Theses and Dissertations

2015

Redundancy, Reliability Updating, and Risk-Based Maintenance Optimization of Aging Structures

Benjin Zhu
Lehigh University

Redundancy, Reliability Updating, and Risk-Based Maintenance Optimization of

Aging Structures

by

Benjin Zhu

Presented to the Graduate and Research Committee

of Lehigh University

in Candidacy for the Degree of

Doctor of Philosophy

in

Structural Engineering

Lehigh University

January 2015

Approved and recommended for acceptance as a dissertation in partial

fulfillment of the requirements for the degree of Doctor of Philosophy.

_____
Date

_____
Dr. Dan M. Frangopol
Dissertation Advisor
Professor of Civil and
Environmental Engineering
Lehigh University

_____
Acceptance Date

Committee Members:

_____
Dr. John L. Wilson
Committee Chairperson
Professor of Civil and
Environmental Engineering
Lehigh University

_____
Dr. Ben T. Yen
Member
Emeritus Professor of Civil and
Environmental Engineering
Lehigh University

_____
Dr. Shamim N. Pakzad
Member
Professor of Civil and
Environmental Engineering
Lehigh University

_____
Dr. Liang Cheng
Member
Professor of Computer
Science and Engineering
Lehigh University

iii

ACKNOWLEDGEMENTS

TABLE OF CONTENTS

LIST OF TABLES

xiv

LIST OF FIGURES

xxii

ABSTRACT

The presence of uncertainties in the structural design process requires the incorporation of system reliability and redundancy concepts in the design specifications. AASHTO Load and Resistance Factor Design specifications utilize a factor relating to redundancy from the load side in the strength limit state to account for system redundancy in the component design. However, the classification of the component redundancy level is very general and the evaluation of values for this factor is also very subjective. Moreover, this factor does not account for several parameters that have significant effects on the system redundancy. Therefore, there is room for further improvement in the classification of the redundancy level and quantification of the associated values.

Structural safety is of paramount importance during the entire lifetime of a structure. Aggressive environmental conditions such as corrosion and / or extreme events such as earthquakes and scour can cause a reduced level of structural safety and functionality under uncertainties. For this reason, assessment of structural performance using probabilistic performance measures such as reliability, redundancy and risk is necessary to determine if maintenance actions need to be applied. Due to the financial constraints on the maintenance budget, optimization tools should be incorporated in the structural maintenance process for seeking the effective and economical solution. The accuracy of performance assessment affects the efficiency of decision making on the maintenance. To enhance the accuracy of the assessment results, objective data

from structural health monitoring can be integrated with the prior information on resistances and / or load effects to obtain a better estimation.

The main objective of this study is two-fold: firstly, to propose a redundancy factor considering the effects of several parameters to provide a rational reliability-based design of structural components; secondly, to develop general approaches for integrating the reliability- and risk-based performance indicators in the life-cycle management framework for structures. Redundancy factors for a wide range of systems consisting of different number of components are evaluated considering several correlation cases. An approach for evaluating time-variant reliability, redundancy, direct and indirect risk considering the effects of resistance deterioration, system modeling type and correlations among failure modes of components is proposed. A risk-based approach for optimum maintenance of bridges under traffic and earthquake loads is also developed. Furthermore, a methodology for assessing risk caused by partially or fully closure of bridge lanes due to traffic load and scour is proposed. Finally, approaches for incorporating structural heath monitoring data in the reliability and redundancy assessment of ship structures by updating one and two parameters using Bayesian method are developed.

The proposed new definition of redundancy factor improves the classification of redundancy levels of structural components and quantification of the factor relating to redundancy used in the current AASHTO Load and Resistance Factor Design specifications by considering several parameters which have significant effects on structural redundancy. The direct, indirect and total risks caused by component failure based on the developed event-tree model can provide guidance on determining the

maintenance priorities of bridge components. The proposed approaches for assessing the time-variant risk due to bridge failure / lanes closure under traffic and earthquake / scour hazards can be efficiently used for obtaining lifetime risk profiles based on which the optimum risk mitigation strategies can be determined through the proposed risk-based optimization process. Finally, the developed Bayesian updating approaches provide a way to make efficient use of the acquired SHM information to improve the accuracy in the performance assessment of naval ships and highway bridges.

CHAPTER 1

INTRODUCTION

1.1 OVERVIEW AND BACKGROUND

Uncertainties exist in almost every aspect of structural design, assessment, maintenance, and monitoring, such as loading, material property, geometry, and modeling, among others. Such uncertainties are generally classified into two types: (a) epistemic uncertainty, which can be reduced through collecting more data, better understanding of the problem, and stricter quality control; and (b) aleatory uncertainty, which has a random nature and cannot be reduced by possession of more knowledge or data (Ang and Tang 2007).

Due to the existence of these uncertainties in the life-cycle of a structure, it is necessary to use probabilistic methods into structural design and assessment process. However, for many years the design of structural systems has been dominated by deterministic thinking: the loads and strengths of structural components were treated as deterministic. A certain safety margin between the strength and load is embedded in determining the component strength. In the conventional allowable stress design (ASD), this margin is considered by using a conservative safety factor which is subjectively defined to attempt to take in account the uncertainties in the design. Due to some inherent weaknesses in the concept of the ASD, the load factor design (LFD) was introduced in the 1970s as an alternative to the ASD specifications. However, no

probabilistic concept was involved in the calibration of the factors for loads and resistances in LFD.

In light of the shortcomings of LFD and the development of the probability-based reliability theory (Ang and Tang 1975, Thoft-Christensen and Baker 1982, Ang and Tang 1984, Thoft-Christensen and Murotsu 1986), the load and resistance factor design (LRFD) was developed through 1990s and 2000s with the intent of implementing a more rational design approach for buildings and bridges. The LRFD specifications utilize the load and resistance factors to quantitatively consider the variability of applied loads and resistances of structural members (Hsiao *et al.* 1990, Lin *et al.* 1992, Paikowsky 2004, Babu and Singh 2011). The load and resistance factors in the strength limit state of LRFD were calibrated using the structural reliability theory to provide a uniform reliability level of safety for components (Kulicki *et al.* 1994). A target reliability index of 3.5 was recommended for the design of main structural elements of a bridge (AASHTO 1994, AASHTO 2007, AASHTO 2010).

The load modifier in the limit state of the AASHTO bridge design specifications (e.g., AASHTO 2010) is a function of a subjective evaluation of the operational importance of a structure, the level of ductility, and the level of redundancy. The level of redundancy concerns the classification of a member's redundancy based on its contribution to the bridge safety. Three values are suggested for the factor relating to redundancy according to the redundancy classification of a member: (a) 1.05 for nonredundant members; (b) 1.0 for conventional level of redundancy; and (c) 0.95 for exceptional levels of redundancy.

This classification of the redundancy level is general and the evaluation of three recommended values is subjective. Since redundancy is defined as the capability of a structure to continue carrying loads after damage or failure of one or more of its members, factors associated with the ability of redistributing and carrying loads (i.e., number of components and post-failure behavior of components, among others) and definition of system failure (i.e., system modeling type) affect the system redundancy. However, these factors are not considered in establishing the classifications and values of the factor relating to redundancy. Therefore, although the factor relating to redundancy is currently being implemented in practice, there is room for its further refinement.

After a structure is constructed, it is expected to perform satisfactorily throughout its anticipated service life. However, due to various environmental and mechanical stressors such as corrosion and fatigue, structures may be subjected to gradual deterioration in strength and performance. In addition, increase of service loads and possible exposure to natural and / or man-made extreme events may cause progressive degradation and sudden damage to structures. In this context, life-cycle performance assessment of structures is playing an increasingly important role in providing information on the structural condition to determine the adequacy of a structure to fulfill the current structural and functional demands.

Due to the uncertainties in the assessment process, probabilistic performance indicators, such as reliability and redundancy, have been proposed and extensively used as the main indicators for decision making (Frangopol 2011). Reliability is defined as the ability of a structure or component to fulfill the specified performance

requirements under the prescribed conditions during the prescribed time (Ayyub *et al.* 2000). Research on reliability and redundancy analysis of different types of structures has been extensively performed in recent decades (Estes 1997, Vu and Stewart 2000, Cheng and Li 2009, Liu and Frangopol 2005b, Ghosh *et al.* 2014, Frangopol and Curley 1987, Frangopol and Nakib 1991, Wen and Song 2003, Liu *et al.* 2001, Cavaco *et al.* 2013). It is noticed from their definitions that these two performance indicators are focused on the abilities of structure itself, without considering the impact of structure failure on the society.

Although the failure probabilities of some structures might be low, the consequences associated with their failures can be enormous and may bring adverse impacts on the society. These consequences can take various forms, such as material / structural damage, human injuries / fatalities, functional downtime, environmental impact, as well as loss of reputation (Janssens *et al.* 2012). Therefore, including the consequences evaluation is essential in structural performance assessment. This necessity leads to the use of another performance indicator: risk.

Risk is defined as the combined effect of probabilities and consequences of some failure or disaster in a given context (Uddin and Ang 2011). Inclusion of hazard analysis and consequences evaluation makes it difficult to assess the risk quantitatively. However, in order to provide clear and accurate results to decision-makers for risk mitigation, studies on risk assessment in recent years have been gradually moved from qualitative to quantitative analysis (Stein *et al.* 1999, Lupoi *et al.* 2003, Adey *et al.* 2003, Decò and Frangopol 2011). Among various extreme events, earthquakes and flood-induced scour are the most common causes of bridge failure in

the United States (Wardhana and Hadipriono 2003). In addition, traffic overloading and corrosion are other potential causes contributing to bridge failure. According to Imam and Chryssanthopoulos (2010), about 10% and 2% of bridge collapse is induced by overloading and corrosion, respectively. Therefore, it is necessary to assess the risks of bridges under these hazards.

The aim of performance assessment is to provide information on the status of structural health to check if the structure will function safely over a specified residual service life according to a prescribed level of safety. If the assessment results indicate that an undesirable performance state is reached or is close to be reached, maintenance or rehabilitation actions need to be applied. Two types of maintenance actions are usually used in current bridge management systems to keep bridges safe and serviceable: essential and preventive maintenance (Kong *et al.* 2000). Essential maintenance actions can lead to significant improvements in the structural performance but they are usually very expensive; while preventive maintenance actions only delay the deterioration rate, but they are more economical.

For a deteriorating structure, the lifetime maintenance cost which may span decades can comprise a large portion of the total lifetime cost (Estes and Frangopol 2001). Since the number of aging structures is increasing while the funding available for maintenance is limited, optimization needs to be involved in the structural maintenance process for seeking effective and economical strategies. Extensive studies on the optimization of maintenance strategies have been performed with respect to different performance indicators, such as system reliability (Augusti *et al.* 1998, Estes and Frangopol 1999), system reliability and redundancy (Okasha and

Frangopol 2009b), lifetime-based reliability (Yang *et al.* 2006), and lifetime-based unavailability and redundancy (Okasha and Frangopol 2010a), among others. However, research on risk-based maintenance strategy optimization is rarely reported.

Accurate prediction of life-cycle performance is very important during structural management because a great deal of decision making often depends on the assessment results of structural performance. The information on the time-variant resistances and load effects of a decaying structure is usually estimated based on mathematical models or previous experience. In order to improve the accuracy in performance assessment, structural health monitoring (SHM) technology has been developed in recent years and extensively used not only in civil engineering but also in marine engineering (Farrar and Worden 2007, Burton and Verijenko 2002, Liu *et al.* 2009, Okasha *et al.* 2010, Hess 2007). SHM is a powerful tool that can provide reliable data for verifying assumptions and parameters used in performance assessment, alarming abnormal load and response, assessing structural safety and functionality after extreme events, issuing early warnings on structural damage / deterioration, and instructing the design of similar structures in future (Ko and Ni 2005).

For structures subjected to long term structural health monitoring, a large amount of input and response data can be collected. Statistical parameters associated with structural resistances and load effects can be directly obtained by analyzing the acquired data. Therefore, structural performance can be evaluated or updated using these parameters. However, in most practical cases, due to the limited funding, SHM is conducted over discrete time intervals instead of throughout the lifetime of structures. It is a challenging task to improve the accuracy of performance assessment

results based on a limited amount of data acquired from SHM. In order to make efficient use of the data, Bayesian updating approach is utilized to combine the objective data from SHM with the prior judgmental information to reach a balanced evaluation of structural performance. Although Bayesian estimation is a very promising method, very few studies have been conducted on its application to structural performance assessment. Therefore, research effort is needed for incorporation of SHM data in the structural performance assessment using Bayesian updating.

1.2 OBJECTIVES

The following are the main objectives of this study:

1. Propose a redundancy factor that considers the effects of several parameters on the system redundancy to provide a rational reliability-based design of components in structural systems.

2. Investigate the reliability of systems whose components have a prescribed uniform reliability level.

3. Develop an approach for the evaluation of time-variant reliability, redundancy, direct and indirect risk of structural systems considering the effect of deterioration, system type and correlation among the failure modes of components.

4. Propose an approach for assessing time-variant risks due to bridge failure under traffic and seismic loads and seeking optimum essential and preventive maintenance strategies.

5. Develop an approach for the quantification of time-variant risks due to the closure of bridge lanes under traffic load and scour.

6. Propose an approach for integrating SHM data in the reliability and redundancy assessment of ship structures by updating single parameter using Bayesian method and extend the approach developed for updating two parameters.

1.3 SUMMARY OF THE APPROACH

Figure 1.1 shows a schematic example of a framework for life-cycle design and management of structures under uncertainty. It consists of the following tasks: structural design, performance assessment and prediction, optimization of maintenance strategies, and performance updating using structural health monitoring information. The approaches proposed for accomplishing these tasks incorporate the probabilistic, structural analysis, and optimization tools based on existing software and self-developed programs. The applications of the developed approaches include structures in both civil and naval engineering fields, such as highway bridges and high speed naval ships.

In the quantification of redundancy factors for bridge component design which is related to the task of "Structural design", the proposed redundancy factor is defined as the ratio of the mean resistance of a component in a system when the system reliability index is prescribed to the mean resistance of the same component when its reliability index is the same as that of the system. Idealized nondeterministic systems are used to study the effects of the statistical parameters that describe the uncertainties of the resistances and load effects of components on the reliability-based redundancy factor.

To obtain the redundancy factors for a wide range of systems consisting of different number of components, a workstation with high computing power is required to generate a large number of simulation samples for hundreds of random variables simultaneously and find the system reliability. The difficulty in evaluating the redundancy factor of brittle systems with many components is solved by using a simplified system model where the number of failure modes considered is significantly reduced without affecting substantially the accuracy in the results.

The performance indicators investigated in "Structural performance assessment and prediction" part of this study include reliability, redundancy and risk. Compared with the reliability and redundancy assessment, analyzing risk of a structure is a more challenging task since it also takes into account the social impacts of structural failure or partial loss of functionality. A complete evaluation of the consequences is required to obtain an accurate assessment of risk. Time effects are considered in performance prediction by mainly using corrosion models to account for the deterioration in resistances and live load models to predict the increase in traffic volume. Probabilistic evaluation of resistances and load effects of structural components and systems is performed by combining several advanced computational techniques, such as Latin hypercube sampling, nonlinear finite element analysis, and first / second reliability analysis.

Maintenance strategies involved in the optimization process are of the essential and preventive types. The optimization criterion which determines the final optimum strategy is associated with minimizing the total life-cycle cost or maximizing the extended service life. The requirements of the performance indicator being higher or

lower than a predefined level are considered as constraints during the optimization process. Genetic algorithm is used to seek the optimum solution after the optimization problem is formulated. The differences in the effects of the optimum essential and preventive strategies on the lifetime safety level and maintenance cost are discussed.

The existence of uncertainties during the performance assessment process may cause the predicted results deviate from the actual performance. Objective information on structural responses collected from SHM can help improving the accuracy in assessment results. Bayesian method is used to combine the prior judgmental information with the objective data to yield a balanced estimation. Approaches for updating one and two parameters of a distribution are developed. Different cases associated with updating one parameter, updating both parameters separately, and updating both parameters simultaneously in a two-parameter distribution are investigated. Data processing tools and slice sampling algorithm are used to extract useful SHM data and generate samples.

The existing software and self-developed programs used in this study include (a) MATLAB (MathWorks 2009, 2010) which is used to develop codes for calculation and connection with other software, (b) OpenSees (OpenSees 2011) for finite element analysis of structural systems under earthquakes, (c) RELSYS (Estes and Frangopol 1998) for component and system reliability analysis, and (d) PDSTRIP (PDSTRIP 2006) which is a hydrodynamic software for seakeeping analysis.

1.4 OUTLINE

This study is divided into nine chapters. The following is a brief description of these chapters.

Chapter 1 serves as introduction.

Chapter 2 proposes a redundancy factor to provide a rational reliability-based design of components in structural systems. The effects of the coefficients of variation of resistance and load, the mean value of load, correlation among the resistances of components, system modeling type, and post-failure material behavior on the redundancy factor are investigated. Redundancy factors of ductile and brittle systems consisting of many components are evaluated considering different correlation cases.

Chapter 3 investigates the reliability of systems consisting of uniform reliability components. The effects of the parameters investigated in Chapter 2 on the system reliability are studied using non-deterministic systems. Reliability indices of ductile and brittle system with many iso-reliability components are evaluated.

Chapter 4 presents an approach for evaluation of the time-variant reliability, redundancy and risk of structural systems considering the effects of the deterioration of structural resistance, type of system modeling and correlations among failure modes of components. The risk caused by the failure of component(s) or system is divided into direct and indirect risk and a method for assessing these two types of risk based on event-tree models is provided. Idealized systems consisting of three components are used to demonstrate the presented approach and study the effects of the aforementioned factors on these performance indicators.

Chapter 5 proposes an approach for assessing the time-variant risks caused by traffic and earthquake loads and establishing the optimal preventive and essential maintenance strategies of bridges. Bridge vulnerability analysis is performed with respect to traffic and earthquake loads. The failure probability under earthquake load is computed by comparing displacement ductility capacity and demand obtained via nonlinear dynamic analysis. Socioeconomic and environmental losses are investigated in a consequence-based framework. Based on the assessment results and the defined risk threshold, the optimal lifetime essential / preventive maintenance strategies for total risk mitigation are developed.

Chapter 6 presents a methodology for evaluating the time-variant risks associated with the closure of bridge lanes due to traffic loading and scour. The annual failure probabilities are estimated for girders under traffic loading and for pier columns under scour. Scenarios of lanes closure due to the two hazards are identified. The occurrence probabilities of the scenarios are computed based on the relations between the scenarios and the failure events of girders and of pier columns. Consequences caused by lanes closure are evaluated considering repair, running, and time loss costs.

Chapter 7 develops an approach for reducing the uncertainty in the reliability and redundancy assessment of ship cross-sections by using the Bayesian updating method. The vertical bending moments associated with ultimate and first failure are evaluated for three ship cross-sections. Based on the extracted wave peaks from the structural health monitoring data, Bayesian method is used to update the Rayleigh-distributed prior load effects obtained based on linear theory. The original and updated reliability

and redundancy indices of the ship cross-sections are evaluated and the results are presented in polar plots.

Chapter 8 extends the approach developed in Chapter 7 for updating one parameter to updating two parameters for improving the accuracy in the reliability assessment of ship structures. Three general cases associated with updating (a) only one parameter, (b) two parameters separately, and (c) two correlated parameters simultaneously are investigated and compared. Bayesian method is used to incorporate the processed SHM data to update the extreme value of wave-induced vertical bending moment modeled by Type I extreme value distribution. Aging effects due to corrosion is considered in the resistance modeling. The original and updated time-variant reliabilities associated with the three general cases are evaluated and compared.

Chapter 9 provides the conclusions drawn from this study and the suggestions for future work.

1.5 CONTRIBUTIONS

The main contributions of this study are (a) the novel definition of a consistent redundancy factor to provide a rational reliability-based design of structural components in nondeterministic systems; and (b) the development of general approaches for life-cycle management process, including quantitative assessment of risks due to structural failure or partial loss of functionality, risk-informed structural maintenance based on optimization, and performance updating using SHM data. Specifically, the contributions include:

- Proposing a redundancy factor whose values are determined based on a detailed classification of redundancy levels considering the effects of several parameters and developing approaches for evaluating the redundancy factors in ductile and brittle systems.

- Developing an approach for assessing the direct and indirect risks due to failure of structural components / system considering time effect.

- Developing an efficient methodology for quantifying lifetime risk for bridge structures subjected to traffic and earthquake loads and seeking the optimum essential and preventive strategies for risk mitigation.

- Developing an approach for assessing time-variant risk of bridges with partially or fully closed lanes due to traffic load and scour considering two correlation cases among the failure modes of bridge components.

- Developing an approach for efficient incorporation of SHM data in the reliability and redundancy assessment of ship cross-sections by updating one parameter using Bayesian method.

- Extending the approach for updating one parameter to two parameters considering two cases where the parameters are updated separately and simultaneously.
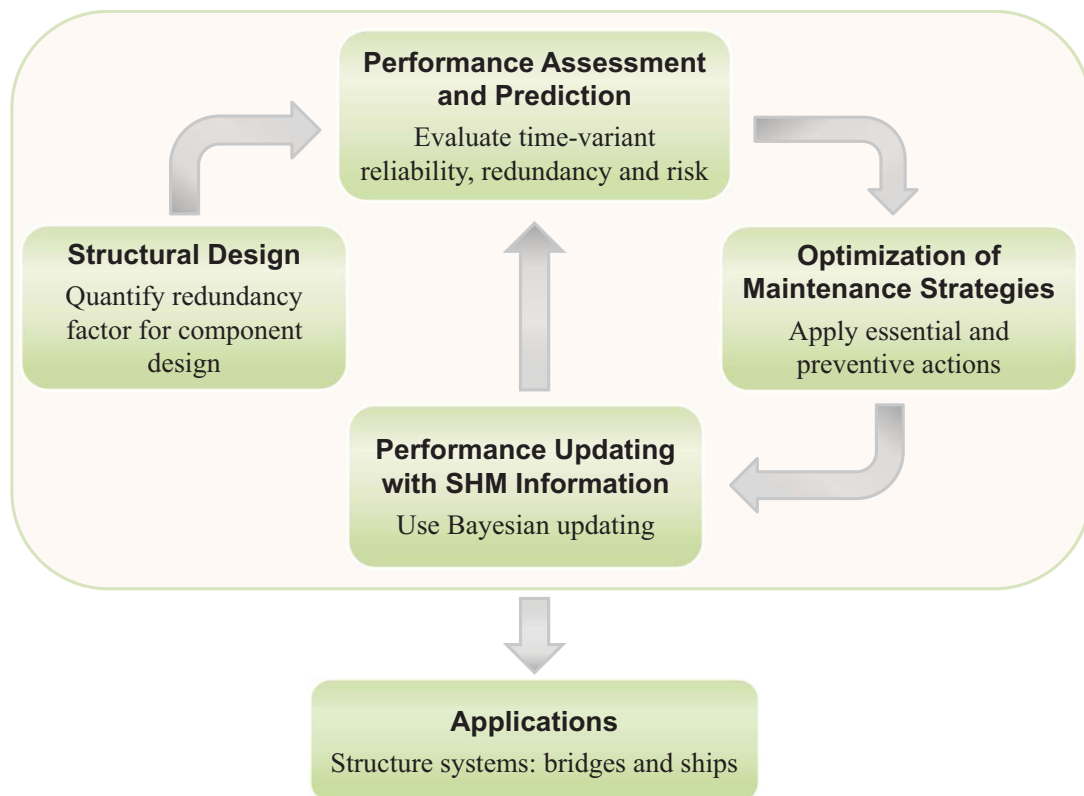
Figure 1.1 Framework for life-cycle design and management of structures under uncertainty.

CHAPTER 2

SYSTEM RELIABILITY-BASED REDUNDANCY FACTORS FOR DESIGN OF STRUCTURAL COMPONENTS IN NONDETERMINISTIC SYSTEMS

2.1 INTRODUCTION

The most important task in structural design is to maximize the safety of structures within economic constraints. This is achieved by making the difference between the designed resistance and the load effect as large as possible. Due to the possible occurrence of some unfavorable events during the construction and / or operation of a structure, a large safety margin needs to be provided to allow for abnormal situations, unexpected loads, misuse, degradation, and ineffective maintenance, among others (Burdekin 2007). In the conventional allowable stress design (ASD), the safety is considered by using a single safety factor. Due to the limitations of the ASD method and the development and application of reliability theory in civil engineering, the design philosophy moved from the allowable stress design to load and resistance factor design (LRFD).

LRFD represents a more rational approach by which the uncertainties associated with resistance and load are incorporated quantitatively into the design process (Babu and Singh 2011, Hsiao *et al.* 1990, Lin *et al.* 1992, Paikowsky 2004). The load and resistance factors are developed from the theory of reliability based on current nondeterministic knowledge of loads and structural performance. The American

Association of State Highway and Transportation Officials (AASHTO) published the first LRFD specification for bridge design in 1994 (AASHTO 1994). Although this specification has been refined, revised, and improved every year since its initial publication, there is still room for improvement because the LRFD code was initiated with a guiding principle that it could and should continually evolve (Tobias 2011). Along these lines, the purpose of this chapter is to provide an improved and rational basis for reliability-based design of components in structural systems by considering redundancy factors.

Research on the redundancy of bridge systems has been extensively performed in the past decades (Frangopol and Curley 1987, Rabi *et al.* 1989, Frangopol and Nakib 1991, Ghosn and Moses 1998, Wen and Song 2003, Tsopelas and Husain 2004, Ghosn *et al.* 2010, Liu *et al.* 2001, Cavaco *et al.* 2013). Different measures have been proposed to quantify the system redundancy. For example, Frangopol and Curley (1987) defined the redundancy as the ratio of the reliability index of the intact system, β_{intact}, to the difference between β_{intact} and the reliability index of the damaged system, $\beta_{damaged}$. Since structural components of a bridge do not behave independently, their interactions with other components in the system should be considered in the bridge component design. Therefore, researchers have attempted to include redundancy which is related to system behavior in the bridge design specifications. Hendawi and Frangopol (1994) introduced a system factor modifier ϕ_R to account for the strength reserve of the bridge system. Ghosn and Moses (1998) proposed a system factor ϕ_s to be used in the limit states to account for the effect of system redundancy in the design of individual components.

In the strength limit state defined by the LRFD bridge design specifications (AASHTO 1994) and the following editions (e.g., AASHTO 2010), the factor relating to redundancy η_R is considered on the load side and its value is determined as follows: (a) $\eta_R \geq 1.05$ for nonredundant members; (b) $\eta_R = 1.00$ for conventional level of redundancy; and (c) $\eta_R \geq 0.95$ for exceptional levels of redundancy. The AASHTO classification of redundancy levels is very general. In fact, the value of this factor relating to redundancy is affected by several parameters, such as system type, number of components in a structure, correlations among the resistances of components, and post-failure behavior of components, among others.

These factors are key points in redundancy assessment and must be considered in establishing redundancy factors for design. As mentioned in section 1.3.2.1 of AASHTO (2010): "improved quantification of ductility, redundancy, and operational classification may be attained with time, and possibly leading to a rearranging of Eq. 1.3.2.1-1, in which these effects may appear on either side of the equation or on both sides", there is still room to improve the quantification of the factor relating to redundancy in the current design code, which is the main objective of this chapter.

This chapter proposes a redundancy factor η_R which considers the effects of the aforementioned parameters (i.e., system modeling type, post-failure behavior of components) to account for the redundancy in the design of structural components. Section 2.2 provides the definition of the proposed redundancy factor and illustrates it with a brief example. Section 2.3 investigates the effects of the coefficients of variation of resistance and load, mean value of load, correlation among the resistances of components, and system type on the redundancy factor. Section 2.4 evaluates the

redundancy factors of systems consisting of many components associated with different correlation cases. Section 2.5 illustrates the procedure for evaluating the redundancy factors of systems considering post-failure material behavior and studies the effects of the post-failure behavior on the redundancy factor. Section 2.6 estimates the redundancy factors of the ductile and brittle systems with many components. Section 2.7 presents two types of limit states in which the redundancy factor is taken into account from the load and resistance side, respectively. In Section 2.8, the application of the proposed redundancy factor for design of structural component is demonstrated using a bridge example. Finally, Section 2.9 provides the conclusions of this chapter.

2.2 REDUNDANCY FACTOR

2.2.1 Definition

Considering a single component, its resistance R and load P are treated as random variables. For the given mean value of load, $E(P)$, the coefficients of variation of resistance and load, denoted as $V(R)$ and $V(P)$, respectively, and the predefined component reliability index $\beta_c = 3.5$, the mean value of the component resistance $E_c(R)$, can be determined (e.g., by using Monte Carlo Simulation (MCS) in MATLAB). For two particular cases in which both R and P of the component are normally or lognormally distributed, $E_c(R)$ can also be calculated by solving the corresponding equations that are used for determining the reliability indices (Tangchawal 2011). $E_c(R)$

obtained herein will be used as the reference value to be compared with the mean value of component resistance in a system to yield the redundancy factor.

For a system consisting of N identical components whose geometries and material properties are the same as the single component just described, different types of systems can be formed: series, parallel, and series-parallel systems (Ditlevsen and Bjerager 1986, Hendawi and Frangopol 1994). The resistances and loads of these components are also considered random variables. Given the distribution type of R and P, the values of $E(P)$, $V(R)$, $V(P)$, the correlation coefficient between the resistances of components i and j, denoted as $\rho(R_i, R_j)$, and the system reliability index β_{sys} that is assumed to be 3.5 herein, the mean value of component resistance $E_{cs}(R)$ can be calculated by using RELSYS (Estes and Frangopol 1998) or MCS-based program in MATLAB (MathWorks 2009). Since the external loads acting on the system are distributed to components, the load effects of each component are correlated. Therefore, the failure modes of the components are always correlated even in the case where $\rho(R_i, R_j)=0$.

Once the mean resistance of a component in a system when the system reliability index is 3.5, $E_{cs}(R)$, and the mean resistance of the same component when the component reliability is 3.5, $E_c(R)$, are obtained, the redundancy factor $\eta_R = E_{cs}(R) / E_c(R)$, can be determined. The procedure for determining the redundancy factor is described in the flowchart shown in Figure 2.1.

2.2.2 Example

An example is provided herein to illustrate the above concepts. In this example, the number of the investigated identical components is three; thus, two different systems are formed: series and parallel, as shown in Figure 2.2. Normal and lognormal distributions are assumed for the resistances and loads of the components. The values of $E(P)$, $V(R)$, and $V(P)$ associated with the three components are assumed as 10, 0.1, and 0.1, respectively. Three correlation cases among the resistances of components are considered: (a) $\rho(R_i,R_j) = 0$, no correlation; (b) $\rho(R_i,R_j) = 0.5$, partial correlation; and (c) $\rho(R_i,R_j) = 1$, perfect correlation.

For a required component reliability index $\beta_c = 3.5$, the mean values of resistance associated with a single component for the normal and lognormal distribution are found to be $E_{c,N}(R) = 16.861$ and $E_{c,LN}(R) = 16.384$, respectively. Assuming the target system reliability index $\beta_{sys} = 3.5$, the mean values of component resistance $E_{cs}(R)$ corresponding to the two systems associated with the normal case are calculated by combining RELSYS (Estes and Frangopol 1998) with MATLAB (MathWorks 2009). The redundancy factors η_R and the corresponding components reliability indices β_{cs} are also obtained, as presented in Table 2.1. By performing the same procedure, the mean values of component resistance $E_{cs}(R)$, the redundancy factors η_R, and the components reliability indices β_{cs} associated with the lognormal case are shown in Table 2.2.

It is seen from Table 2.1 and Table 2.2 that in the no correlation and partial correlation cases (a) the redundancy factors η_R associated with series system are greater than 1.0; this indicates that the mean resistance required for each component in

24

series system is larger than that needed for a single component; therefore, the component reliability indices β_{cs} in the two correlation cases are larger than 3.5; and (b) in the parallel system, the obtained conclusion is contrary to that of the series system.

2.3 EFFECTS OF PARAMETERS ON REDUNDANCY FACTOR

It is observed from the above example that the mean value of the component resistance $E_{cs}(R)$ is affected by the coefficient of variation of resistance $V(R)$, coefficient of variation of load $V(P)$, mean value of load $E(P)$, correlation among the resistances of components $\rho(R_i,R_j)$, and system type. In addition to these parameters, the number of components N in a system has an impact on $E_{cs}(R)$. Therefore, different types of systems consisting of two, three, and four components are investigated herein to study the effects of $V(R)$, $V(P)$, $E(P)$, $\rho(R_i,R_j)$, and N on the redundancy factor η_R in these systems. The probability distribution types of R and P of the components in these systems are assumed to be normal, and $\beta_c = \beta_{cs} = 3.5$.

The effects of $V(R)$, $V(P)$, and $E(P)$ on the redundancy factor η_R in two-component systems associated with two extreme correlation cases are plotted Figure 2.3. It is seen that in the no correlation case, (a) as $V(R)$ increases, η_R increases in the series system while it decreases significantly in the parallel system; (b) as $V(P)$ increases, η_R increases in both systems but more significantly in the parallel system; and (c) η_R is not affected by changes in the mean values of the load in both systems. However, in the perfect correlation case, η_R in both systems is equal to 1.0 and it is not affected by changes in $V(R)$, $V(P)$, and / or $E(P)$.

These observations can be explained by the results presented in Figure 2.4 which shows the effects of $V(R)$ and $V(P)$ on the mean resistance of the single component $E_c(R)$ and the mean component resistance $E_{cs}(R)$ in the two systems associated with two correlation cases. It is found that (a) as $V(R)$ or $V(P)$ increases, $E_c(R)$ and $E_{cs}(R)$ in the two systems associated with both correlation cases increase; (b) in the no correlation case, the variation of $E_{cs}(R)$ in the series system due to the change of $V(R)$ or $V(P)$ is more significant than that of $E_c(R)$; therefore, $\eta_R = E_{cs}(R) / E_c(R)$ will increase as $V(R)$ or $V(P)$ increases; (c) however, in the parallel system, the increase of $E_{cs}(R)$ due to the increase of $V(R)$ in the no correlation case is less significant than the increase of $E_c(R)$; therefore, η_R associated with the no correlation case in the parallel system decreases (see Figure 2.3(a)); (d) as $V(P)$ increases in the no correlation case, the distance between the curves associated with $E_c(R)$ and $E_{cs}(R)$ of the parallel system decreases; thus, η_R increases along with the increase of $V(P)$ (see Figure 2.3(b)); and (e) for the perfect correlation case, $E_{cs}(R) = E_c(R)$; hence, $\eta_R = 1.0$ and $V(R)$ and $V(P)$ have no effect on the redundancy factor.

The redundancy factor as function of $V(R)$, $V(P)$ and $E(P)$ in three-component systems is plotted in Figure 2.5. The conclusions obtained from this figure are similar to those associated with two-component systems drawn from Figure 2.3. The effects of the aforementioned parameters on η_R are also investigated for the four-component systems in which three different systems can be composed: series, parallel, and series-parallel systems, as shown in Figure 2.6. An additional correlation case in which the correlation coefficients among the components resistances are 0.5 is studied. The results are presented in Figure 2.7 and Figure 2.8. It is seen from Figure 2.7 that in the

no correlation and partial correlation cases, as $V(R)$ increases, η_R associated with the series system increases while η_R associated with both the parallel and series-parallel systems show a decreasing tendency. It is also seen that as the correlation among the resistances becomes stronger, the sensitivity of η_R to the changes in $V(R)$ decreases.

In the no correlation and partial correlation cases, Figure 2.8 shows that increasing $V(P)$ leads to a larger redundancy factor in series, parallel and series-parallel systems. In the perfect correlation case, η_R of all systems is 1.0 for any value of $V(P)$. The effect of $E(P)$ on η_R in four-component systems is the same as that associated with Figure 2.3(c) and Figure 2.5(c). The effects of number of components N on the redundancy factor η_R in different systems with variations of $V(R)$, $V(P)$, and $E(P)$ are plotted in Figure 2.9. As N increases in the no correlation case, it is observed that (a) η_R in series systems increases while its counterpart in parallel systems decreases; and (b) the change of η_R due to the variation of $V(R)$ or $V(P)$ is more significant than that due to the variation of $E(P)$.

2.4 REDUNDANCY FACTOR OF SYSTEM WITH MANY COMPONENTS

In the previous section, η_R is evaluated with respect to the systems consisting of no more than four components. However, in most practical cases, a structure usually consists of dozens or hundreds of members; therefore, it is necessary to investigate the redundancy factors of systems with many components. In this section, two different computer programs are used to determine the redundancy factor.

2.4.1 Using the RELSYS Program

RELSYS is a program used to compute the system reliability of a structure which can be modeled as a series-parallel combination of its components (Estes and Frangopol 1998). It initially calculates the reliability of each individual component using the first-order reliability method and then computes the system reliability by successively reducing the series and parallel systems until the system is simplified to a single equivalent component.

A search algorithm is used herein in combination with the program RELSYS to find the redundancy factor for a system with many components. The algorithm is described as follows:

1. Give the mean value of the load effect $E(P)$, coefficients of variation of resistance and load effect $V(R)$ and $V(P)$, correlation between the resistances of components $\rho(R_i, R_j)$, probability distribution types of resistance and load, number of components N, and a group of initial guess for $E_{cs}(R)$: $\boldsymbol{x}=[x_1, x_2,\dots x_i,\dots, x_k]$, where k is the dimension of the array (i.e., $k = 20$); it should be noted that the elements in the vector $\boldsymbol{x}$ need to be arranged in an ascending order and the increment is 1.0; also define a counter number $c = 0$;

2. Starting from x_1, check if $(\beta_{sys} \mid x_i) < 3.5$ and $(\beta_{sys} \mid x_{i+1}) > 3.5$; if yes, go to Step 3; otherwise repeat this step, $i = i+1$ ($i =1,2, \dots, k\text{-}1$);

3. Checkpoint: if $|(\beta_{sys} \mid x_i) - 3.5| \leq Tol$ or $|(\beta_{sys} \mid x_{i+1}) - 3.5| \leq Tol$ (Tol is set to be 10^{-4} herein), stop and return x_i or x_{i+1} as the final value of $E_{cs}(R)$; otherwise continue, $c = c+1$;

4. Clear the original vector $\boldsymbol{x}$; use x_i as the first element and generate a new initial guess vector $\boldsymbol{x}$ for $E_{cs}(R)$; the increment of the adjacent array elements is 10^{-c}; the size of this vector is also $1 \times k$;

5. Repeat steps 2 to 4 until $E_{cs}(R)$ is found.

A flowchart for this algorithm is presented in Figure 2.10. The redundancy factor can usually be found before $c = 5$. For systems with many components, evaluation of all the redundancy factors with respect to different combinations of $V(R)$ and $V(P)$ is a computationally expensive task. Therefore, focusing on a specific case where $V(R)$ and $V(P)$ are commonly used values is most efficient and practical. Since the uncertainty associated with load effect is usually larger than that associated with resistance, $V(P)$ is assumed to be 0.3 and $V(R)$ is set to be 0.05. Since the mean value of the load effect $E(P)$ has no effect on the redundancy factor, $E(P)$ is still assumed to be 10.

For the specified case (i.e., $E(P)$=10, $V(R)$=0.05, and $V(P)$=0.3), the redundancy factors associated with different types of systems (i.e., series, parallel, and series-parallel systems) and different correlation cases (i.e., $\rho(R_i,R_j) = 0$, 0.5, and 1.0) in N-component systems (N = 100, 300, and 500) are intended to be evaluated using the search algorithm described previously.

For a system consisting of N components, different series-parallel (SP) systems can be formed. Therefore, the following rule is used to describe different SP systems: (a) if the subsystem of the series-parallel (SP) system is a parallel system consisting of m components and it is repeated n times in the system model, as shown in Figure 2.11(a), the series-parallel system is denoted as $mp \times ns$ SP system; and (b) if the subsystem of the series-parallel system is a series system consisting of m components

and it is repeated *n* times in the system model, as shown in Figure 2.11(b), the series-parallel system is denoted as *ms×np* SP system. In this subsection, only the *mp×ns* SP systems in which *m* equals to 5, 10 and 20 are investigated.

Assuming β_c = 3.5 and normal distributions for resistances and load effects, the mean value of resistance associated with a single component is found to be $E_c(R)$ =21.132. Then, starting with the no correlation case, the mean values of component resistance $E_{cs}(R)$ and redundancy factors associated with the *N*-component systems are evaluated by combining RELSYS with MATLAB based on the aforementioned search algorithm. However, a limitation of RELSYS was found during the computation: for systems with more than 200 components and parallel systems consisting of more than 50 components, the computational time is excessive. Therefore, the mean component resistances and redundancy factors associated with the systems with only 100 and 200 components are determined, as presented in Table 2.3.

By comparing the results associated with 100- and 200-component systems, it is observed that (a) η_R of the series system increases as the number of components becomes larger; and (b) for the *mp×ns* SP systems having the same number of parallel components (i.e., *m* in these systems are identical), η_R also shows an increasing tendency as the number of total components increases.

2.4.2 Using the MCS-based Program

In some practical cases, a structure may consist of more than 200 components, such as a truss bridge or a high-rise building. Therefore, it is necessary to study the redundancy factors of systems that have a high number of components ($N \geq 200$).

Since the computational time needed by RELSYS to obtain the probability of failure for systems with more than 200 components is excessive, the Monte Carlo Simulation-based program is used herein to find the probability of failure, P_f, of the N-component systems (N = 100, 300, and 500). In this subsection, the $mp{\times}ns$ and $ms{\times}np$ SP systems where m equals to 5, 10 and 20 are investigated.

The algorithm of the MCS-based program for the calculation of P_f using MATLAB is described as follows:

1. Give the mean value of the load effect $E(P)$, coefficients of variation of resistance and load effect $V(R)$ and $V(P)$, correlation between the resistances of components $\rho(R_i,\ R_j)$, probability distribution types of resistance and load, number of components N, number of simulation samples w, and the initial guess for the mean value of component resistance $E_{cs}(R)$;

2. Generate the random samples of resistance R_i and load effect P based on the above parameters, and the dimensions of the R_i and P vectors are $w \times 1$;

3. Obtain the performance function for each component $g_i = R_i - P$ (i=1, 2, …, N); the dimensions of g_i is also $w \times 1$;

4. For series system, define a $w \times 1$ zero vector L, and the ratio of the number of $\left[L\,|\,(g_1 < 0)\,|\,...\,|\,(g_N < 0)\right]$ to the total sample size w represents the failure probability of series system ("|" is logical OR in MATLAB; it refers to union herein); for the parallel system, define a $w \times 1$ unit vector Q, and the ratio of the number of $\left[Q\,\&\,(g_1 < 0)\,\&\,...\,\&\,(g_N < 0)\right]$ to the sample size w is the P_f of parallel system ("&" is logical AND in MATLAB; it refers to intersection herein); for the $mp \times ns$ SP

31

system, define a $w \times 1$ zero vector L and a $w \times 1$ unit vector Q, and the ratio of the

number of $\{L \mid [Q \& (g_1 < 0) \& ... \& (g_m < 0)] \mid ... \mid [Q \& (g_{m \cdot (n-1)+1} < 0) \& ... \& (g_{m \cdot n} < 0)]\}$

to the sample size w is the P_f of the SP system; and for the $ms \times np$ SP system,

define a $w \times 1$ zero vector L and a $w \times 1$ unit vector Q, and the ratio of the number

of $\{Q \& [L \mid (g_1 < 0) \mid ... \mid (g_m < 0)] \& ... \& [L \mid (g_{m \cdot (n-1)+1} < 0) \mid ... \mid (g_{m \cdot n} < 0)]\}$ to the sample

size w is the P_f of the SP system; it should be noted that in the series-parallel

systems, $n \times m$ is equal to the number of components N.

5. Repeat steps 1 to 4 for t times (e.g., $t = 50$) to obtain the average probability of

   failure of the system; then, convert it to the reliability index.

   When using the MCS-based program to find the reliability index of systems, it is

noticed that as N increases, the computational time required increases dramatically.

Therefore, the aforementioned search algorithm that requires a group of initial values

is not efficient when combined with the MCS-based program. In order to reduce the

computing time, a simple algorithm based on the effects of the number of components

on the redundancy factor is used herein in combination with the MCS-based program

to find $E_{cs}(R)$ and η_R. The procedure of this algorithm is as follows:

1. Determine an initial guess value of $E_{cs}(R)$ based on the effects of number of

   components N on the redundancy factors. For example, it was found previously that

   $E_{cs}(R)$ associated with series (or series-parallel) system increases as N increases;

   however, this increase is less significant as N becomes larger. Therefore, the initial

   guess of $E_{cs}(R)$ for the 300-component series system can be obtained by increasing

   the $E_{cs}(R)$ of 200-component series system by Δ percent ($0.5 \leq \Delta \leq 1$). On the

   contrary, increasing N leads to lower $E_{cs}(R)$ in parallel systems. Hence, the initial

guess of $E_{cs}(R)$ for the 500-component parallel system can be determined by reducing the $E_{cs}(R)$ of 400-component parallel system by Δ percent ($0.5 \leq \Delta \leq 1$).

2. Substitute the initial value to the MCS-based method described above to obtain the system reliability index β_{sys};

3. Checkpoint: if $|\beta_{sys} - 3.5| \leq Tol$ (*Tol* is set to be 10^{-4} herein), then return this initial value; otherwise go to the next step;

4. Checkpoint: if the $\beta_{sys} < 3.5$, increase the initial value by δ percent ($0.1 \leq \delta \leq 0.3$); if $\beta_{sys} > 3.5$, reduce the initial value by δ percent ($0.1 \leq \delta \leq 0.3$);

5. Repeat steps 2-4 until $E_{cs}(R)$ is found.

$E_{cs}(R)$ can usually be found within four loops. A flowchart for this algorithm combined with the MCS-based program is presented in Figure 2.12. It is seen that this algorithm is similar to the search algorithm that is combined with RELSYS; however, since the initial values in this algorithm are selected based on the conclusions from the effects of N on the redundancy factors, they are much closer to the final value of $E_{cs}(R)$ than those in the search algorithm; therefore, the number of trials is drastically reduced and, therefore, the computational time is decreased.

As stated previously, the coefficients of variation of resistance and load are 0.05 and 0.3, respectively. The mean value of load acting on each component $E(P)$ is assumed to be 10. Three correlation cases ($\rho(R_i,R_j) = 0$, 0.5 and 1.0) among the resistances of components and two probability distribution types (normal and lognormal) of the loads and resistances are investigated herein. Based on these parameters, the mean values of resistance associated with a single component for the normal and lognormal distribution are found to be $E_c(R) = 21.132$ and $E_c(R) = 27.194$,

respectively. By combining the MCS-based program with the simple algorithm, the redundancy factors of different types of N-component systems ($N = 100$, 300 and 500) are evaluated. The mean resistances of components and redundancy factors associated with the no correlation ($\rho(R_i,R_j) = 0$) and partial correlation ($\rho(R_i,R_j) = 0.5$) cases are presented in Table 2.4 and Table 2.5.

It is observed that in the no correlation and partial correlation cases (a) η_R of the series and $mp \times ns$ SP systems that have the same number of parallel components (i.e., m is the same in these SP systems) becomes larger as N increases; however, the contrary is observed in the parallel and $ms \times np$ SP systems which have the same number of series components (i.e., m is the same); and (b) the redundancy factors associated with the normal and lognormal distributions are very close; this indicates that the effect of distribution type on the redundancy factor is not significant.

In the perfect correlation case ($\rho(R_i,R_j) = 1.0$), $\eta_R = 1.0$ for different types of systems with different number of components associated with both normal and lognormal distributions. This was expected since for systems whose components are identical and perfectly correlated, the system can be reduced to a single component; therefore, the redundancy factors in the perfect correlation case do not change as the system type and number of components vary.

For the investigated systems associated with different correlation cases, the component reliability indices β_{cs} can be found after $E_{cs}(R)$ is obtained. Figure 2.13 illustrates the variations of the component reliability index and redundancy factor in the series and parallel systems due to the increase in the number of components. It is noticed that (a) as the number of components increases, the component reliability

increases in series systems, while it decreases in parallel systems; (b) for the series systems, the component reliability associated with the normal distribution is higher than that associated with the lognormal distribution in the no correlation and partial correlation cases; however, contrary conclusion is found in the parallel systems; (c) the effect of the probability distribution type of R and P on η_R is not significant, especially in the series systems; and (d) in the perfect correlation case, the component reliability index is equal to 3.5 and the redundancy factor equals 1.0.

2.5 REDUNDANCY FACTORS OF SYSTEMS CONSIDERING POST-FAILURE MATERIAL BEHAVIOR

The systems investigated in Sections 2.3 and 2.4 do not consider the post-failure behavior of components. However, this behavior of components affects the load redistribution in a damaged system and, consequently, it affects the system redundancy. Therefore, it is necessary to include the post-failure behavior of structural components in the evaluation of redundancy factors. The failure mode of a system accounting for post-failure material behavior of its components is determined not only by the system type but also by the failure sequence of components. Therefore, the step for identifying the failure modes and limit state equations is more complicated than that associated with the systems without considering the post-failure behavior. Several systems consisting of two, three, and four components are used in this section to illustrate the process of evaluating the redundancy factor of a system considering the post-failure behavior of its components.

2.5.1 Redundancy Factors of Ductile Systems

As mentioned previously, the first step in determining the redundancy factor in a system is to find the mean resistance of its component when the component reliability is prescribed as $\beta_c = 3.5$. Consider a single component whose resistance R and load P are modeled as normally distributed random variables. The coefficients of variation of resistance and load $V(R)$ and $V(P)$, and the mean value of load $E(P)$ are assumed to be 0.05, 0.3, and 10, respectively. Therefore, the mean resistance of component $E_c(R)$ is found to be 21.132.

For a system consisting of two ductile components which are identical with the single component just mentioned, two different systems can be formed: series and parallel. Since failure of the series system can be caused by failure of any component, the redundancy factor of series system is not affected by the post-failure behavior of the components. Therefore, the evaluation of redundancy factors in this section is mainly focused on the parallel and series-parallel systems.

For a two-component parallel system subject to load $2P$, the resistances of its ductile components are denoted as R_1 and R_2, respectively. Three correlation cases among the resistances of components are considered herein: (a) $\rho(R_1,R_2) = 0$, no correlation; (b) $\rho(R_1,R_2) = 0.5$, partial correlation; and (c) $\rho(R_1,R_2) = 1.0$, perfect correlation. The statistical parameters associated with R and P are the same as those associated with the single component mentioned previously. Since the failure modes of ductile systems are independent of the failure sequence of components, the limit state equation of the two-component parallel system is

$$g = R_1 + R_2 - 2P = 0 \tag{2.1}$$

By using the MCS-based method described in Section 2.4.2, the mean resistances $E_{cs}(R)$ of ductile components in the two-component parallel system associated with the three correlation cases are found to be 20.810, 20.950, and 21.132, respectively. The corresponding redundancy factors η_R are 0.985, 0.991, and 1.0, respectively. Consequently, the reliability indices of components in the ductile system β_{cs} associated with three correlation cases are 3.40, 3.45, and 3.50, respectively.

Next, the three- and four-component ductile parallel system and the $2p \times 2s$ ductile series-parallel system (see Figure 2.6(c)) are studied. The loads applied on these systems are $3P$, $4P$, and $2P$, respectively. The limit state equations of three- and four-component system, respectively, are

$$g = R_1 + R_2 + R_3 - 3P = 0 \tag{2.2}$$

$$g = R_1 + R_2 + R_3 + R_4 - 4P = 0 \tag{2.3}$$

where R_i (i=1,2,3,4) is the resistance of component i. The $2p \times 2s$ ductile series-parallel system has two failure modes and the associated limit state equations are

$$g_1 = R_1 + R_2 - 2P = 0 \tag{2.4}$$

$$g_2 = R_3 + R_4 - 2P = 0 \tag{2.5}$$

By performing the same procedure used in the two-parallel system, the mean resistances, redundancy factors, and reliability indices of components associated with three- and four-component parallel and series-parallel systems are presented in Table 2.6.

It is noticed from the results associated with two- to four-component systems that (a) as the number of components in the parallel system increases, the redundancy

factor and component reliability index decrease slightly in the no correlation and partial correlation cases; (b) increasing the correlation among the resistances of components leads to higher redundancy factor and component reliability index in the parallel system; and (c) compared with the four-component parallel system, the redundancy factor and component reliability index associated with the series-parallel system are higher in the no correlation and partial correlation cases.

2.5.2 Redundancy Factors of Brittle Systems

Contrary to ductile components, brittle components do not take loads after their fracture failure; therefore, the applied loads will distribute to other remaining components in brittle systems. Due to this property, different failure sequences lead to different load distributions and thus different failure modes in brittle systems. All the possible failure modes must be accounted for and the associated limit state equations need to be identified to determine the redundancy factors. The two-component parallel system described in Section 2.5.1 is used herein to demonstrate the procedure for calculating the redundancy factors of brittle systems.

Assuming both components are brittle, two different failure modes are anticipated and their respective limit state equations are given as

$$g_1 = R_1 - P = 0 \qquad\qquad g_3 = R_2 - 2P = 0 \qquad\qquad (2.6)$$

and

$$g_2 = R_2 - P = 0 \qquad\qquad g_4 = R_1 - 2P = 0 \qquad\qquad (2.7)$$

Assuming the same statistical parameters of the normally distributed resistances and load as those described in Section 2.5.1 (e.g., $V(R_i) = 0.05$; $V(P) = 0.3$), the mean

resistances of brittle components in the two-component parallel system associated with the three correlation cases are 21.585 if $\rho(R_i,R_j) = 0$; 21.481 if $\rho(R_i,R_j) = 0.5$; and 21.132 if $\rho(R_i,R_j) = 1.0$. Therefore, the associated redundancy factors are 1.021, 1.017, and 1.0, respectively.

Similarly, the failure modes of three-component parallel system can be identified, as shown in Figure 2.14. The limit state equations associated with all the failure modes are

$$g_1 = R_1 - P = 0 \qquad g_2 = R_2 - P = 0 \qquad g_3 = R_3 - P = 0 \qquad (2.8)$$

$$g_4 = R_2 - 1.5P = 0 \qquad g_5 = R_3 - 1.5P = 0 \qquad g_6 = R_1 - 1.5P = 0 \qquad (2.9)$$

$$g_7 = R_3 - 1.5P = 0 \qquad g_8 = R_1 - 1.5P = 0 \qquad g_9 = R_2 - 1.5P = 0 \qquad (2.10)$$

$$g_{10} = R_3 - 3P = 0 \qquad g_{11} = R_2 - 3P = 0 \qquad g_{12} = R_1 - 3P = 0 \qquad (2.11)$$

The redundancy factors of the three-component parallel system associated with three correlation cases when R and P follow normal distribution are found to be 1.033 if $\rho(R_i,R_j) = 0$; 1.026 if $\rho(R_i,R_j) = 0.5$; and 1.0 if $\rho(R_i,R_j) = 1.0$.

It is observed from the results related to the two- and three-component brittle systems that (a) the redundancy factor of the parallel system becomes smaller as the correlation among the resistances of components increases; and (b) in the no correlation and partial correlation cases, the redundancy factors associated with the two-component parallel system are less than those associated with the three-component parallel system.

2.5.3 Redundancy Factors of Mixed Systems

The systems investigated in Sections 2.5.1 and 2.5.2 consist of only ductile or brittle components. However, there are some cases where both types of material behavior are included in the system. One of the examples is the steel truss railway bridge in Kama River of Russia. Its superstructure consists of multi-span steel trusses while its substructure has many single column piers that are made of stones. Therefore, it is necessary to study the redundancy factors of systems having both ductile and brittle components (called "mixed systems"). Mixed systems consisting of two, three, and four components are used herein to investigate the redundancy factors.

For the two-component mixed parallel system, there is only one combination possible: one component is ductile and the other one is brittle (denoted as "1 ductile & 1 brittle"). As more components are included in the mixed system, the number of combinations increases. For the three-component parallel system, two mixed systems are considered: 1 ductile & 2 brittle, and 2 ductile & 1 brittle. Similarly, three mixed systems can be formed for four-component parallel system: 1 ductile & 3 brittle, 2 ductile & 2 brittle, and 3 ductile & 1 brittle. For the four-component $2p \times 2s$ series-parallel system, there are two combinations associated with the 2 ductile & 2 brittle case: (a) 2 ductile & 2 brittle Case A, where the two ductile components are located in the same sub-parallel system; and (b) 2 ductile & 2 brittle Case B, where the two ductile components locate in two sub-parallel systems, as shown in Figure 2.15. Therefore, four different mixed systems can be formed for the $2p \times 2s$ series-parallel system: 1 ductile & 3 brittle, 2 ductile & 2 brittle Case A, 2 ductile & 2 brittle Case B, and 3 ductile & 1 brittle.

Assuming the resistances of components and the loads are normally distributed random variables with the coefficients of variation 0.05 and 0.3, respectively, the mean resistances, redundancy factors, and reliability indices of components of the mixed systems associated with the no correlation and partial correlation cases are presented in Table 2.7 and Table 2.8, respectively. It is found that (a) the redundancy factors of the parallel systems are all at least 1.0 due to the existence of brittle component(s) in the systems; and (b) for the $2p \times 2s$ series-parallel system, the redundancy factors associated with the two cases in which the number of brittle components is two are the same; this means that the redundancy factor is not affected by the location of the brittle components in this series-parallel system. In the perfect correlation case ($\rho(R_i, R_j) = 1.0$), $\eta_R = 1.0$ and $\beta_{cs} = 3.5$ for all the mixed systems.

Figure 2.16 shows the effects of the number of brittle components in the parallel system on the redundancy factor. It is noticed that (a) as the number of brittle components in the parallel system increases, the redundancy factor becomes larger in the no correlation and partial correlation cases; and (b) as the correlation among the resistances of components increases, the redundancy factor increases in the ductile case but decreases in the mixed and brittle cases.

2.5.4 Effects of Post-failure Behavior Factor on the Redundancy Factor

The post-failure behavior factor δ of a material describes the percentage of remaining strength after failure. The value of δ varies from 0 (i.e., brittle) to 1 (i.e., ductile). The previous sections focus on the redundancy factors associated with only the two extreme post-failure behavior cases. However, in addition to the ductile and brittle

materials, there are some materials whose post-failure behavior factors are between 0 and 1. Therefore, it is necessary to study the redundancy factors associated with these intermediate post-failure behavior cases. In this section, parallel systems consisting of two to four components are used to investigate the effects of post-failure behavior factor on the redundancy factor.

The post-failure behavior factors of all components are assumed to be the same. The resistances and load associated with the components are considered as normally distributed variables with the coefficients of variation equal to 0.05 and 0.3, respectively. After identifying the failure modes of the parallel system and formulating the associated limit state equations, the redundancy factors of the two-, three-, and four-component parallel systems associated with different post-failure behavior factors are calculated using the MCS-based method. The results are plotted in Figure 2.17 and Figure 2.18.

It is noted that (a) as δ increases from 0 to 1 in the no correlation and partial correlation cases, η_R in the three systems firstly remains the same and then decreases dramatically; (b) as the correlation among the resistances of components becomes stronger, the region of δ during which η_R remains the same increases; (c) η_R is not affected by δ in the perfect correlation case; (d) the differences in the redundancy factors associated with the three systems are almost the same for $\delta < 0.6$ and become less significant with increasing δ above 0.6; and (e) the redundancy factors reach almost the same value when δ is close to 1.0 (i.e., ductile).

During the calculation of redundancy factor, the mean resistance of components ($E_{cs}(R)$) when the system reliability index is 3.5 is obtained. Substituting $E_{cs}(R)$ into

the component reliability analysis yields the reliability indices of components. Figure 2.19 and Figure 2.20 show the effects of the post-failure behavior factor on the component reliability index in the parallel systems associated with three correlation cases. Most of the conclusions drawn from these two figures are similar to those regarding redundancy factors obtained from Figure 2.17 and Figure 2.18. Moreover, it is seen that the reliability index of components when $\delta = 0$ (i.e., brittle) is greater than 3.5 while its value when $\delta = 1.0$ (i.e., ductile) is less than 3.5. This is because brittle systems are much less redundant than ductile systems and, therefore, a larger redundancy factor ($\eta_R > 1.0$) needs to be applied to penalize the brittle components by designing them conservatively ($\beta_{cs} > 3.5$); while in the ductile case, smaller redundancy factors ($\eta_R < 1.0$) can be used to achieve a more economical component design ($\beta_{cs} < 3.5$).

2.6 REDUNDANCY FACTORS OF DUCTILE AND BRITTLE SYSTEMS WITH MANY COMPONENTS

In Sections 2.5.1 and 2.5.2, redundancy factors are investigated with respect to the ductile and brittle systems having up to four components and it is found that η_R is affected by the number of components in the system. In most practical cases, structures are composed of dozens or hundreds of components. Therefore, it is necessary to evaluate the redundancy factors of ductile and brittle systems that consist of many components so that standard tables of redundancy factors can be generated to facilitate the component design process.

As stated previously, the redundancy factors of series systems are independent of the material behavior of its components; therefore, only the parallel and series-parallel systems are studied in this section. The redundancy factors associated with N-component series systems have been provided in Section 2.4. Based on the conclusion that the redundancy factor associated with a certain system is not affected by the mean value of the applied load, which was obtained in Section 2.3, the following assumption is made for the loads acting on the parallel and series-parallel systems: (a) for a N-component parallel system, the load it is subject to is $N \cdot P$, where P is the load applied to a single component which is used to calculate $E_c(R)$; (b) for a $mp \times ns$ series-parallel system that has n sub-parallel systems and each sub-parallel system consists of m components, the load acting on the system is $m \cdot P$; and (c) for a $ms \times np$ series-parallel system which has n sub-series systems and each sub-series system consists of m components, the load on it is $n \cdot P$. In this way, the load effect of each component in the intact parallel and series-parallel systems is P so that the obtained mean resistance $E_{cs}(R)$ can be compared with $E_c(R)$ to calculate the redundancy factor η_R.

2.6.1 Redundancy Factors of Ductile Systems with Many Components

A ductile component continues to carry its share of the load equal to its capacity after it fails. Therefore, for an N-component ductile parallel system, the load acting on an intact component j after m components in the system fail is $\dfrac{N \cdot P - \sum\limits_{i=1}^{m} R_i}{N - m}$. This value is not affected by the failure sequence of the m components. Since the failure modes of

ductile systems are independent of the failure sequence, the limit state equation of an

N-component parallel system can be written as

$$g = \sum_{i=1}^{N} R_i - N \cdot P = 0 \qquad (2.12)$$

For a $mp \times ns$ series-parallel system which has n possible failure modes, the limit state

equation associated with failure mode k is

$$g = \sum_{i=m(k-1)+1}^{m \cdot k} R_i - m \cdot P = 0 \qquad (2.13)$$

where $m(k-1)+1$ and $m \cdot k$ denote the first and last component in the k_{th} sub-parallel

system, respectively. For a $ms \times np$ series-parallel system, the number of its possible

failure modes is m^n. The limit state equation associated with one of the failure modes

can be written as

$$g = \sum_{i=k}^{k+n-1} R_i - n \cdot P = 0 \qquad (2.14)$$

where components k, $k+1$,…, $k+n$-1 locate in different sub-series systems.

With the identified the limit state equations of the N-component (N = 100, 300,

and 500) ductile parallel and series-parallel systems and the assumed coefficients of

variation of resistance and load equal to 0.05 and 0.3, respectively, the redundancy

factors associated with two probability distribution types (i.e., normal and lognormal)

and three correlation cases (i.e., $\rho(R_i,R_j)$ = 0; 0.5; and 1.0) when the system reliability

index is 3.5 are obtained using the MCS-based method. The redundancy factors for the

$ms \times np$ series-parallel systems are calculated only up to N = 25 because the number of

the failure modes for the $5s \times 10p$ series-parallel systems (N = 50) is 9765625, which

far exceeds the memory usage of the server (a Dell Precision R5500 rack workstation

equipped with two six cores X5675 Intel Xeon processors with 3.06 GHz clock speed and 24 GB DDR3 memory). Hence, the results of the $ms \times np$ series-parallel systems are not shown herein.

In the perfect correlation case ($\rho(R_i, R_j) = 1.0$), $\eta_R = 1.0$ and $\beta_{cs} = 3.5$ for different types of systems with different number of components for both normal and lognormal distributions. Table 2.9 and Table 2.10 present the redundancy factors associated with the correlation cases $\rho(R_i, R_j) = 0$ and 0.5, respectively, for the parallel and $mp \times ns$ series-parallel ($m = 5$, 10, and 20 herein) ductile systems along with the results of series systems to facilitate the comparison analysis. In these tables, $E_{c,N}(R) = 21.132$ and $E_{c,LN}(R) = 27.194$ denote the mean resistance of a single component with 3.5 reliability index when its R and P follow normal and lognormal distributions, respectively. These results are also plotted in Figure 2.21 which shows the effects of number of components on the redundancy factors of series and parallel ductile systems.

It is observed that (a) the effect of N on η_R in the parallel ductile system depends on the value of N: when N is small ($N \leq 5$), increasing N leads to lower η_R in the parallel system, and the change is less significant as the correlation among the resistances of component increases; however, when $N > 5$, η_R remains almost the same as N increases; (b) for the $mp \times ns$ series-parallel ductile systems that have the same number of parallel components (m is the same in these systems), η_R increases with N; (c) as the correlation among the resistances of components becomes stronger, η_R decreases and increases in the series and parallel system, respectively; and (d) in the series system, the redundancy factors associated with normal and lognormal distributions are very close; however, in the parallel system, the differences in the

redundancy factors associated with these two probability distribution cases are more significant.

The component reliability indices β_{cs} of the N-component ductile systems associated with the normal and lognormal cases are shown in Table 2.11. The results are also plotted in Figure 2.22 to directly display the effects of N on the component reliability index. It is found that (a) the effects of N and $\rho(R_i, R_j)$ on the reliability index of components are similar to those on the redundancy factor just discussed; and (b) in the series and parallel systems, the component reliability index associated with normal distribution is higher and lower than that associated with lognormal distribution, respectively.

2.6.2 Redundancy Factors of Brittle Systems with Many Components

As indicated previously, for the evaluation of redundancy factors of brittle systems, all the possible failure modes and associated limit state equations need to be identified and accounted for to perform a correct reliability analysis. The number of failure modes for an N-component parallel system is N factorial ($N!$). When N is small ($N \leq 4$), the approach described in the Section 2.5.2 for determining the failure modes and limit state equations can be used; however, when $N > 4$, the number of failure modes will exceed 120 and it becomes difficult and computationally expensive to consider all the failure modes and associated limit states. Therefore, an alternative approach that can be combined with MATLAB (Mathworks 2010) is introduced herein.

The number of limit state equations of the three-component parallel system is 12, as shown in Equations (2.8) to (2.11). It is noticed that some limit state equations can

be merged because they are actually the same (i.e., g_4 and g_9, g_5 and g_7, and g_6 and g_8).

After merging the identical ones, the limit state equations associated with the three-component parallel system are renumbered as follows:

$$g_1 = R_1 - P = 0 \qquad g_2 = R_2 - P = 0 \qquad g_3 = R_3 - P = 0 \qquad (2.15)$$

$$g_4 = R_1 - 1.5P = 0 \qquad g_5 = R_2 - 1.5P = 0 \qquad g_6 = R_3 - 1.5P = 0 \qquad (2.16)$$

$$g_7 = R_1 - 3P = 0 \qquad g_8 = R_2 - 3P = 0 \qquad g_9 = R_3 - 3P = 0 \qquad (2.17)$$

It is seen that the number of the limit state equations after merging is nine. Similarly, the four-component parallel system has 16 limit state equations after merging. Therefore, the number of the limit state equations associated with an N-component parallel system is N^2. The failure modes of the three-component parallel system with renumbered limit state equations are shown in Figure 2.23. It is observed that (a) g_1, g_2, and g_3 correspond to the cases where component 1, 2, and 3 fails first, respectively; (b) g_4, g_5, and g_6 correspond to the cases where component 1, 2, and 3 fails second, respectively; and (c) g_7, g_8, and g_9 correspond to the cases where component 1, 2, and 3 fails last, respectively. Therefore, for an N-component brittle parallel system, its limit state equations can be formulated as a matrix

$$G = \begin{bmatrix} g_1 & g_2 & \cdots & g_N \\ g_{N+1} & g_{N+2} & \cdots & g_{2N} \\ \cdots & \cdots & \cdots & \cdots \\ g_{N(N-1)+1} & g_{N(N-1)+2} & \cdots & g_{N^2} \end{bmatrix} \qquad (2.18)$$

The element $G(i, j)$ in this matrix denotes that the failure sequence of component j is i. The limit state equation associated with the element $G(i, j)$ in the matrix is

$$G(i, j) = R_j - \frac{N \cdot P}{N - i + 1} = 0 \qquad (2.19)$$

48

where $i, j = 1, 2, 3,...N$. For example, the coordinate of the limit state equation g_2 in the matrix is (1,2) (i.e., first row and second column); therefore, g_2 represents the case where component 2 fails first, and the associated limit state equation is $R_2 - P = 0$ (see Equation (2.15)). Similarly, $g_{N(N-1)+1}$ stands for the case in which component 1 fails last; when $N = 3$ (three-component system), $g_7 = G(3,1) = R_1 - 3P = 0$ (see Equation (2.17)).

After placing all the limit state equations into a matrix, the failure modes of the N-component parallel system can be easily obtained by selecting N elements that are in different rows and columns from the matrix and the set consisting of these selected N elements is one possible failure mode of the system. For example, the limit state equation matrix of the aforementioned three-component parallel system is

$$G = \begin{bmatrix} g_1 & g_2 & g_3 \\ g_4 & g_5 & g_6 \\ g_7 & g_8 & g_9 \end{bmatrix} \tag{2.20}$$

where g_i ($i=1,2,..,9$) are defined in Equations (2.15) to (2.17). According to the selection process indicated previously, six possible failure modes can be found from the matrix: (a) $g_1 \rightarrow g_5 \rightarrow g_9$; (b) $g_1 \rightarrow g_6 \rightarrow g_8$; (c) $g_2 \rightarrow g_4 \rightarrow g_9$; (d) $g_2 \rightarrow g_6 \rightarrow g_7$; (e) $g_3 \rightarrow g_4 \rightarrow g_8$; and (f) $g_3 \rightarrow g_5 \rightarrow g_7$. These are the same as the failure modes shown in Figure 2.23.

By using the limit state equation matrix G, the process of generating limit state equations associated with different failure sequences and identifying the failure modes can be achieved with MATLAB codes. The procedure for estimating the redundancy factor in brittle systems using this approach is summarized as follows:

(1) Determine the limit state equation of component j when it fails at the sequence i using Equation (2.19), where $i, j = 1,2,\ldots, N$;

(2) Form the limit state equation matrix G by defining g_k $(k = 1,2,\ldots,N^2)$ using the format shown in Equation (2.18);

(3) Identify all the combinations, each consisting of N elements located in different rows and columns of the matrix G; the obtained combinations are the failure modes of the system;

(4) Based on the obtained limit state equations and failure modes, and other statistical information associated with the resistances and load, the mean resistance of component when the system reliability index is prescribed (i.e., 3.5) can be determined;

(5) Calculate the redundancy factor.

This approach is used to compute the redundancy factor of the brittle parallel systems with up to eight components. However, the nine-component parallel system has 362880 different failure modes and the reliability analysis becomes very time consuming and in most servers (such as a Dell Precision R5500 rack workstation equipped with two six cores X5675 Intel Xeon processors with 3.06 GHz clock speed and 24 GB DDR3 memory) the memory usage is exceeded. Therefore, in order to calculate the redundancy factors of brittle parallel systems consisting of more than eight components, another method has to be introduced.

Consider the two-component brittle parallel system described in Section 2.5.2. It has two different failure modes and the associated limit state equations are shown in

Equations (2.6) and (2.7). Its system failure can be expressed in terms of components failure events as:

$$F_1 = [(g_1 < 0) \cap (g_3 < 0)] \cup [(g_2 < 0) \cap (g_4 < 0)] \tag{2.21}$$

Denoting the event $g_i < 0$ as D_i, the above equation can be rewritten as

$$F_1 = (D_1 \cap D_3) \cup (D_2 \cap D_4) \tag{2.22}$$

The probability of event F_1 is approximately equal to the probability of the following event F_2

$$F_2 = (D_1 \cup D_2) \cap (D_3 \cup D_4) = [(g_1 < 0) \cup (g_2 < 0)] \cap [(g_3 < 0) \cup (g_4 < 0)] \tag{2.23}$$

This is explained using Figure 2.24. The sample spaces generated by the events F_1 and F_2 are shown in Figure 2.24(a) and (b), respectively. It is seen that

$$F_2 = F_1 \cup A \cup B \tag{2.24}$$

where event A is $(R_1 > 2P) \cap (R_2 < P)$ and event B is $(R_2 > 2P) \cap (R_1 < P)$, as shown in the Figure 2.24(b). Since R_1 and R_2 have the same mean value and standard deviation, the probabilities of occurrence of events A and B are very small and can be neglected. Therefore, the event F_2 in Equation (2.24) can be used to find the failure probability of the two-component brittle parallel system. Extending this conclusion to the N-component brittle parallel system yields the system failure event as follows

$$F = [(g_1 < 0) \cup (g_2 < 0) \cup ... \cup (g_N < 0)] \cap [(g_{N+1} < 0) \cup (g_{N+2} < 0) \cup ... \cup (g_{2N} < 0)] \cap ...$$
$$\cap [(g_{N(N-1)+1} < 0) \cup (g_{N(N-1)+2} < 0) \cup ... \cup (g_{N^2} < 0)]$$

$$\tag{2.25}$$

where $g_1, g_2, ..., g_{N^2}$ are the performance functions listed in Equation (2.18). Therefore, by simplifying the system model from an $N! \times N$ series-parallel system to an $N \times N$

series-parallel system, the redundancy factors can be computed for brittle parallel systems having a large number of components.

It should be noted that this approach for estimating the failure probability of the brittle parallel system with many components is based on the assumption that the resistances of components in the system are the same. With this assumption, the limit state equations can be merged to form the limit state equation matrix for the failure modes identification and failure probability estimation. In most practical cases, the components in parallel positions are usually designed to have the same (or very similar) dimensions (e.g., pier columns, beam girders). Therefore, if the material of the components is brittle, the system failure probability can be approximately evaluated using this approach.

With the coefficients of variation of resistances and load being 0.05 and 0.3, respectively, the redundancy factors associated with two probability distribution types (i.e., normal and lognormal) and three correlation cases (i.e., $\rho(R_i,R_j) = 0$; 0.5; and 1.0) are calculated with respect to the N-component (N = 10, 20, 25 and 50) parallel and series-parallel brittle systems. Similar to the ductile systems, the redundancy factors associated with the perfect correlation case (i.e., $\rho(R_i,R_j) = 1.0$) in the brittle systems are also 1.0. The redundancy factors associated with the other two correlation cases are shown in Table 2.12 and Table 2.13. Figure 2.25 plots the effects of number of components on the redundancy factors in brittle systems.

It is noted that (a) the redundancy factors η_R of the brittle parallel systems are all greater than 1.0, which implies that the brittle components have to be designed conservatively ($\beta_{cs} > 3.5$) even in the parallel systems; (b) when the number of brittle

52

components are fixed, η_R associated with series, parallel, and series-parallel systems are the same; this indicates that for a N-component brittle structure, η_R is independent of the system type; (c) as the number of components in the brittle system increases, η_R associated with all types of systems become larger; (d) η_R of all types of systems decreases when the correlation among the resistances of components becomes stronger; (e) in the no correlation case, η_R associated with the lognormal distribution case is higher than that associated with the normal distribution case; and (f) in the partial correlation case, η_R associated with normal and lognormal distributions are almost the same.

It should be noted that although the redundancy factors of the N-component series and parallel systems in brittle case are identical, the designs of components (i.e., the mean resistances) in the two systems are not the same. This is because the loads applied on the series and parallel systems are different when calculating the redundancy factors. The mean resistances of the N-component series and parallel systems listed in the tables are computed with respect to the loads P and $N \cdot P$, respectively. Therefore, when the load is fixed, the mean resistance associated with the brittle parallel system is lower than that associated with the series system, which clearly indicates that the parallel system is more economical than the series system.

The component reliability indices of the N-component brittle systems when the system reliability indices are 3.5 are presented in Table 2.14 and Figure 2.26. It is observed that (a) for the brittle systems, increasing the number of components leads to higher reliability indices of components in both series and parallel systems; (b) in the no correlation and partial correlation cases, the reliability indices of components

associated with the normal distribution are higher than those associated with the lognormal distribution; and (c) as the correlation among the resistances of components increases, the component reliability indices in both series and parallel systems decrease.

2.7 LIMIT STATES FOR COMPONENT DESIGN

In the AASHTO bridge design specifications (AASHTO 2010), each component and connection shall satisfy the following equation for each limit state during the design:

$$\sum \eta_i \gamma_i Q_i \leq \phi R_n = R_r \tag{2.26}$$

where γ_i = load factor, Q_i = force effect, ϕ = resistance factor, R_n = nominal resistance, R_r = factored resistance, and η_i = load modifier relating to ductility, redundancy, and operational classification, given as

$$\eta_i = \eta_D \eta_R \eta_l \tag{2.27}$$

where η_D = factor relating to ductility, η_R = factor relating to redundancy, and η_l = factor relating to operational classification. Therefore, Equation (2.26) can be rewritten as follows

$$\sum \eta_D \eta_R \eta_l \gamma_i Q_i \leq \phi R_n = R_r \tag{2.28}$$

As stated previously, η_R is considered on the load effect side in the above limit state equation and its value is determined based on a very general classification of redundancy levels: (a) $\eta_R \geq 1.05$ for nonredundant members; (b) $\eta_R = 1.00$ for conventional level of redundancy; and (c) $\eta_R \geq 0.95$ for exceptional levels of

redundancy (AASHTO 2010). However, in this chapter, the proposed redundancy factor, which is also denoted as η_R, is more specifically investigated for different system modeling types, different correlation cases among the resistances of components, and different number of components in the system.

The procedure for applying this redundancy factor in component design consists of two steps: (1) calculating the resistance $R_r^{'}$

$$\phi R_n^{'} = R_r^{'} \geq \sum \eta_D \eta_l \gamma_i Q_i \tag{2.29}$$

Equation (2.29) doesn't consider the factor relating to redundancy on the load effect side; therefore, the effect of redundancy is not reflected in the resistance $R_r^{'}$; and (2) applying the redundancy factor η_R to the resistance $R_r^{'}$ to obtain the final factored resistance R_r, as:

$$R_r = \eta_R R_r^{'} \tag{2.30}$$

This procedure is demonstrated in the numerical example in the following section.

By substituting Equation (2.30) into Equation (2.29), Equation (2.29) can be rewritten as follows:

$$\sum \eta_D \eta_l \gamma_i Q_i \leq \phi R_n^{'} = R_r^{'} = \frac{R_r}{\eta_R} \tag{2.31}$$

Multiplying both sides of Equation (2.31) by η_R yields

$$\sum \eta_D \eta_R \eta_l \gamma_i Q_i \leq \phi \eta_R R_n^{'} = \eta_R R_r^{'} = R_r \tag{2.32}$$

where $\eta_R R_n^{'} = R_n$ and $\eta_R R_r^{'} = R_r$. It is seen that Equation (2.32) is actually the same as Equation (2.28) which is the limit state equation used in the current AASHTO

specifications. The only difference is that the value of η_R in Equation (2.32) is based on a more detailed classification (i.e., considering the effects of system modeling type, correlation among components resistances, and number of components, among others) than that used in Equation (2.28). Therefore, if the redundancy factor η_R is considered from the load side, Equation (2.32) is used as the limit state equation for component design; however, if the redundancy factor η_R is taken into account from the resistance side, the limit state equation becomes

$$\sum \eta_D \eta_l \gamma_i Q_i \leq \phi \phi_R R_n = \phi_R R_r \qquad (2.33)$$

where ϕ_R = redundancy modifier given by

$$\phi_R = \frac{1}{\eta_R} \qquad (2.34)$$

2.8 CASE STUDY: A BRIDGE EXAMPLE

A bridge example is presented herein to demonstrate the application of the proposed redundancy factor. The span length of the simply supported bridge is 20 m. The deck consists of 18 cm of reinforced concrete and 8 cm surface layer of asphalt. The roadway width is 8.2 m with 0.2 m wide railing on each side. The space between two adjacent railing columns is 3 m; therefore, there are 7 railing columns on each side of the bridge. The slab is supported by four I-beam steel girders as shown Figure 2.27. Assuming the same dimensions of the steel girders, the goal of the design is to determine the bending resistance of the girders using the proposed redundancy factors.

The total bending moment acting on each girder consists of the moments due to both dead and live loads. The maximum bending moment occurs at the mid-span cross-section of the girder. Therefore, the moment capacity at mid-span cross-section governs during the design and the limit state equation for flexure failure of the girder i at the mid-span cross-section is:

$$g_i = M_{U,i} - M_{L,i} = 0 \tag{2.35}$$

where $M_{U,i}$ and $M_{L,i}$ = ultimate moment capacity and total bending moments acting on girder i, respectively. The next step is to estimate the load effects on each girder due to dead and live loads.

2.8.1 Live Load Bending Moments

According to AASHTO (2010), vehicular live loading on the roadways of bridges, designated HL-93, shall consist of the design truck or design tandem and the design lane load. In this example, a combination of the design truck and lane load is used. Based on the influence line for the bending moment at the mid-span cross-section, the most unfavorable longitudinal loading position associated with the design truck is determined, as shown in Figure 2.28. In addition, the bridge is subject to the lane load of 9.34 kN/m that is uniformly distributed along the bridge. The loadings shown in Figure 2.28 correspond to the case in which only one lane is loaded; therefore, the maximum bending moment at the mid-span cross-section when both lanes are loaded is $M_{LL}' = 3379$ kN·m.

In order to find the live load bending moment distributed to each girder, lever rule is used herein to obtain the lateral load distribution factors of the girders. For the exterior and interior girders, the transverse placements of truck wheels are shown in Figure 2.29(a) and (b), respectively. Since only one lane is loaded for exterior girders, the multiple presence factor is 1.2 and, thus, the associated lateral load distribution factors are found to be $q_{ext} = 0.81$. However, for interior girders, the multiple presence factor is 1.0 because both lanes are loaded; therefore, the lateral load distribution factor is $q_{int} = 0.81$. With the maximum bending moment at mid-span cross-section and the lateral load distribution factors of each girder, the maximum bending moments acting on exterior and interior girders due to live load are: $M_{LL,ext} = M_{LL,int} = 2736$ kN·m. Since the lateral load distribution factors of exterior and interior girders are identical, the obtained maximum live load bending moments of exterior and interior girders are the same.

2.8.2 Dead Load Bending Moments

The dead load herein refers to the self-weight of the superstructure. For exterior girders, the dead load consists of the weights of the slab, asphalt pavement, railings, and steel girder; however, for interior girders, the self-weight of the railings is not included since it is generally taken by the exterior girders. Therefore, only the weights of the slab, asphalt pavement, and steel girders are considered. Assuming the weights of the slab and asphalt pavement between the exterior and interior girders are uniformly distributed, the weights of slab and asphalt pavement distributed on exterior and interior girder are $w_{s,ext} = 7.99$ kN/m (slab, exterior girder), $w_{s,int} = 9.5$ kN/m (slab,

interior girder), $w_{a,ext} = 3.0$ kN/m (asphalt pavement, exterior girder), and $w_{a,int} = 4.0$ kN/m (asphalt pavement, interior girder), respectively. The uniform railing weight on the exterior girder is $w_{r,ext} = 0.44$ kN/m. The self-weight of each girder is assumed to be $w_{g,i} = 1.96$ kN/m. With all the uniform loads obtained previously, the total distributed dead loads for the exterior and interior girder are $w_{ext} = 13.41$ kN/m and $w_{int} = 15.46$ kN/m, respectively. Therefore, the dead load bending moments acting on the exterior and interior girders at the mid-span cross-section are: $M_{DL,ext} = 671$ kN·m and $M_{DL,int} = 773$ kN·m.

2.8.3 Mean Resistance of Girders

Based on the live load and dead load bending moments obtained previously, the total bending moment is found to be $M_{L,ext} = 3407$ kN·m (for exterior girder) and $M_{L,int} = 3509$ kN·m (for interior girder). Assuming that the resistance and load effect in Equation (2.35) are normally distributed random variables, the total bending moments associated with exterior and interior girders just mentioned are used herein as the mean value of the load effects acting on girders. The coefficients of variation of girder resistance and load effect are assumed to be 0.05 and 0.3, respectively. Therefore, the mean resistances for exterior and interior girders when the reliability index of each girder is 3.5 are found to be $E_c(M_{U,ext}) = 7200$ kN·m (for exterior girder) and $E_c(M_{U,int}) = 7415$ kN·m (for interior girder), respectively.

For the analyzed bridge, three types of systems are studied herein based on three different definitions of system failure: (a) the system fails if any girder fails (series system); (b) the system fails only if all girders fail (parallel system); and (c) the system fails if any two adjacent girders fail (series-parallel system), as shown in Figure 2.30. In addition, three correlation cases among the resistances of girders are investigated herein: (a) $\rho(R_i,R_j)=0$; (b) $\rho(R_i,R_j)=0.5$; and (c) $\rho(R_i,R_j)=1.0$.

By using the idealized systems consisting of identical components, the redundancy factors of the three systems associated with the three correlation cases are calculated, as shown in Table 2.15. Multiplying the mean resistances of girders obtained previously by the redundancy factors yields the designed mean resistances of girders in series, parallel, and series-parallel systems, as listed in Table 2.16. Since the dimensions of the girders are assumed to be the same, as previously mentioned, the larger bending moment between the exterior and interior girders is selected as the final mean resistance of girder $E_{cs}(M_U)$, as shown in the last column of Table 2.16. It is seen that the final design resistance of girder is the same as that of the interior girder because the total load effect acting on interior girder is larger than that on exterior girder.

The corresponding component reliability indices of exterior (β_{ext}) and interior (β_{int}) girders and the associated system reliability indices (β_{sys}) of the three systems are presented in Table 2.17. It is observed that the system reliability indices in all correlation cases are no less than 3.5. Therefore, they satisfy the predefined reliability level $\beta_{sys,target}=3.5$. For the no correlation and partial correlation cases, the component reliability indices (β_{ext} and β_{int}) associated with series system are much higher than

those associated with other systems while their counterparts associated with parallel system are much lower. This reflects the effect of system type on the design of structural components.

When computing the redundancy factors presented in Table 2.15 associated with series-parallel system, different correlations among the resistances of six components are considered: $\rho(R_i,R_j)$= 0, 0.5, and 1.0 (i, j=1, 2, 3,…,6). However, it should be noted that in Figure 2.30(c), components 2 and 3 refer to the same girder (Girder 2) and Girder 3 also represents both components 4 and 5, which indicates that components 2, 3 and components 4, 5 are perfectly correlated. Hence, the series-parallel system actually consists of four components instead of six components. In order to distinguish these two cases, the system considering the perfect correlation between components 2, 3 and components 4, 5 is named "4-component series-parallel system" while the system that doesn't take perfect correlation into account is called "6-component series-parallel system". Therefore, for the no correlation and partial correlation cases, the redundancy factors in Table 2.15 associated with the 6-component series-parallel system are slightly higher than the redundancy factors associated with the 4-component series-parallel system.

By taking the perfect correlation between components 2, 3 and components 4, 5 into account, the redundancy factors associated with the 4-component series-parallel system are found to be 0.983 (no correlation case) and 0.991 (partial correlation case), and 1.0 (perfect correlation case). The designed mean resistances of girders and the associated reliability indices of girders and system based on these redundancy factors are listed in Table 2.18 and Table 2.19, respectively.

It is observed that the final mean resistance $E_{cs}(M_U)$ and the system reliability index β_{sys} without considering perfect correlation (Table 2.16 and Table 2.17) are slightly higher than those considering perfect correlation (Table 2.18 and Table 2.19); this indicates that the design based on the 6-component series-parallel system is safer than that based on the 4-component series-parallel system. Therefore, the redundancy factors from the regular idealized system that doesn't consider the perfect correlation among some components can be used as a good approximation of the true redundancy factors associated with the series-parallel system to determine the designed mean resistance of girders. This finding shows the necessity of generating standard tables using the regular idealized systems for different number of components, different system models, and different correlations. After these standard tables are generated, the redundancy factor corresponding to a specific system can be found from these tables and then directly used in the design.

2.8.4 An Additional Case: Target System Reliability is 4.0

The previous results are associated with the case in which the target system reliability index is 3.5. However, if the analyzed bridge is classified as a critical or essential bridge (i.e., it is part of a very important highway system), its designed reliability index is expected to be higher. Therefore, an additional case in which the target system reliability index is 4.0 is investigated. The redundancy factor herein is defined as the ratio of the mean resistance of a component in a system when the system reliability index is 4.0 to the mean resistance of the same component when its reliability index is 3.5.

62

By performing the same procedure as in the previous $\beta_{sys,target} = 3.5$ case, the redundancy factors associated with three different systems are obtained using the idealized systems, as shown in Table 2.20. Correspondingly, the designed mean resistances of girders and the associated component and system reliability indices are calculated (see Table 2.21 and Table 2.22, respectively). It is found from these tables that (a) the redundancy factors in this case are all greater than those in the previous $\beta_{sys,target} = 3.5$ case; this is because the target system reliability index herein is higher; (b) all the redundancy factors are greater than 1.0; therefore, all the component reliability indices are larger than 3.5 (even in the parallel system when $\rho(R_i,R_j)=0$); this is different from the finding in the previous $\beta_{sys,target} = 3.5$ case; (c) the final mean resistance of girders is still governed by the interior girder; hence, the reliability indices of exterior girders are larger than those of interior girders; and (d) the system reliability indices of all the systems meet the predefined system reliability level $\beta_{sys,target} = 4.0$.

Similar to the previous $\beta_{sys,target} = 3.5$ case, the redundancy factors associated with the 4-component series-parallel system that considers the perfect correlation between components 2, 3 and 4, 5 are also calculated: 1.058 (no correlation case), 1.070 (partial correlation case), and 1.081 (perfect correlation case). The associated designed mean resistances of girders and the reliability indices of girders and the system for this $\beta_{sys,target} = 4.0$ case are listed in Table 2.23 and Table 2.24, respectively. Comparing the results in Table 2.21 to Table 2.24, it is observed that the results with / without considering the perfect correlation among some components are very close and the

designed mean resistances of girders based on the 6-component system (without considering the perfect correlation) are slightly conservative.

2.9 CONCLUSIONS

In this chapter, a redundancy factor is proposed to provide a rational system reliability-based design of structural components. By using idealized systems consisting of identical components, the effects of the system type, correlations among the resistances of components, number of components in a system, coefficients of variation of load and resistances, and mean value of the load on the redundancy factor are investigated. For a representative case, the redundancy factors of N-component systems without considering the post-failure material behavior are evaluated with respect to different correlation cases and system types.

Next, systems consisting of two to four components are used to demonstrate the procedure for evaluating the redundancy factors of ductile, brittle, and mixed systems. The effects of number of brittle components in a system and post-failure behavior factor on the redundancy factor are also studied using these systems. Then, the redundancy factors of N-component ductile and brittle systems with large number of components are calculated for the aforementioned representative case. Two types of limit states in which system redundancy is taken into account from the load and resistance side, respectively, are provided. Finally, a bridge example is presented to demonstrate the application of the redundancy factor. The following conclusions are drawn:

1. The redundancy factor η_R proposed in this chapter and the factor relating to redundancy in the AASHTO bridge design specifications are of the same nature. The major difference is that the factor relating to redundancy in the AASHTO specifications is determined based on a general classification of redundancy levels while the proposed redundancy factor η_R in this chapter is more rational since it is based on a comprehensive system reliability-based approach considering several parameters including the system type, correlation among the resistances of components, number of components in the system, and post-failure material behavior of components.

2. An approach for simplifying the system model in the redundancy factor analysis of brittle systems is proposed. By reducing the $N! \times N$ series-parallel system model to the $N \times N$ series-parallel system model, this approach makes it possible to calculate the redundancy factor of brittle parallel systems with large number of components.

3. For the systems without considering the post-failure material behavior, (a) increasing the coefficient of variation of resistance leads to higher redundancy factors in series systems but lower redundancy factors in parallel systems; (b) as the coefficient of variation of load increases, the redundancy factors associated with both series and parallel systems increase; (c) the mean value of load has no effect on the redundancy factors; and (d) the effect of N on the redundancy factors in $mp \times ns$ series-parallel systems having the same number of parallel components (i.e., m is same in these systems) is similar to that in the series system; while the effect of N on the redundancy factors in $ms \times np$ series-parallel systems having the

same number of series components (i.e., *m* is same) is similar to that in the parallel system.

4. In the ductile case, (a) the difference in the redundancy factors between the normal and lognormal distributions is significant in the parallel system; and (b) when the number of components in the parallel system is small, increasing *N* leads to a significant decrease of the redundancy factor; however, as *N* continues increasing this decrease becomes insignificant.

5. In the brittle case, the redundancy factors associated with series, parallel, and series-parallel systems are almost the same; this indicates that for an *N*-component brittle structure, the redundancy factor is independent of the system type.

6. In the mixed case, the redundancy factors are at least 1.0 due to the existence of brittle component(s) in the systems. As the number of brittle components increases in an *N*-component mixed system, the redundancy factor becomes larger and closer to the redundancy factor associated with the brittle case. Increasing the correlation among the resistances of components leads to a lower redundancy factor in the mixed parallel systems.

7. This chapter is for codification purpose. The proposed approach can be used to calculate the redundancy factors for a wide range of systems with different number of components, different system types, and different correlation cases.

8. This chapter presents standard tables of redundancy factors associated with a representative $V(R)$ and $V(P)$ case. Further effort is necessary to generate standard tables with respect to different combinations of $V(R)$ and $V(P)$. When this

information becomes available, the redundancy factors corresponding to a specific

system will be determined from these tables and then directly used in the design.

Table 2.1 $E_{cs}(R)$, η_R and β_{cs} of three-component systems when R and P follow normal distribution.

System type / Correlation	Series system $E_{cs}(R)$; η_R; β_{cs}	Parallel system $E_{cs}(R)$; η_R; β_{cs}
$\rho(R_i, R_j) = 0$	17.685; 1.049; 3.78	13.684; 0.812; 2.17
$\rho(R_i, R_j) = 0.5$	17.651; 1.047; 3.77	14.817; 0.879; 2.69
$\rho(R_i, R_j) = 1$	16.861; 1.000; 3.50	16.861; 1.000; 3.50

Note: $E(P) = 10$; $V(P) = 0.1$; $V(R) = 0.1$; $\beta_c = 3.5$; $\beta_{sys} = 3.5$; $E_{c,N}(R) = 16.861$.

Table 2.2 $E_{cs}(R)$, η_R and β_{cs} of three-component systems when R and P follow lognormal distribution.

System type Correlation	Series system $E_{cs}(R)$; η_R ; β_{cs}	Parallel system $E_{cs}(R)$; η_R ; β_{cs}
$\rho(R_i,R_j) = 0$	17.045; 1.040; 3.78	14.092; 0.860; 2.43
$\rho(R_i,R_j) = 0.5$	16.985; 1.037; 3.76	14.969; 0.914; 2.86
$\rho(R_i,R_j) = 1$	16.384; 1.000; 3.50	16.384; 1.000; 3.50

Note: $E(P) = 10$; $V(P) = 0.1$; $V(R) = 0.1$; $\beta_c = 3.5$; $\beta_{sys} = 3.5$; $E_{c,LN}(R) = 16.384$.

Table 2.3 $E_{cs}(R)$ and η_R of N-component systems using RELSYS when R and P follow normal distribution.

System		$E_{cs}(R)$	η_R
100-component system	Series system	24.185	1.144
	$5p \times 20s$ SP system	20.655	0.977
	$10p \times 10s$ SP system	19.618	0.928
	$20p \times 5s$ SP system	18.853	0.892
200-component system	Series system	24.723	1.17
	$5p \times 40s$ SP system	21.019	0.995
	$10p \times 20s$ SP system	19.915	0.942
	$20p \times 10s$ SP system	19.069	0.902

Note: $E(P) = 10$; $V(P) = 0.3$; $V(R) = 0.05$; $\rho(R_i, R_j) = 0$; $\beta_c = 3.5$; $\beta_{sys} = 3.5$; $E_{c,N}(R) = 21.132$.

Table 2.4 $E_{cs}(R)$ and η_R of different systems associated with the case $\rho(R_i,R_j) = 0$ using the MCS-based program.

System		Normal distribution		Lognormal distribution	
		$E_{cs}(R)$	η_R	$E_{cs}(R)$	η_R
100-component system	Series system	23.631	1.118	30.470	1.120
	Parallel system	18.306	0.866	23.695	0.871
	$5p \times 20s$ SP system	20.551	0.972	26.831	0.986
	$10p \times 10s$ SP system	19.846	0.939	25.874	0.951
	$20p \times 5s$ SP system	19.293	0.913	25.147	0.925
	$5s \times 20p$ SP system	20.550	0.972	26.825	0.986
	$10s \times 10p$ SP system	21.300	1.008	27.790	1.022
	$20s \times 5p$ SP system	21.980	1.040	28.643	1.053
300-component system	Series system	24.110	1.141	31.024	1.141
	Parallel system	17.970	0.850	23.249	0.855
	$5p \times 60s$ SP system	20.810	0.985	27.147	0.998
	$10p \times 30s$ SP system	20.059	0.949	26.213	0.964
	$20p \times 15s$ SP system	19.495	0.923	25.413	0.934
	$5s \times 60p$ SP system	20.279	0.960	26.460	0.973
	$10s \times 30p$ SP system	21.010	0.994	27.450	1.009
	$20s \times 15p$ SP system	21.680	1.026	28.254	1.039
500-component system	Series system	24.315	1.151	31.242	1.149
	Parallel system	17.843	0.844	23.058	0.848
	$5p \times 100s$ SP system	20.905	0.989	27.283	1.003
	$10p \times 50s$ SP system	20.151	0.954	26.290	0.967
	$20p \times 25s$ SP system	19.570	0.926	25.538	0.939
	$5s \times 100p$ SP system	20.160	0.954	26.330	0.968
	$10s \times 50p$ SP system	20.887	0.988	27.290	1.004
	$20s \times 25p$ SP system	21.565	1.020	28.092	1.033

Note: $E(P) = 10$; $V(P) = 0.3$; $V(R) = 0.05$; $\beta_c = 3.5$; $\beta_{sys} = 3.5$; $E_{c,N}(R) = 21.132$; $E_{c,LN}(R) = 27.194$.

Table 2.5 $E_{cs}(R)$ and η_R of different systems associated with the case $\rho(R_i,R_j) = 0.5$ using the MCS-based program.

System		Normal distribution		Lognormal distribution	
		$E_{cs}(R)$	η_R	$E_{cs}(R)$	η_R
100-component system	Series system	23.005	1.089	29.537	1.086
	Parallel system	19.124	0.905	24.748	0.910
	5p×20s SP system	20.840	0.986	27.038	0.994
	10p×10s SP system	20.305	0.961	26.344	0.969
	20p×5s SP system	19.890	0.941	25.784	0.948
	5s×20p SP system	20.840	0.986	27.000	0.993
	10s×10p SP system	21.385	1.012	27.690	1.018
	20s×5p SP system	21.880	1.035	28.247	1.039
300-component system	Series system	23.310	1.103	29.912	1.100
	Parallel system	18.861	0.893	24.414	0.898
	5p×60s SP system	21.025	0.995	27.255	1.002
	10p×30s SP system	20.477	0.969	26.553	0.976
	20p×15s SP system	20.050	0.949	26.020	0.957
	5s×60p SP system	20.635	0.976	26.770	0.984
	10s×30p SP system	21.182	1.002	27.474	1.010
	20s×15p SP system	21.669	1.025	28.010	1.030
500-component system	Series system	23.458	1.110	30.068	1.106
	Parallel system	18.780	0.889	24.265	0.892
	5p×100s SP system	21.110	0.999	27.335	1.005
	10p×50s SP system	20.546	0.972	26.630	0.979
	20p×25s SP system	20.115	0.952	26.119	0.960
	5s×100p SP system	20.555	0.973	26.624	0.979
	10s×50p SP system	21.110	0.999	27.373	1.007
	20s×25p SP system	21.584	1.021	27.874	1.025

Note: $E(P) = 10$; $V(P) = 0.3$; $V(R) = 0.05$; $\beta_c = 3.5$; $\beta_{sys} = 3.5$; $E_{c,N}(R) = 21.132$; $E_{c,LN}(R) = 27.194$.

Table 2.6 $E_{cs}(R)$, η_R, and β_{cs} of three- and four-component ductile systems associated with normal distribution.

Correlation	Three-component parallel system $E_{cs}(R);\ \eta_R\ ;\beta_{cs}$	Four-component parallel system $E_{cs}(R);\ \eta_R\ ;\beta_{cs}$	Four-component $2p{\times}2s$ series-parallel system $E_{cs}(R);\ \eta_R\ ;\beta_{cs}$
$\rho(R_i,R_j) = 0$	20.699; 0.980; 3.37	20.660; 0.978; 3.36	21.160; 1.001; 3.51
$\rho(R_i,R_j) = 0.5$	20.910; 0.989; 3.44	20.893; 0.989; 3.43	21.231; 1.005; 3.53
$\rho(R_i,R_j) = 1$	21.132; 1.000; 3.50	21.132; 1.000; 3.50	21.132; 1.000; 3.50

Note: $V(R) = 0.05$; $V(P) = 0.3$; $\beta_c = 3.5$; $\beta_{sys} = 3.5$; $E_c(R) = 21.132$

Table 2.7 $E_{cs}(R)$, η_R, and β_{cs} of mixed systems associated with the case $\rho(R_i,R_j) = 0$ when R and P are normal distributed.

System		$E_{cs}(R)$	η_R	β_{cs}
2-component parallel system	1 ductile & 1 brittle	21.280	1.007	3.55
3-component parallel system	1 ductile & 2 brittle	21.630	1.024	3.65
	2 ductile & 1 brittle	21.300	1.008	3.55
4-component parallel system	1 ductile & 3 brittle	21.850	1.034	3.71
	2 ductile & 2 brittle	21.640	1.024	3.65
	3 ductile & 1 brittle	21.319	1.009	3.56
4-component series-parallel system ($2p \times 2s$ SP system)	1 ductile & 3 brittle	21.850	1.034	3.71
	2 ductile & 2 brittle Case A	21.680	1.026	3.66
	2 ductile & 2 brittle Case B	21.680	1.026	3.66
	3 ductile & 1 brittle	21.440	1.015	3.59

Note: $V(P) = 0.3$; $V(R) = 0.05$; $\beta_c = 3.5$; $\beta_{sys} = 3.5$; $E_c(R) = 21.132$.

Table 2.8 $E_{cs}(R)$, η_R, and β_{cs} of mixed systems associated with the case $\rho(R_i,R_j) = 0.5$ when R and P are normal distributed.

System		$E_{cs}(R)$	η_R	β_{cs}
2-component parallel system	1 ductile & 1 brittle	21.260	1.006	3.53
3-component parallel system	1 ductile & 2 brittle	21.530	1.019	3.62
	2 ductile & 1 brittle	21.290	1.007	3.55
4-component parallel system	1 ductile & 3 brittle	21.700	1.027	3.67
	2 ductile & 2 brittle	21.550	1.020	3.62
	3 ductile & 1 brittle	21.318	1.009	3.55
4-component series-parallel system ($2p \times 2s$ SP system)	1 ductile & 3 brittle	21.700	1.027	3.67
	2 ductile & 2 brittle Case A	21.585	1.021	3.63
	2 ductile & 2 brittle Case B	21.585	1.021	3.63
	3 ductile & 1 brittle	21.420	1.014	3.59

Note: $V(P) = 0.3$; $V(R) = 0.05$; $\beta_c = 3.5$; $\beta_{sys} = 3.5$; $E_c(R) = 21.132$.

75

Table 2.9 $E_{cs}(R)$ and η_R of ductile systems associated with the case $\rho(R_i,R_j) = 0$.

System		Normal distribution		Lognormal distribution	
		$E_{cs}(R)$	η_R	$E_{cs}(R)$	η_R
100-component system	Series system	23.626	1.118	30.457	1.120
	Parallel system	20.519	0.971	26.759	0.984
	$5p \times 20s$ SP system	21.428	1.014	27.928	1.027
	$10p \times 10s$ SP system	21.026	0.995	27.439	1.009
	$20p \times 5s$ SP system	20.794	0.984	27.085	0.996
300-component system	Series system	24.112	1.141	31.028	1.141
	Parallel system	20.498	0.970	26.759	0.984
	$5p \times 60s$ SP system	21.639	1.024	28.227	1.038
	$10p \times 30s$ SP system	21.195	1.003	27.656	1.017
	$20p \times 15s$ SP system	20.921	0.990	27.303	1.004
500-component system	Series system	24.323	1.151	31.246	1.149
	Parallel system	20.498	0.970	26.759	0.984
	$5p \times 100s$ SP system	21.745	1.029	28.309	1.041
	$10p \times 50s$ SP system	21.280	1.007	27.738	1.020
	$20p \times 25s$ SP system	20.963	0.992	27.357	1.006

Note: $E(P) = 10$; $V(P) = 0.3$; $V(R) = 0.05$; $\beta_c = 3.5$; $\beta_{sys} = 3.5$; $E_{c,N}(R) = 21.132$;
$E_{c,LN}(R) = 27.194$.

Table 2.10 $E_{cs}(R)$ and η_R of ductile systems associated with the case $\rho(R_i,R_j) = 0.5$.

System		Normal distribution		Lognormal distribution	
		$E_{cs}(R)$	η_R	$E_{cs}(R)$	η_R
100-component system	Series system	23.013	1.089	29.533	1.086
	Parallel system	20.815	0.985	26.976	0.992
	$5p \times 20s$ SP system	21.449	1.015	27.847	1.024
	$10p \times 10s$ SP system	21.195	1.003	27.439	1.009
	$20p \times 5s$ SP system	21.026	0.995	27.221	1.001
300-component system	Series system	23.309	1.103	29.913	1.100
	Parallel system	20.815	0.985	26.949	0.991
	$5p \times 60s$ SP system	21.660	1.025	28.010	1.030
	$10p \times 30s$ SP system	21.322	1.009	27.602	1.015
	$20p \times 15s$ SP system	21.132	1.000	27.330	1.005
500-component system	Series system	23.457	1.110	30.077	1.106
	Parallel system	20.815	0.985	26.949	0.991
	$5p \times 100s$ SP system	21.703	1.027	28.064	1.032
	$10p \times 50s$ SP system	21.364	1.011	27.656	1.017
	$20p \times 25s$ SP system	21.132	1.000	27.357	1.006

Note: $E(P) = 10$; $V(P) = 0.3$; $V(R) = 0.05$; $\beta_c = 3.5$; $\beta_{sys} = 3.5$; $E_{c,N}(R) = 21.132$;
$E_{c,LN}(R) = 27.194$.

Table 2.11 Component reliability index β_{cs} of ductile systems.

System		Normal distribution		Lognormal distribution	
		$\rho = 0$	$\rho = 0.5$	$\rho = 0$	$\rho = 0.5$
100-component system	Series system	4.23	4.05	3.88	3.77
	Parallel system	3.32	3.40	3.44	3.48
300-component system	Series system	4.36	4.14	3.94	3.81
	Parallel system	3.31	3.40	3.44	3.47
500-component system	Series system	4.42	4.18	3.96	3.83
	Parallel system	3.31	3.40	3.44	3.47

Note: ρ denotes $\rho(R_i, R_j)$; $E(P) = 10$; $V(P) = 0.3$; $V(R) = 0.05$; $\beta_c = 3.5$; $\beta_{sys} = 3.5$;
$E_{c,N}(R) = 21.132$; $E_{c,LN}(R) = 27.194$.

Table 2.12 $E_{cs}(R)$ and η_R of brittle systems associated with the case $\rho(R_i,R_j) = 0$.

System		Normal distribution		Lognormal distribution	
		$E_{cs}(R)$	η_R	$E_{cs}(R)$	η_R
10-component system	Series system	22.484	1.064	29.098	1.070
	Parallel system	22.506	1.065	29.125	1.071
	5p×2s SP system	22.506	1.065	29.125	1.071
	5s×2p SP system	22.506	1.065	29.125	1.071
20-component system	Series system	22.865	1.082	29.560	1.087
	Parallel system	22.865	1.082	29.560	1.087
	5p×4s SP system	22.865	1.082	29.560	1.087
	10p×2s SP system	22.865	1.082	29.560	1.087
	5s×4p SP system	22.865	1.082	29.560	1.087
	10s×2p SP system	22.865	1.082	29.560	1.087
25-component system	Series system	22.992	1.088	29.641	1.090
	Parallel system	22.992	1.088	29.641	1.090
	5p×5s SP system	22.992	1.088	29.641	1.090
	5s×5p SP system	22.992	1.088	29.641	1.090
50-component system	Series system	23.330	1.104	30.104	1.107
	Parallel system	23.330	1.104	30.104	1.107
	5p×10s SP system	23.330	1.104	30.104	1.107
	10p×5s SP system	23.330	1.104	30.104	1.107
	5s×10p SP system	23.330	1.104	30.104	1.107
	10s×5p SP system	23.330	1.104	30.104	1.107

Note: $E(P) = 10$; $V(P) = 0.3$; $V(R) = 0.05$; $\beta_c = 3.5$; $\beta_{sys} = 3.5$; $E_{c,N}(R) = 21.132$;

$E_{c,LN}(R) = 27.194$.

Table 2.13 $E_{cs}(R)$ and η_R of brittle systems associated with the case $\rho(R_i,R_j) = 0.5$.

System		Normal distribution		Lognormal distribution	
		$E_{cs}(R)$	η_R	$E_{cs}(R)$	η_R
10-component system	Series system	22.189	1.050	28.608	1.052
	Parallel system	22.189	1.050	28.608	1.052
	5p×2s SP system	22.189	1.050	28.608	1.052
	5s×2p SP system	22.189	1.050	28.608	1.052
20-component system	Series system	22.463	1.063	28.880	1.062
	Parallel system	22.442	1.062	28.880	1.062
	5p×4s SP system	22.442	1.062	28.880	1.062
	10p×2s SP system	22.442	1.062	28.880	1.062
	5s×4p SP system	22.442	1.062	28.880	1.062
	10s×2p SP system	22.442	1.062	28.880	1.062
25-component system	Series system	22.527	1.066	28.962	1.065
	Parallel system	22.527	1.066	28.962	1.065
	5p×5s SP system	22.527	1.066	28.962	1.065
	5s×5p SP system	22.527	1.066	28.962	1.065
50-component system	Series system	22.759	1.077	29.288	1.077
	Parallel system	22.759	1.077	29.288	1.077
	5p×10s SP system	22.759	1.077	29.288	1.077
	10p×5s SP system	22.759	1.077	29.288	1.077
	5s×10p SP system	22.759	1.077	29.288	1.077
	10s×5p SP system	22.759	1.077	29.288	1.077

Note: $E(P) = 10$; $V(P) = 0.3$; $V(R) = 0.05$; $\beta_c = 3.5$; $\beta_{sys} = 3.5$; $E_{c,N}(R) = 21.132$; $E_{c,LN}(R) = 27.194$.

Table 2.14 Component reliability index β_{cs} of brittle systems.

System		Normal distribution		Lognormal distribution	
		$\rho = 0$	$\rho = 0.5$	$\rho = 0$	$\rho = 0.5$
5-component system	Series system	3.79	3.73	3.67	3.62
	Parallel system	3.79	3.73	3.67	3.62
10-component system	Series system	3.90	3.81	3.72	3.67
	Parallel system	3.90	3.81	3.72	3.67
15-component system	Series system	3.97	3.86	3.76	3.69
	Parallel system	3.97	3.86	3.76	3.69
20-component system	Series system	4.01	3.89	3.78	3.70
	Parallel system	4.01	3.89	3.78	3.70
25-component system	Series system	4.04	3.91	3.79	3.71
	Parallel system	4.04	3.91	3.79	3.71
50-component system	Series system	4.14	3.98	3.84	3.74
	Parallel system	4.14	3.98	3.84	3.74

Note: $E(P) = 10$; $V(P) = 0.3$; $V(R) = 0.05$; $\beta_c = 3.5$; $\beta_{sys} = 3.5$; $E_{c,N}(R) = 21.132$;

$E_{c,LN}(R) = 27.194$.

Table 2.15 The redundancy factors of the three systems.

Correlation case	Series system	Parallel system	Series-parallel system
$\rho(R_i, R_j) = 0$	1.041	0.934	0.987
$\rho(R_i, R_j) = 0.5$	1.032	0.956	0.995
$\rho(R_i, R_j) = 1.0$	1.000	1.000	1.000

Note: $V(R) = 0.05$; $V(P) = 0.3$.

Table 2.16 The designed mean resistances of exterior $E_{cs}(M_{U,ext})$ and interior girders $E_{cs}(M_{U,int})$ in the four-component systems.

System type	Correlation case	$E_{cs}(M_{U,ext})$, kN·m	$E_{cs}(M_{U,int})$, kN·m	$E_{cs}(M_U)$, kN·m
Series system	$\rho(R_i, R_j) = 0$	7495	7719	7719
	$\rho(R_i, R_j) = 0.5$	7430	7652	7652
	$\rho(R_i, R_j) = 1.0$	7200	7415	7415
Parallel system	$\rho(R_i, R_j) = 0$	6725	6926	6926
	$\rho(R_i, R_j) = 0.5$	6883	7089	7089
	$\rho(R_i, R_j) = 1.0$	7200	7415	7415
Series-parallel system	$\rho(R_i, R_j) = 0$	7106	7319	7319
	$\rho(R_i, R_j) = 0.5$	7164	7378	7378
	$\rho(R_i, R_j) = 1.0$	7200	7415	7415

Note: $E(M_{L,ext})$=3407 kN·m; $E(M_{L,int})$=3509 kN·m; $V(R)$=0.05; $V(P)$=0.3; $E_{c,N}(M_{U,ext})$=7200 kN·m; $E_{c,N}(M_{U,int})$=7415 kN·m.

Table 2.17   The reliability indices of exterior and interior girders and the system reliability indices.

System type	Correlation case	β_{ext}	β_{int}	β_{sys}
Series system	$\rho(R_i, R_j) = 0$	3.95	3.75	3.58
	$\rho(R_i, R_j) = 0.5$	3.89	3.70	3.60
	$\rho(R_i, R_j) = 1.0$	3.69	3.50	3.50
Parallel system	$\rho(R_i, R_j) = 0$	3.26	3.08	3.61
	$\rho(R_i, R_j) = 0.5$	3.40	3.22	3.63
	$\rho(R_i, R_j) = 1.0$	3.69	3.50	3.69
Series-parallel system	$\rho(R_i, R_j) = 0$	3.60	3.42	3.62
	$\rho(R_i, R_j) = 0.5$	3.65	3.47	3.61
	$\rho(R_i, R_j) = 1.0$	3.69	3.50	3.50

Note: $E(M_{L,ext})$=3407 kN·m; $E(M_{L,int})$=3509 kN·m; $V(R)$=0.05; $V(P)$=0.3;

$E_{c,N}(M_{U,ext})$=7200 kN·m; $E_{c,N}(M_{U,int})$=7415 kN·m.

Table 2.18   The designed mean resistance associated with the 4-component series-parallel system.

System type	Correlation case	$E_{cs}(M_{U,ext})$, kN·m	$E_{cs}(M_{U,int})$, kN·m	$E_{cs}(M_U)$, kN·m
Series-parallel system	$\rho(R_i, R_j) = 0$	7078	7289	7289
	$\rho(R_i, R_j) = 0.5$	7135	7348	7348
	$\rho(R_i, R_j) = 1.0$	7200	7415	7415

Note: $E(M_{L,ext})$=3407 kN·m; $E(M_{L,int})$=3509 kN·m; $V(R)$=0.05; $V(P)$=0.3;

$E_{c,N}(M_{U,ext})$=7200 kN·m; $E_{c,N}(M_{U,int})$=7415 kN·m.

Table 2.19 The reliability indices of exterior and interior girders and the system reliability indices associated with the 4-component series-parallel system.

System type	Correlation case	β_{ext}	β_{int}	β_{sys}
Series-parallel system	$\rho(R_i, R_j) = 0$	3.58	3.39	3.59
	$\rho(R_i, R_j) = 0.5$	3.63	3.44	3.58
	$\rho(R_i, R_j) = 1.0$	3.69	3.50	3.50

Note: $E(M_{L,ext})$=3407 kN·m; $E(M_{L,int})$=3509 kN·m; $V(R)$=0.05; $V(P)$=0.3;

$E_{c,N}(M_{U,ext})$=7200 kN·m; $E_{c,N}(M_{U,int})$=7415 kN·m.

Table 2.20 The redundancy factors of the four-component systems when $\beta_{sys,target} = 4.0$.

Correlation case	Series system	Parallel system	Series-parallel system
$\rho(R_i, R_j) = 0$	1.123	1.004	1.062
$\rho(R_i, R_j) = 0.5$	1.113	1.030	1.072
$\rho(R_i, R_j) = 1.0$	1.081	1.081	1.081

Note: $V(R)$=0.05; $V(P)$=0.3.

Table 2.21 The designed mean resistances of exterior $E_{cs}(M_{U,ext})$ and interior girders $E_{cs}(M_{U,int})$ when $\beta_{sys,target}=4.0$.

System type	Correlation case	$E_{cs}(M_{U,ext})$, kN·m	$E_{cs}(M_{U,\text{int}})$, kN·m	$E_{cs}(M_{U})$, kN·m
Series system	$\rho(R_i,R_j)=0$	8085	8327	8327
	$\rho(R_i,R_j)=0.5$	8012	8251	8251
	$\rho(R_i,R_j)=1.0$	7782	8014	8014
Parallel system	$\rho(R_i,R_j)=0$	7231	7447	7447
	$\rho(R_i,R_j)=0.5$	7416	7637	7637
	$\rho(R_i,R_j)=1.0$	7782	8014	8014
Series-parallel system	$\rho(R_i,R_j)=0$	7644	7872	7872
	$\rho(R_i,R_j)=0.5$	7721	7952	7952
	$\rho(R_i,R_j)=1.0$	7782	8014	8014

Note: $E(M_{L,ext})$=3407 kN·m; $E(M_{L,int})$=3509 kN·m; $V(R)$=0.05; $V(P)$=0.3;

$E_{c,N}(M_{U,ext})$=7200 kN·m; $E_{c,N}(M_{U,int})$=7415 kN·m.

Table 2.22 The reliability indices of exterior and interior girders and the system reliability indices when $\beta_{sys,target} = 4.0$.

System type	Correlation case	β_{ext}	β_{int}	β_{sys}
	$\rho(R_i, R_j) = 0$	4.46	4.26	4.08
Series system	$\rho(R_i, R_j) = 0.5$	4.40	4.20	4.08
	$\rho(R_i, R_j) = 1.0$	4.20	4.00	4.00
	$\rho(R_i, R_j) = 0$	3.71	3.53	4.11
Parallel system	$\rho(R_i, R_j) = 0.5$	3.88	3.69	4.12
	$\rho(R_i, R_j) = 1.0$	4.20	4.00	4.20
	$\rho(R_i, R_j) = 0$	4.08	3.88	4.11
Series-parallel system	$\rho(R_i, R_j) = 0.5$	4.14	3.95	4.10
	$\rho(R_i, R_j) = 1.0$	4.20	4.00	4.00

Note: $E(M_{L,ext})$=3407 kN·m; $E(M_{L,int})$=3509 kN·m; $V(R)$=0.05; $V(P)$=0.3;

$E_{c,N}(M_{U,ext})$=7200 kN·m; $E_{c,N}(M_{U,int})$=7415 kN·m.

Table 2.23 The designed mean resistance associated with the 4-component series-parallel system when $\beta_{sys,target} = 4.0$.

System type	Correlation case	$E_{cs}(M_{U,ext})$, kN·m	$E_{cs}(M_{U,int})$, kN·m	$E_{cs}(M_U)$, kN·m
Series-parallel system	$\rho(R_i, R_j) = 0$	7618	7845	7845
	$\rho(R_i, R_j) = 0.5$	7701	7931	7931
	$\rho(R_i, R_j) = 1.0$	7782	8014	8014

Note: $E(M_{L,ext})$=3407 kN·m; $E(M_{L,int})$=3509 kN·m; $V(R)$=0.05; $V(P)$=0.3;

$E_{c,N}(M_{U,ext})$=7200 kN·m; $E_{c,N}(M_{U,int})$=7415 kN·m.

Table 2.24 The reliability indices of exterior and interior girders and the system reliability indices associated with the 4-component series-parallel system when $\beta_{sys,target} = 4.0$.

System type	Correlation case	β_{ext}	β_{int}	β_{sys}
Series-parallel system	$\rho(R_i, R_j) = 0$	4.05	3.86	4.08
	$\rho(R_i, R_j) = 0.5$	4.13	4.24	4.09
	$\rho(R_i, R_j) = 1.0$	4.20	4.00	4.00

Note: $E(M_{L,ext})$=3407 kN·m; $E(M_{L,int})$=3509 kN·m; $V(R)$=0.05; $V(P)$=0.3;

$E_{c,N}(M_{U,ext})$=7200 kN·m; $E_{c,N}(M_{U,int})$=7415 kN·m.
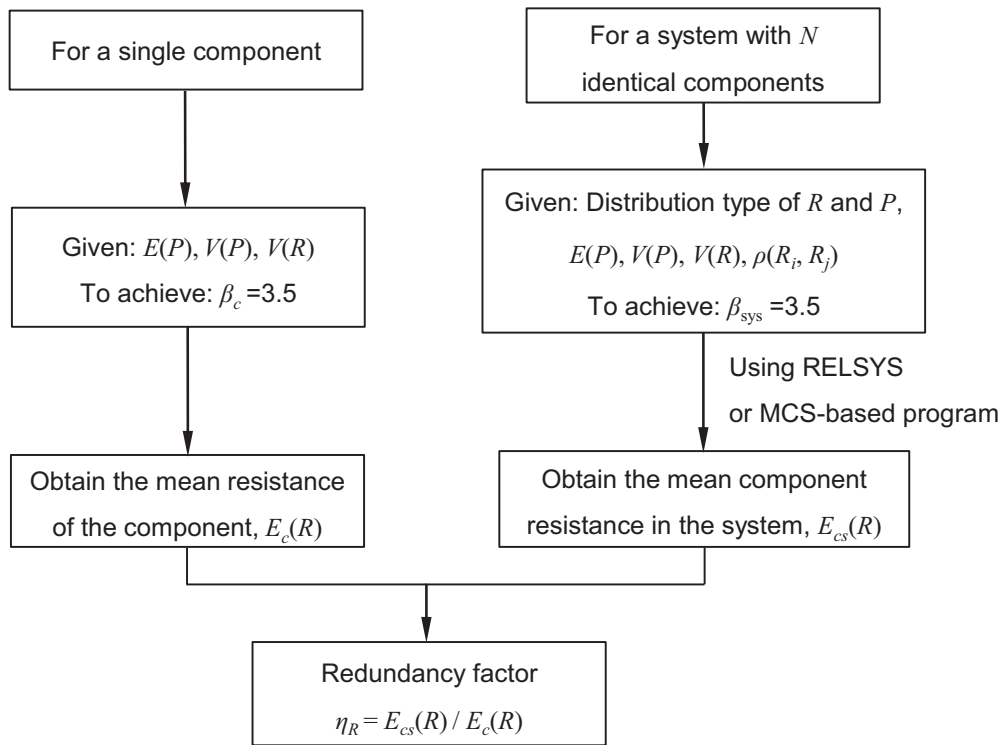
Figure 2.1 Flowchart of the procedure for determining the redundancy factor η_R.
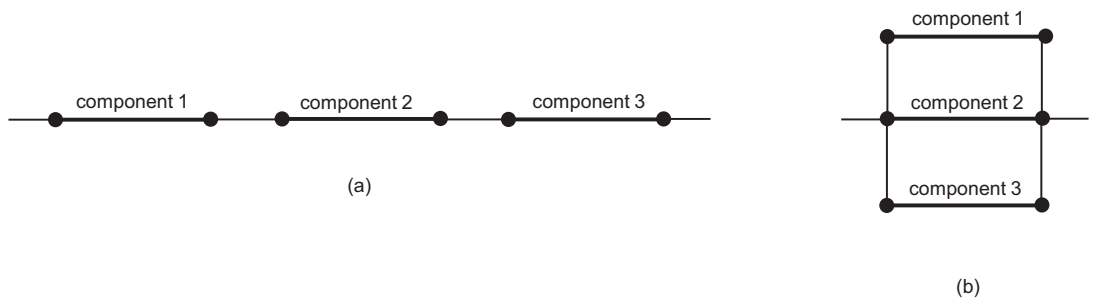
Figure 2.2 Three-component systems: (a) series system; and (b) parallel system.
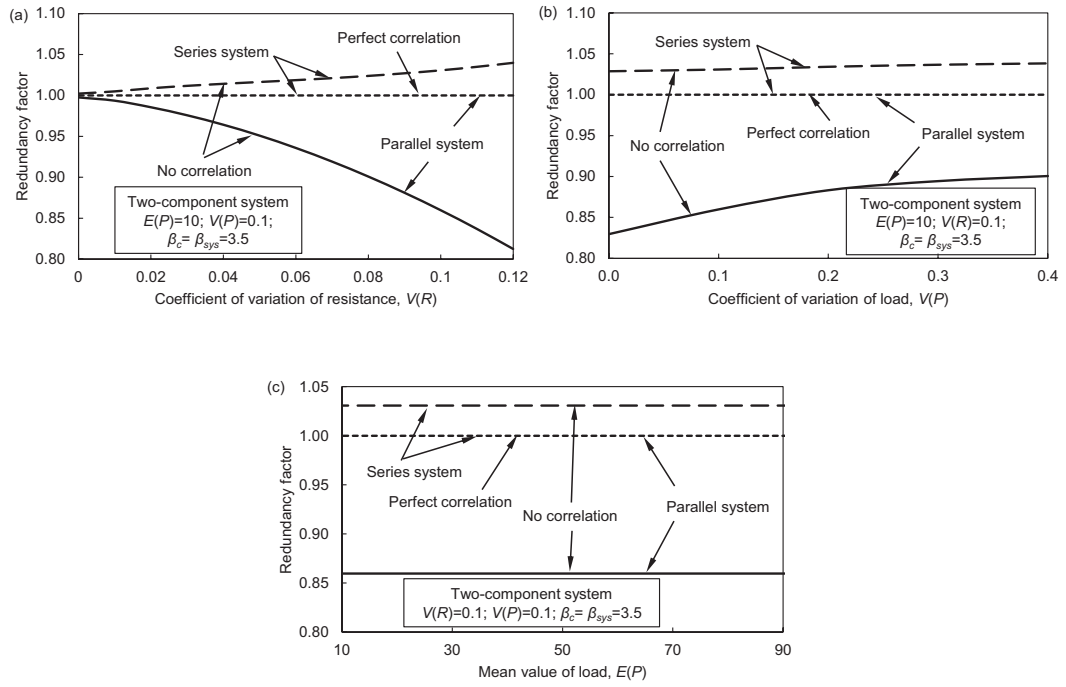
Figure 2.3 Effects of (a) $V(R)$; (b) $V(P)$; and (c) $E(P)$ on η_R in two-component systems.
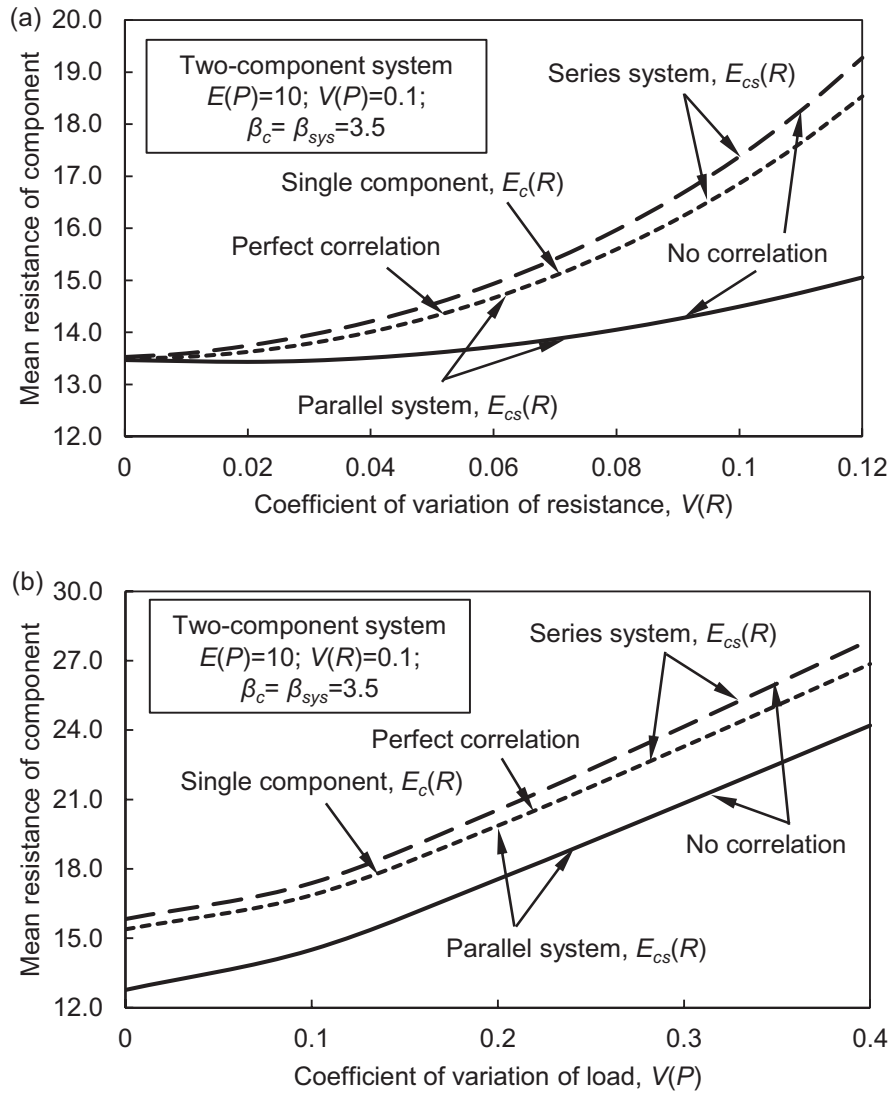
Figure 2.4 Effects of (a) $V(R)$; and (b) $V(P)$ on $E_c(R)$ and $E_{cs}(R)$ in two-component systems.
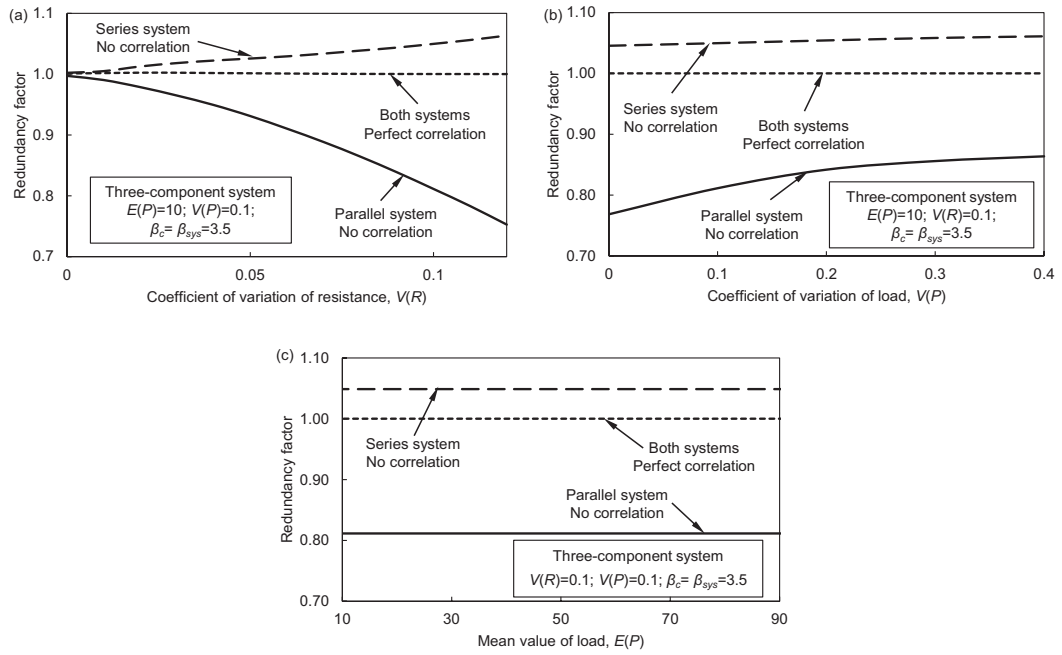
Figure 2.5 Effects of (a) $V(R)$; (b) $V(P)$; and (c) $E(P)$ on η_R in three-component systems.
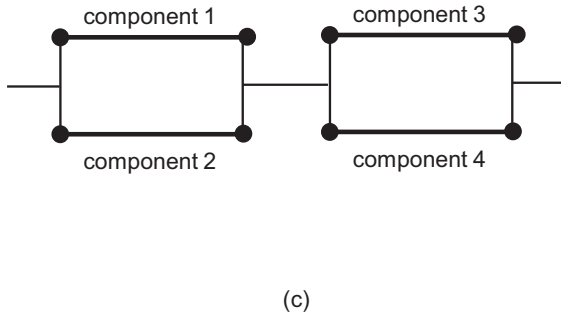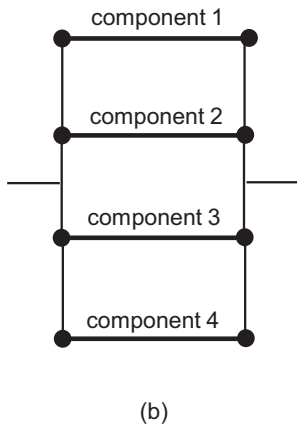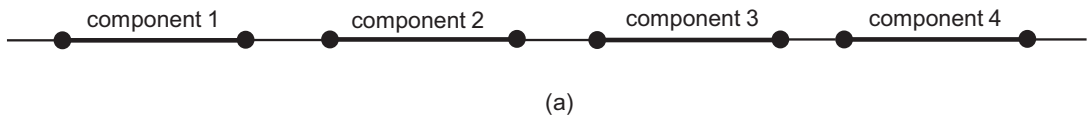
Figure 2.6 Four-component systems: (a) series system; (b) parallel system; and (c) series-parallel system.
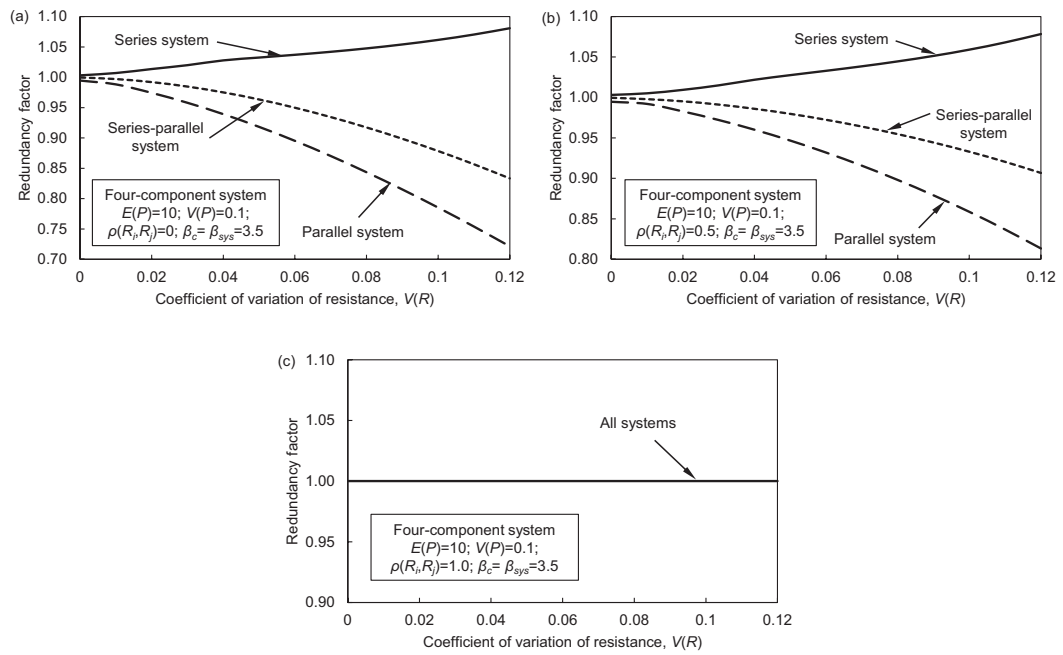
Figure 2.7 Effects of $V(R)$ on η_R in four-component systems associated with the case of (a) no correlation; (b) partial correlation; and (c) perfect correlation.
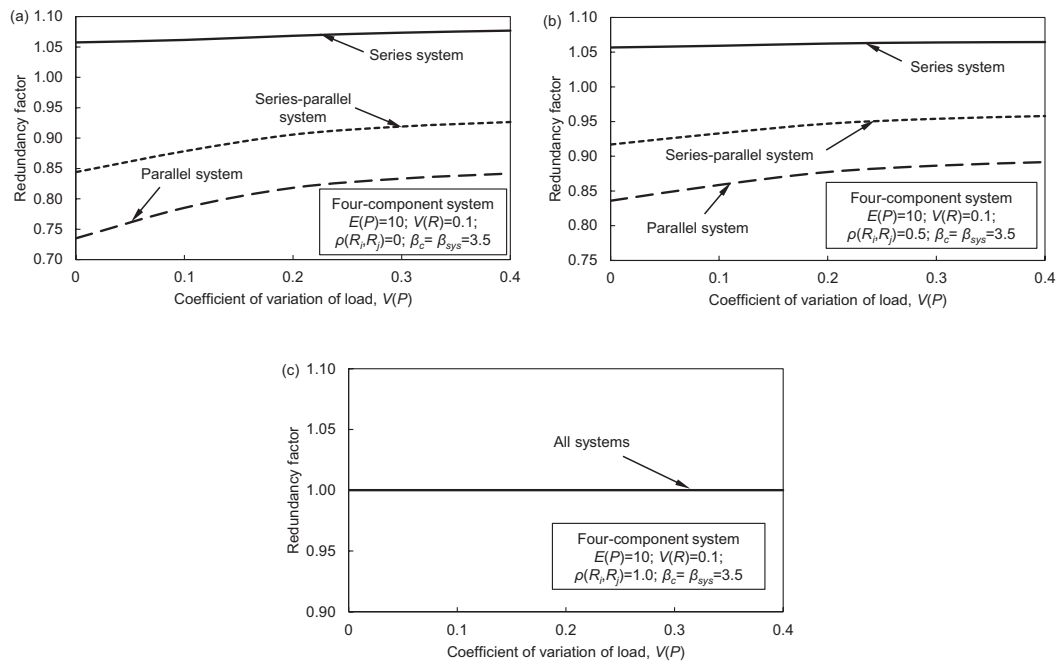
Figure 2.8 Effects of $V(P)$ on η_R in four-component systems associated with the case of (a) no correlation; (b) partial correlation; and (c) perfect correlation.

99
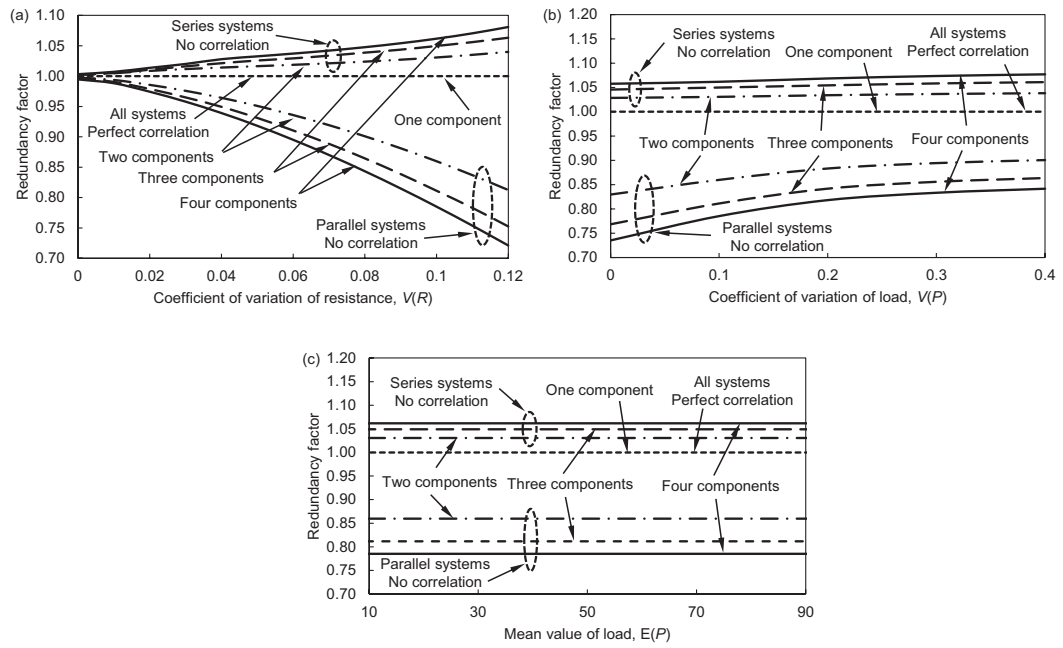
Figure 2.9 Effects of number of components on η_R with the variations of (a) $V(R)$; (b) $V(P)$; and (c) $E(P)$ in two extreme correlation cases.

Given: $E(P)$, $V(R)$, $V(P)$, $\rho(R_i,R_j)$, N,
distribution type of R and P, system type,
and a group of initial guess for $E_{cs}(R)$:
$x=[x_1, x_2, x_3, \ldots, x_k]$;
also define $k = 20$; $c = 0$; $Tol = 10^{-4}$

Starting from x_1, find the x_i that satisfies:
$(\beta_{sys}| x_i) < 3.5$ and $(\beta_{sys}| x_{i+1}) > 3.5$

Use x_i as the first element to
generate a new x vector:
$x=[x_i, x_i+10^{-c}, \ldots, x_i+ (k-1)\times10^{-c}]$;

Is $|(\beta_{sys}| x_i) - 3.5| < Tol$
or
$|(\beta_{sys}| x_{i+1}) - 3.5| < Tol$
?

NO

$c = c+1$;
clear the original x vector

YES

$E_{cs}(R) = x_i$ or x_{i+1}
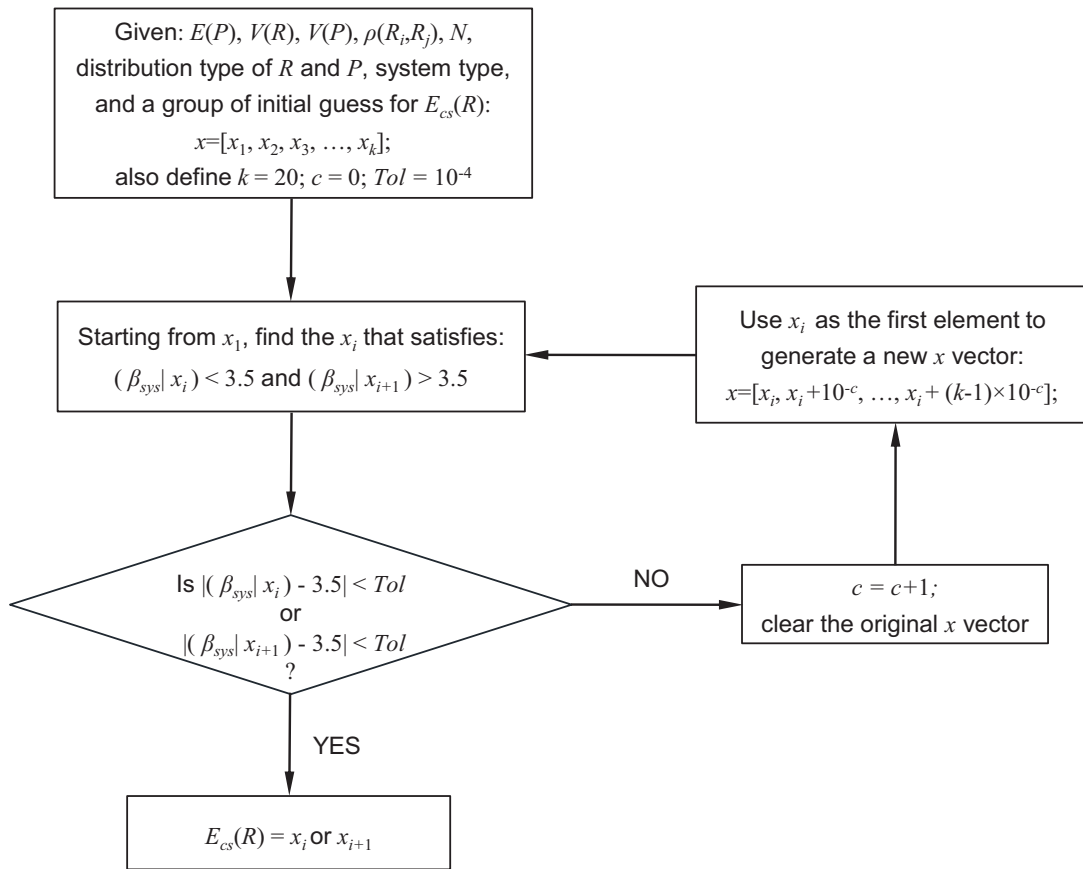
Figure 2.10 Flowchart for the algorithm combined with RELSYS.

101
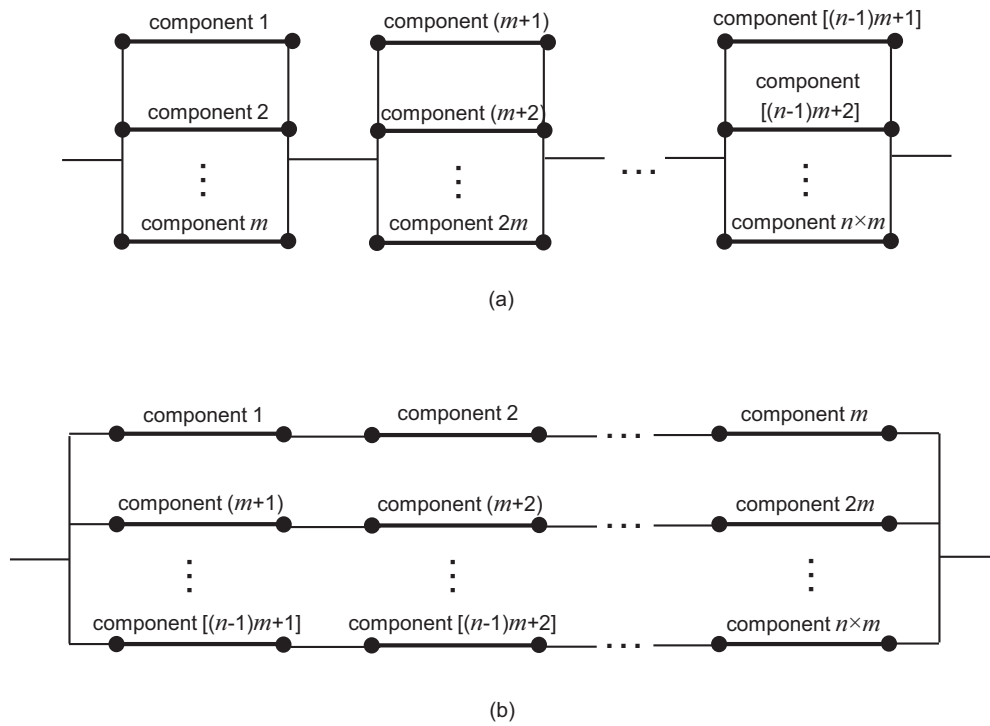
Figure 2.11 Schematic figure of (a) $mp \times ns$ series-parallel system (n series of m components in parallel); and (b) $ms \times np$ series-parallel system (n parallel of m components in series).

Given: $E(P)$, $V(R)$, $V(P)$, $\rho(R_i,R_j)$, N, distribution type of R and P, system type, number of simulation samples w, and an initial guess for $E_{cs}(R)$; define $c = 1$

Adjust the initial value for $E_{cs}(R)$; define $c = 1$

Generate w random samples for each R_i and P

Obtain the limit state equations of each component: $g_i = R_i - P$

Series system

Define an $w \times 1$ zero vector L:
$P_f(c) = \{sum\ [\ L\ |\ (g_1 < 0)\ |\ \ldots\ |\ (g_N < 0)\ ]\}/w$

Parallel system

Define an $w \times 1$ unit vector Q:
$P_f(c) = \{sum\ [\ Q\ \&\ (g_1 < 0)\ \&\ \ldots\ \&\ (g_N < 0)\ ]\}/w$

$mp \times ns$ SP system

Define an $w \times 1$ zero vector L and an $w \times 1$ unit vector Q:
$P_f(c) = \{sum\ \{\ L\ |\ [\ Q\ \&\ (g_1 < 0)\ \&\ \ldots\ \&\ (g_m < 0)\ ]\ |\ \ldots\ |\ [\ Q\ \&\ (g_{m\cdot(n-1)+1} < 0)\ \&\ \ldots\ \&\ (g_{m\cdot n} < 0)\ ]\ \}\}/w$

$ms \times np$ SP system

Define an $w \times 1$ zero vector L and an $w \times 1$ unit vector Q:
$P_f(c) = \{sum\ \{\ Q\ \&\ [\ L\ |\ (g_1 < 0)\ \&\ \ldots\ \&\ (g_m < 0)\ ]\ \&\ \ldots\ \&\ [\ Q\ |\ (g_{m\cdot(n-1)+1} < 0)\ |\ \ldots\ |\ (g_{m\cdot n} < 0)\ ]\ \}\}/w$

$c = c + 1$

NO

Is $c = 50$?

YES

Find the average failure probability and convert it to reliability index β_{sys}

Is $|\beta_{sys} - 3.5| < Tol$?

NO

YES

Return the initial value as final $E_{cs}(R)$

Figure 2.12 Flowchart for the algorithm combined with MCS-based program.

103
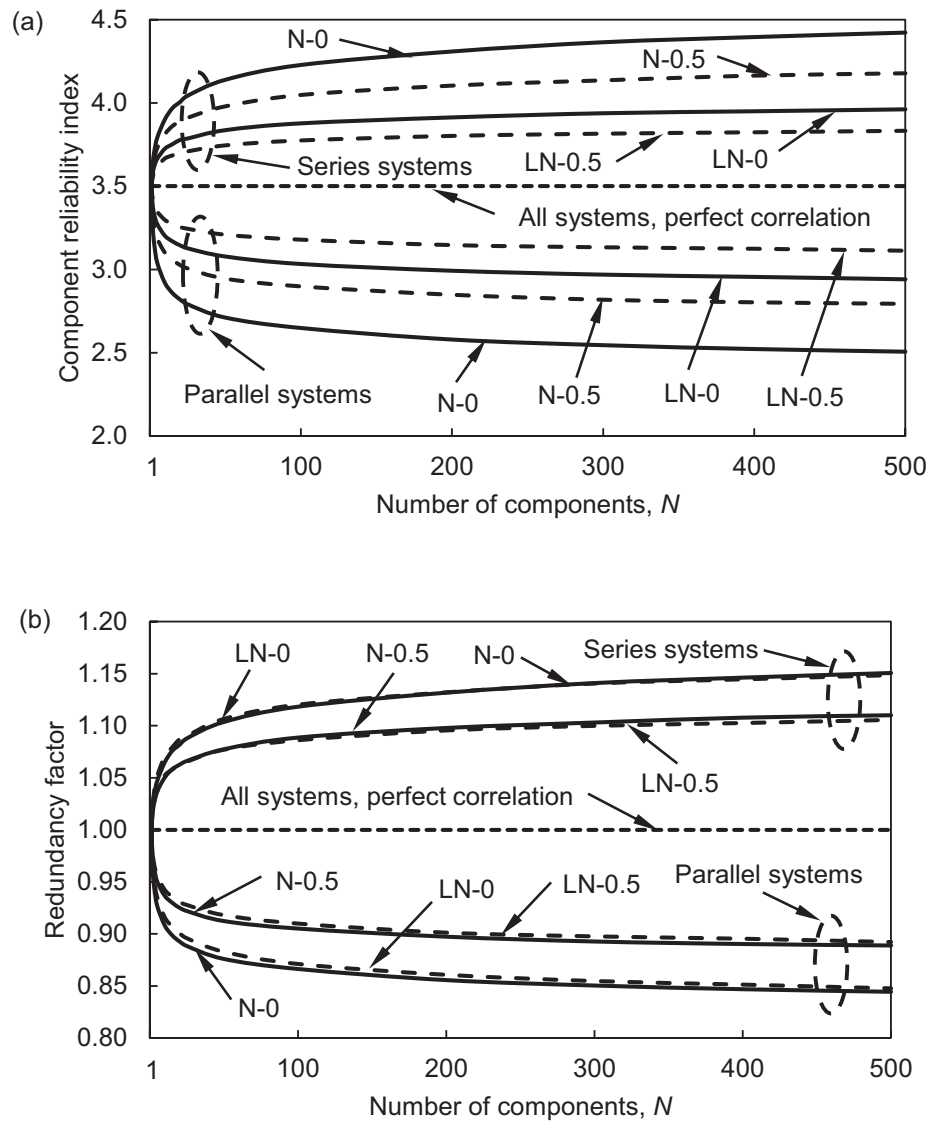
Figure 2.13 The effects of number of component on (a) component reliability index β_{cs}; and (b) redundancy factor η_R (Note: "N" is normal distribution; "LN" is lognormal distribution; "0" denotes $\rho(R_i,R_j) = 0$; "0.5" denotes $\rho(R_i,R_j) = 0.5$).
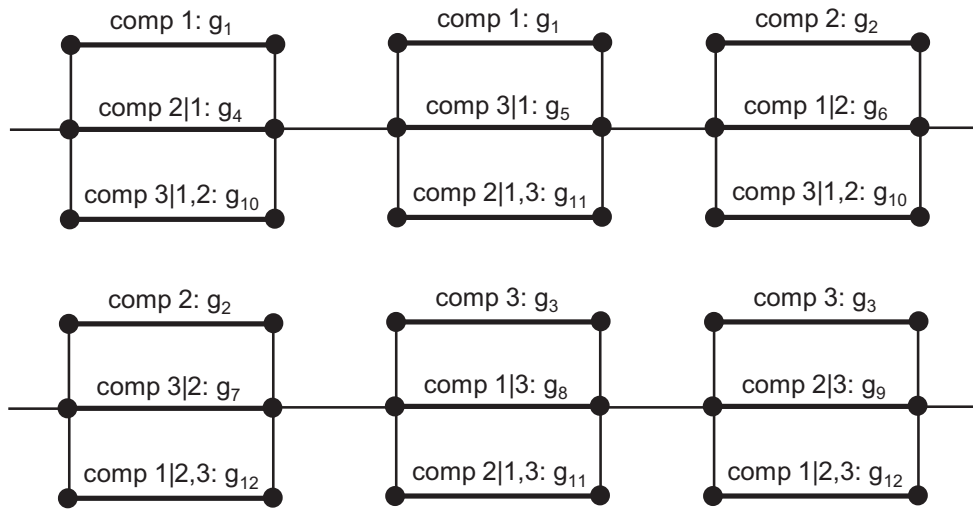
Figure 2.14 Failure modes of three-component brittle parallel system.
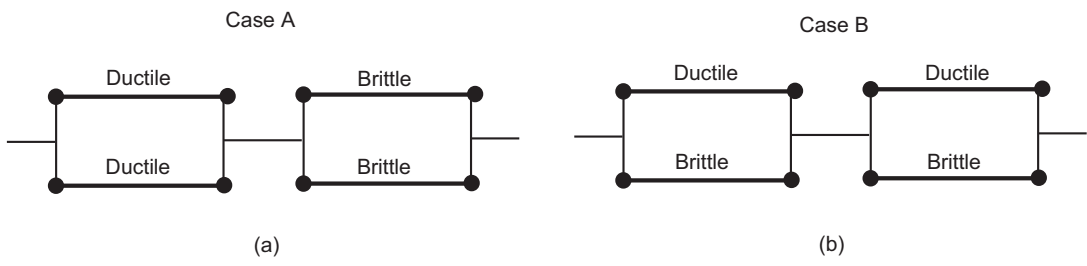
Figure 2.15 Four-component series-parallel systems: (a) 2 ductile & 2 brittle Case A; and (b) 2 ductile & 2 brittle Case B.
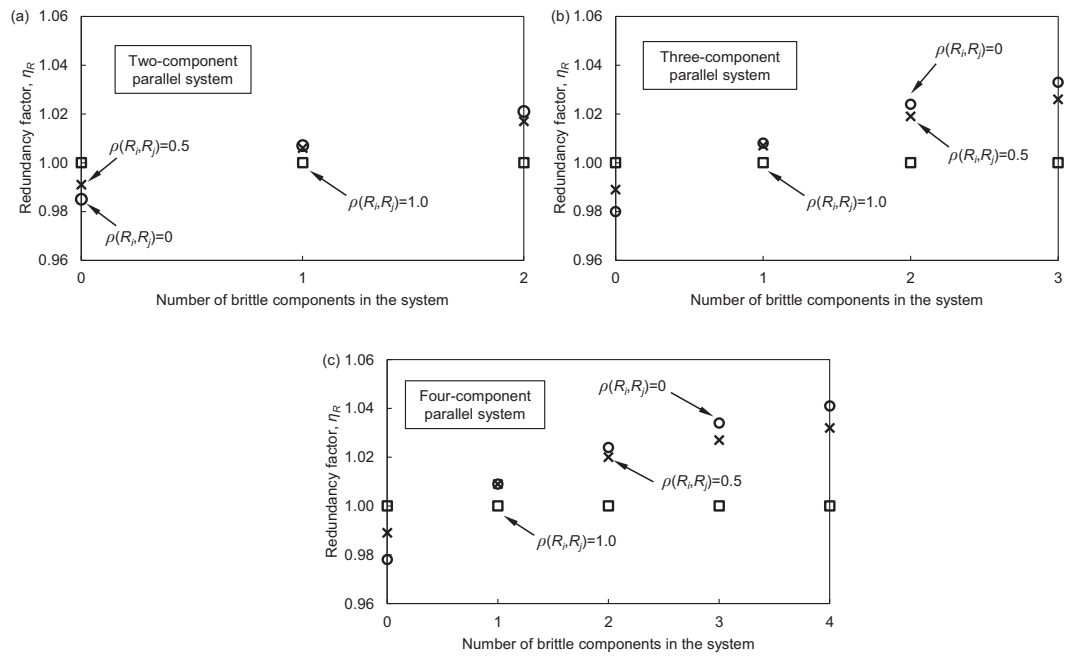
Figure 2.16 Effects of number of brittle components on the redundancy factor in the parallel systems consisting of (a) two components; (b) three components; and (c) four components.
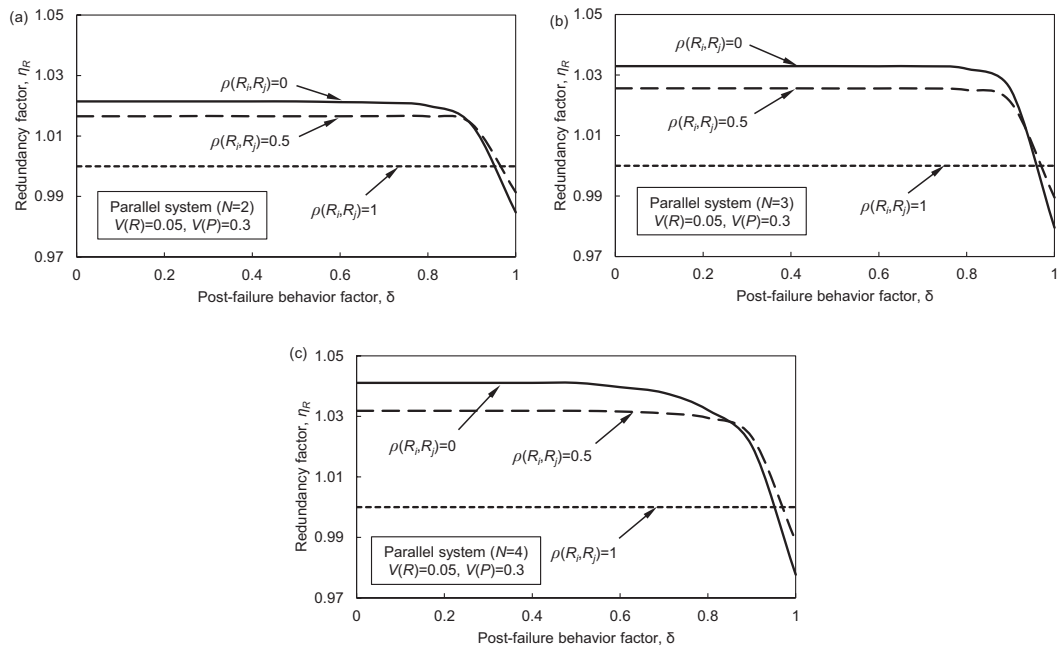
Figure 2.17 Effects of post-failure behavior factor δ on redundancy factor η_R in the parallel systems consisting of (a) two components; (b) three components; and (c) four components.
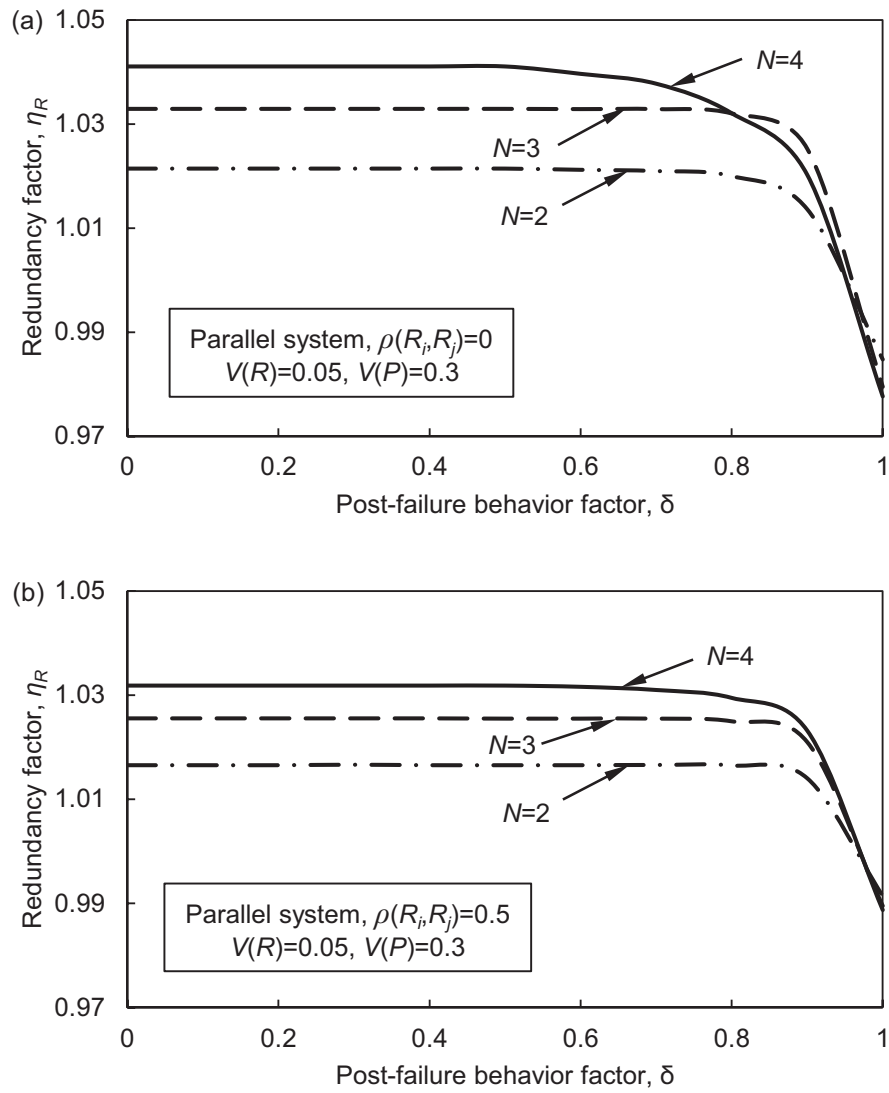
Figure 2.18 Effects of post-failure behavior factor δ on redundancy factor η_R in: (a) no correlation case; and (b) partial correlation case.
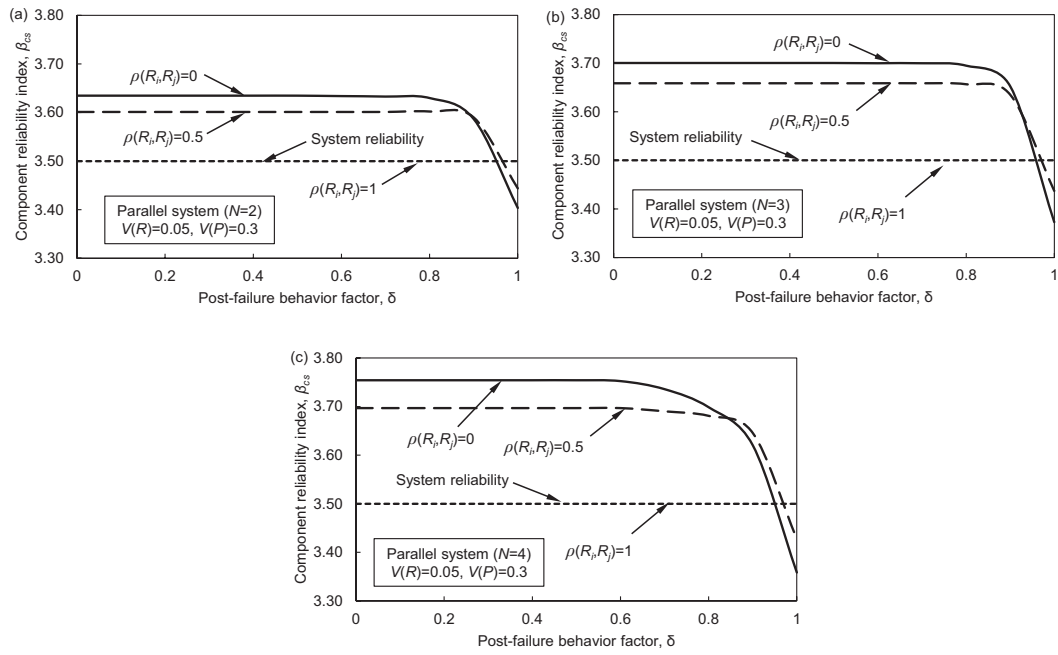
Figure 2.19 Effects of post-failure behavior factor δ on component reliability index in the parallel systems consisting of (a) two components; (b) three components; and (c) four components.
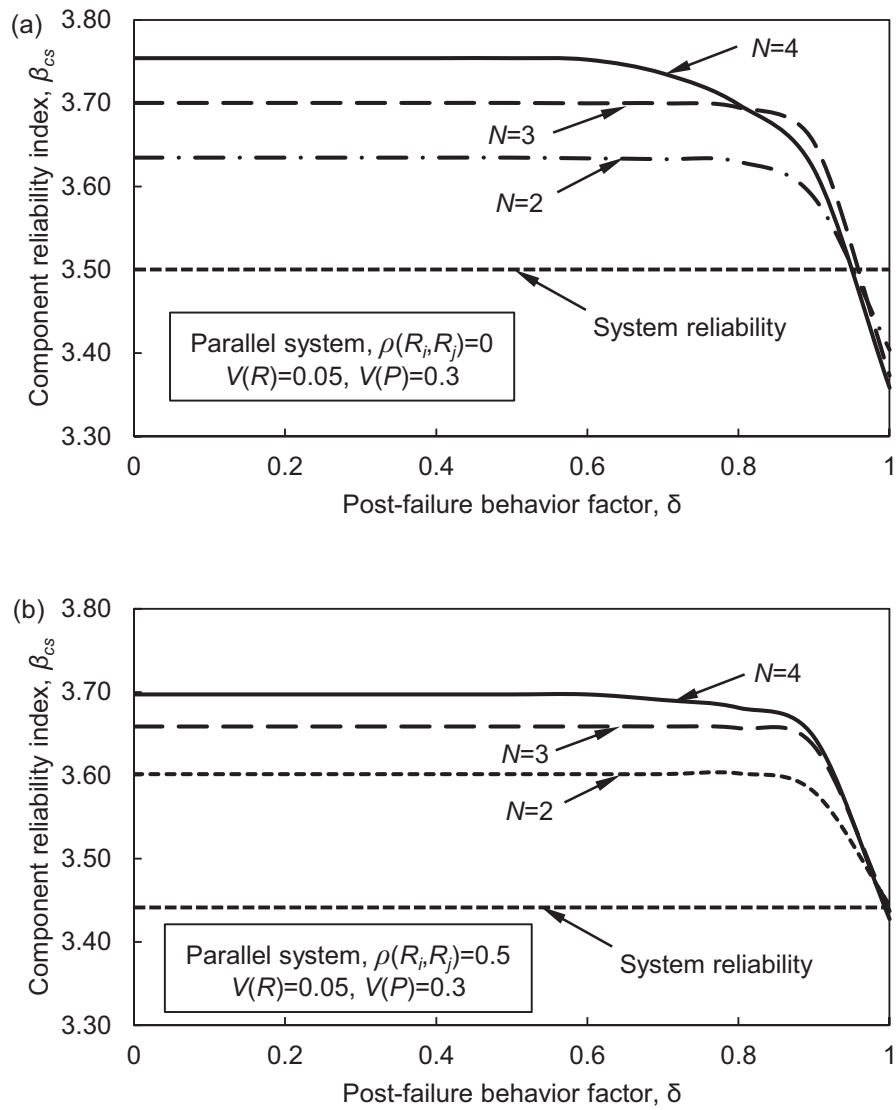
Figure 2.20 Effects of post-failure behavior factor δ on component reliability index in the (a) no correlation case; and (b) partial correlation case.
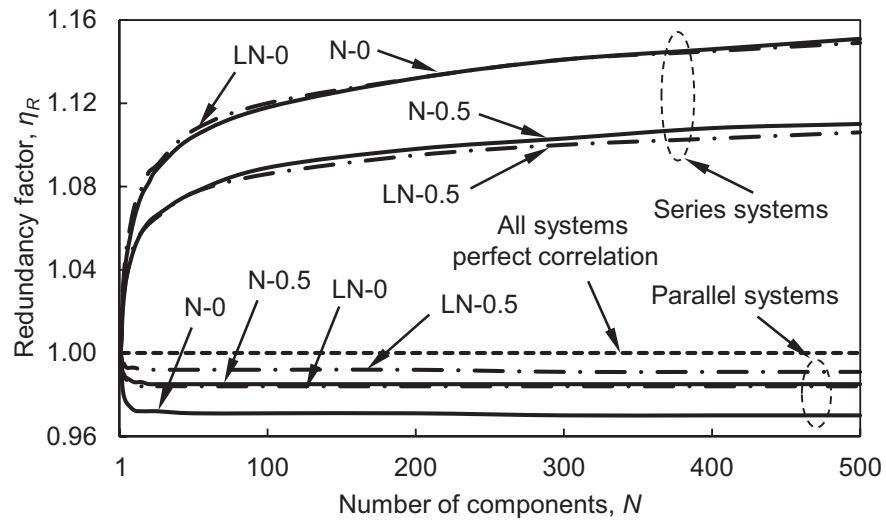
Figure 2.21 Effects of number of components on the redundancy factor in ductile
systems (Note: "N" denotes normal distribution; "LN" denotes lognormal
distribution; "0" denotes $\rho(R_i, R_j) = 0$; "0.5" denotes $\rho(R_i, R_j) = 0.5$).
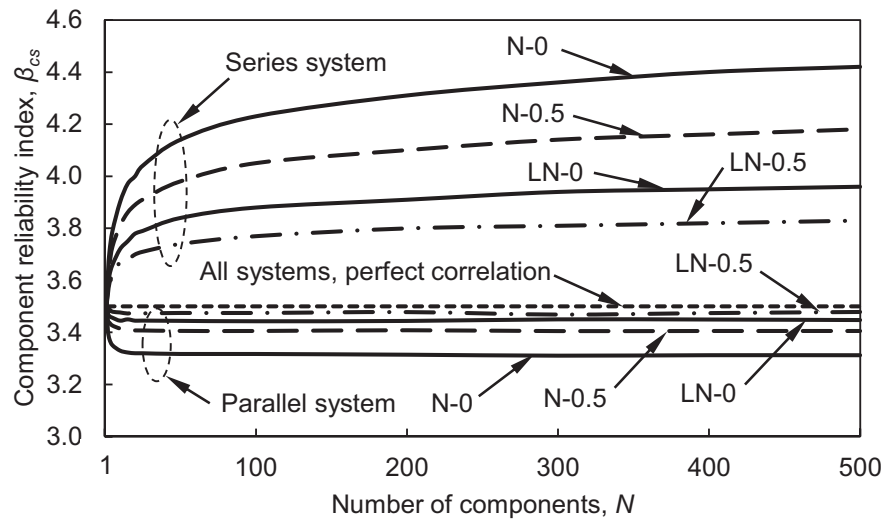
Figure 2.22 Effects of number of components on the component reliability index in ductile systems (Note: "N" denotes normal distribution; "LN" denotes lognormal distribution; "0" denotes $\rho(R_i, R_j) = 0$; "0.5" denotes $\rho(R_i, R_j) = 0.5$).
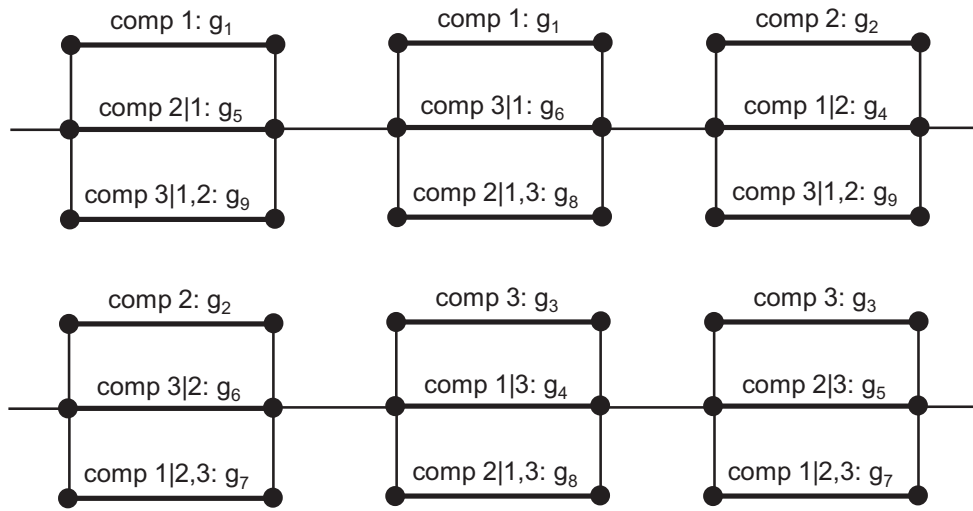
Figure 2.23 Failure modes of the three-component parallel system with renumbered limit state equations.

114
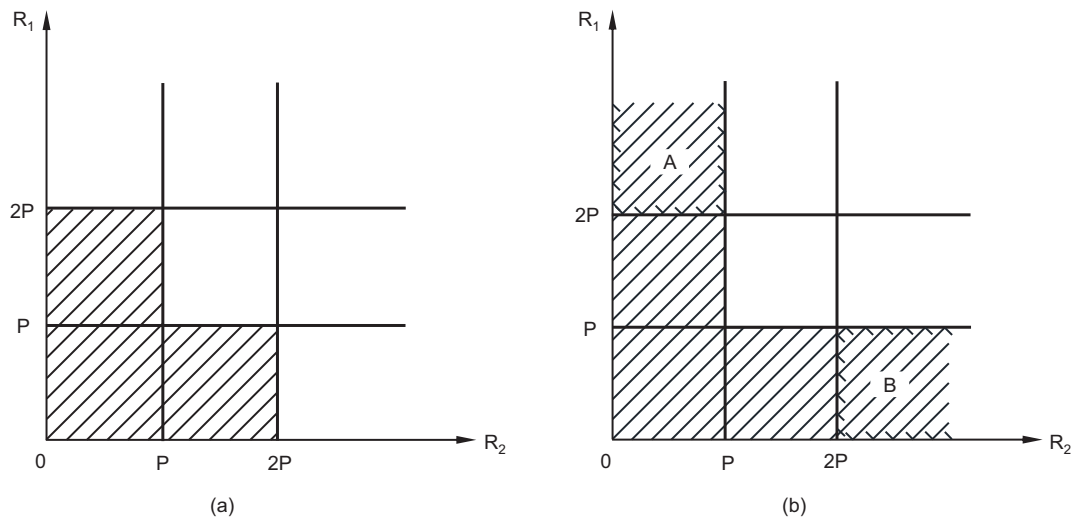
Figure 2.24 Sample space of (a) event F_1; and (b) event F_2.
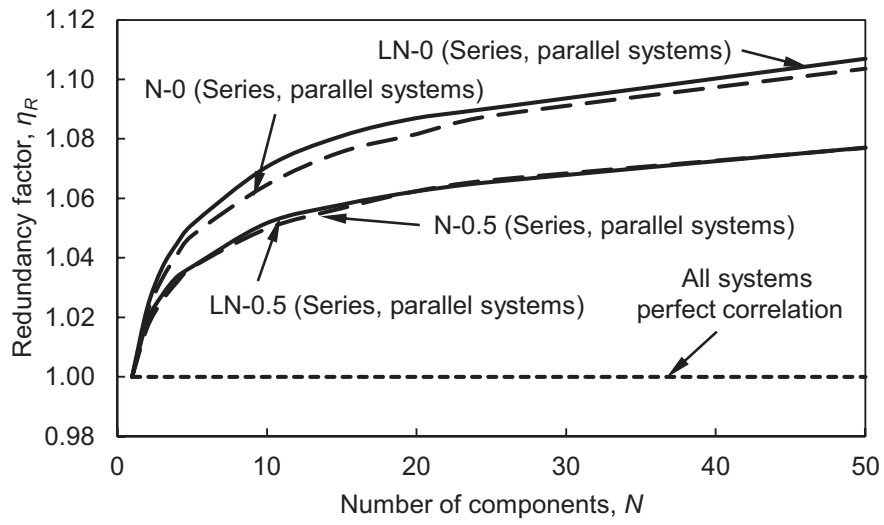
Figure 2.25 Effects of number of components on the redundancy factor in brittle systems (Note: "N" denotes normal distribution; "LN" denotes lognormal distribution; "0" denotes $\rho(R_i, R_j) = 0$; "0.5" denotes $\rho(R_i, R_j) = 0.5$).
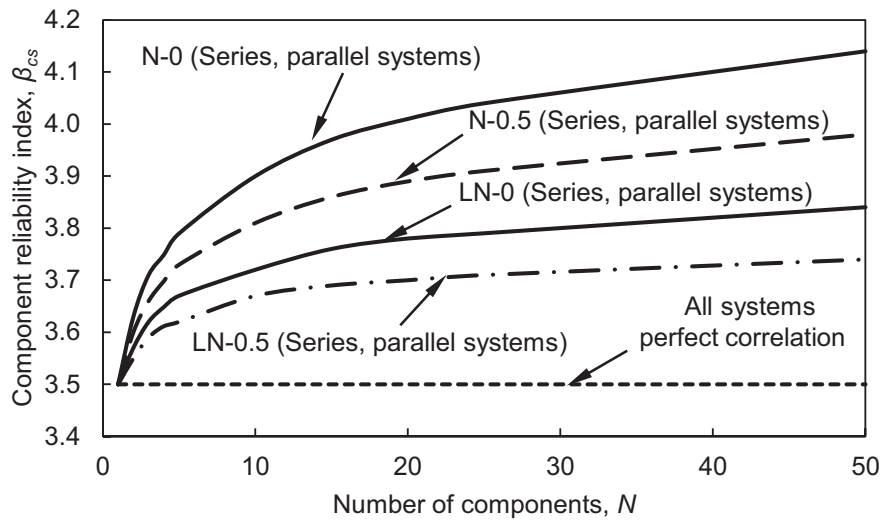
Figure 2.26 Effects of number of components on the reliability index of components in brittle systems (Note: "N" denotes normal distribution; "LN" denotes lognormal distribution; "0" denotes $\rho(R_i,R_j) = 0$; "0.5" denotes $\rho(R_i,R_j) = 0.5$).
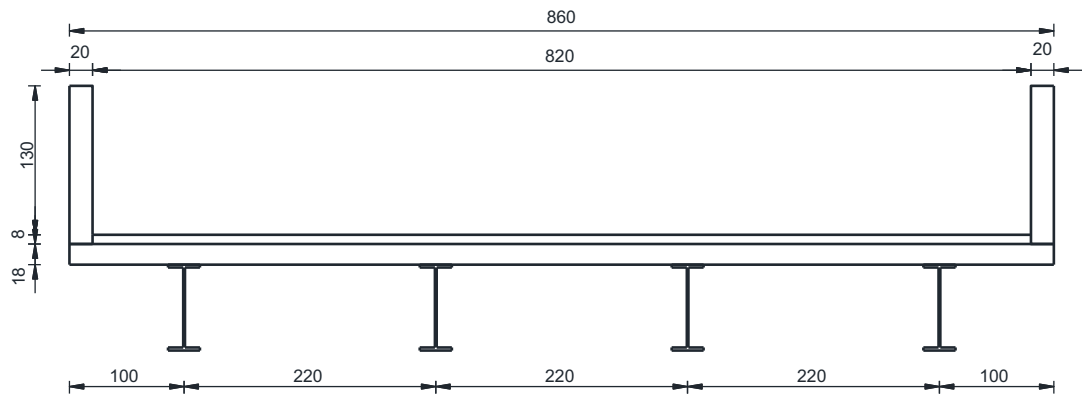
Figure 2.27 The cross-section of the bridge (dimensions are in cm).
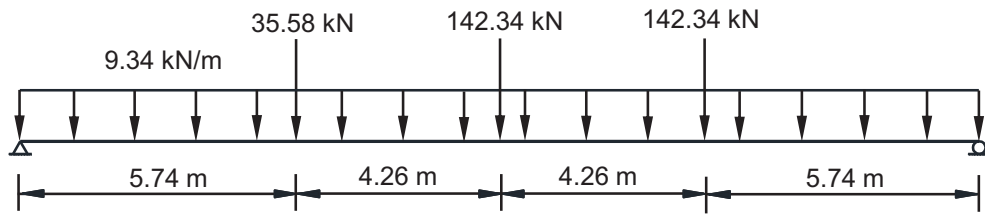
Figure 2.28 The most unfavorable longitudinal loading position of the design truck for the bridge.
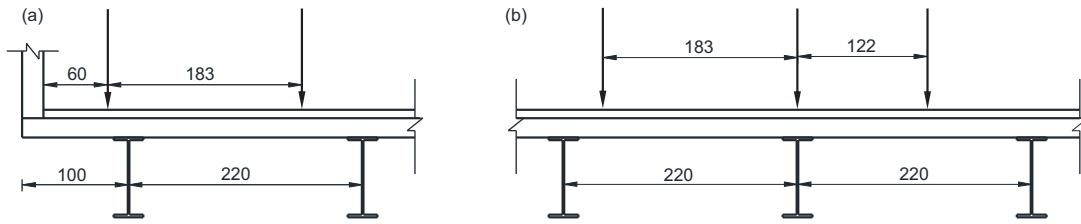
Figure 2.29 The transverse position of truck wheels associated with (a) exterior girder; and (b) interior girder for determining the lateral distribution factors (dimensions are in cm).
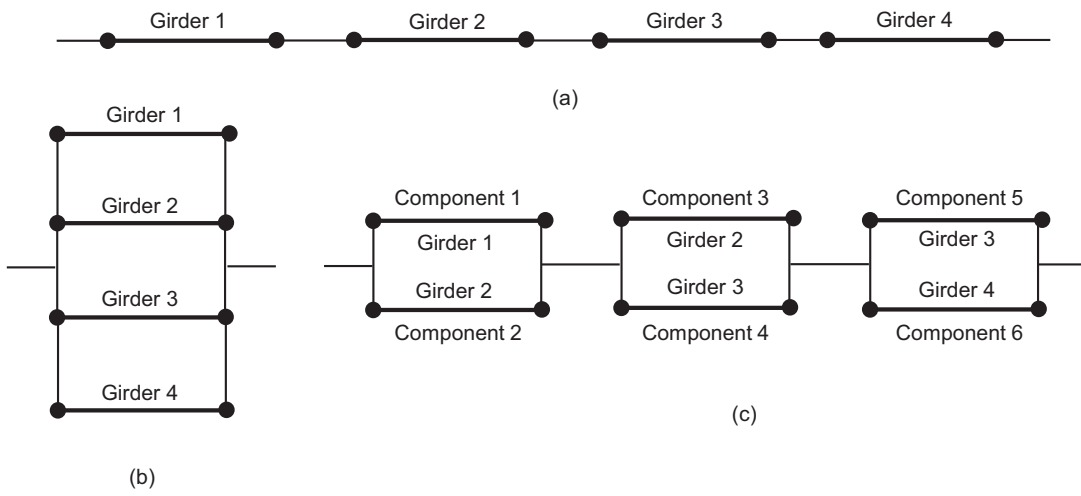
Figure 2.30 Three types systems of for the analyzed bridge: (a) series system; (b) parallel system; and (c) series-parallel system.

CHAPTER 3

RELIABILITY OF SYSTEMS WITH CODIFIED ISO-RELIABILITY COMPONENTS

3.1 INTRODUCTION

Due to the increased understanding of structural behavior and loading processes, the structural design theory has evolved significantly in the past decades. During the years 1930 to 1970, the sole design philosophy associated with the bridge design standards prescribed by the American Association of State Highway and Transportation Officials (AASHTO) was allowable stress design (ASD). The allowable stresses are calculated by dividing the material ultimate strength by a safety factor subjectively determined to account for uncertainties. Beginning in early 1970s, a new design philosophy referred to as load factor design (LFD) was introduced. The preliminary effort made in LFD is to recognize that the live load has more variability than the dead load and uncertainties in load prediction are considered through the load factors (Hansell and Viest 1971). However, no probabilistic concept was involved in the calibration of the factors for loads and resistances in LFD. In early 1990s, with the development of probability-based reliability theory (Ang and Tang 1975, Thoft-Christensen and Baker 1982, Ang and Tang 1984, Thoft-Christensen and Murotsu 1986), the bridge design philosophy moved from LFD to the load and resistance factor design (LRFD). This new design approach is probability-based and the uncertainties

associated with resistances and loads are incorporated quantitatively into the design process (Hsiao *et al.* 1990, Lin *et al.* 1992, Paikowsky 2004, Babu and Singh 2011).

According to LRFD bridge design specifications (e.g., AASHTO 2010), load and resistance factors in the strength limit state are calibrated using statistical studies. In the calibration process, a target reliability index is first selected to provide a minimum acceptable safety margin and then the load and resistances factors are determined to achieve a uniform level of reliability for all components (Kulicki *et al.* 1994). The target reliability index is currently provided only for the design of individual components of the bridge instead of the bridge system. It was recommended to use a target reliability index of 3.5 for the component design of bridge structures (AASHTO 2007, Kulicki *et al.* 1994, Kulicki *et al.* 2007). For bridge structures, the system reliability that reflects the overall level of structural safety is of paramount importance (Moses 1974, Bruneau 1992, Estes and Frangopol 1999, 2001, Imai and Frangopol 2002, Rakoczy 2012, Moses 1982). Moreover, as all components have a uniform reliability, the system reliability may not reach the predefined target since it is affected by several factors, such as system type, correlation among resistances of components, coefficients of variation of loads and resistances, and post-failure behavior of components. Therefore, it is necessary to investigate the impact of these factors on the system reliability and assess the reliability of systems consisting of components following uniform reliability design approach.

Among these factors, post-failure behavior describes the response of a material beyond the elastic limit. Ductile behavior is characterized by significant inelastic deformations before the material failure; while brittle behavior exhibits sudden loss of

load-carrying capacity immediately after the elastic limit is reached. Therefore, the post-failure behavior of components determines the load sharing and redistribution in the damaged system after component failure (Chen and Duan 1999). Consequently, this behavior has significant effects on both the reliability and redundancy of structural systems. The effects of post-failure material behavior on the redundancy factor for the design of structural components have been studied in the previous chapter. However, the evaluation of these effects on the reliability of systems, especially systems with large number of components, has not been investigated in detail for reliability-based design. Most structures consist of dozens or hundreds of members. It is computationally expensive to calculate the system reliability of these structures to check if they satisfy the predefined reliability design threshold. Therefore, obtaining results of reliability values for various types of systems consisting of large number of components considering different correlation cases will facilitate the reliability-based design process.

This study investigates the effects of several parameters on the system reliability and evaluates the reliability of various systems considering the post-failure behavior of components. Section 3.2 provides the procedure for calculating the reliability of a system consisting of uniform reliability components. Section 3.3 studies the effects of the coefficients of variation of resistance and load, mean value of load, correlation among the resistances of components, and system type on the system reliability. Section 3.4 illustrates the procedure for calculating the reliability of ductile, brittle, and mixed systems and investigates the effects of post-failure behavior factor on the reliability of parallel system. Section 3.5 evaluates the reliability of ductile and brittle

system with many components considering different correlation cases. In Section 3.6, a bridge example is used to demonstrate the application of the obtained results of systems reliability. Finally, Section 3.7 provides the conclusions of this chapter.

3.2 RELIABILITY OF SYSTEMS WITH UNIFORM RELIABILITY COMPONENTS

As mentioned previously, achieving a uniform reliability level of all components is the purpose of the LRFD design process. During the probabilistic design process, the goal is to find the mean values of the resistances of structural components since the probability distribution types, the associated statistical parameters (e.g., coefficients of variation of resistance and load, mean value of load), and the target reliability are usually provided. Therefore, for a system consisting of uniform reliability components, the mean resistances of components need to be determined to evaluate the system reliability index.

Consider a system consisting of N identical components and assume that the load effect acting on each component is P and the resistance of component i is R_i ($i = 1$, 2, …, N). Given the mean value of load $E(P)$, coefficients of variation of resistance and load $V(R_i)$ and $V(P)$, and probability distribution types of R_i and P, the mean resistance of component i, $E_{cs}(R_i)$, can be determined to meet a prescribed target reliability index $\beta_{cs} = 3.5$ in the component design. With these parameters and the correlation coefficients between the resistances of components i and j, denoted as $\rho(R_i, R_j)$, the system reliability index β_{sys} can be computed.

A brief example is provided herein to illustrate the above procedure. Assuming a three-component structure, three different systems can be formed: series, parallel, and series-parallel systems. The values of $E(P)$, $V(R_i)$, and $V(P)$ associated with the three components are assumed 10, 0.1, and 0.1, respectively. Three correlation cases among the resistances are considered: (a) $\rho(R_i,R_j) = 0$, no correlation; (b) $\rho(R_i,R_j) = 0.5$, partial correlation; and (c) $\rho(R_i,R_j) = 1$, perfect correlation. Two types of probability distribution are assumed for the resistances and loads of the components: normal and lognormal. Based on the above parameters, the mean resistances associated with the normal and lognormal distribution when the component reliability index is 3.5 are found to be $E_{cs,N}(R_i) = 16.861$ and $E_{cs,LN}(R_i) = 16.384$, respectively. By using these mean resistances, the reliability indices associated with the three systems are listed in Table 3.1.

It is observed that in the no correlation and partial correlation cases: (a) the reliability index of the series system is less than 3.5 while its counterpart of the parallel system is greater than 3.5; and (b) the system reliability associated with the normal distribution is slightly higher than that associated with the lognormal distribution. In the perfect correlation case, the system reliability is the same as the component reliability. This is because the correlation among the failure modes of the components in the perfect correlation cases is 1.0, and, therefore, the system can be reduced to a single component. Hence, the system reliability in this case is independent of system type and distribution type.

3.3 EFFECTS OF SEVERAL PARAMETERS ON THE SYSTEM RELIABILITY

The reliability of a system is affected by the statistical parameters associated with the resistances and loads of the components, such as $V(R_i)$, $V(P)$, $E(P)$, and $\rho(R_i,R_j)$. In this section, the effects of these parameters on the system reliability are investigated using non-deterministic systems with up to four components. The resistance and load associated with component i are assumed to be normally distributed random variables with $V(R_i) = 0.1$, and $V(P) = 0.1$, $E(P) = 10$, respectively.

The system reliability as function of $V(R)$, $V(P)$ and $E(P)$ in two-component systems associated with two extreme correlation cases (i.e., $\rho(R_i,R_j) = 0$ and 1) is plotted in Figure 3.1. It is noticed that (a) as $V(R)$ increases, the system reliability β_{sys} associated with the no correlation case ($\rho(R_i,R_j) = 0$) increases significantly in the parallel system, while it decreases slightly in the series system; (b) as $V(P)$ increases, β_{sys} associated with the no correlation case almost remains the same in the series system, while it decreases significantly in the parallel system; (c) β_{sys} is not affected by $E(P)$ in both systems associated with the no correlation case; and (d) in the perfect correlation case, β_{sys} in both systems is 3.5 and it is not affected by the change of $V(R)$, $V(P)$, and or $E(P)$.

Similarly, the effects of these parameters on the reliability of three-component systems are shown in Figure 3.2. It is found that (a) the variations of reliability associated with the series and parallel systems along with the increase of $V(R)$, $V(P)$, and $E(P)$ are similar to the observations for the two-component systems; and (b) the

reliability of series-parallel system almost remains the same as $V(R)$ or $V(P)$ increases in the no correlation case and it is also not affected by $E(P)$.

The effects of the aforementioned parameters on the system reliability are also investigated for the four-component systems, where four different systems can be obtained: series, parallel, series-parallel system A and series-parallel system B, as shown in Figure 3.3. An additional correlation case where $\rho(R_i, R_j) = 0.5$ is studied. The results associated with the effects of $V(R)$, $V(P)$, and $E(P)$ are presented in Figure 3.4 to Figure 3.6. In addition to the observations that are similar to those drawn from the two- and three-component systems, it is also found that (a) as the correlation among the resistances of component increases, the effects of $V(R)$ and $V(P)$ on the system reliability become less significant; while in the perfect correlation case, the reliability of all systems is independent of $V(R)$ and $V(P)$; (b) the effects of $V(R)$ and $V(P)$ on the reliability in the series-parallel system B are similar to those in the parallel system, but less significant than those of the parallel system; and (c) the reliability of series-parallel system A is almost not affected by $V(R)$ and $V(P)$ in the no correlation and partial correlation cases.

3.4 EFFECTS OF POST-FAILURE MATERIAL BEHAVIOR ON THE SYSTEM RELIABILITY

3.4.1 Reliability of Ductile System

The post-failure behavior affects the load redistribution in the system after the failure of component(s). Therefore, the failure modes of a system and the associated limit state equations are dependent on the post-failure behavior of components. Consider

the two-component ductile parallel system described in Section 2.5.1. It is subject to load $2P$; therefore, the load distributed to each component is P. Assuming that the resistance R_i ($i =1, 2$) and the load P follow normal distribution with $V(R_i)$, $V(P)$, and $E(P)$ equal to 0.05, 0.3, and 10, respectively, the mean resistance of each component $E_{cs}(R_i)$ is found to be 21.132 to meet the target component reliability index β_{cs} of 3.5. Substituting $E_{cs}(R_i) = 21.132$ into the system reliability analysis yields the reliability index associated with the three correlation cases ($\rho(R_1, R_1)$ =0, 0.5, and 1.0) are 3.60, 3.55, and 3.50, respectively.

Similarly, the reliability of three- and four-component ductile parallel systems described in Section 2.5.1 can be evaluated using the same procedure. The statistical parameters (i.e., $V(R_i)$, $V(P)$, and $E(P)$) of R and P herein are the same as those used in the above two-component ductile parallel system. Two probability distribution cases (i.e., normal and lognormal) are considered. For the lognormal distribution case, the mean resistance of each component $E_{cs}(R_i)$ when the component reliability index is 3.5 is found to be 27.194. Assuming that the load acting on the three- and four-component parallel system is $3P$ and $4P$, respectively, the reliability indices of the three- and four-component ductile parallel system associated with the two distributions are presented in Table 3.2. It is found that (a) as the correlation among the resistances of components increases, the system reliability associated with both distributions decreases; (b) the results associated with lognormal distribution is slightly lower than those associated with normal distribution; and (c) the reliability associated with the four-component ductile parallel system is higher than that associated with the three-component parallel system in both distribution cases.

129

3.4.2 Reliability of Brittle System

The two- and three-component brittle parallel system presented in Section 2.5.2 are used herein to study the reliability of brittle systems. Assuming that the load effect acting on the system is $2P$ and $3P$, respectively, the limit state equations associated two- and three-component systems are provided in Equations (2.6) and (2.11). Similarly, the failure modes and limit state equations for a four-component brittle parallel system subjected to load $4P$ can also be identified. Assuming that the resistances and load are normally distributed with the aforementioned parameters (i.e., $V(R_i) = 0.05$, $V(P) = 0.3$, and $E(P) = 10$), the reliability indices of the two-, three-, and four-component brittle parallel system associated with three correlation cases are shown in Table 3.3.

In addition to the four-component brittle parallel system, a $2p \times 2s$ brittle series-parallel system consisting of four components is analyzed herein (see Figure 3.3(d)). The load applied on this system is $2P$. Assuming the same resistance for all components, the initial load effect acting on each component is P. For each sub-parallel system, its failure modes are similar to those associated with the two-component brittle parallel system discussed previously. Therefore, the $2p \times 2s$ brittle series-parallel system has four failure modes: (a) mode I caused by failure of component 1 followed by component 2; (b) mode II caused by failure of component 2 followed by component 1; (c) mode III caused by failure of component 3 followed by component 4; and (d) mode IV caused by failure of component 4 followed by component 3. The limit state equations associated with modes I, II, III, and IV are, respectively,

$$g_1 = R_1 - P = 0 \qquad\qquad g_2 = R_2 - 2P = 0 \tag{3.1}$$

$$g_3 = R_2 - P = 0 \qquad\qquad g_4 = R_1 - 2P = 0 \tag{3.2}$$

$$g_5 = R_3 - P = 0 \qquad\qquad g_6 = R_4 - 2P = 0 \tag{3.3}$$

$$g_7 = R_4 - P = 0 \qquad\qquad g_8 = R_3 - 2P = 0 \tag{3.4}$$

where R_i (i =1, 2, 3, and 4) is the resistance of component i. By performing the same procedure, the reliability index of the $2p \times 2s$ brittle series-parallel system associated with three correlation cases is also presented in Table 3.3. It is observed that (a) increasing the correlation among resistances of brittle components leads to a higher system reliability; (b) the reliability of the brittle parallel system decreases as the number of components increases; and (c) the reliability indices associated with the four-component parallel and series-parallel systems are the same.

It should be noted that in addition to the ductile and brittle behavior discussed in this chapter, there are other types of post-failure behavior, such as strain hardening and softening where the load acting on a component increases and decreases after yielding, respectively. The procedure for identifying the failure modes and limit state equations in the strain hardening and softening cases are similar to that in the brittle case. Since the failed components in the strain hardening case still have the ability to take additional loads, the loads distributed to the survived components are less than those in the ductile case. Therefore, for the parallel and series-parallel systems having equally reliable components, the system reliability associated with the strain hardening case is higher than that associated with the ductile case. However, in the strain softening case, the opposite conclusion is valid.

3.4.3 Reliability of Mixed System

A system that has both ductile and brittle components is denoted as a mixed system, as mentioned in Section 2.5.3. Since a mixed system has brittle component(s), the system failure modes are affected by the failure sequence of its components. The process of identifying the limit state equations of a mixed system is similar to that of a brittle system discussed previously. The two-, three-, and four-component mixed parallel system and the $2p \times 2s$ mixed series-parallel system described in Section 2.5.3 are analyzed herein. The loads acting on these systems are $2P$, $3P$, $4P$, and $2P$, respectively. The number of possible mixed combinations for the two- to four-component systems is provided in Section 2.5.3.

Assuming that the load and resistances of the components in all systems follow normal distribution with $V(R_i) = 0.05$ and $V(P) = 0.3$, the reliability indices of the mixed systems consisting of two to four components associated with three correlation cases are presented in Table 3.4. It is noted that (a) the reliability indices of these mixed systems are at most 3.5 due to the existence of the brittle component(s) in the systems; (b) as the correlation among the resistances of the components increases, the reliability of the mixed system exhibits an increasing trend; and (c) for the $2p \times 2s$ mixed series-parallel system, the system reliability indices associated with the two combinations in which the number of brittle components is two are almost the same although the locations of the brittle components in the system are different; this indicates that the system reliability is not affected by the location of the brittle components in this series-parallel system.

Figure 3.7 shows the effect of the number of brittle components in the mixed parallel system on the system reliability index. It is noticed that (a) the system reliability decreases in the no correlation and partial correlation cases as the number of brittle components in the parallel system increases; and (b) increasing the correlation among the resistances of components leads to a lower system reliability in the ductile case, while a higher system reliability in both brittle and mixed cases.

3.4.4 Effects of Post-failure Behavior Factor

The two-, three-, and four-component systems discussed in Section 2.5.4 are used herein to examine the effect of post-failure behavior factor on the system reliability. All the components in a given system are assumed to have the same post-failure behavior factor δ ($0 \leq \delta \leq 1$). The procedure for identifying the failure modes and the associated limit state equations of a system where the post-failure behavior factors of its components are δ is similar to that of a brittle or mixed system.

Assuming that the load and resistances of the components follow normal distribution with $V(R_i) = 0.05$ and $V(P) = 0.3$, the reliability indices of the parallel systems associated with different post-failure behavior cases are calculated. The results are plotted in Figure 3.8 and Figure 3.9. It is noted that (a) as δ increases in the no correlation and partial correlation cases, the system reliability associated with the three parallel systems initially remains the same and then increases dramatically; (b) as the correlation among the resistances of components becomes stronger, the region of δ in which the system reliability remains the same increases; in the perfect correlation case, the system reliability is not affected by δ; (c) in the brittle case (i.e., δ

= 0) and most intermediate post-failure behavior cases (i.e., $0 < \delta < 1$), the system reliability associated with the perfect correlation case is the highest among the reliabilities associated with the three correlation cases; however, in the ductile case, the system reliability associated with the no correlation case is the highest; and (d) the differences in the system reliability associated with the three systems become less significant along with the increase of δ; more specifically, when $\delta = 1$ (i.e., ductile case), the reliabilities associated with the three parallel systems are almost the same.

3.5 RELIABILITY OF DUCTILE AND BRITTLE SYSTEMS WITH MANY COMPONENTS

According to the current AASHTO bridge design specifications, structural components are expected to have a uniform reliability index (i.e., 3.5). In order to ensure structural safety, the resulted system reliability needs to meet the target reliability level. However, evaluation of the reliability for systems consisting of many components is a very time-consuming task in the preliminary design stage. Therefore, it is necessary to generate standard tables of reliability indices for different types of ductile and brittle systems with many uniform reliability components. The values of system reliability index from these tables can provide a quick estimation of the system reliability in the preliminary design stage.

3.5.1 Reliability of Ductile Systems with Many Components

The assumptions for the loads acting on the N-component parallel and series-parallel systems associated with the ductile and brittle cases are provided in Section 2.6. For

134

an N-component series system, the load on the system is assumed to be P so that the load effect of each component is P, which is the same as the load applied to each component in the parallel and series-parallel systems. An N-component series system has N different failure modes and the limit state equation associated with the i_{th} failure mode is

$$g_i = R_i - P = 0 \tag{3.5}$$

where R_i and P = resistance and load associated with component i, respectively. This equation is independent of the post-failure behavior of components. The limit state equations for an N-component parallel system, a $mp \times ns$ series-parallel system, and a $ms \times np$ series-parallel system associated with ductile case are presented in Equations (2.12) to (2.14), respectively.

For the representative case where $V(R_i) = 0.05$, $V(P) = 0.3$ and $E(P) = 10$, the mean resistances lead to component reliability index 3.5 associated with the normal and lognormal case are 21.132 and 27.194, respectively, as mentioned in Section 3.4.1. Based on the limit state equations and aforementioned parameters (i.e., $V(R_i) = 0.05$, $V(P) = 0.3$ and $E(P) = 10$), the reliability indices of N-component (N = 100, 300, and 500) ductile systems associated with three correlation cases ($\rho(R_i,R_j) = 0$, 0.5 and 1.0) are computed by substituting the obtained mean resistance into the reliability analysis. The results are shown in Table 3.5 and Table 3.6. The impact of number of components on the reliability of series and parallel systems is plotted in Figure 3.10. It should be noted that the reliability index for the $ms \times np$ series-parallel systems can be calculated only up to $N = 25$ and the reason is provided in Section 2.6.1. Therefore, the

135

reliability indices of the *ms×np* series-parallel systems are not shown in the above tables.

It is observed that (a) when N is small ($N \leq 5$), the reliability of parallel systems becomes higher along with the increase of N; however, when $N > 5$, the system reliability is almost not affected by N; (b) as the correlation among the resistances of components increases, the system reliability exhibits an increasing trend in the series systems, while a decreasing tendency in the parallel systems; (c) the system reliability associated with the normal distribution is higher than that associated with the lognormal distribution in the parallel systems; however, an opposite conclusion can be drawn for the series systems; (d) the effect of the correlation among the resistance of components on the system reliability is more significant in the series systems than in the parallel systems; and (e) for the *mp×ns* series-parallel systems that have the same number of parallel components (i.e., m is the same in these systems), the system reliability decreases along with the increase of N.

3.5.2 Reliability of Brittle Systems with Many Components

As mentioned in Chapter 2, the number of failure modes of brittle parallel system increases dramatically as the number of components increases. In order to evaluate the reliability of brittle systems consisting of many components, an approximate method for estimation of the probability of system failure by simplifying the system model from an $N! \times N$ series-parallel system to an $N \times N$ series-parallel system is developed in Section 2.6.2. In this manner, the system reliability can be calculated for brittle systems consisting of up to 50 components.

The loads acting on the brittle systems are the same as those applied to the ductile systems so that the load associated with each component in the intact system is P. For the representative parameter case (i.e., $V(R_i) = 0.05$, $V(P) = 0.3$, and $E(P) = 10$), the reliability indices of N-component brittle systems are evaluated with respect to two probability distributions (normal and lognormal) and three correlation cases ($\rho(R_i,R_j) = 0$, 0.5 and 1.0) using the approximate approach. The results are listed in Table 3.7 and Table 3.8. Figure 3.11 illustrates the effects of number of components on the reliability of brittle systems.

It is observed that (a) when the number of components is fixed, the reliability indices associated with the series, parallel, and series-parallel systems are the same; this shows that for a brittle structure consisting of N equally reliable components, the system reliability is independent of the system type; (b) the reliability associated with all types of systems decreases as the number of components in the brittle system increases in the no correlation and partial correlation cases; this is different from the finding associated with the ductile systems; (c) as the correlation among the resistances of components becomes stronger, the reliability of all types of brittle systems associated with both distributions increases; and (d) in the no correlation and partial correlation cases, the system reliability associated with the lognormal distribution is higher than that associated with the normal distribution.

3.6 CASE STUDY: A BRIDGE EXAMPLE

A bridge example similar to the bridge described in Section 2.8 is used herein to demonstrate (a) the procedure for evaluating the reliability index of systems consisting

of equally reliable components; and (b) the effects of post-failure material behavior on the system reliability. Most parameters of this bridge are the same as those of the bridge in Section 2.8. The main difference between the two bridges is two post-failure behavior cases are considered for the girders in this bridge example.

According to Section 2.8, the maximum total bending moments acting on the exterior and interior girders due to both dead and live loads are $M_{L,ext} = 3407$ kN·m and $M_{L,int} = 3509$ kN·m, respectively. Assuming that the ultimate moment capacity of a girder $M_{U,i}$ and the total bending moment $M_{L,i}$ follow normal distribution with $V(M_{U,i}) = 0.05$ and $V(M_{L,i}) = 0.3$, respectively, the mean resistances of the exterior and interior girders when their reliability indices equal to 3.5 are obtained as $E_{cs}(M_{U,ext}) = 7200$ kN·m (exterior girder) and $E_{cs}(M_{U,int}) = 7415$ kN·m (interior girder).

Based on different definitions of the bridge system failure related to girders, three systems are formed: (a) series system (failure of any girder leads to system failure); (b) parallel system (system failure is caused by failure of all girders); and (c) series-parallel system consisting of three series of two adjacent girders in parallel (failure of any two adjacent girders leads to system failure), as shown in Figure 2.30. Two different material behavior cases associated with girders are considered herein: ductile and brittle. Based on the mean resistances, load effects and distribution parameters, the reliability indices of the three systems associated with ductile and brittle cases are obtained. The results are presented in Table 3.9.

It is noticed that (a) the reliability indices of the parallel system in ductile case are the same as those associated with the four-component ductile systems listed in Table 3.2; and (b) the reliability indices of the parallel systems in brittle case are identical to those associated with the four-component brittle systems presented in Table 3.3. This is because when the coefficients of variation of resistances and load associated with components are fixed (i.e., $V(R_i) = 0.05$, $V(P) = 0.3$), the reliability of system whose components have the same reliability is not affected by the mean value of the load acting on the system.

By comparing the reliability indices associated with the ductile and brittle cases, it is observed that the material behavior of girders has no effect on the reliability index of series system; however, for the parallel and series-parallel systems, the system reliability indices associated with ductile case are higher than those associated with brittle case, and the difference in the system reliability index between the two cases is more significant in the parallel system than that in the series-parallel system.

If a threshold for system reliability index is predefined (e.g., 3.5), it is seen that only the design of girders in the parallel system associated with the ductile case satisfies this threshold. This indicates the girders in the other systems require to be designed to have higher resistances. When the reliability index of girders is increased to 4.0, the mean resistances of girders are $E_{cs}(M_{U,ext}) = 7782$ kN·m (exterior girder) and $E_{cs}(M_{U,\mathrm{int}}) = 8015$ kN·m (interior girder). The reliability indices of the series and series-parallel systems associated with the ductile case and the series, parallel, and series-parallel systems associated with the brittle case are also presented in Table 3.9.

139

It is observed that they all satisfy the predefined system reliability threshold after the component reliability index of girders is increased.

3.7 CONCLUSIONS

In this chapter, the effects of several parameters on the reliability of systems consisting of uniform reliability components are studied and the reliability indices of ductile and brittle systems with many components are evaluated. The procedure for calculating the reliability of a system having equally reliable components is formulated. The impacts of the coefficients of variation of resistance and load, mean value of load, correlation between the resistances of components, and post-failure material behavior of components on the system reliability are investigated. Based on the proposed procedure, the system reliability evaluation is extended to ductile and brittle systems with large number of components. Finally, a bridge example is used to illustrate the above procedure and also demonstrate the effects of post-failure material behavior of components on the system reliability. The following conclusions are drawn:

1. For the no correlation and partial correlation cases, increasing the coefficient of variation of resistance leads to an increase and a decrease of reliability in the parallel and series systems, respectively. Conversely, the reliability of parallel system decreases significantly as the coefficient of variation of load increases while its counterpart of series system is slightly affected by this coefficient.

2. As the number of components (N) increases in the no correlation and partial correlation cases, the reliability of series system decreases; however, its effect

140

on the reliability of ductile parallel system depends on the value of N. When N is small, increasing it leads to a significant increase of the system reliability; however, as N becomes larger, this increase is less significant.

3. In the no correlation and partial correlation cases, the reliability associated with all types of brittle systems decreases as the number of components increases.

4. The reliability associated with all types of brittle systems increases as the correlation among the resistances of components becomes stronger.

5. The effect of the correlation among the resistances of components on the reliability in mixed system is similar to that in the brittle system. In the no correlation and partial correlation cases, the reliability of mixed parallel systems decreases as the number of brittle components increases.

6. As the post-failure behavior factor increases in the no correlation and partial correlation cases, the reliability of parallel systems initially remains the same and then increases dramatically. Increasing the correlation among the resistances of the components results in an extended region of the post-failure behavior factor during which the system reliability is almost not affected.

Table 3.1 Reliability indices of three-component systems.

Correlation	Normal			Lognormal		
	Series	Parallel	Series-parallel	Series	Parallel	Series-parallel
$\rho(R_i,R_j) = 0$	3.205	5.478	3.507	3.201	4.761	3.491
$\rho(R_i,R_j) = 0.5$	3.222	4.460	3.494	3.234	4.187	3.474
$\rho(R_i,R_j) = 1$	3.500	3.500	3.500	3.500	3.500	3.500

Note: $V(R_i) = 0.1$; $V(P) = 0.1$; $E(P) = 10$; $\beta_{cs} = 3.5$; $E_{cs,N}(R_i) = 16.861$; $E_{cs,LN}(R_i) = 16.384$.

Table 3.2   Reliability indices of three- and four-component ductile parallel systems associated with normal and lognormal distribution.

Correlation	Three-component parallel		Four-component parallel	
	Normal	Lognormal	Normal	Lognormal
$\rho(R_i,R_j) = 0$	3.645	3.538	3.670	3.543
$\rho(R_i,R_j) = 0.5$	3.568	3.519	3.576	3.521
$\rho(R_i,R_j) = 1$	3.500	3.500	3.500	3.500

Note: $V(R_i) = 0.05$; $V(P) = 0.3$; $E(P) = 10$; $\beta_{cs} = 3.5$; $E_{c,N}(R_i) = 21.132$; $E_{c,LN}(R_i) = 27.194$.

Table 3.3 Reliability indices of the two-, three-, and four-component brittle systems when R and P follow normal distribution.

Correlation	Two-component parallel	Three-component parallel	Four-component parallel	Four-component series-parallel
$\rho(R_i,R_j) = 0$	3.368	3.293	3.245	3.243
$\rho(R_i,R_j) = 0.5$	3.393	3.338	3.305	3.300
$\rho(R_i,R_j) = 1$	3.50	3.50	3.50	3.50

Note: $V(R_i) = 0.05$; $V(P) = 0.3$; $\beta_{cs} = 3.5$; $E_{c,N}(R_i) = 21.132$.

Table 3.4 Reliability indices of mixed systems when R and P follow normal distribution.

System		$\rho(R_i,R_j) = 0$	$\rho(R_i,R_j) = 0.5$	$\rho(R_i,R_j) = 1$
2-component parallel system	1 ductile & 1 brittle	3.458	3.462	3.50
3-component parallel system	1 ductile & 2 brittle	3.353	3.385	3.50
	2 ductile & 1 brittle	3.452	3.444	3.50
4-component parallel system	1 ductile & 3 brittle	3.286	3.332	3.50
	2 ductile & 2 brittle	3.345	3.381	3.50
	3 ductile & 1 brittle	3.444	3.447	3.50
4-component series-parallel system ($2p{\times}2s$ SP system)	1 ductile & 3 brittle	3.283	3.337	3.50
	2 ductile & 2 brittle Case A	3.335	3.368	3.50
	2 ductile & 2 brittle Case B	3.335	3.368	3.50
	3 ductile & 1 brittle	3.405	3.413	3.50

Note: $V(P) = 0.3$; $V(R) = 0.05$; $\beta_{cs} = 3.5$; $E_{c,N}(R) = 21.132$.

Table 3.5 Reliability indices of ductile systems associated with different correlation cases when R and P follow normal distribution.

	System	$\rho(R_i,R_j) = 0$	$\rho(R_i,R_j) = 0.5$	$\rho(R_i,R_j) = 1$
100-component system	Series system	2.793	2.977	3.50
	Parallel system	3.709	3.604	3.50
	$5p\times20s$ SP system	3.409	3.390	3.50
	$10p\times10s$ SP system	3.531	3.478	3.50
	$20p\times5s$ SP system	3.615	3.532	3.50
300-component system	Series system	2.669	2.892	3.50
	Parallel system	3.711	3.607	3.50
	$5p\times60s$ SP system	3.339	3.344	3.50
	$10p\times30s$ SP system	3.475	3.439	3.50
	$20p\times15s$ SP system	3.571	3.510	3.50
500-component system	Series system	2.617	2.855	3.50
	Parallel system	3.712	3.610	3.50
	$5p\times100s$ SP system	3.306	3.328	3.50
	$10p\times50s$ SP system	3.456	3.426	3.50
	$20p\times25s$ SP system	3.550	3.494	3.50

Note: $E(P) = 10$; $V(P) = 0.3$; $V(R) = 0.05$; $\beta_{cs} = 3.5$.

Table 3.6 Reliability indices of ductile systems associated with different correlation cases when R and P follow lognormal distribution.

System		$\rho(R_i,R_j) = 0$	$\rho(R_i,R_j) = 0.5$	$\rho(R_i,R_j) = 1$
100-component system	Series system	3.116	3.219	3.50
	Parallel system	3.556	3.526	3.50
	5p×20s SP system	3.409	3.426	3.50
	10p×10s SP system	3.469	3.469	3.50
	20p×5s SP system	3.509	3.500	3.50
300-component system	Series system	3.055	3.180	3.50
	Parallel system	3.557	3.527	3.50
	5p×60s SP system	3.375	3.401	3.50
	10p×30s SP system	3.439	3.451	3.50
	20p×15s SP system	3.490	3.476	3.50
500-component system	Series system	3.026	3.159	3.50
	Parallel system	3.558	3.529	3.50
	5p×100s SP system	3.361	3.392	3.50
	10p×50s SP system	3.432	3.442	3.50
	20p×25s SP system	3.481	3.474	3.50

Note: $E(P) = 10$; $V(P) = 0.3$; $V(R) = 0.05$; $\beta_{cs} = 3.5$.

Table 3.7 Reliability indices of brittle systems associated with different correlation cases when R and P follow normal distribution.

System		$\rho(R_i,R_j) = 0$	$\rho(R_i,R_j) = 0.5$	$\rho(R_i,R_j) = 1$
10-component system	Series system	3.097	3.196	3.50
	Parallel system	3.097	3.196	3.50
	5p×2s SP system	3.097	3.196	3.50
	5s×2p SP system	3.097	3.196	3.50
20-component system	Series system	2.996	3.122	3.50
	Parallel system	2.996	3.122	3.50
	5p×4s SP system	2.996	3.122	3.50
	10p×2s SP system	2.996	3.122	3.50
	5s×4p SP system	2.996	3.122	3.50
	10s×2p SP system	2.996	3.122	3.50
25-component system	Series system	2.967	3.102	3.50
	Parallel system	2.967	3.102	3.50
	5p×5s SP system	2.967	3.102	3.50
	5s×5p SP system	2.967	3.102	3.50
50-component system	Series system	2.877	3.035	3.50
	Parallel system	2.877	3.035	3.50
	5p×10s SP system	2.877	3.035	3.50
	10p×5s SP system	2.877	3.035	3.50
	5s×10p SP system	2.877	3.035	3.50
	10s×5p SP system	2.877	3.035	3.50

Note: $V(R) = 0.3$; $V(P) = 0.05$; $\beta_{cs} = 3.5$.

Table 3.8 Reliability indices of brittle systems associated with different correlation cases when R and P follow lognormal distribution.

System		$\rho(R_i,R_j) = 0$	$\rho(R_i,R_j) = 0.5$	$\rho(R_i,R_j) = 1$
10-component system	Series system	3.273	3.331	3.50
	Parallel system	3.273	3.331	3.50
	$5p\times2s$ SP system	3.273	3.331	3.50
	$5s\times2p$ SP system	3.273	3.331	3.50
20-component system	Series system	3.216	3.295	3.50
	Parallel system	3.216	3.295	3.50
	$5p\times4s$ SP system	3.216	3.295	3.50
	$10p\times2s$ SP system	3.216	3.295	3.50
	$5s\times4p$ SP system	3.216	3.295	3.50
	$10s\times2p$ SP system	3.216	3.295	3.50
25-component system	Series system	3.204	3.281	3.50
	Parallel system	3.204	3.281	3.50
	$5p\times5s$ SP system	3.204	3.281	3.50
	$5s\times5p$ SP system	3.204	3.281	3.50
50-component system	Series system	3.158	3.251	3.50
	Parallel system	3.158	3.251	3.50
	$5p\times10s$ SP system	3.158	3.251	3.50
	$10p\times5s$ SP system	3.158	3.251	3.50
	$5s\times10p$ SP system	3.158	3.251	3.50
	$10s\times5p$ SP system	3.158	3.251	3.50

Note: $V(R) = 0.3$; $V(P) = 0.05$; $\beta_{cs} = 3.5$.

Table 3.9 Four-girder bridge: reliability indices associated with ductile and brittle cases.

Correlation	Ductile			Brittle		
	Series	Parallel	Series-parallel	Series	Parallel	Series-parallel
$\rho(R_i,R_j) = 0$	3.245 (3.76*)	3.670	3.482 (4.02*)	3.245 (3.76*)	3.245 (3.76*)	3.245 (3.76*)
$\rho(R_i,R_j) = 0.5$	3.305 (3.79*)	3.576	3.455 (3.96*)	3.305 (3.79*)	3.305 (3.79*)	3.305 (3.79*)
$\rho(R_i,R_j) = 1$	3.50 (4.0*)	3.50	3.50 (4.0*)	3.50 (4.0*)	3.50 (4.0*)	3.50 (4.0*)

Note: * denotes the case where the reliability indices of girders are 4.0.
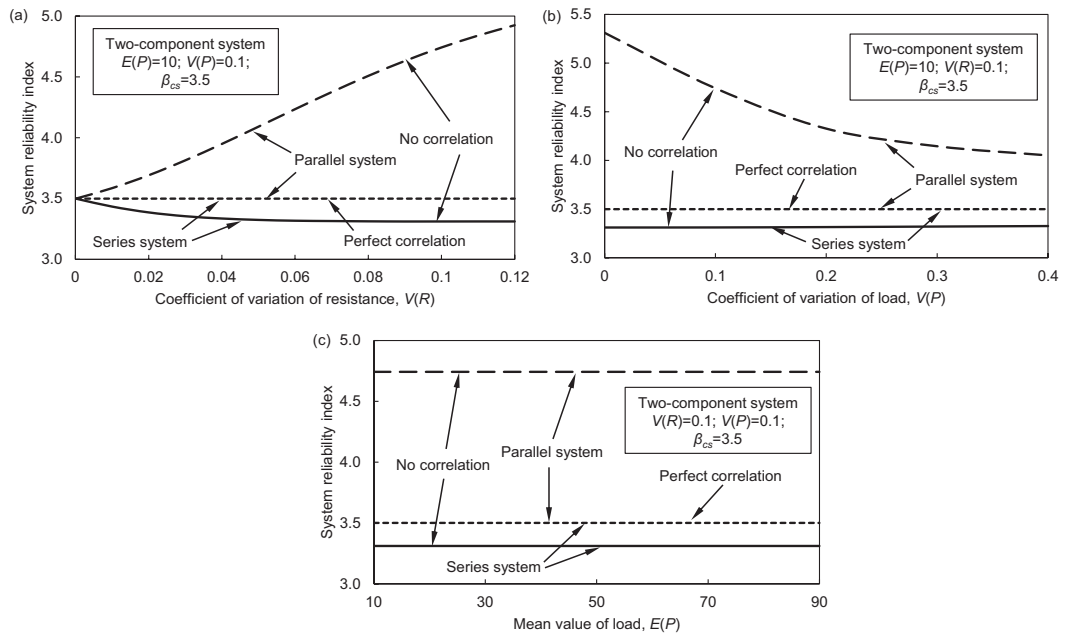
Figure 3.1   Effects of (a) $V(R)$; (b) $V(P)$; and (c) $E(P)$ on the reliability of two-component systems associated with no correlation and perfect correlation cases.
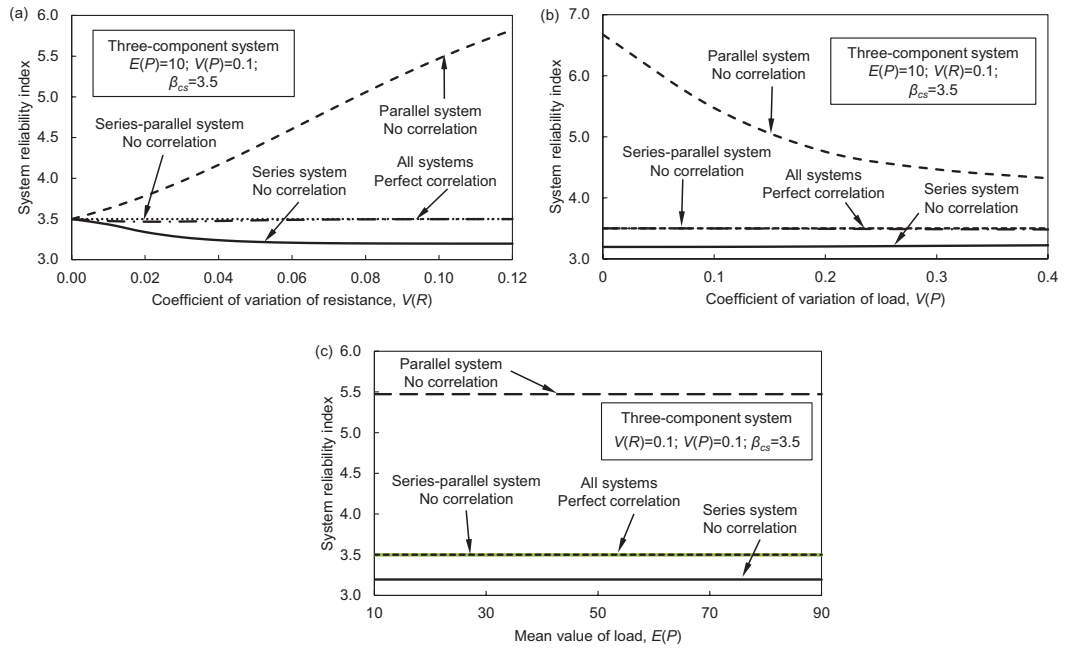
Figure 3.2   Effects of (a) $V(R)$; (b) $V(P)$; and (c) $E(P)$ on the reliability of three-component systems associated with no correlation and perfect correlation cases.
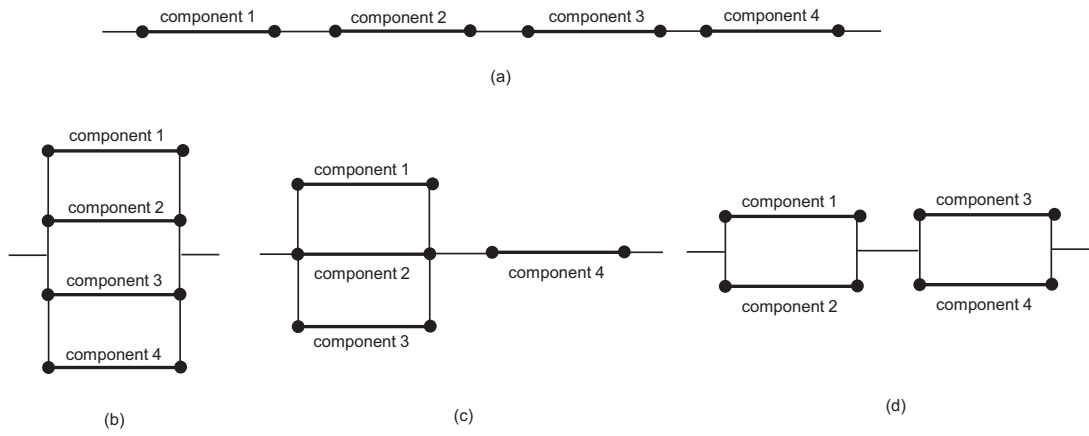
Figure 3.3 Four-component systems: (a) series system; (b) parallel system; (c) series-parallel system A; and (d) series-parallel system B.
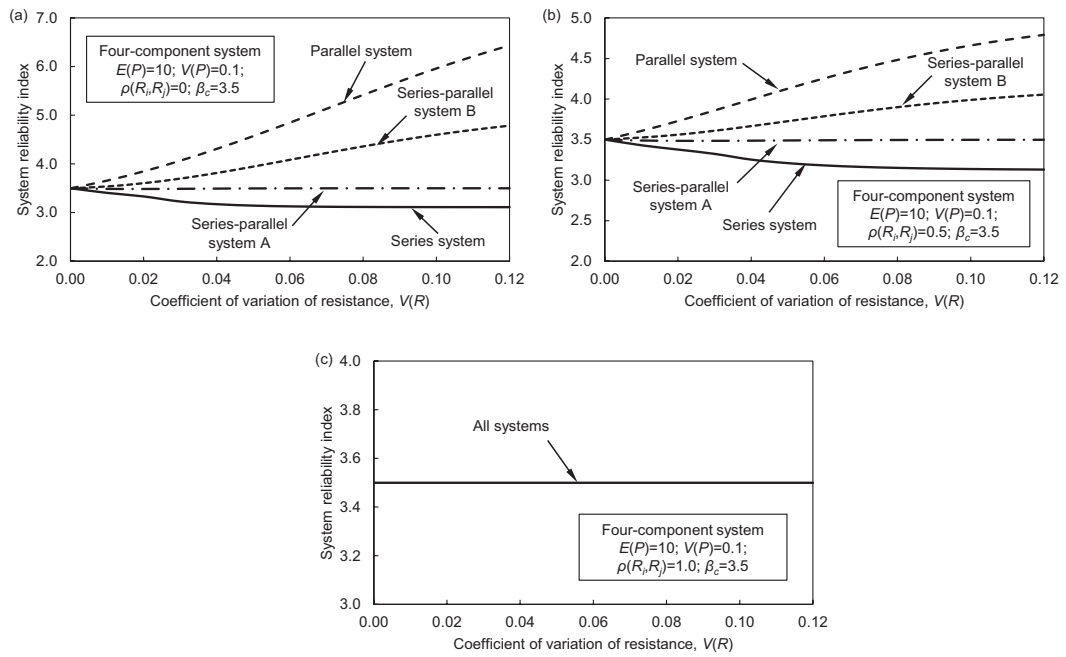
Figure 3.4   Effects of $V(R)$ on the reliability of four-component systems associated with the (a) no correlation; (b) partial correlation; and (c) perfect correlation case.
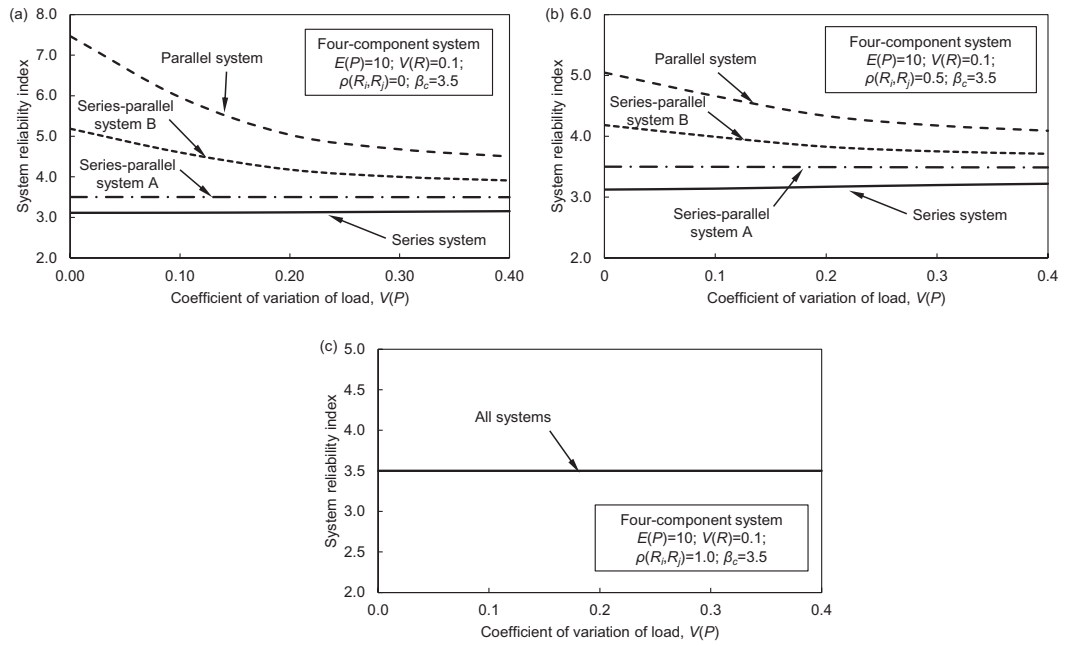
Figure 3.5 Effects of $V(P)$ on the reliability of four-component systems associated with the (a) no correlation; (b) partial correlation; and (c) perfect correlation case.

155
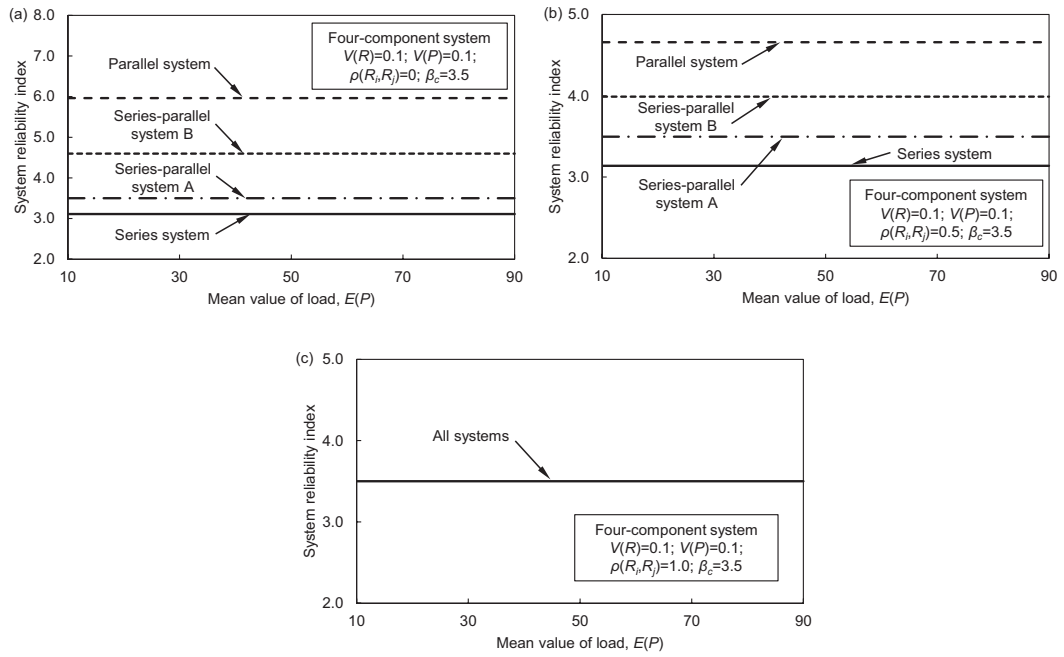
Figure 3.6 Effects of $E(P)$ on the reliability of four-component systems associated with the (a) no correlation; (b) partial correlation; and (c) perfect correlation case.

156
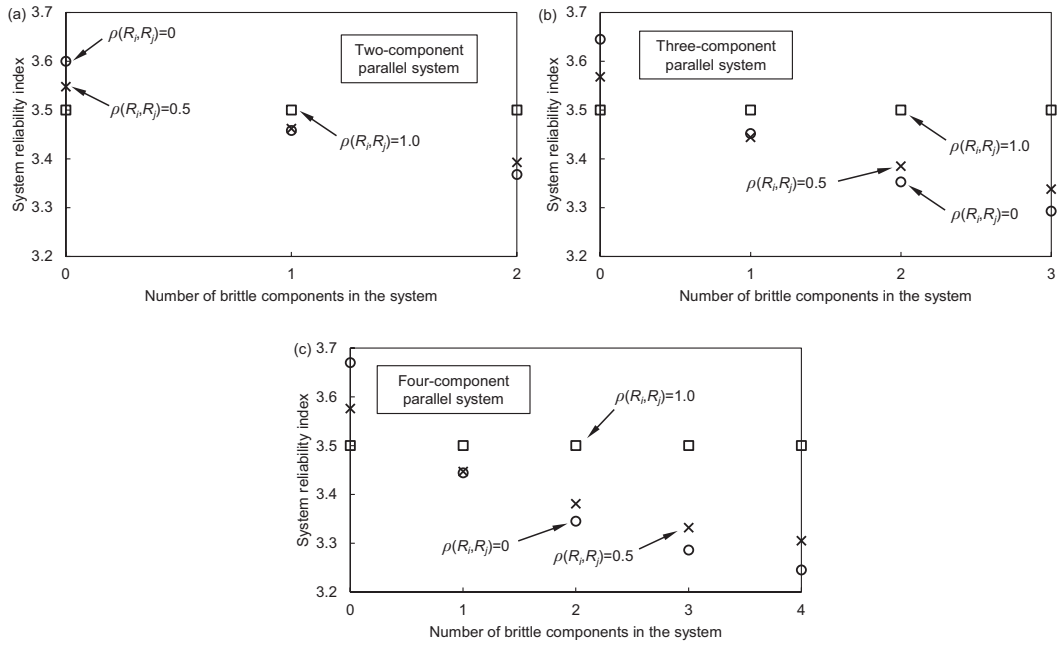
Figure 3.7 Effects of number of brittle components on the reliability of mixed systems consisting of: (a) two components; (b) three components; and (c) four components.
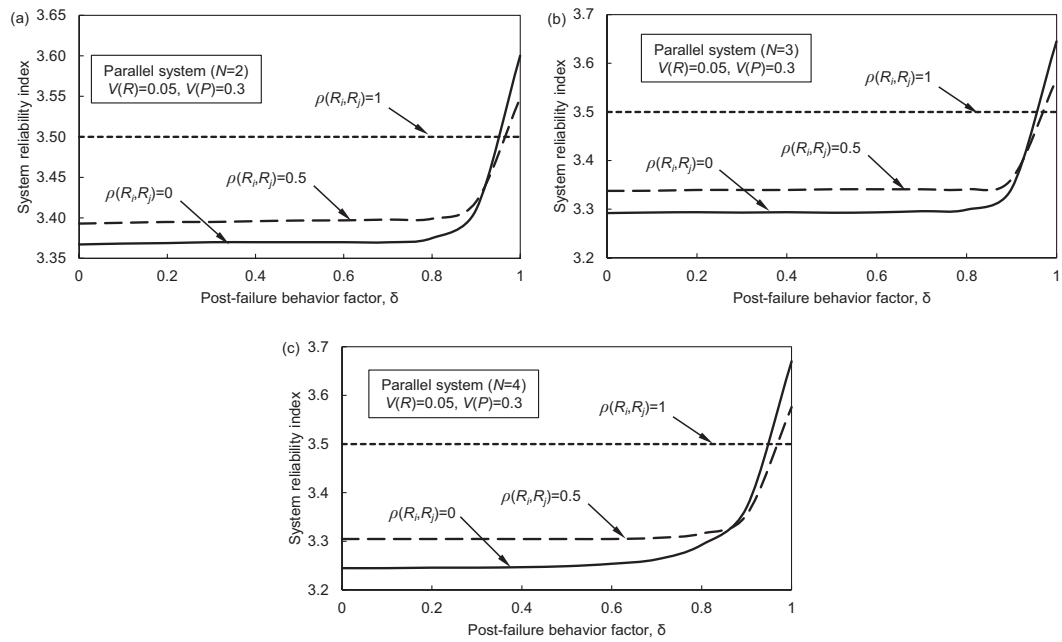
Figure 3.8   Effects of post-failure behavior factor δ on the reliability of parallel systems consisting of (a) two components; (b) three components; and (c) four components.

158
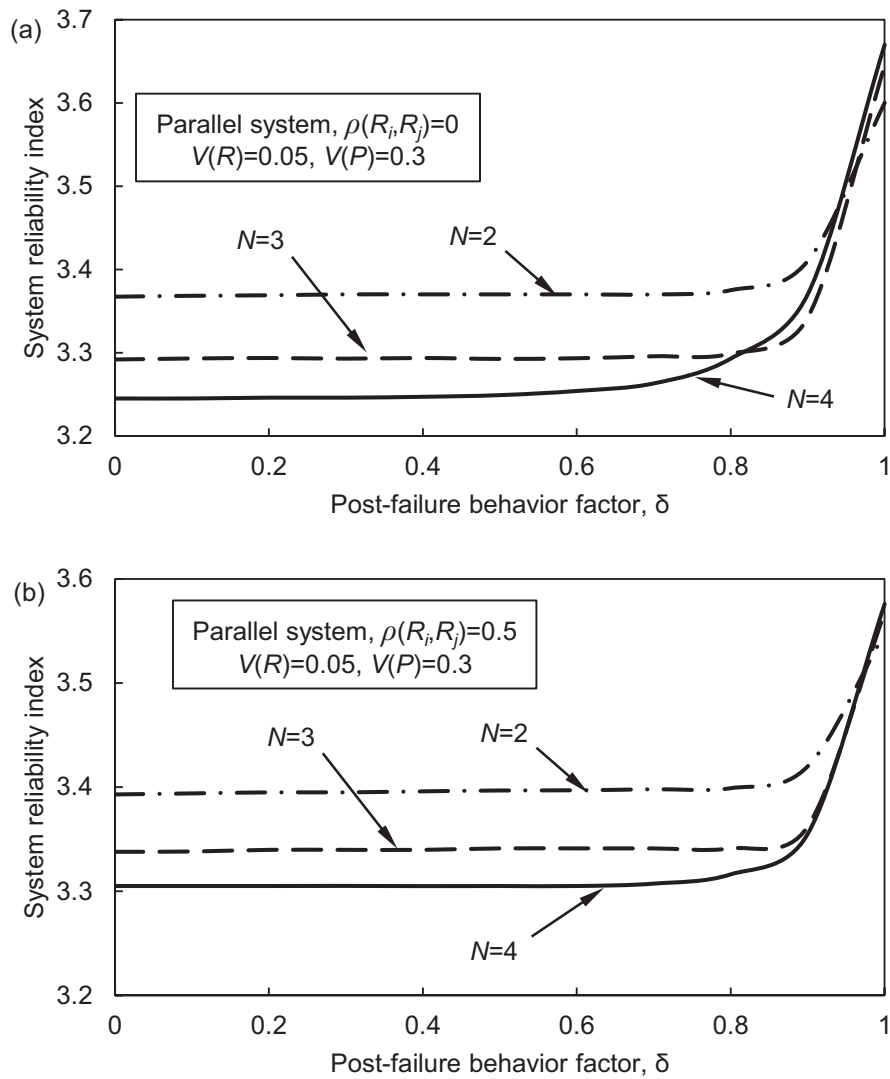
Figure 3.9 Effects of post-failure behavior factor δ on the system reliability associated with (a) no correlation; and (b) partial correlation case.
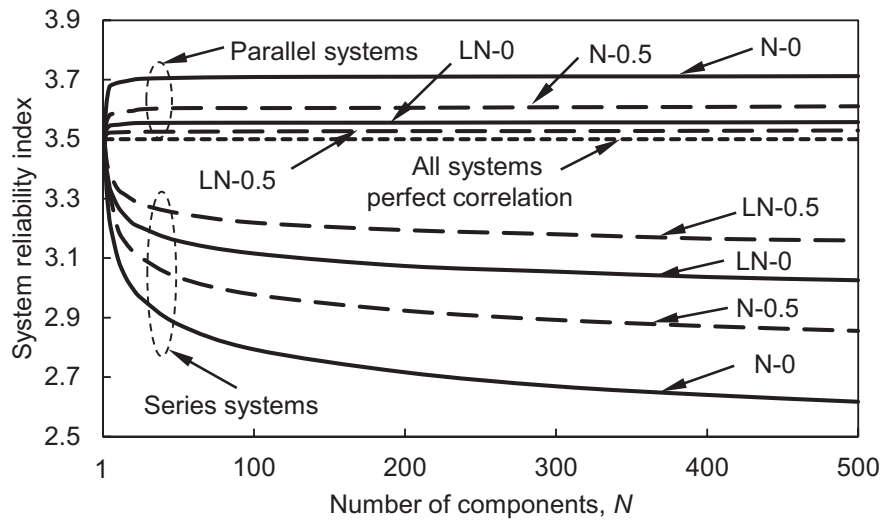
Figure 3.10   Effects of number of components on the reliability of ductile systems (Note: "N" denotes normal distribution; "LN" denotes lognormal distribution; "0" denotes $\rho(R_i,R_j) = 0$; "0.5" denotes $\rho(R_i,R_j) = 0.5$).
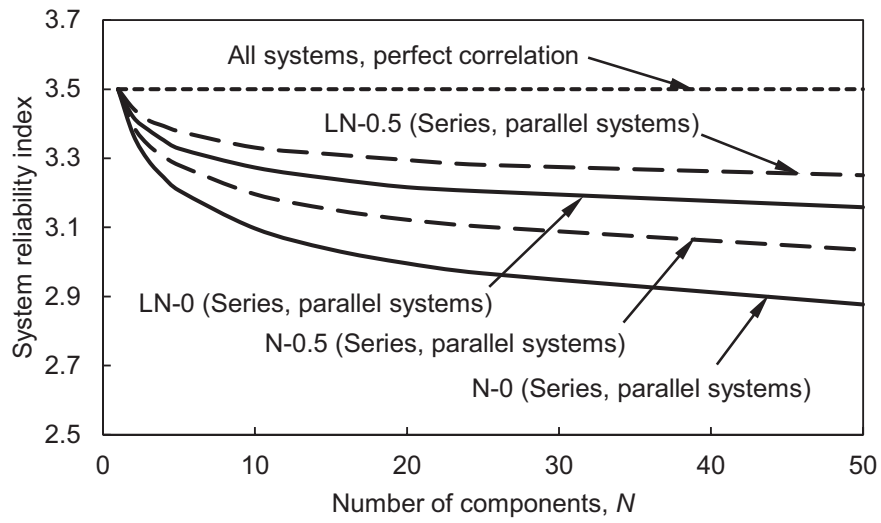
Figure 3.11 Effects of number of components on reliability of brittle systems (Note: "N" denotes normal distribution; "LN" denotes lognormal distribution; "0" denotes $\rho(R_i,R_j) = 0$; "0.5" denotes $\rho(R_i,R_j) = 0.5$).

CHAPTER 4

RELIABILITY, REDUNDANCY AND RISK AS PERFORMANCE INDICATORS OF STRUCTURAL SYSTEMS DURING THEIR LIFE-CYCLE

4.1 INTRODUCTION

It has been widely accepted that uncertainties exist in every aspect of the assessment process of structural safety. Due to these uncertainties, probabilistic methods have been proposed and applied in structural engineering planning and design (Ang and Tang 1984, Leemis 1995, Thoft-Christensen and Baker 1982). Probability-based system performance indicators, such as reliability index, redundancy index, and risk, have been introduced and used in design, assessment, inspection, maintenance, monitoring and prediction of the performance of structural systems (Frangopol and Curley 1989, Mansour 1997, Ellingwood 2005, Okasha and Frangopol 2009a, Moan 2005, Kim *et al.* 2011, Saydam and Frangopol 2011).

Due to mechanical and environmental stressors, structural systems start to deteriorate even before they are put into service. In addition, the loads acting on the structural systems may change over time as well. Therefore, the values of structural performance indicators are expected to time-variant. Structural systems can be generally modeled as series, parallel or series-parallel combination of the potential failure modes, depending on the definition of system failure. Therefore, studying the effect of time and system modeling type on the performance indicators can provide a

162

realistic description of structural performance over time and help improving the design and management of structural systems.

This chapter investigates the effects of the deterioration of structural resistance, system modeling type, and correlations among failure modes on the time-variant reliability, redundancy and risk of structural systems. Section 4.2 introduces the models for evaluation of the time-variant probability of failure, reliability index, redundancy index, direct and indirect risk, and total risk. Section 4.3 utilizes the systems consisting of three components to demonstrate the analysis of these structural performance indicators considering the aforementioned factors. In Section 4.4, the proposed approach is applied to an existing highway bridge in Colorado, USA. Finally, Section 4.5 provides the conclusion of this chapter.

4.2 TIME-VARIANT PERFORMANCE INDICATORS

4.2.1 Time-Variant Reliability

In structural reliability theory, the safe condition is the one in which the failure of the investigated component / system does not occur. For a structural component with resistance r and load effect s, its performance function is:

$$g = r - s \tag{4.1}$$

The probability that this component fails is:

$$P_{f(component)} = P[g < 0] \tag{4.2}$$

For a structural system with at least two failure modes, its failure probability is defined as the probability of violating any of the limit states that are defined by its failure modes:

$$P_{f(system)} = P[any\ g_i < 0] \tag{4.3}$$

where g_i = system performance function with respect to failure mode i. Due to the usual assumption of Gaussian distribution of performance functions, the reliability index associated with the evaluated structural component / system is given by:

$$\beta = -\Phi^{-1}(P_f) \tag{4.4}$$

where Φ = standard normal cumulative distribution function.

In many previous studies, loads and resistances are considered as time-independent random variables (Hendawi and Frangopol 1994, Wang and Wen 2000, Imai and Frangopol 2001, Zhao and Ono 2001, Lin and Frangopol 1996). Accordingly, the probability of failure obtained from Equation (4.3) is kept unchanged during the lifetime of a structure. However, in most practical cases, resistances and loads of a structure vary with time. In general, the resistances deteriorate and loads increase over time. Therefore, Equations (4.1) to (4.4) considering the time effects can be rewritten as:

$$g(t) = r(t) - s(t) \tag{4.5}$$

$$P_{f(component)}(t) = P[g(t) < 0] \tag{4.6}$$

$$P_{f(system)}(t) = P[any\ g_i(t) < 0] \tag{4.7}$$

$$\beta(t) = -\Phi^{-1}(P_f(t)) \tag{4.8}$$

where t = time. It should be noted that the probabilities of failure obtained from Equations (4.6) and (4.7) are instantaneous. They define the probability of failure at a point-in-time, rather than evaluate the probability within a specified time interval, which is known as cumulative probability of failure. Since the instantaneous probability of failure changes over time, it is time-variant. In this chapter, the "time-variant" performance indicators (reliability, redundancy, and risk) are considered as "point-in-time".

4.2.2 Time-Variant Redundancy

System redundancy has been defined as the availability of system warning before the occurrence of structural collapse (Okasha and Frangopol 2009a). Several studies have been performed in presenting measures of quantifying redundancy for structural design or assessment (Frangopol and Curley 1987, Okasha and Frangopol 2009a, Blagojevic and Ziha 2008, Ghosn and Moses 1998, Liu *et al.* 2001, Frangopol 2011). However, no agreement has been reached on redundancy measures yet. In this chapter, the time-variant redundancy index provided in (Frangopol 2011) is used:

$$RI(t) = \beta_s(t) - \beta_{fc}(t) \tag{4.9}$$

where $\beta_s(t)$ = system reliability index at time t, and $\beta_{fc}(t)$ = reliability index associated with the probability of the first component failure at time t.

The larger the difference between these two reliability indices, the higher redundancy the system has. This difference can be interpreted as the availability of system warning before failure. However, the redundancy defined in Equation (4.9) cannot be used as the only metric for assessing structural safety. For example, consider

two structures whose system reliability indices are 5.0 and 3.0, respectively, and the reliability indices of first component failure are 3.0 and 1.0, respectively. Obviously, the two systems have the same redundancy index (i.e. 2.0); however, the first system is much more reliable than the second one. Therefore, the redundancy index defined in Equation (4.9) should be combined with the information on other performance indicators (such as system reliability and risk) to obtain a more complete assessment of time-variant structural performance.

4.2.3 Time-Variant Risk

Risk has become an increasingly important performance indicator. It is defined as the combined effect of probabilities and consequences of some failure or disaster in a given context:

$$R(t) = P_f(t) \times C(t) \tag{4.10}$$

where $R(t)$ = risk caused by a failure in a given context at time t, $P_f(t)$ = probability of failure at time t, and $C(t)$ = consequences caused by the failure at time t. The time-variant probability of a component or system failure, $P_f(t)$, can be obtained after identifying the performance function of the component or the failure modes of the system.

Consequences caused by the failure of components or system consist of two parts: (a) direct consequences, $C_{DIR}(t)$, which are related to local components failure; and (b) indirect consequences, $C_{IND}(t)$, which are associated with subsequent system failure (Baker *et al.* 2006). Direct consequences are considered proportional to the initial damage since they include only the commercial loss aspect (i.e., the cost required to

replace the damaged component / system), while the indirect consequences are not proportional to the initial damage because they consist of several loss aspects, such as safety loss, commercial loss and environmental loss (Hessami 1999). An event-tree model for a general case where component i fails is shown in Figure 4.1. In this figure, $F_{comp,i}$ denotes the event that component i fails; $F_{subsys} \mid F_{comp,i}$ and $\overline{F}_{subsys} \mid F_{comp,i}$ represent the events that the subsequent system fails and survives given the failure of component i, respectively. The subsequent system discussed herein is the system without component i. In branch b_1, only direct consequence exists since only component i fails and the subsequent system survives. However, in branch b_2, both direct and indirect consequences occur because the subsequent system fails after failure of component i.

Based on the classification of the consequences (i.e., direct and indirect consequences), the risk at time t caused by the failure of component i can be divided into direct risk $R_{DIR,i}(t)$ and indirect risk $R_{IND,i}(t)$, which are computed as:

$$R_{DIR,i}(t) = P_{f,comp,i}(t) \times C_{DIR,i}(t) \tag{4.11}$$

$$R_{IND,i}(t) = P_{f,comp,i}(t) \times P_{f,subsys|comp,i}(t) \times C_{IND,i}(t) \tag{4.12}$$

where $P_{f,comp,i}(t)$ = failure probability of component i at time t, $P_{f,subsys|comp,i}(t)$ = probability of subsequent system failure at time t given the failure of component i, $C_{DIR,i}(t)$ = direct consequences at time t associated with the failure of component i (i.e., the cost to replace this component), and $C_{IND,i}(t)$ = indirect consequences at time t caused by the failure of component i (i.e., the cost to rebuild the subsequent system,

safety loss, and environmental loss). Finally, the total risk caused by the failure of component i is:

$$R_{TOT,i}(t) = R_{DIR,i}(t) + R_{IND,i}(t) \tag{4.13}$$

4.3 PERFORMANCE INDICATORS OF THREE-COMPONENT SYSTEMS

As mentioned previously, most structures can be modeled as series, parallel, or series-parallel systems. Three types of three-component systems shown in Figure 4.2 are used herein to study the effects of the resistance deterioration, system modeling type, and correlations among the failure modes of components on the time-variant reliability, redundancy, and risk.

To study the effects of time on the performance indicators of components and systems, a resistance deterioration model presented in Okasha and Frangopol (2009a) is used herein. It is assumed that the deterioration in resistance is mainly due to a continuous cross-section loss over time. The mean $\mu_{Ri}(t)$ and standard deviation $\sigma_{Ri}(t)$ of the resistance of component i at time t are:

$$\mu_{Ri}(t) = \left[1 - DR_i(t)\right]^t \times A_i(0) \times \left(\mu_{Fy}\right)_i \tag{4.14}$$

$$\sigma_{Ri}(t) = \left[1 + DR_i(t)\right]^t \times A_i(0) \times \left(\sigma_{Fy}\right)_i \tag{4.15}$$

where $A_i(0)$ = initial cross-sectional area of component i, $DR_i(t)$ = deterioration rate of component i at time t, and $\left(\mu_{Fy}\right)_i$ and $\left(\sigma_{Fy}\right)_i$ = mean and standard deviation of the material yield stress F_y of component i, respectively. The yield stress F_y and load effect

on the system are assumed to be lognormally distributed and F_y is also considered as constant over time.

The distribution parameters of the yield stress and load effect associated with each component are presented in Table 4.1. The initial cross-sectional areas and deterioration rates of components are assumed to be deterministic. The deterioration rates of components 1 and 2 are constant during lifetime, while their counterpart of component 3 follows an exponential function so that it increases over time. With the parameters given in Table 4.1, the mean and standard deviation of the resistance of each component at time t can be obtained using the deterioration models presented in Equations (4.14) and (4.15).

Two cases of correlations among the failure modes of components are considered: statistically independent case, i.e., $\rho(g_i, g_j) =0$, and perfectly correlated case, i.e., $\rho(g_i, g_j) =1$, where ρ is the correlation efficient. It should be noted that perfect correlation doesn't mean that all the components will fail together. This situation occurs only when the performance functions of all the components are identical. Assuming that the service life of the system is 50 years, reliability, redundancy and risk for the three-component systems associated with two extreme correlation cases are evaluated.

4.3.1 Reliability Analysis

The time-variant reliability indices of the three systems (Figure 4.2) are calculated using RELSYS (Estes and Frangopol 1998). The results are plotted in Figure 4.3. It is observed that (a) in the perfect correlation case, the reliability of series system is decided by the lowest component reliability during lifetime, i.e., $\min[\beta_1; \beta_2; \beta_3]$, while

the reliability of parallel system is determined by the highest component reliability

during lifetime, i.e., $\max[\beta_1; \beta_2; \beta_3]$; (b) for the series-parallel system with perfectly

correlated failure modes, the system reliability can be obtained by comparing the

reliability of series component and the reliability of the subsequent system consisting

of two parallel components, i.e., $\min[\beta_3; \max(\beta_1; \beta_2)]$; (c) for the series system, the

system reliability in the independent case is slightly lower than that associated with the

perfectly correlated case; and (d) for the parallel system, the system reliability in the

independent case is much higher than that associated with the perfectly correlated case.

Given a predefined reliability index threshold, the lifetime of a component /

system is considered as the period of time during which the reliability index of the

component / system is not lower than the threshold. It is computed by finding the time

when the reliability index reaches its threshold. For different reliability index

thresholds, the lifetimes of components and systems are listed in Table 4.2. It is

observed that (a) component 2 has the longest lifetime among three components due to

its lowest deterioration rate; (b) for the series and series-parallel system, correlations

among failure modes of components have no significant effect on system lifetime;

however, for the parallel system, the lifetime associated with the independent case is

longer than that associated with the perfectly correlated case; and (c) the lifetime of

parallel system is much longer than the lifetimes associated with the other two types of

systems regardless of the correlation cases.

In order to find the effects of the components combination on the reliability of

series-parallel system, three combinations of components are investigated herein, as

shown in Figure 4.4. The reliability profiles associated with combinations II and III

170

are plotted in Figure 4.5. Figure 4.3(d) and Figure 4.5 show that in the independent case, system reliability is usually controlled by the reliability of the series component; however, if the reliability of the series component decreases much more slowly than those of the other parallel components (i.e., in "Combination II"), system reliability will be lower than the reliability of the series component.

Table 4.3 shows the lifetimes of the series-parallel systems with different combinations of components. For "Combination I" and "Combination III", the lifetimes associated with the independent and perfectly correlated cases are almost the same. However, for "Combination II", the difference in lifetime between the two correlation cases is significant. In the perfectly correlated case, the lifetimes of "Combination I" and "Combination II" are the same while "Combination III" has slightly shorter lifetime than the other two combinations. However, in the independent case, the effect of components combination on system lifetime is significant; it is observed that "Combination II" has the longest lifetime. Therefore, although the components of series-parallel system are the same, different combinations of components could lead to different lifetimes of system.

To study the effect of the correlation among the failure modes on the reliability of series-parallel system, five correlation cases listed in Table 4.4 are considered for "Combination I": (a) the failure modes of all components are statistically independent, denoted as "IN_{123}"; (b) the failure modes of all components are perfectly correlated, denoted as "PC_{123}"; (c) only the failure modes of component 1 and 2 are perfectly correlated, denoted as "IN_{13}, IN_{23}, PC_{12}"; (d) only the failure modes of component 1

171

and 3 are perfectly correlated, denoted as "IN_{12}, IN_{23}, PC_{13}"; and (e) only the failure modes of component 2 and 3 are perfectly correlated, denoted as "IN_{12}, IN_{13}, PC_{23}".

The system reliability indices associated with the five different correlation cases are plotted in Figure 4.6. It is found that (a) the effect of the correlations among the failure modes of components on the reliability of series-parallel system is not significant; therefore, the system lifetimes associated with these five correlation cases are almost the same; (b) in the three correlation cases where the two parallel components are independent, their system reliability indices are almost the same during the whole lifetime, and their reliability indices are the highest among these five cases; and (c) the case in which only the two parallel components are perfectly correlated has the lowest system reliability.

4.3.2 Redundancy Analysis

A series system has no redundancy because the system will fail if any component fails. Therefore, only parallel and series-parallel systems are studied in this section. The time-variant redundancy of the two systems associated with the two extreme correlation cases are plotted in Figure 4.7, Figure 4.8 and Figure 4.9. It is noticed that (a) the system redundancy index can decrease or increase over time; (b) for both systems, redundancy associated with the independent case is higher than that associated with the perfectly correlated case; and (c) the difference of system redundancy between the two extreme correlation cases is more significant in the parallel system than in the series-parallel system.

4.3.3 Risk Analysis

This section investigates the time-variant direct, indirect and total risk caused by: (a) only one component failure; and (b) system failure in two extreme correlation cases. For a three-component system, risk caused by component or system failure can be evaluated using an event-tree model. The event-tree model for risk analysis associated with only one component failure is shown in Figure 4.10. In the three main branches, $E_i \overline{E_j} \overline{E_k}$ denotes the event that component i fails while components j and k survive. For the independent (INDP) and perfectly correlated (PC) cases, the probabilities of the event $E_i \overline{E_j} \overline{E_k}$, respectively, are:

$$P(E_i \overline{E_j} \overline{E_k})_{INDP} = P(E_i) \cdot [1 - P(E_j)] \cdot [1 - P(E_k)] \tag{4.16}$$

$$P(E_i \overline{E_j} \overline{E_k})_{PC} = \max \left\{ 0; P(E_i) - \max \left[P(E_j), P(E_k) \right] \right\} \tag{4.17}$$

where $P(E_i)$, $P(E_j)$, and $P(E_k)$ = failure probabilities associated with components i, j and k, respectively. In the following six branches, $F_i \mid E_i \overline{E_j} \overline{E_k}$ and $\overline{F_i} \mid E_i \overline{E_j} \overline{E_k}$ represent the events that the damaged system (without component i) fails and survives, respectively. Therefore, the probabilities of occurrence of the paths b_{i0} and b_{i1}, respectively, are

$$P(b_{i0}) = P(E_i \overline{E_j} \overline{E_k}) \cdot [1 - P(F_i \mid E_i \overline{E_j} \overline{E_k})] \tag{4.18}$$

$$P(b_{i1}) = P(E_i \overline{E_j} \overline{E_k}) \cdot P(F_i \mid E_i \overline{E_j} \overline{E_k}) \tag{4.19}$$

For the branches corresponding to the path b_{i0}, only direct consequences exist since only component i fails. However, for the branches related to the path b_{i1}, both

173

direct and indirect consequences are present because both component i and the damaged system (i.e., without component i) fail. Therefore, the direct and indirect risks caused by only component i failure, respectively, are

$$R_{DIR,i} = P(b_{i0}) \cdot C_{DIR,i} + P(b_{i1}) \cdot C_{DIR,i} = P(E_i \overline{E_j} \overline{E_k}) \cdot C_{DIR,i} \tag{4.20}$$

$$R_{IND,i} = P(b_{i1}) \cdot C_{IND,i} = P(E_i \overline{E_j} \overline{E_k}) \cdot P(F_i \mid E_i \overline{E_j} \overline{E_k}) \cdot C_{IND,i} \tag{4.21}$$

which are similar to those presented in Equations (4.11) and (4.12).

In this chapter, the direct consequences associated with each component failure and the indirect consequences associated with subsystem failure are assumed to be $10,000 and $100,000 respectively. The risk threshold is assumed to be 10^{-2} and risks below this threshold are neglected. By using the event-tree model and the equations above, the direct and indirect risks caused by the failure of only one component associated with two extreme correlation cases in different systems are plotted in Figure 4.11 and Figure 4.12.

It is observed from Figure 4.11 that (a) even under the assumption that direct loss is the same for each component (i.e., $10,000), the direct risks caused by the failures of different components are still different due to the differences in their failure probabilities; (b) the direct risks due to component failure is independent of system type and it is only related to the failed component itself; and (c) in the independent case, all the direct risks increase over time; however, in the perfect correlation case, the direct risks associated with components 1 and 3 have a dramatic decrease and increase at $t = 38$ and 39 years, respectively; the direct risk associated with component 2 in the perfect correlation case is much lower than the predefined threshold; therefore,

it is not shown in this figure. The results in this figure indicate that the correlation among the failure modes of components has significant effect on the direct risks.

Figure 4.12 shows that (a) the indirect risks due to the failures of different components are significantly different in all systems; (b) failure of the same component leads to different indirect risks in different systems; among all the three systems, the indirect risks associated with the parallel systems due to the failure of single component is the lowest; and (c) in the series and series-parallel systems, the indirect risks associated with the independent case are higher than those associated with the perfectly correlated case; however, in the parallel system, the indirect risk due to failure of component 3 associated with the independent case is lower than that associated with the independent case.

The total risks due to the failure of single component in different systems are shown in Figure 4.13. It is found that (a) the total risks due to the failure of single component associated with the independent case are higher than those perfectly correlated case; (b) in the independent case, failure of component 1 (or 2) causes higher total risk to the series system than to the other systems; however, the total risks due to failure of component 3 associated with the series and series-parallel systems are almost the same and they are higher thant that associated with the parallel system; and (c) the total risk caused by failure of component 2 is much lower than those caused by failure of component 1 or 3. Therefore, it can be concluded that the failure of the same component in different systems could cause different total risks to these systems. In general, if a component is part of a series system, and an identical component is part

175

of a parallel system, the component failure will cause higher total risk to the series system than to the parallel system.

The total risks due to the failure of single component and the system associated with the independent and perfectly correlated cases are plotted in Figure 4.14 and Figure 4.15, respectively. Figure 4.14 shows that in the independent case (a) the total risk due to the failure of series system is slightly higher than that associated with component failure; however, contrary finding is observed in the parallel system due to the very low failure probability of the parallel system; (b) the total risk associated with the failure of series-parallel system is determined by its counterpart associated with the failure of component 3 which is in the series position of the system; and (c) failure of the parallel system leads to much lower total risk than failure of the other two systems.

It is observed from Figure 4.15 that in the perfectly correlated case (a) the total risk due to the failure of series system is slightly higher than those due to component failure; however, in the parallel system, the total risk caused by system failure is lower than those caused by component failure; this is similar to the conclusion drawn in the independent case; and (b) the risk profiles associated with failure of components 1 and 3 have a sudden decrease and increase, respectively; the total risks due to failure of component 2 are not shown in the figure because they are much lower than the predefined risk threshold in all the systems.

It is noted from Figure 4.10 that, for a system consisting of three components, the event-tree model has already six branches if only one component failure is considered. For a real structure with many members, using this event-tree model may lead to

combinatorial explosion problem which threatens the assessment of direct / indirect risk of the structure. Since the combinatorial explosion problem usually arises in risk assessment and decision-making areas which are closely related to event-tree and fault-tree models, research on this problem has been extensively performed in the recent decades. Kirkwood (1993) developed an algebraic approach to address the combinatorial explosion of decision tree scenarios. Later, Binary Decision Diagrams (BDD) was introduced and proved to be an efficient approach to perform event-tree and fault-tree analysis (Andrews and Dunnett 2000, Jung *et al.* 2004). Therefore, considering the available computational resources, the application of the risk assessment event-tree model in this chapter to real structures is feasible.

4.4 CASE STUDY: AN EXISTING HIGHWAY BRIDGE

An exsiting highway bridge in Colorado is presented herein as a case study. Bridge E-17-AH is located on 40th Avenue (State Highway 33) between Madison and Garfield Streets in Denver, Colorado. The bridge has three simple spans of equal length (13.3 m) and a total length of 42.1m as shown in Figure 4.16 (Estes 1997, Estes and Frangopol 1999). The deck consists of a 22.9 cm layer of reinforced concrete and a 7.6 cm surface layer of asphalt. The east–west bridge has two lanes of traffic in each direction with an average daily traffic of 8,500 vehicles. The roadway width is 12.18 m with 1.51 m pedestrian sidewalks and handrailing on each side. The slab is supported by nine standard-rolled, compact, and non-composite steel girders as shown in Figure 4.17 (Estes 1997, Estes and Frangopol 1999). Each girder is supported at one

end by a fixed bearing and an expansion bearing at the other end (Estes 1997, Estes and Frangopol 1999). The service life of this bridge is assumed to be 80 years.

Since the main objective of this case study is to demonstrate the effects of corrosion, system modeling type, and correlations among the failure modes of components on the system performance indicators rather than perform an accurate assessment of bridge safety, the failure modes of the bridge's substructure and deck are not taken into account and the system failure is modeled as the combination of only girders' flexural failure. Three types of system failure modes are considered: (a) failure of any girder leads to system failure; (b) system failure is caused by failure of all girders; and (c) failure of any two adjacent girders leads to system failure. Considering the symmetry within the span, the system models can be simplified, as shown in Figure 4.18 (the girders are numbered in Figure 4.17). The limit-state equations of girders 1 to 5 are listed as follows (Estes 1997):

$$g(1) = Z_e(t)F_y\gamma_{mfg} - 145.32\lambda_{conc} - 37.3\lambda_{steel} - M_{trk-e}(t)DF_e I_{beam} = 0 \tag{4.22}$$

$$g(2) = Z_i(t)F_y\gamma_{mfg} - 244.08\lambda_{conc} - 28.8\lambda_{asph} - 31.7\lambda_{steel} - M_{trk-i}(t)DF_{i-e} I_{beam} = 0 \tag{4.23}$$

$$g(3,4,5) = Z_i(t)F_y\gamma_{mfg} - 197.65\lambda_{conc} - 57.64\lambda_{asph} - 31.7\lambda_{steel} - M_{trk-i}(t)DF_i I_{beam} = 0 \tag{4.24}$$

where Z_e and Z_i = plastic section modulus of girder 1 (G1) and girders 2-5 (G2-G5), respectively, F_y = yield strength of steel girders, γ_{mfg} = modeling uncertainty factor of steel girder, λ_{asph}, λ_{conc} and λ_{steel} = weight uncertainty factors of asphalt, concrete, and steel, respectively, DF_e, DF_{i-e} and DF_i = traffic load distribution factors of girder 1 (G1), girder 2 (G2), and girders 3-5 (G3-G5), respectively, M_{trk-e} and M_{trk-i} =

traffic load moment on girder 1 (G1) and girders 2-5 (G2-G5), respectively, and I_{beam} = impact factor of traffic load. The parameters of these random variables are listed in Table 4.5 (Estes 1997).

4.4.1 Live Load Model and Corrosion Model

To study the time effect on system reliability, redundancy and risk, the variations of girder capacity and live load over time need to be known. In this case study, the live load model discussed in Estes (1997) is used herein to predict the time-variant traffic volume and estimate the distribution type of the maximum traffic load moment and its associated distribution parameters. According to this model, the maximum traffic load moment follows a type I extreme value distribution and its parameters at the year t can be obtained as follows:

$$\mu_M(t) = \sigma\,u(t) + \mu + (\gamma\sigma/\alpha(t)) \tag{4.25}$$

$$\sigma_M(t) = (\pi/\sqrt{6})(\sigma/\alpha(t)) \tag{4.26}$$

where

$$\mu = lM_{max} \tag{4.27}$$

$$\sigma = \delta\mu \tag{4.28}$$

$$\alpha(t) = \sqrt{2\ln(365A_{DTT}t)} \tag{4.29}$$

$$u(t) = \alpha(t) - \frac{\ln[\ln(365A_{DTT}t)] + \ln(4\pi)}{2\alpha(t)} \tag{4.30}$$

in which, A_{DTT} = average daily truck traffic considered to be 850 trucks per day for this bridge, l = ratio between the traffic load moment and the HS-20 moment, δ =

179

coefficient of variation, M_{max} = critical traffic load moment under the HS-20 truck load, which is equal to 351.2 kNm, and $\gamma = 0.5772$ (the Euler number). The values associated with the parameters k and δ are 0.65 and 0.32, respectively (Estes 1997).

The corrosion model used for the steel girders is based on Albrecht and Naeemi (1984). The average corrosion penetration $c(t)$ at time t is:

$$c(t) = pt^q \tag{4.31}$$

where p and q = regression random variables based on the environment and type of steel. For exterior (G1) and interior-exterior (G2) girders, the mean values of p and q are 80.2 and 0.593, respectively, and their coefficients of variation are 0.42 and 0.4, respectively. The correlation coefficient between p and q is assumed to be 0.68. For interior girders (G3, G4, and G5), these two random variables are assumed to be uncorrelated. The mean values of p and q are 34.0 and 0.65, respectively, and their coefficients of variation are 0.09 and 0.1, respectively.

4.4.2 Reliability Analysis

Based on the parameters of random variables and limit-state equations of girders, the time-variant reliability indices of each girder are plotted in Figure 4.19(a). It is noticed that the exterior girder (G1) has the highest lifetime reliability while an interior girder (G3, G4 or G5) has the lowest reliability up to 60 years. After that time, the reliability of exterior-interior girder (G2) becomes the lowest due to its larger corrosion rate.

The reliability indices of three types of systems considering three correlation cases among the failure modes of girders (independent case: $\rho=0$; partially correlated case: $\rho=0.5$; and perfectly correlated case: $\rho=1$) are plotted in Figure 4.19(b-d). It is

observed that (a) for the series system (Figure 4.19(b)), the reliability index associated with the perfectly correlated case is determined by an interior girder (G3, G4, or G5) in the first 60 years, and then, by the exterior-interior girder (G2) in the next 40 years; the reliability index associated with the independent case is smaller than that associated with the perfectly correlated case; (b) for the parallel system and series-parallel systems, the reliability index in the perfectly correlated case is decided by the exterior girder (G1) and an interior girder (G3, G4 or G5) during the entire lifetime, respectively; contrary to the series system, the reliability indices of parallel and series-parallel systems associated with the independent case are much higher than those associated with the perfectly correlated case; and (c) compared with the average value of the reliability indcies associated with the two extreme cases, the reliability index associated with the partially correlated case is slightly lower in the series system but higher in the parallel and series-parallel systems.

4.4.3 Redundancy Analysis

The time-variant redundancy profiles of the parallel and series-parallel systems considering three correlation cases are shown in Figure 4.20. It is found that (a) the redundancy indices of both systems decrease slightly over time in all correlation cases; (b) the redundancy index of series-parallel system associated with the perfectly correlated case is almost zero; (c) for both systems, the redundancy index associated with the independent case is higher than that associated with the perfectly correlated case; and (d) the redundancy indcies of the two systems associated with the partially correlated case are higher than the average values of the two extreme correlation cases.

181

4.4.4 Risk Analysis

When assessing the risk of a bridge under a hazard, the following factors need to be identified: the type of hazard, the probability of failure of a component / system given this hazard, and the associated consequences due to failure. The hazards considered in this case study are corrosion and traffic load. The failure probability of a certain component or system under these two hazards can be obtained from the reliability analysis above. Therefore, the only unknown factor is the consequences caused by the bridge failure.

Quantification of the consequences due to the failure of a bridge system is a difficult task since it includes several aspects related to commercial, safety, and environmental losses (Hessami 1999). Based on Rackwitz (2002) and Stein *et. al* (1999), the commercial and safety losses associated with the failure of E-17-AH bridge are evaluated as follows:

1. Commercial loss: rebuilding cost C_{Reb}

Based on the repair costs of replacement options in Estes and Frangopol (1999), the rebuilding costs of each item in the superstructure are listed in Table 4.6.

2. Commercial loss: running cost $C_{Running}$

Based on the length of the detour that users are forced to follow in the case of bridge failure, a general formula provided by Stein *et. al* (1999) is:

$$C_{Ruuning} = C_{Veh}DA_{DT}d \tag{4.32}$$

where C_{Veh} = average running cost for vehicles ($/km), A_{DT} = average daily traffic (vehicles/day), D = length of detour (km), and d = duration of detour (days). The values of these parameters used for this bridge are presented in Table 4.7.

3. Commercial loss: time loss cost C_{TL}

Based on the time loss for users and goods traveling through the detour, a formula given by Stein *et. al* (1999) is:

$$C_{TL} = \left[C_{Tva}O_{Car}\left(1 - \frac{T_{Trk}}{100}\right) + C_{Tvrk}\frac{T_{Trk}}{100} \right] \frac{DA_{DT}d}{S} \tag{4.33}$$

where C_{Tva} = value of time per adult (\$/h), O_{Car} = average vehicle occupancy for cars, T_{Trk} = average daily truck traffic (%), C_{Tvtk} = value of time for truck (\$/h), and S = average detour speed (km/h). The values of these parameters used for this bridge are also presented in Table 4.7.

4. Safety loss cost C_{SL}

Based on the number of casualties in the bridge failure accident and the Implied Cost of Averting a Fatality for Bridge Engineering (*ICAFB*) (Rackwitz 2002), the safety loss cost can be estimated as:

$$C_{SL} = (\frac{L}{D_S} + 1)\left[(1 - \frac{T_{Trk}}{100})O_{Car} + \frac{T_{Trk}}{100}O_{Trk} \right](ICAFB) \tag{4.34}$$

where L = total bridge length (m), D_S = safe following distance during driving (m), and O_{Trk} = average vehicle occupancy for trucks. Rackwitz (2002) investigated the values of the *ICAFB* in different countries. It should be noted that the *ICAFB* should never be taken as the value of a human life since "the value of a human life is infinite and beyond measure" (Rackwitz 2002). It is just an indication for the magnitude of a possible monetary compensation of the relatives of victims in the bridge failure event. The values of these parameters used for this bridge are also listed in Table 4.7.

For the failure of the bridge system, the direct consequence $C_{DIR,S}$ is the rebuilding cost of the whole superstructure while the indirect consequence $C_{IND,S}$ consists of the running cost, time loss cost, and safety loss cost. For the component (girder) failure, the direct consequence $C_{DIR,C}$ is the cost to replace the girder and its adjacent deck parts. Due to the symmetry consideration in system modeling, the failure of girder Gi (except G5) in Figure 4.18 actually represents the failure of two girders: girder Gi and the symmetrical girder G(10-i). Therefore, the replacing cost of girder Gi (except G5) included in the direct consequence analysis is $2C_G$, as listed in Table 4.8. For the girder G5, since it is located in the center of the cross-section and has no symmetrical counterpart, its replacing cost is C_G.

Based on the assumption that the failure of a girder will cause the failure of its adjacent deck parts, the costs to replace these deck parts are also included in the direct consequence evaluation. The failed deck parts associated with the failure of different girders are different. For the exterior girder (G1), its associated deck parts are defined as the sidewalk, guard rails, and the portion of slab under the sidewalk; for the exterior-interior girder (G2), its associated deck parts are the sidewalk, guard rails, the portion of slab under the sidewalk, and the portion of slab between G2 and G3; and for an interior girder (G3, G4 or G5), its associated deck parts are the portions of slab which are adjacent to the girder. The indirect consequence $C_{IND,C}$ includes the rebuilding cost of the damaged bridge system (without the girder and its affiliated deck parts), running cost, time loss cost, and safety loss cost. The detailed items

184

included in the direct and indirect consequences associated with the system or component failure are presented in Table 4.8.

Considering an annual money discount rate r_m of 2%, the future monetary value of the consequences C_{FV} at the year t is given by:

$$C_{FV} = C_{PV}(1+r_m)^t \hspace{4cm} (4.35)$$

where C_{PV} = present monetary value of the consequences. Based on the time-variant failure probabilities and consequences, the direct, indirect and total risks due to component or system failure are assessed using the risk event-tree model. The risk threshold in this case study is also defined as $\$10^{-2}$ and the risks below this limit are neglected.

The direct risks caused by the failure of each girder considering two extreme correlation cases are shown in Figure 4.21. It is observed that in the independent case (a) the highest risk is caused by the failure of an interior girder (G3 or G4) in the first 40 years and then by the exterior-interior girder (G2) in the next 40 years; and (b) the lowest risk is caused by the failure of exterior girder (G1). However, in the perfect correlation case, only the risk due to the failure of G2 is shown and the risks associated with the failure of exterior girder (G1) and an interior girder (G3, G4, or G5) are neglected because they are much lower than the predefined threshold. It can be concluded that the correlation among the failure modes of components has significant effects on the direct risk caused by the failure of single girder.

The indirect risks due to the failure of each girder considering two extreme correlation cases are plotted in Figure 4.22. The indirect risks in the parallel system

185

associated with the independent case are not shown in Figure 4.22(b) because they are much lower than the risk threshold (10^{-2}). It is found that in the independent case (a) the indirect risks associated with the failure of G1 in the series and series-parallel systems are much lower than those associated with the failure of other girders; (b) the highest indirect risk in the series system is governed by an interior girder (G3, G4, or G5) in the first 60 years then by the exterior-interior girder (G2) in the next 20 years; however, the highest indirect risk in the series-parallel system is determined by an interior girder (G3, G4, or G5) during the entire lifetime; (c) the indirect risks due to the failure of any interior girder (G3, G4 or G5) are the same in the series system but slightly different in the series-parallel system; and (d) failure of single girder leads to the highest indirect risk to the series system but the lowest indirect risk to the parallel system. However, in the perfect correlation case, only the indirect risks caused by failure of G2 in the last 18 years are higher than the risk threshold (10^{-2}). Therefore, the indirect risk due to the failure of single girder is significantly affected by the correlation among the failure modes of girders in a system.

The total risks due to the failure of system and each girder associated with the independent case are plotted in Figure 4.23. It is observed that (a) in the series system, failure of the system leads to higher total risk than failure of a single girder; however, in the parallel system, the opposite conclusion is drawn; (b) in the series-parallel system, the total risk due to failure of the system is very close to that due to the failure of G4; and (c) failure of G1 leads to the lowest total risk to all the three systems;

Figure 4.24 plots the total risks due to the failure of system and each girder associated with the perfect correlation case. It is noticed that (a) the total risks due to

186

failure of G1, G3, G4, and G5 are neglected in the three systems; (b) in the series and series-parallel systems, the highest total risk is caused by failure of the system; and (c) in the parallel and series-parallel systems, the total risk due to failure of the system associated with the perfect correlation case is higher than that associated with the independent case.

4.5 CONCLUSIONS

In this chapter, the effects of the deterioration of structural components, type of system modeling, and correlation among the failure modes of components on the time-variant reliability, redundancy, and risk of structural systems are investigated. An approach for assessing the lifetime reliability, redundancy and risk is presented and illustrated using an existing highway bridge. The following conclusions are drawn:

1. The effect of correlation among the failure modes of components on the direct risk due to a single component failure is independent of the system type. For the systems investigated in this chapter, the direct risk due to failure of a single component associated with the independent case is higher than that associated with the perfect correlation case.

2. Deterioration of structural components will cause the degradation of reliability and the increase of risk over time. However, the tendency of redundancy changing with time is uncertain. It may decrease, remain the same, or even increase within the lifetime.

3. The event-tree model used in this chapter considers the direct and indirect consequences caused by the failure of component / system and can be used to

assess the direct, indirect and total risk associated with the component / system failure for different systems.

4. The direct risk due to failure of a single component is independent of the system type. However, the indirect risk is affected not only by the system type but also by the position of component in the system. For a given system, the indirect risk associated with failure of a component in series position is usually higher than that associated with failure of a component in parallel position.

5. In the series system, the total risk due to system failure is higher than that due to component failure; however, contrary finding is observed in the parallel system due to the lower failure probability of the parallel system. Failure of the parallel system leads to much lower total risk than failure of the series and series-parallel systems. The total risk due to failure of the system or a single component is significantly affected by the correlation among the failure modes of components.

Table 4.1 Parameters of the three-component system.

Parameters		Component 1	Component 2	Component 3
Initial cross-section area $A_i(0)$ (cm^2)		2.5	2.0	4.8
Initial deterioration rate $DR_i(0)$ (per year)		0.015	0.004	0.005
Deterioration rate $DR_i(t)$ at time t (per year)		$DR_1(0)$	$DR_2(0)$	$DR_3(0)\times(1+0.025)^t$
Yield stress F_y (kN/cm^2)	mean μ_{Fyi}	11.0	6.5	10.0
	std. dev. σ_{Fyi}	2.0	1.0	2.0
Load (kN)	mean μ_{Qi}	5.0	4.5	9.5
	std. dev. σ_{Qi}	0.5	0.45	0.95

Table 4.2 Lifetime of components and systems (years).

Components and systems		$\beta_{target} = 2.0$	$\beta_{target} = 3.0$	$\beta_{target} = 4.0$
Component 1		36	27	20
Component 2		94	62	35
Component 3		37	31	25
Series system	Independent	35	27	20
	Perfectly correlated	36	27	20
Parallel system	Independent	104	69	51
	Perfectly correlated	94	62	35
Series-parallel system	Independent	37	31	25
	Perfectly correlated	37	31	25

Table 4.3 Lifetime of series-parallel systems (years).

Series-parallel systems		$\beta_{target} = 2.0$	$\beta_{target} = 3.0$	$\beta_{target} = 4.0$
Components combination I	Independent	37	31	25
	Perfectly correlated	37	31	25
Components combination II	Independent	46	39	32
	Perfectly correlated	37	31	25
Components combination III	Independent	36	27	20
	Perfectly correlated	36	27	20

Table 4.4 Five correlation cases associated with the series-parallel system.

IN_{123}	PC_{123}	$IN_{13}, IN_{23}, PC_{12}$	$IN_{12}, IN_{23}, PC_{13}$	$IN_{12}, IN_{13}, PC_{23}$
$\rho(g_i, g_j) = 0$ $i,j=1,2,3$	$\rho(g_i, g_j) = 1$ $i,j=1,2,3$	$\rho(g_1, g_2) = 1$ $\rho(g_1, g_3) = 0$ $\rho(g_2, g_3) = 0$	$\rho(g_1, g_3) = 1$ $\rho(g_1, g_2) = 0$ $\rho(g_2, g_3) = 0$	$\rho(g_2, g_3) = 1$ $\rho(g_1, g_2) = 0$ $\rho(g_1, g_3) = 0$

Note: IN = independent failure modes; PC = perfectly correlated failure modes.

Table 4.5 Parameters of the random variables associated with the material properties and traffic load effects of the Bridge E-17-AH (Estes 1997).

Variables	Distribution parameters	Variables	Distribution parameters
F_y (Mpa)	N[250, 30]	λ_{asph}	N[1.0, 0.25]
γ_{mfg}	N[1.11, 0.128]	λ_{conc}	N[1.05, 0.105]
DF_e	N[0.982, 0.122]	λ_{steel}	N[1.03, 0.082]
$DF_{i\text{-}e}$	N[1.14, 0.142]	I_{beam}	N[1.14, 0.114]
DF_i	N[1.309, 0.163]	-	-

Note: N[μ, σ] = the random variable is normally distributed with the mean of μ and standard deviation of σ.

Table 4.6 Rebuilding cost of each item in the superstructure of Bridge E-17-AH.

Rebuilding item	Notation	Cost ($)
Each girder	C_G	29,050
Sidewalk, guard rails, the portion of slab under sidewalk (both sides)	C_W	113,000
Slab (without the portion under sidewalk)	C_S	112,600
Superstructure	C_{Sup}	487,100

Table 4.7 Parameters for the consequences evaluation of Bridge E-17-AH.

Definition and units of parameters	Notation	Value	Reference
Average daily traffic (ADT) (vehicles/day)	A_{DT}	8500	Estes (1997)
Average daily truck traffic (ADTT) (%)	T_{Trk}	10	Estes (1997)
Length of detour (km)	D	0.64	Based on the local transportation network
Duration of detour (days)	d	180	Decò and Frangopol (2011)
Average running costs for vehicles ($/km)	C_{Veh}	0.16	Stein et al. (1999)
Value of time per adult ($/h)	C_{Tva}	7.05	Stein et al. (1999)
Value of time for truck ($/h)	C_{Tvtk}	20.56	Stein et al. (1999)
Average vehicle occupancy for cars	O_{Car}	1.5	Decò and Frangopol (2011)
Average vehicle occupancy for trucks	O_{Trk}	1.05	Decò and Frangopol (2011)
Safe following distance during driving (m)	D_S	30	Colorado State Patrol (2011)
Average detour speed (km/h)	S	64	Stein et al. (1999)
Implied cost of averting a fatality for bridge engineering ($)	$ICAFB$	2.6×10^6	Rackwitz (2002)
Total bidge length (m)	L	42.1	Estes (1997)

Table 4.8 Direct and indirect consequences caused by the failure of component or system of Bridge E-17-AH.

Failure item	Direct consequence	Indirect consequence
Exterior girder (G1)	$2C_G + C_W$	$(C_{Sup} - 2C_G - C_W) + C_{Running} + C_{TL} + C_{SL}$
Exterior-interior girder (G2)	$2C_G + C_W + C_S/3$	$(C_{Sup} - 2C_G - C_W - C_S/3) + C_{Running} + C_{TL} + C_{SL}$
Interior girder (G3 or G4)	$2C_G + 2C_S/3$	$(C_{Sup} - 2C_G - 2C_S/3) + C_{Running} + C_{TL} + C_{SL}$
Interior girder (G5)	$C_G + C_S/3$	$(C_{Sup} - C_G - C_S/3) + C_{Running} + C_{TL} + C_{SL}$
Superstructure	C_{Sup}	$C_{Running} + C_{TL} + C_{SL}$

$$F_{comp,i}$$

$$\overline{F}_{subsys}\,|F_{comp,i}$$

$$F_{subsys}\,|F_{comp,i}$$

Consequences	Branches
$C_{DIR,i}$	b_1
$C_{IND,i} + C_{DIR,i}$	b_2
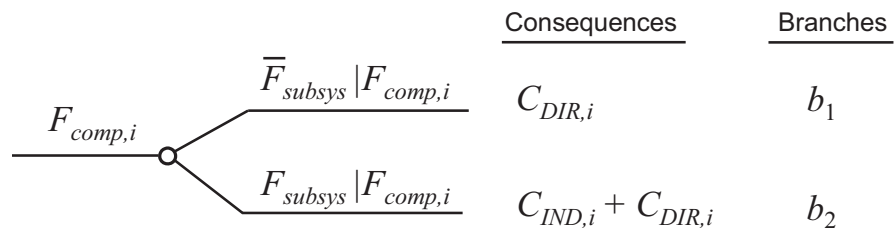
Figure 4.1 Event-tree risk model for the failure of component i.
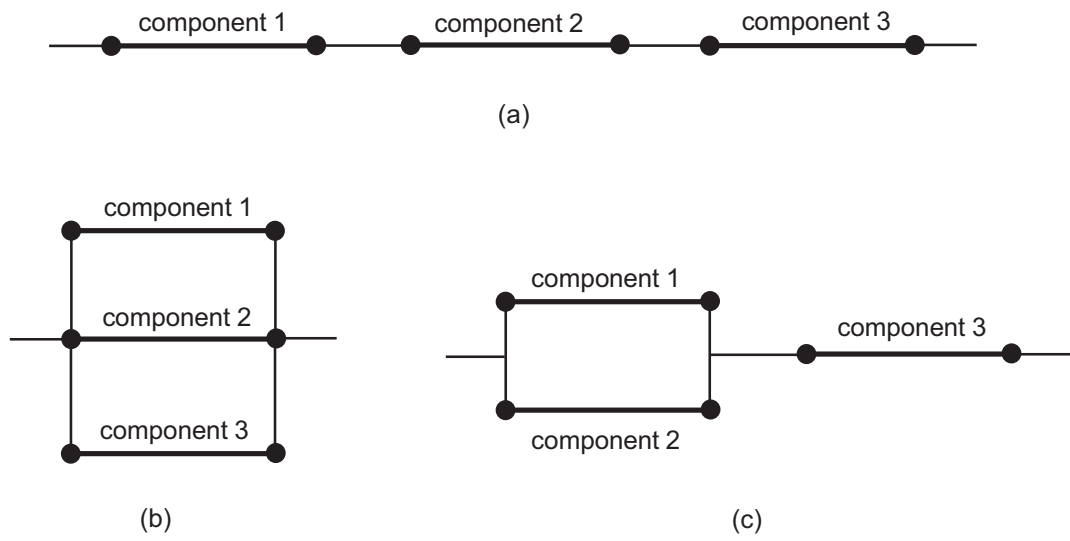
Figure 4.2 Three-component systems: (a) series system; (b) parallel system; and (c) series-parallel system.
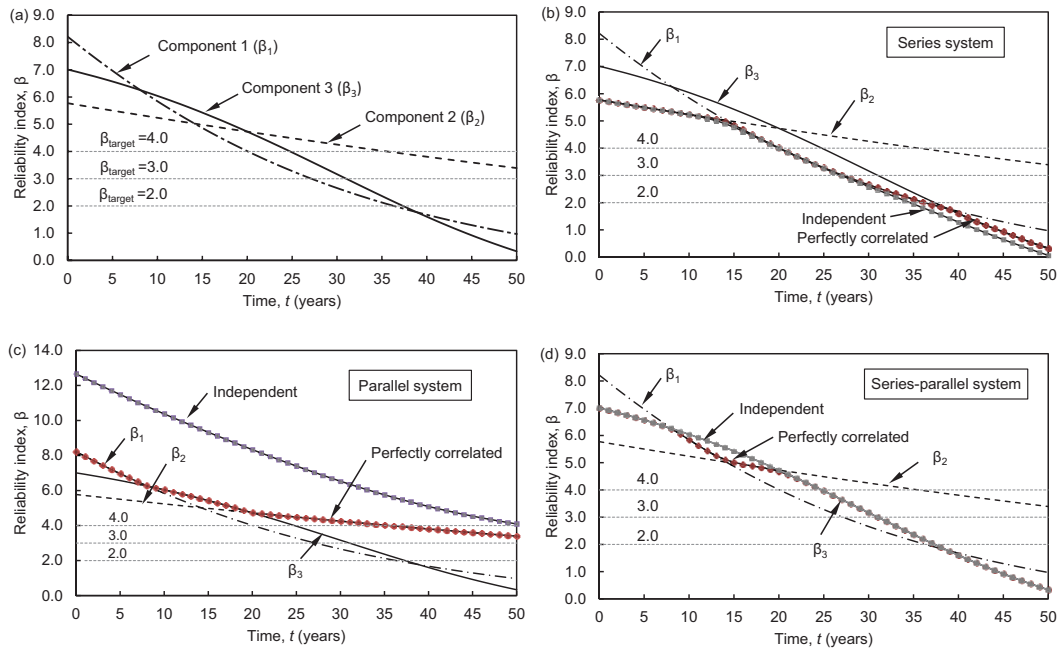
Figure 4.3 Profiles of reliability of (a) three components; (b) series system; (c) parallel system; and (d) series-parallel system.
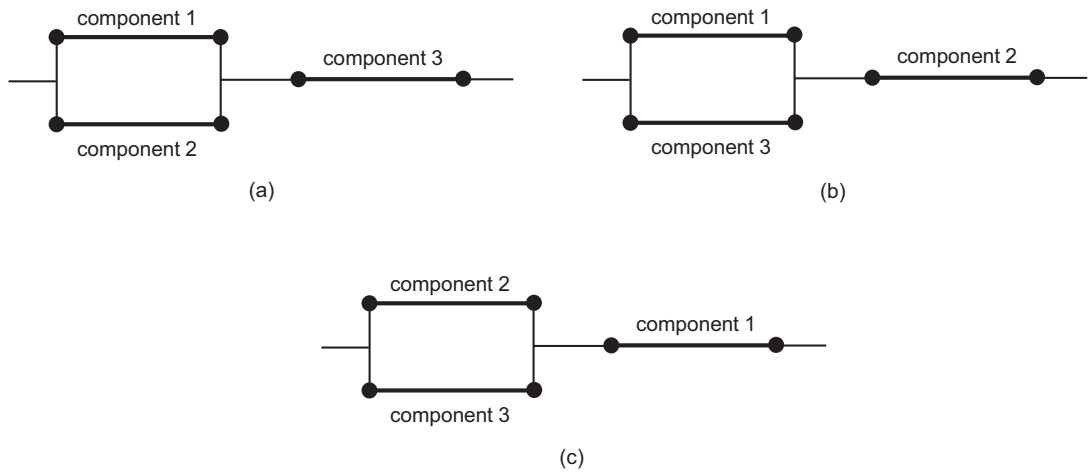
Figure 4.4 Three types of components combinations of series-parallel system: (a) combination I; (b) combination II; and (c) combination III.
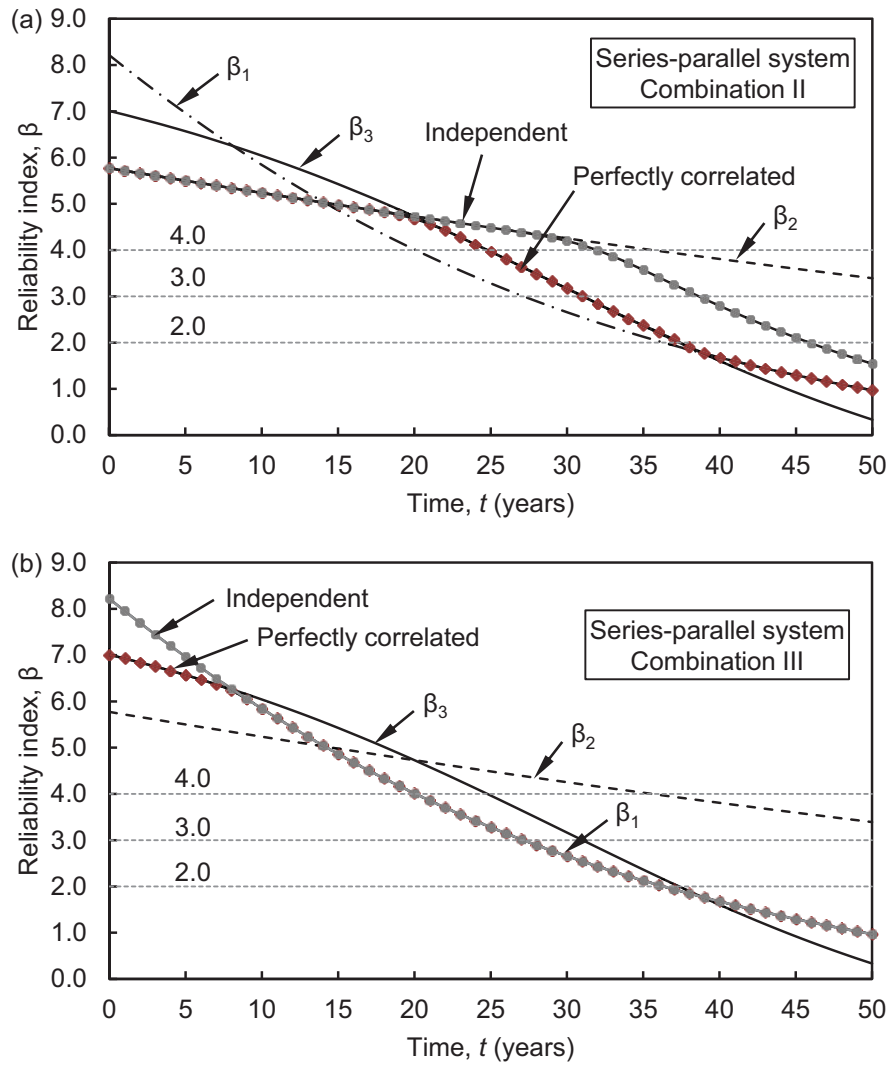
Figure 4.5 Profiles of reliability of series-parallel systems: (a) combination II; and (b) combination III.

(a)

Series-parallel system
Combination I

Detail A

(b)

Detail A

IN_{123}

$IN_{12}, IN_{13}, PC_{23}$

PC_{123}

$IN_{12}, IN_{23}, PC_{13}$

$IN_{13}, IN_{23}, PC_{12}$
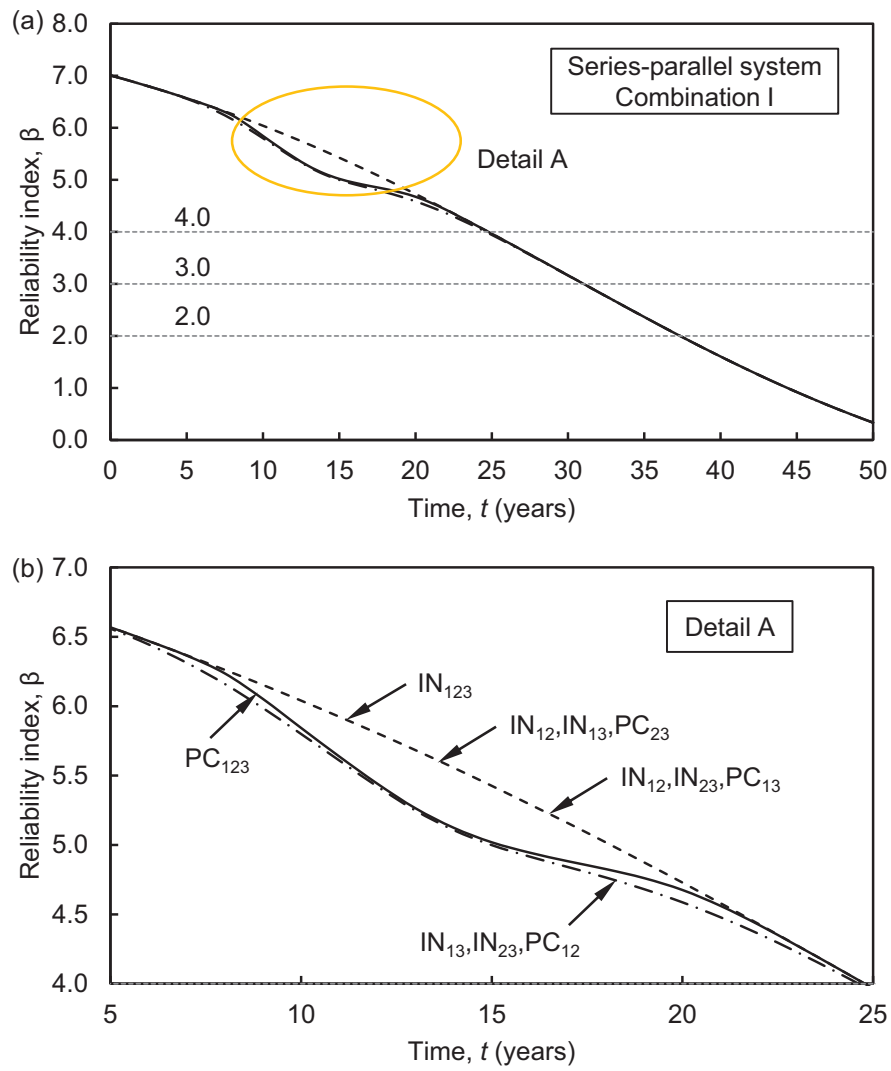
Figure 4.6 Profiles of reliability of series-parallel system in different correlation cases.
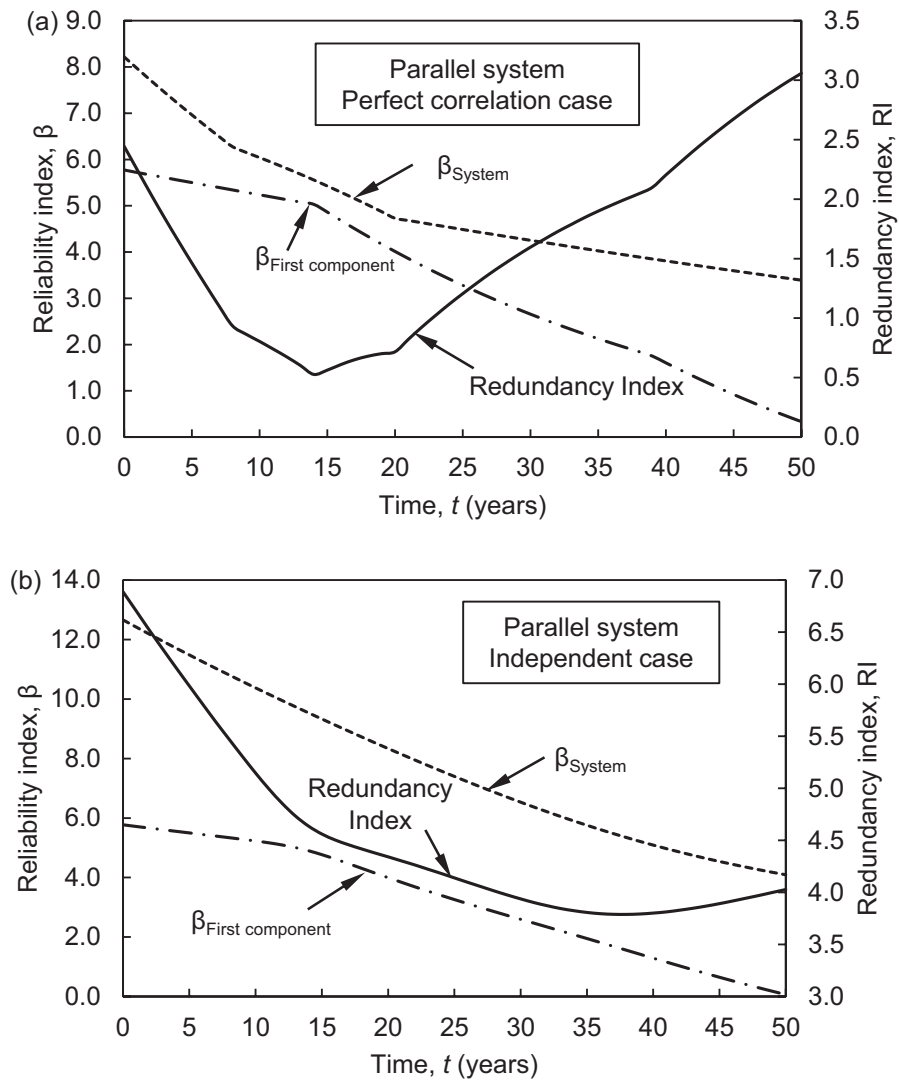
Figure 4.7 Profiles of redundancy of parallel system in: (a) perfect correlation case; and (b) independent case.
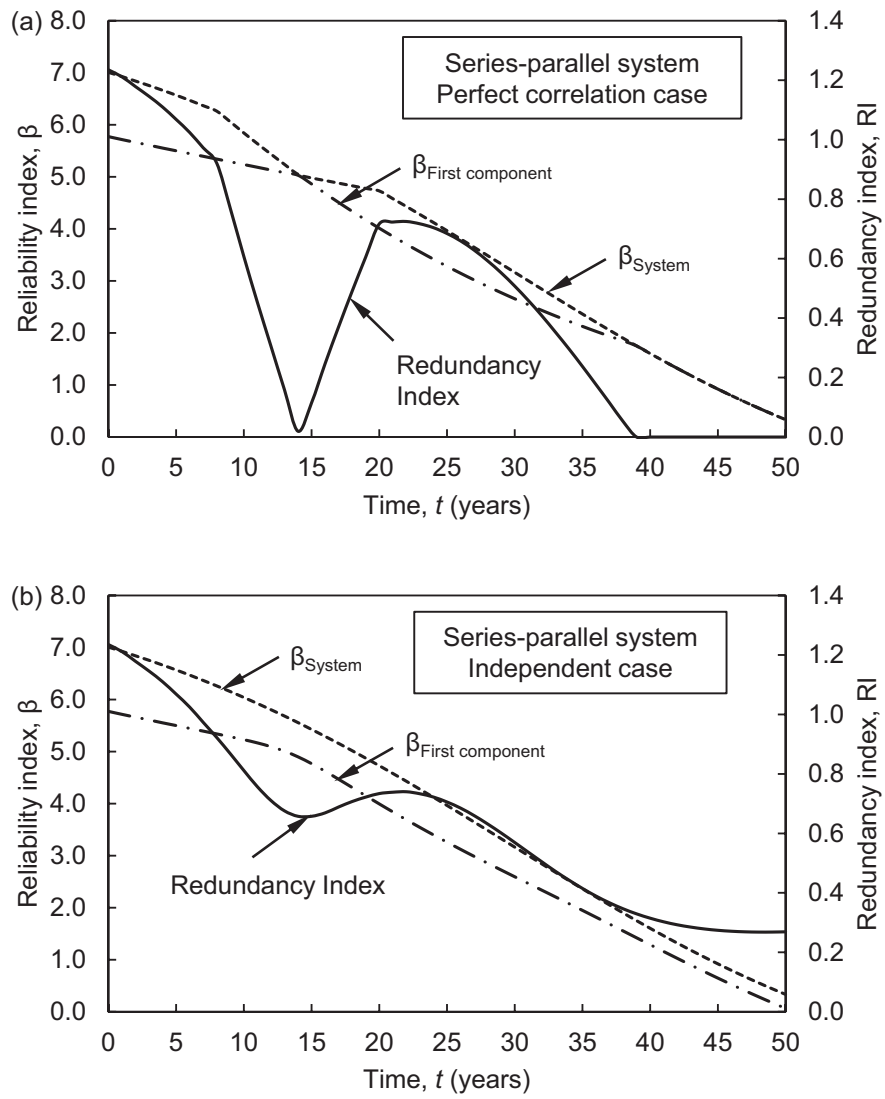
Figure 4.8 Profiles of redundancy of series-parallel system in: (a) perfect correlation case; and (b) independent case.
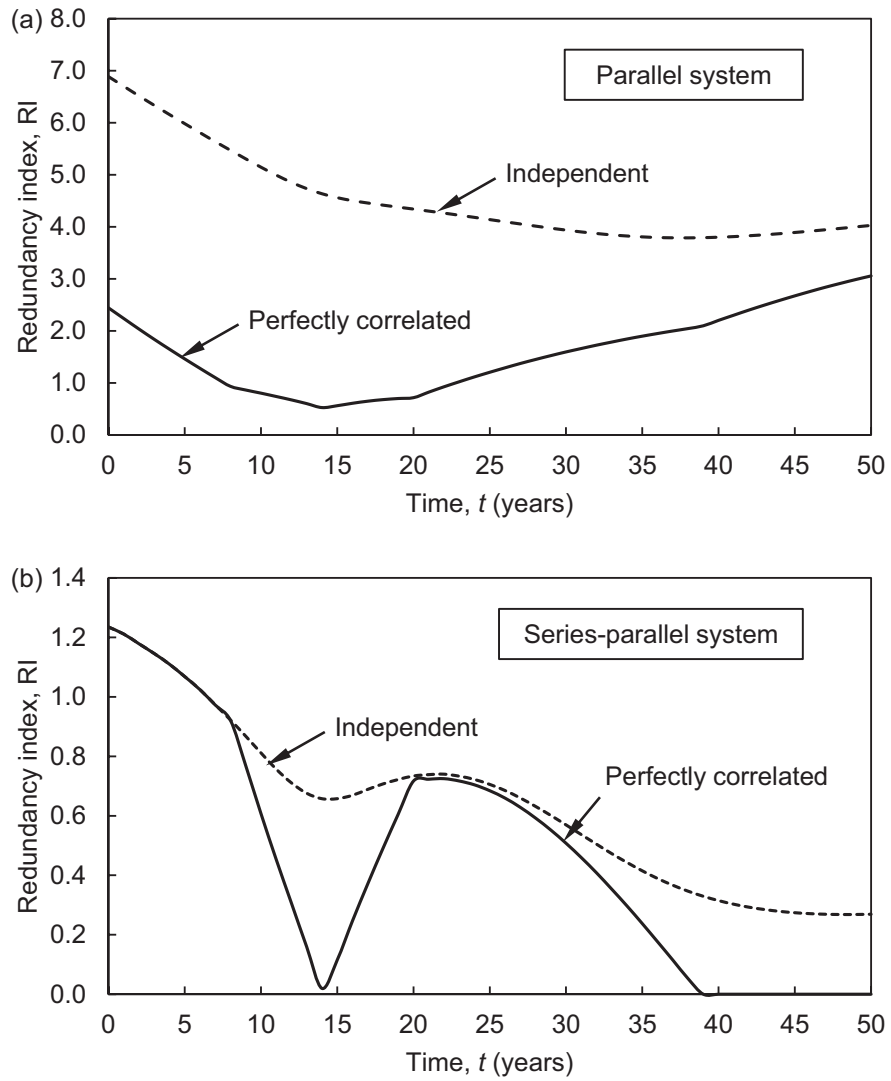
Figure 4.9 Profiles of redundancy of two types of systems: (a) parallel system; and (b) series-parallel system.
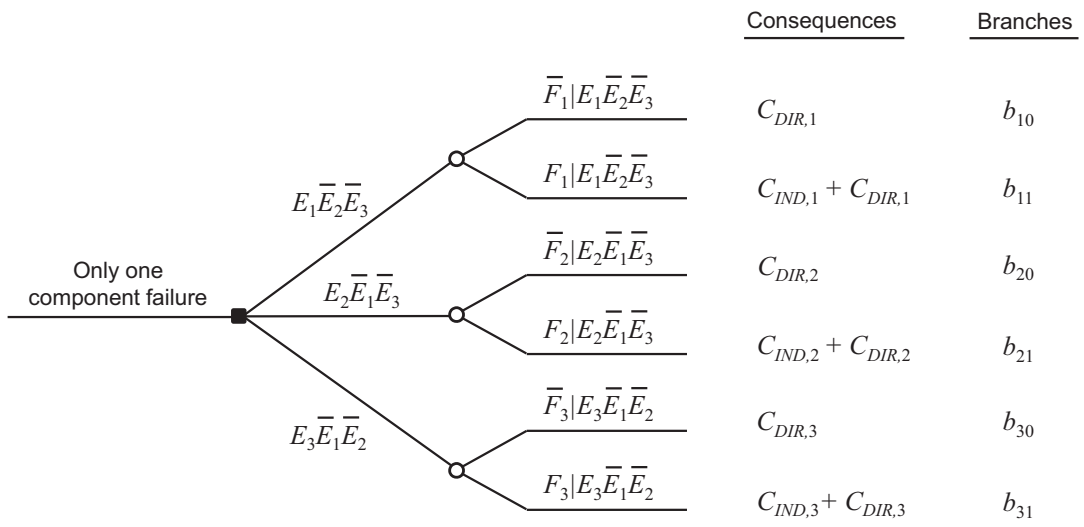
Figure 4.10 Event-tree risk model for only one component failure in a three-component system.
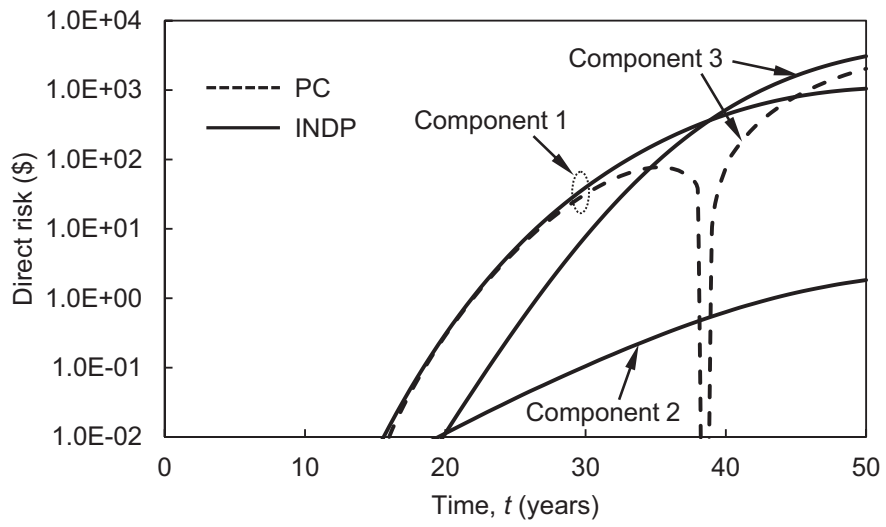
Figure 4.11 Profiles of direct risk due to the failure of only one component (INDP = independent failure modes, PC = perfectly correlated failure modes).
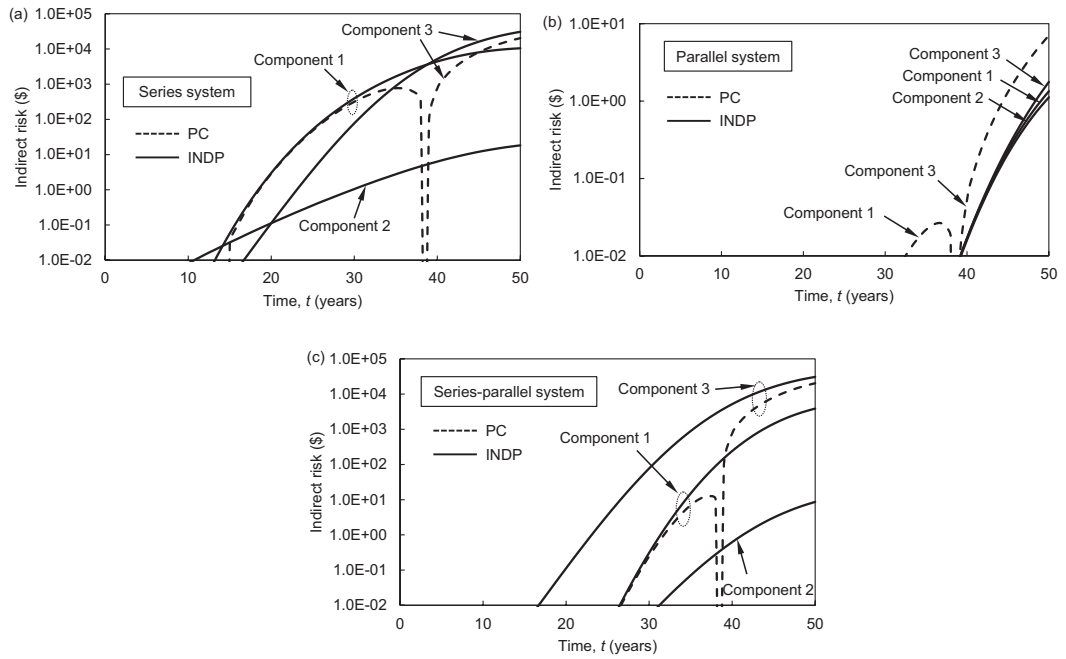
Figure 4.12 Profiles of indirect risk due to the failure of only one component in: (a) series system; (b) parallel system; and (c) series-parallel system.
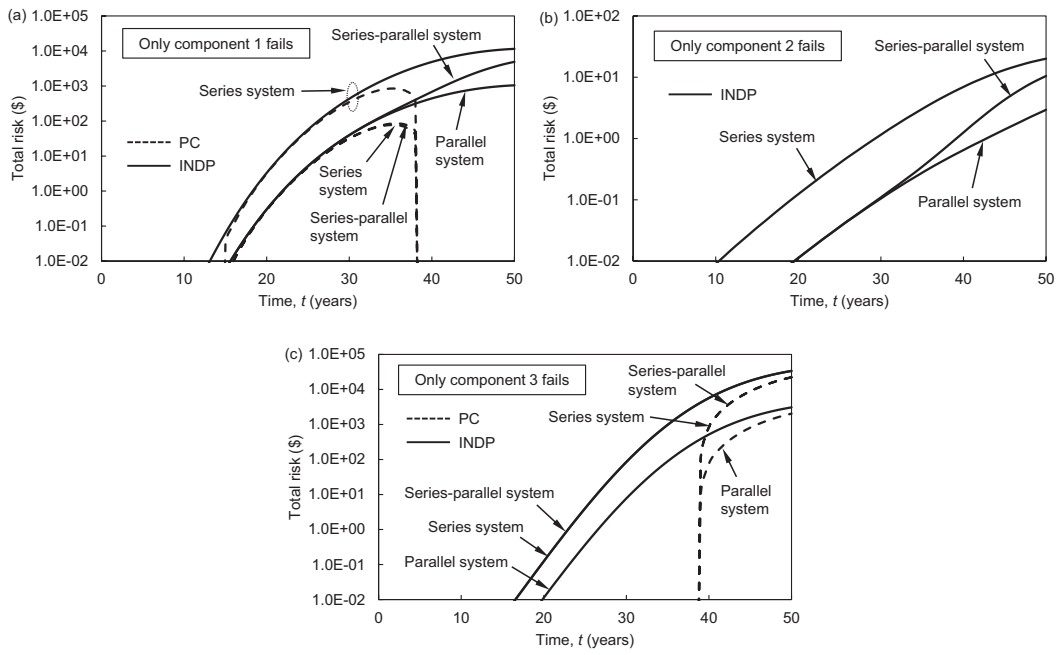
Figure 4.13 Profiles of total risk of different systems due to the failure of (a) component 1; (b) component 2; and (c) component 3.
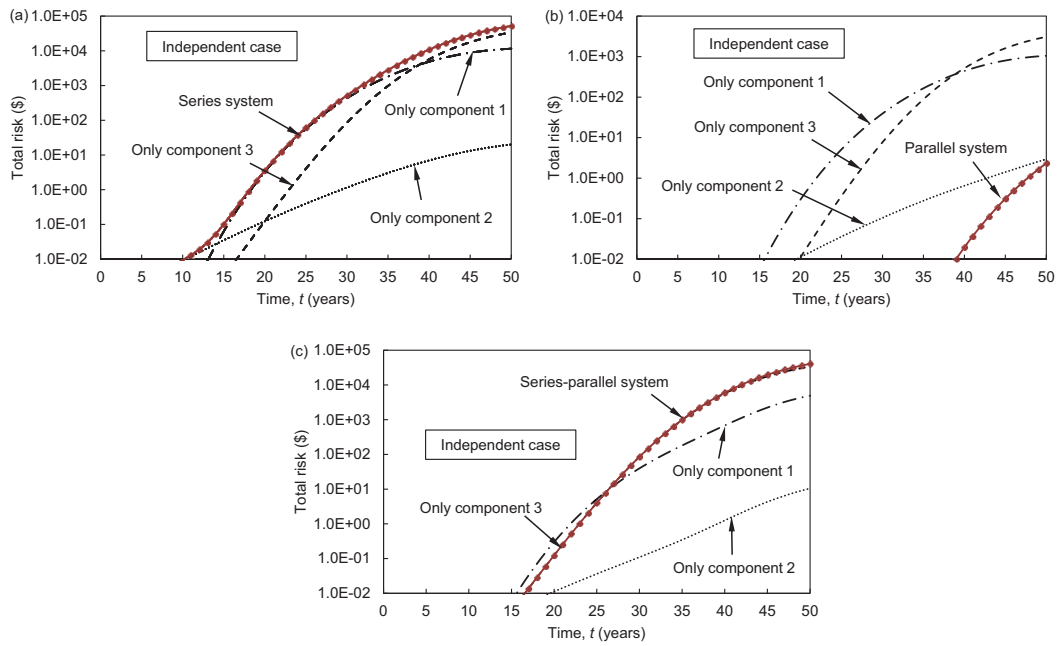
Figure 4.14 Profiles of total risk due to the failure of component and system in the independent case: (a) series system; (b) parallel system; and (c) series-parallel system.
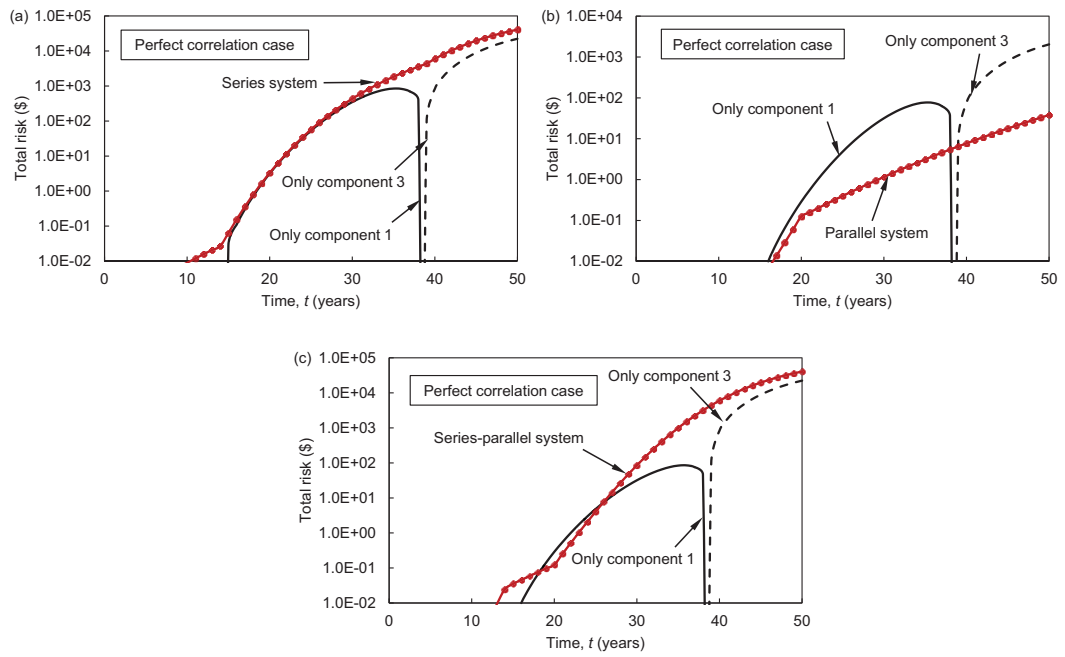
Figure 4.15   Profiles of total risk due to the failure of component and system in the
perfect correlation case: (a) series system; (b) parallel system; and (c)
series-parallel system.

211
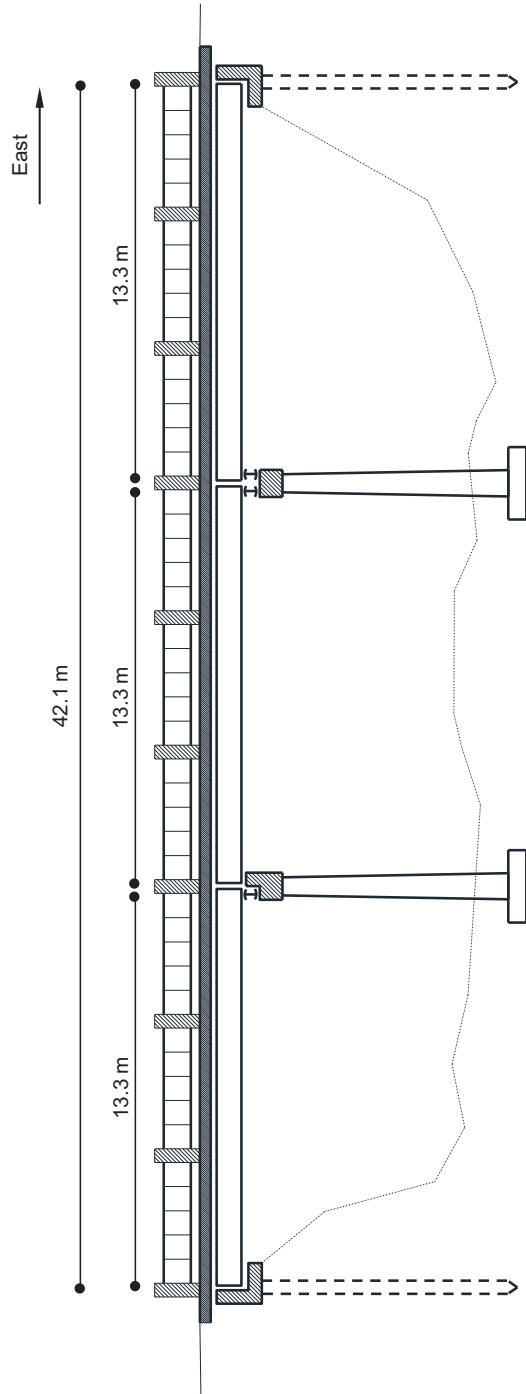
Figure 4.16 Elevation of Colorado State Highway Bridge E-17-AH.
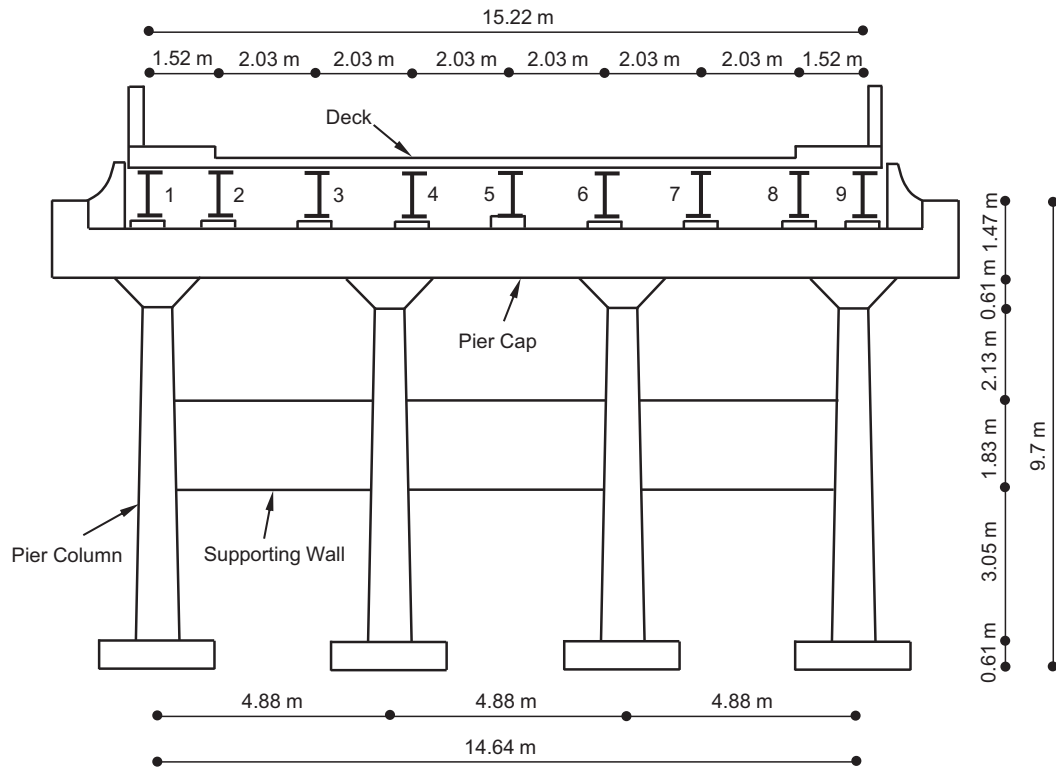
Figure 4.17 Cross-section of Colorado State Highway Bridge E-17-AH.
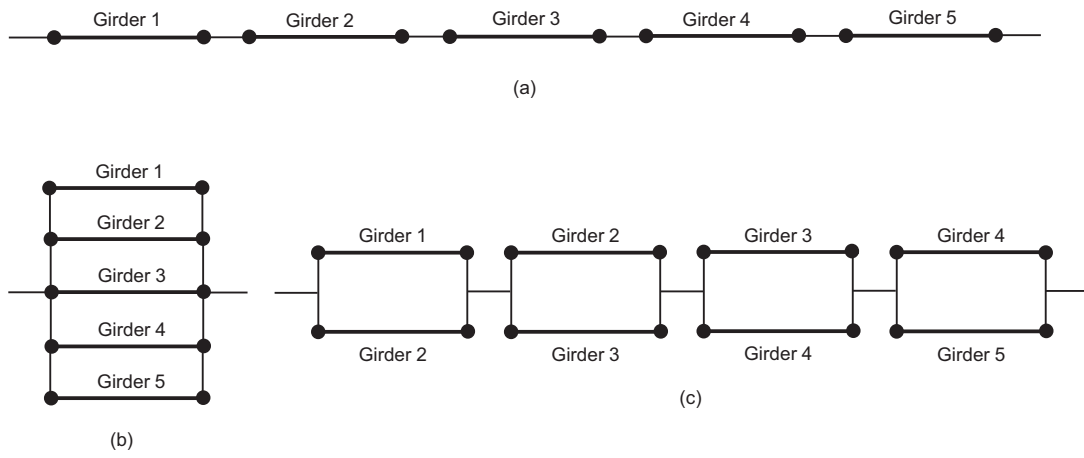
Figure 4.18   Simplified system models for Bridge E-17-AH: (a) series system; (b) parallel system; and (c) series-parallel system.
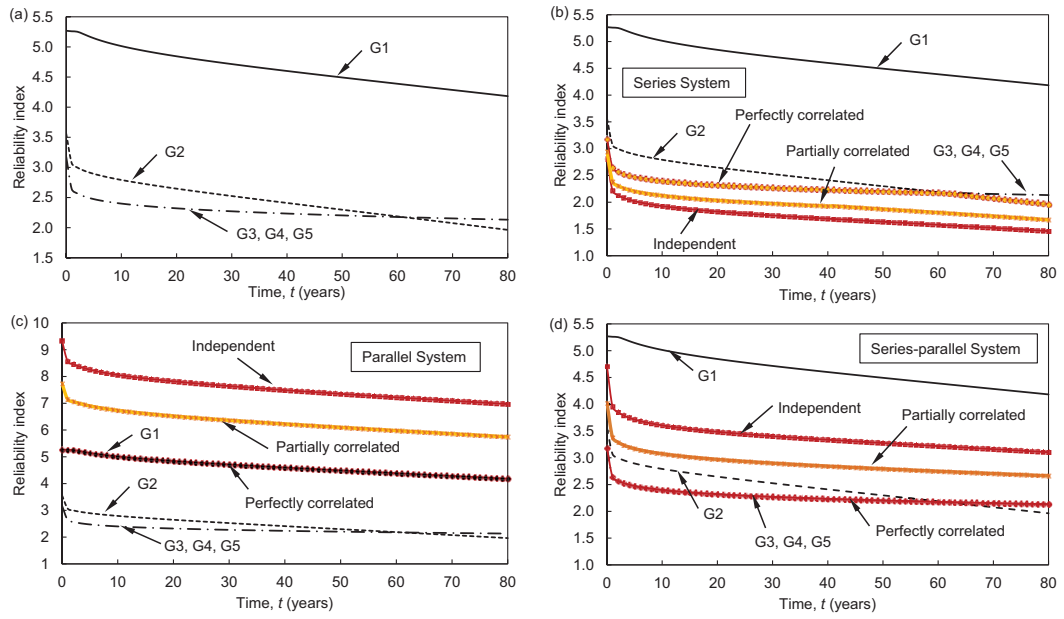
Figure 4.19 Profiles of reliability of Bridge E-17-AH: (a) girders; (b) series system; (c) parallel system; and (d) series-parallel system.
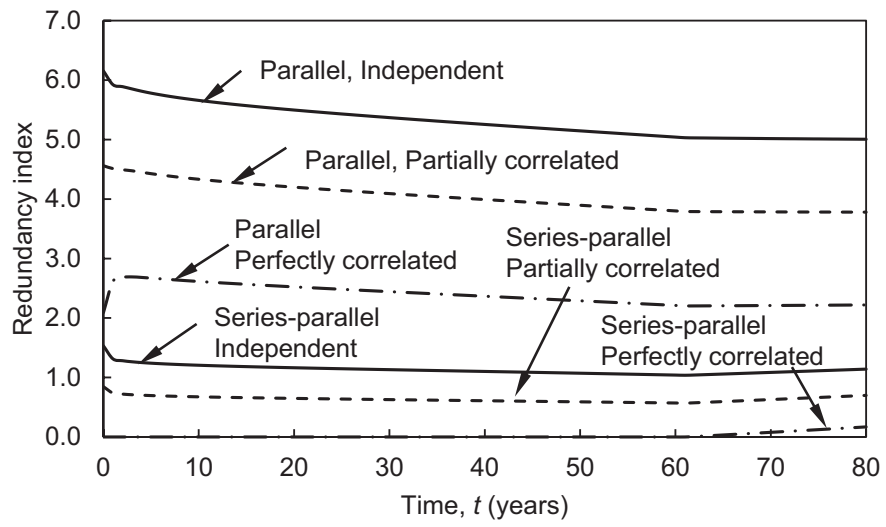
Figure 4.20 Profiles of redundancy for different systems of Bridge E-17-AH.
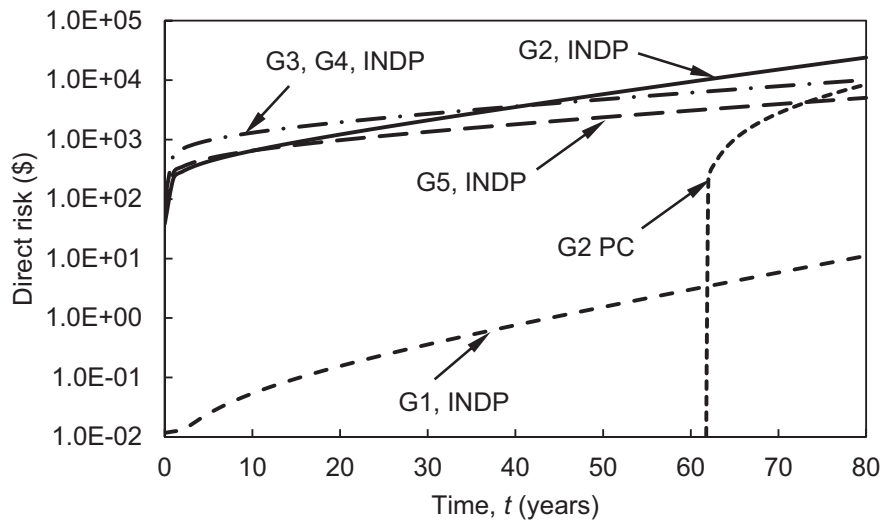
Figure 4.21 Profiles of direct risk due to the failure of only one girder.
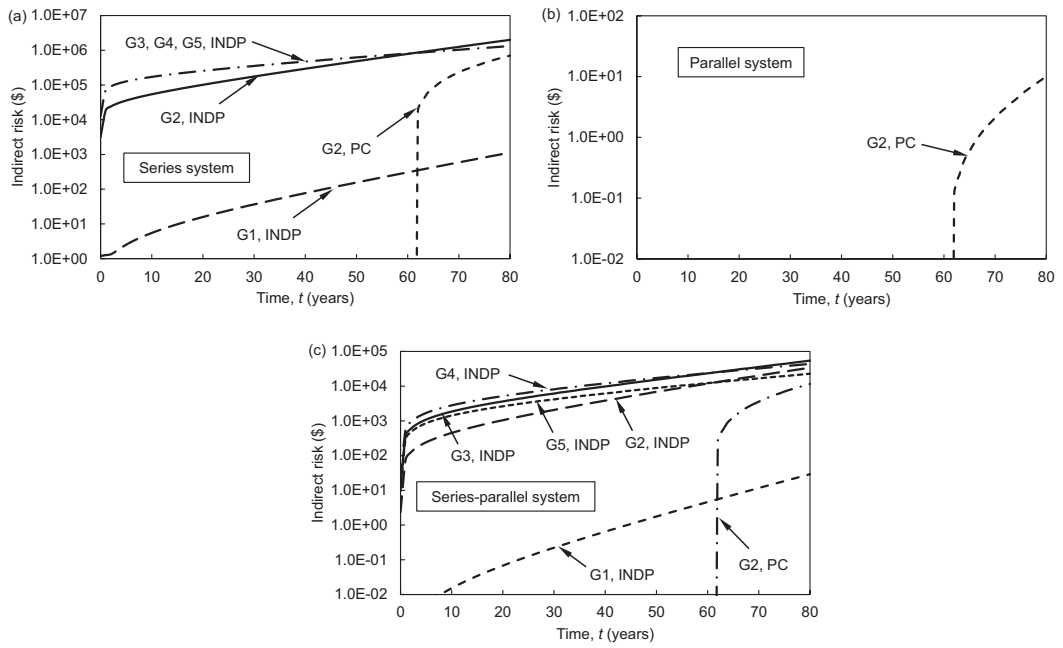
Figure 4.22 Profiles of indirect risk due to the failure of only one girder in: (a) series system; (b) parallel system; and (c) series-parallel system.
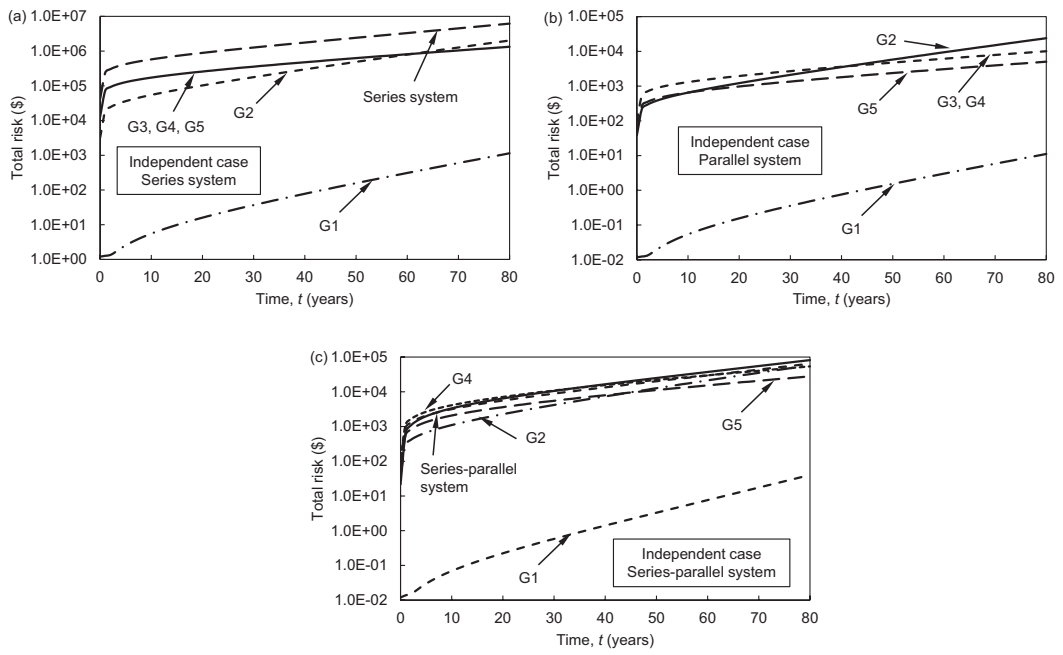
Figure 4.23 Profiles of total risk due to the failure of component and system in the independent case: (a) series system; (b) parallel system; and (c) series-parallel system.
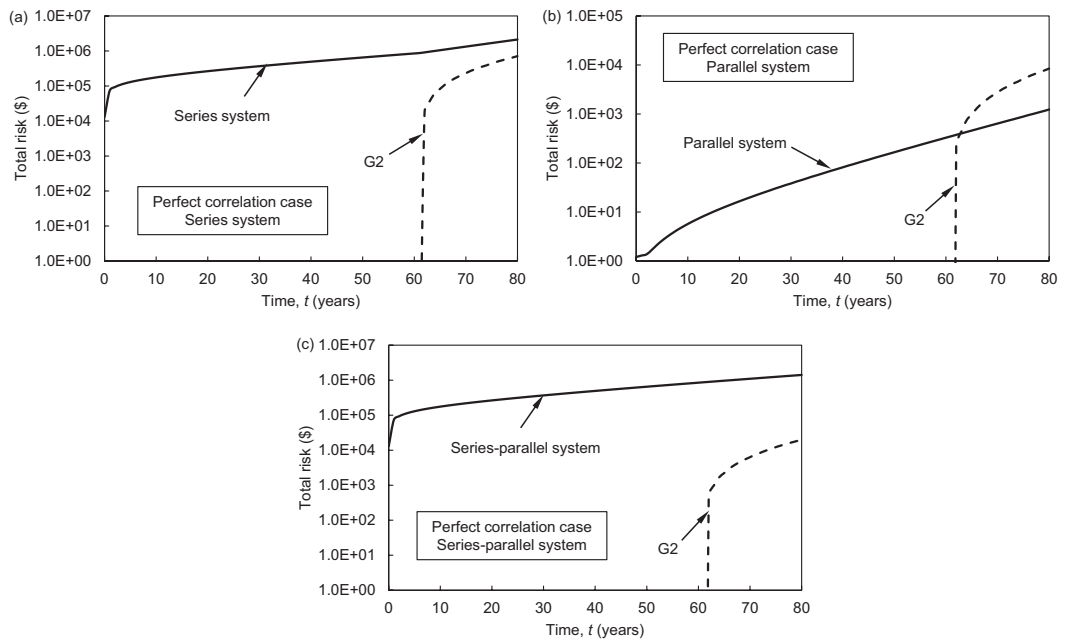
Figure 4.24 Profiles of total risk due to the failure of component and system in the perfect correlation case: (a) series system; (b) parallel system; and (c) series-parallel system.

CHAPTER 5

RISK-BASED APPROACH FOR OPTIMUM MAINTENANCE OF BRIDGES UNDER TRAFFIC AND EARTHQUAKE LOADS

5.1 INTRODUCTION

Material aging, aggressive environmental conditions, and increasing loads may lead to deterioration of structures. In addition, structures may encounter adverse events during their lifetime, such as earthquakes and floods. The consequences associated with structural failure due to progressive deterioration or extreme events can be enormous and may bring adverse impacts on the society. In this context, risk assessment and mitigation is essential to maintain structural performance within satisfactory levels (Ellingwood 2005, Frangopol 2011). Different from other performance indicators, such as reliability index and redundancy index, which are only focused on the probability of failure of a member or a structure, risk also includes the necessity to study the occurrences of extreme events and the economic effects due to structure failure. Therefore, quantitative risk assessment is a very complicated task, and explains the fact that most previous research on risk was qualitative (Ellingwood 2001, Hessami 1999). However, researchers and engineers gradually realized that evaluation of risk only in qualitative terms could not provide clear and accurate results to decision-makers for assessing and managing risk effectively. Therefore, more recent studies on risk tend to focus on quantitative risk assessment for structures under

different hazards (Pedersen 2002, Adey *et al.* 2003, Decò and Frangopol 2011, Uddin and Ang 2011, Zhu and Frangopol 2012, Decò and Frangopol 2013).

The ultimate purpose of risk assessment is to manage risk, such as finding a proper maintenance plan to keep the lifetime risk below a target level. Since the funds used for lifetime maintenance are usually limited, it is crucial to seek the optimum maintenance strategies to allocate the available funds reasonably. Optimization of maintenance strategy based on performance indicators such as reliability and redundancy have been extensively studied (Yang *et al.* 2006, Kong and Frangopol 2003, Okasha and Frangopol 2010a, Bocchini and Frangopol 2012). However, maintenance strategy optimization based on risk has been rarely reported.

This chapter develops a risk-based approach for optimum essential and preventive maintenance strategies of bridge structures under traffic and seismic hazards. Section 5.2 proposes the methods for performing the hazard analysis, vulnerability analysis under traffic and seismic loads, respectively, and consequences analysis. Section 5.3 introduces two types of maintenance options for risk mitigation. In Section 5.4, an existing highway bridge located in Colorado is used to illustrate the effectiveness of the presented approach. In Section 5.5, the bridge is assumed to be located in California which is a high seismicity region and different optimum maintenance strategies are obtained. Finally, Section 5.6 provides the conclusions of this chapter.

5.2 RISK ASSESSMENT

Risk assessment is the first step in the risk management process since it is the basis for the development of risk mitigation strategy to prevent malfunctions or collapse of

structures during their lifetime. Quantitative risk assessment consists of three main parts: hazard analysis, vulnerability analysis and consequence analysis. The approaches for performing these analyses will be presented in the following subsections.

5.2.1 Hazard Analysis

In civil engineering applications, hazards are the situations or circumstances causing unavoidable danger to the structural system so that structural failures or malfunctioning may occur. Hazards that are most commonly studied can generally be classified into two types: natural hazards (such as earthquakes, floods and tornadoes) and man-made hazards (such as fires, and explosions). Any type of hazard has usually two properties: (a) its occurrence is uncertain; and (b) it may cause damages or collapse to structures. Therefore, hazard analysis is considered as an important step in the risk assessment process.

The aim of analyzing a hazard is to determine its probability of occurrence, denoted as $P(H)$. In this chapter, the hazards investigated are traffic and earthquake loads. For bridge structures which are constructed for the daily passage use for vehicles and pedestrians, the probability of traffic load occurrence can be assumed to be 1.0. For probabilistic analysis of seismic hazard, four steps are required: (1) identify all possible seismic sources that can generate strong ground shaking at the site; (2) characterize each seismic source in terms of location and geometry; (3) determine the magnitudes of earthquakes that might occur in the investigated region; and (4) estimate the probabilities of occurrence of selected earthquakes using Earthquake

Probability Mapping. Earthquake Probability Maps is a valuable tool developed by USGS for probabilistic seismic hazard analysis in the United States. These maps are derived from seismic hazard curves calculated on a grid of sites across the country that describe the frequency of exceeding a set of ground motions. After the location of the epicenter (latitude and longitude), the desired time interval, the earthquake magnitude, and the radius of the investigated region are provided, the probability of an earthquake equaling or exceeding the given magnitude within the radius of the given location and within the time interval can be estimated (USGS 2009a).

5.2.2 Vulnerability Analysis

Given a particular hazard, there is a possibility that the maximum load that it imposes to the structure exceeds its resisting capacity, and thus, structural failure might occur. Therefore, the second step of risk assessment is to determine this failure probability, which is generally referred to vulnerability analysis. The failure probability of a structural system for a given hazard, denoted as $P(F \mid H)$, is defined as the probability of violating any of its limit states. These limit states are expressed by equations relating the resistance of the structural system to the loads acting on it:

$$g_i = R_i - Q_i = 0 \tag{5.1}$$

where g_i = performance function with respect to failure mode i; and R_i and Q_i = resistance and load effect associated with failure mode i, respectively. The limit state is violated when the value of respective performance function is less than zero. Once a limit state is violated, the structure fails in the mode defined by that limit state.

Therefore, the probability of system failure of a structure with n possible failure modes for a certain hazard is:

$$P(F \mid H) = P([any\, g_i < 0] \mid H), \quad i = 1, 2, ..., n \tag{5.2}$$

The detailed procedures of estimating the system failure probability under traffic and seismic loads are presented in the following two subsections.

5.2.2.1 *Traffic load*

Traffic loads are the most common type of hazard for bridge structures. Since it is the basic type of loading that bridge designers need to deal with during the design process, the reliability index of a new structure under traffic loads is usually controlled at a satisfactory level. However, due to the progressive deterioration of bridge members' resistance and the increase of traffic load effects, the probability of structural system failure tends to increase with time. Although structural members may fail in different modes under traffic loads, only flexural failure mode is studied herein with respect to bridge superstructure members. According to the AASHTO specifications, the moment capacities of members and the maximum moment loading effects acting on them can be determined.

As both bending capacities and maximum loads contain variability and uncertainty, the obtained flexural moment capacities and the acting moments need to be represented with respective random variables and associated probability distributions. Moreover, the epistemic uncertainty factors are also required to be included in the limit state equations to take into account modeling uncertainty. Estes (1997) provided a detailed approach to obtain the limit state equations of concrete

225

deck and steel girders based on AASHTO (1992). The limit state equations derived from this approach are listed as follows:

for concrete deck:

$$\gamma_{mfc} M_u(t) - \lambda_{asph} M_{dl\_asph}(t) - \lambda_{conc} M_{dl\_conc}(t) - M_{ll}(t) = 0 \tag{5.3}$$

for steel girder:

$$\gamma_{mfg} M_u(t) - \lambda_{steel} M_{dl\_steel}(t) - \lambda_{conc} M_{dl\_conc}(t) - \eta I M_{ll}(t) = 0 \tag{5.4}$$

where γ_{mfc} = modeling uncertainty factor of concrete deck, M_u and M_{ll} = ultimate moment capacity and the traffic load moment, respectively, M_{dl_asph}, M_{dl_conc} and M_{dl_steel} = dead load moment caused by asphalt, concrete and steel, respectively, η = traffic load distribution factor of girder, I = impact factor of traffic load, and t = time. γ_{mfg}, λ_{asph}, λ_{conc} and λ_{steel} are defined in Chapter 4.

The live load model presented in Chapter 4 is used herein to predict the time-dependent traffic volume and estimate the distribution type of the maximum traffic load moment and its associated distribution parameters. The corrosion of concrete deck reinforcement and steel girder is considered as deterioration mechanism. The evolution of corrosion of the deck reinforcement is assumed to be uniform, therefore the remaining cross-sectional area of the reinforcement $A_r(t)$ at time t is:

$$A_r(t) = \frac{\pi}{4}[d_o - C_{corr} i_{corr}(t - T_{i,rebar})]^2 \qquad \text{for} \quad t > T_{i,rebar} \tag{5.5}$$

where d_o = initial diameter of the reinforcing bar, C_{corr} = corrosion coefficient, i_{corr} = parameter related to the rate of corrosion, and $T_{i,rebar}$ = corrosion initiation time of reinforcing bar, which can be determined by

226

$$T_{i,rebar} = \frac{x^2}{4D\left[erfc^{-1}(\frac{C_{cr}}{C_0})\right]^2}$$ (5.6)

where x = concrete cover depth, D = chloride diffusion coefficient; $erfc$ = complementary error function, C_{cr} = critical chloride concentration, and C_0 = surface chloride concentration. The corrosion model used for the steel girder is based on Albrecht and Naeemi (1984) (see Chapter 4).

Before performing the vulnerability analysis of the structural system, the definition of the system failure needs to be clarified. Taking a steel girder bridge as an example, the system can be modeled as series system (failure of deck or any girder) or series-parallel system (failure of deck or any two (or three) adjacent girders). Obviously, different definitions of system failure lead to different vulnerability analysis results. After determining the system model and substituting the results obtained from capacity and traffic load models into the limit state equations above, the system vulnerability analysis can be performed using the computer program RELSYS (Estes and Frangopol 1998).

5.2.2.2 *Seismic load*

The losses caused by earthquake hazard depend not only on the magnitude of earthquake, but also on the structural vulnerability, site conditions, directivity and basin effects, existence of previous damage, etc. Sometimes small earthquakes can also cause severe economic loss or safety loss if the structure is vulnerable to earthquake hazards. Therefore, analyzing structural vulnerability under seismic loads

is important in risk assessment and studies on this topic have been conducted by many researchers (Wen and Song 2003, Ghosh and Padgett 2010, Balendra *et al.* 1999, Wilson and Holmes 2007, Seo and Linzell 2010). Based on the assumption that seismic vulnerability analysis is mainly related to the bridge substructure, the approach proposed by Akiyama *et al.* (2011) for evaluation of the time-variant seismic reliability of reinforcement concrete (RC) piers is adopted herein and other possible failure mechanisms (such as unseating) under seismic loads are not considered.

In this approach, the failure probability under seismic loads is estimated by comparing the demand and capacity of ductile displacement of an RC pier. The limit state equation is given as:

$$g = C_a - \Delta_e = 0 \tag{5.7}$$

where C_a = seismic displacement ductility capacity, which is evaluated based on the buckling model of longitudinal rebars in RC piers, and Δ_e = seismic displacement ductility demand, which can be obtained by nonlinear dynamic analysis. According to this model, the ductile displacement capacity is achieved when the buckling of longitudinal rebars occurs. Therefore, for a single degree of freedom RC pier with the bottom fixed, its displacement capacity can be estimated as (Akiyama *et al.* 2011, Naito *et al.* 2011):

$$\delta_u = \frac{\phi_y h^2}{3} + (\phi_u - \phi_y)(h - \frac{0.5d + 0.05h}{2})h \tag{5.8}$$

where h = shear span of RC pier; d = effective cross-sectional depth; ϕ_y = yield curvature of rebar; and ϕ_u = ultimate curvature, which is the curvature at the onset of buckling of longitudinal rebars, given by (Akiyama *et al.* 2011):

$$\phi_u = -\frac{1}{180d'}\ln\left[\left(\frac{f_y}{E_s} - \frac{\Delta\varepsilon_B}{100}\right)\left(\frac{2SN_B}{\pi d_o}\right)^2 - 0.0045\right] + \frac{\Delta\varepsilon_B}{d'} \tag{5.9}$$

$$\Delta\varepsilon_B = \left[\frac{2(d_o/S)}{1.95N_B}\left(g(N_B)\frac{f_m}{f_y} - 1\right)\right]^2 \tag{5.10}$$

$$g(N_B) = 1 + \frac{0.65\pi N_B}{16(d_o/S)A_{rl}f_m}\left[a_{wle}f_{wy}f(N_B) + 0.03\alpha_1\alpha_2 d_{se}d_r f_c^{\frac{2}{3}}N_B S\right] \tag{5.11}$$

$$a_{wle} = \begin{cases} N_w A_{rt}/N_L & \text{if } N_L < 5 \\ N_w A_{rt}/(0.2N_L + 4) & \text{if } N_L \geq 5 \end{cases} \tag{5.12}$$

$$f(N_B) = \begin{cases} (N_B^2 - 1)/N_B & \text{if } N_B \text{ is odd} \\ (N_B^2 + 2)/N_B & \text{if } N_B \text{ is even} \end{cases} \tag{5.13}$$

$$\alpha_2 = \exp\left(-7.4\frac{w - w_2}{w}\right) \tag{5.14}$$

where d' = distance from extreme compression longitudinal rebar to extreme tensile longitudinal rebar, f_y and f_m = yield and tensile strength of the longitudinal rebar, respectively, f_{wy} =yield strength of the tie, E_s = elastic modulus of the longitudinal rebar, S = ties' spacing of the RC pier, d_o and d_r = intact and remaining diameter of the longitudinal rebar, respectively, A_{rl} and A_{rt} = cross-sectional areas of the longitudinal rebar and tie, respectively, f_c = concrete compressive strength, d_{se} = distance from the center of cross-section of the longitudinal rebar to the edge of the

229

cover, N_w = number of ties in the region involved in the instability of the rebar, N_L = number of longitudinal rebars perpendicular to the loading direction, α_1 = reduction parameter, w = weight of intact cross-section of rebar, w_2 = remaining weight after removing the rust, and N_B = number of spaces between ties associated with buckling length. The corrosion effect on cross-section weakening of rebars is taken into account by the reduction factor α_2 and the remaining rebar diameter d_r.

With the seismic displacement ductility capacity given by Equations (5.8) to (5.14) and the seismic displacement demand obtained by performing nonlinear dynamic analysis of the bridge substructure, the seismic failure probability of each pier can be evaluated. For a multi-pier substructure whose piers are of same dimensions, it is assumed that all the piers are perfectly correlated. Therefore, the vulnerability analysis of the substructure can be reduced to the vulnerability analysis of a pier.

5.2.3 Consequence Analysis

Estimation of consequences of structure failure is one of the key steps in the risk assessment process. The inclusion of consequences evaluation distinguishes risk from other structural performance indicators, such as reliability and redundancy, which are only focused on the structure itself, without considering the influence of structure failure on the society. However, quantification of the consequences caused by a structure failure is a difficult task since it includes several aspects related to commercial, safety, and environmental losses.

As discussed in Chapter 4, the consequences associated with bridge failure can be evaluated from the following four aspects: rebuilding cost, running cost, time loss cost, and safety loss cost. However, in addition to these costs, failure of bridge structures may also lead to environmental losses. Different from some other structures, such as nuclear power stations and gas stations, bridge failure barely causes severe pollution to the environment. Therefore, environmental losses it causes can be evaluated as the cost to remove the collapsed bridge, which can be estimated as follows:

$$C_{\mathrm{Rem}} = C_1 WL \tag{5.15}$$

where C_1 = removal cost per square meter ($\$/m^2$), W = bridge width (m), and L = bridge length.

All the losses discussed above are only related to the bridge itself. However, if the bridge crosses a sea / river, its failure may also cause the running cost and the time loss cost due to the unavailability of the channel of the sea/river. If the bridge crosses a highway / railway, the rebuilding cost for the part of highway / railway under the bridge should also be counted in addition to the running cost and the time loss cost due to the unavailability of the highway / railway. The running cost and time loss cost can be estimated by using the same formulas presented in Equations (4.32) and (4.33) but all the parameters in these equations should be updated with the values associated with channel, highway or railway. Therefore, considering the annual money discount rate r_m, the future monetary value of the consequences C_{FV} caused by bridge failure at the year t is:

$$C_{FV} = \left[\left(C_{\mathrm{Reb}} + C_{Running} + C_{TL} + C_{SL} + C_{\mathrm{Rem}}\right) + C_{under}\right]\left(1 + r_m\right)^t \tag{5.16}$$

where C_{under} = loss associated with the channel, highway or railway under the failed bridge. C_{Reb}, $C_{Running}$, C_{TL}, and C_{SL} are defined in Chapter 4.

5.2.4 Risk Evaluation

After evaluating the occurrence probabilities of traffic loads and earthquake, performing the vulnerability analysis of the bridge under these two hazards, and investigating the associated consequences caused by the bridge failure, the instantaneous total risk R_{Total} is given as:

$$R_{Total} = C_{FV}\left[P(H_L)P(F\,|\,H_L) + P(H_E)P(F\,|\,H_E) - P(H_L)P(H_E)P(F\,|\,H_L H_E)\right] \quad (5.17)$$

where $P(H_L)$ and $P(H_E)$ = occurrence probabilities of traffic loads and earthquake, respectively, and $P(F\,|\,H_L)$, $P(F\,|\,H_E)$ and $P(F\,|\,H_L H_E)$ = failure probabilities of bridge under the occurrence of traffic loads, earthquake loads and both of them, respectively. It should be noted that Equation (5.17) is based on the assumption that the occurrences of traffic and earthquake loads are statistically independent.

5.3 RISK MITIGATION

Due to the deterioration of structural members and increase of loads, risk of bridge failure tends to increase over time. In order to ensure the structure's safety during its lifetime, a risk threshold is required. If the results from risk assessment indicate that the current system risk is lower than the predefined risk threshold, the structure is considered to be safe. In contrast, if the assessed risk is higher than the threshold, then an efficient mitigation strategy is required to reduce structural vulnerability. It is

obvious that strategies for risk mitigation should be structured aiming to: (a) reducing the occurrence probabilities of hazards; (b) reducing the failure probabilities of the structure for the specific hazards; and (c) reducing the consequences caused by structure failure. In this chapter, the efforts for risk mitigation are focused on the second aspect mentioned above: reducing structural failure probability, which can be achieved by applying maintenance actions to structures. These actions can be divided in: (a) essential maintenance; and (b) preventive maintenance.

5.3.1 Essential Maintenance

Essential maintenance (EM) is performance-based, since EM actions are normally applied when the performance indicator is close to or reaches the defined threshold. It comprises actions such as repair and replacement of members to improve structural performance substantially. Due to the limitation of financial resources, cost-oriented optimum EM strategies usually need to be sought. EM options used in this chapter are to replace certain structural members with new ones when the threshold of total risk is reached.

5.3.2 Preventive Maintenance

Preventive maintenance (PM) actions are usually performed at predetermined timings during the lifetime of a structure; therefore PM is time-based. It is composed of actions to repair defects or slow down the rate of deterioration, such as repainting, recoating, and re-waterproofing. PM actions applied before the deterioration of structural members are called proactive PM and their purpose is to delay the

deterioration initiation time (Yang *et al.* 2006, Kececioglu 1995). PM actions applied to deteriorating members are called reactive PM and the aim is to reduce the deterioration rate. PM can be performed at uniform or non-uniform time intervals. Liu and Frangopol (2005a) and Frangopol *et al.* (1997) studied the non-uniform PM strategies and found that they are more economical than the uniform ones. Therefore, PM actions considered in this chapter are at nonuniform time intervals, and both proactive and reactive PM actions are included.

5.4 CASE STUDY 1: A HIGHWAY BRIDGE IN LOW SEISMICITY REGION

The existing highway bridge described in Chapter 4 is used hrein to illustrate the effectiveness of the proposed approach. The elevation and cross-section of the bridge are shown in Figure 4.16 and Figure 4.17, respectively. The lifetime of this bridge is assumed to be 100 years.

5.4.1 Hazard Analysis

Hazards analyzed for this bridge are traffic and seismic loads. As mentioned previously, since the bridge was built for daily traffic use, the occurrence probability of traffic loads is assumed to be 1.0. Therefore, the unknown quantity in the hazard analysis part is the occurrence probability of earthquake. According to USGS (2009b), Colorado is considered a region of minor earthquake activity and the magnitude of the strongest earthquake it ever experienced is 6.6. Since the occurrence of earthquakes is relatively infrequent in Colorado and the historical earthquake record is relatively short (only about 130 years), it is not possible to accurately estimate the timing or

location of future dangerous earthquake in this state. However, based on the available historical earthquake record and geologic studies in Colorado, the seismologists predict that an earthquake of magnitude 6.5 to 7.0 could occur somewhere in the state in the future. Therefore, the largest magnitude considered for this bridge is 7.0.

Since sudden movements on faults are mainly responsible for strong ($6.0 \leq$ *magnitude* <7.0) and major earthquakes ($7.0 \leq$ *magnitude* <8.0), the magnitude 7.0 earthquake is assumed to occur at some faults around the bridge location. According to the Colorado's Earthquake and Fault Map, it is found that there are three faults near the bridge location: Golden Fault, Rampart Range Fault and Ute Pass Fault. The lengths of these faults are 30km, 46km and 71km, respectively. Their approximate positions and minimum distances from the bridge are shown in Figure 5.1. More detailed information about these faults can be found at the USGS website. Based on the latitudes and longitudes of the epicenters presented in Figure 5.1, the occurrence probabilities of the magnitude 7.0 earthquake at Golden, Rampart Range and Ute Pass Fault can be obtained using the 2009 Earthquake Probability Mapping (USGS 2009a), which are 2.02×10^{-5}, 3.51×10^{-5}, and 7.75×10^{-5}, respectively.

Moderate earthquakes ($5.0 \leq$ *magnitude* <6.0) can be caused by some other reasons besides fault movements; therefore, these earthquakes may occur at the places where no fault exists. In this context, an earthquake of magnitude 5.9 which is the maximum magnitude in the range of moderate earthquake is assumed to occur at the bridge location to generate the maximum earthquake intensity. According to the National Bridge Inventory (NBI), the latitude and longitude of the bridge location is found to be 39.76˚ and -104.93˚ (Figure 5.1). Based on the above information and

considering the radius of the investigated region as 10 km, the occurrence probability of the magnitude 5.9 earthquake at the bridge location is found to be 4.71×10^{-5} by using the 2009 Earthquake Probability Mapping (USGS 2009a).

5.4.2 Vulnerability Analysis

5.4.2.1 *Traffic load*

Vulnerability analysis of the bridge under traffic loads is only related to the superstructure which is composed of deck and girders. Based on Estes (1997), the limit state equations of the deck is:

$$g_{deck} = 0.563A(t)f_y\gamma_{mfc} - \frac{A^2(t)f_y^2\gamma_{mfc}}{244.8f_c} - 0.137\lambda_{asph} - 0.471\lambda_{conc} - M_{deck}(t) = 0 \qquad (5.18)$$

where A = cross-sectional area of reinforcement, f_c = compressive strength of concrete, f_y = yield stress of reinforcement, and M_{deck} = traffic load moment acting on the deck. The limit state equations of girders are presented in Equations (4.22) to (4.24) of Chapter 4. The probability distribution type of the random variables f_y, f_c, and γ_{mfc} are assumed to be normal. Their mean values are 390 Mpa, 19 Mpa, and 1.02, respectively, and the associated standard deviations are 45 Mpa, 3.4 Mpa, and 0.061, respectively. The parameters of other random variables in the above equations are listed in Table 4.5.

Failure of the system is defined as the failure of the deck or of any two adjacent girders. Therefore, the system can be modeled as a series-parallel system which consists of the deck and nine girders. Assuming the spans are perfectly correlated and considering the symmetry within the span, the system model can be simplified to the

model which is composed of the deck and five girders, as shown in Figure 5.2. It indicates that failure of the deck or any two adjacent girders (among girders 1 to 5) will cause bridge failure under traffic load. The correlations among the resistances of girders are assumed to be 0.5.

The point-in-time system failure probabilities under traffic load are evaluated using RELSYS and the results are plotted in Figure 5.3. It is observed that (a) the failure probability of exterior girder (girder 1) is the lowest among the deck and girders; (b) the changes of the failure probabilities of exterior-interior girder (girder 2) and interior girders (girders 3, 4 and 5) are not significant during the lifetime; and (c) the system failure probability is mainly governed by the deck. These findings are very helpful for the explanation of the optimum essential and preventive maintenance strategies which will be discussed later.

5.4.2.2 *Seismic load*

As mentioned previously, vulnerability analysis under seismic loads is focused on the substructure of the bridge. If the piers are assumed to be perfectly correlated, the vulnerability analysis of the substructure can be reduced to the vulnerability analysis of a pier. For a pier consisting of four columns, the failure of the pier is defined as the failure of any column, i.e., the system model is a weakest-link model. The limit state equation of each column under seismic loads is presented in Equation (5.7).

In order to find the probability distribution type and the associated parameters of ductile displacement capacity, the parameters of the assumed random variables associated with geometrical and material properties of column, as listed in Table 5.1,

are simulated by using Latin Hypercube sampling (1000 trials). The number of the ties and longitudinal rebars N_w and N_L are considered 4 and 12, respectively (Estes 1997). By using the approach defined by Equations (5.9) to (5.14), the displacement capacity matrix with the dimension of 1000 (number of samples) $\times$100 (bridge lifetime) is obtained. By applying this matrix into the Minitab (2010) and performing the distribution fitting for each year, it is found that lognormal distribution is the best fitting distribution and the associated distribution parameters for each year are also obtained. Figure 5.4 plots the lognormal distribution fitting result of the displacement capacity at the year $t = 0$.

To analyze the ductile displacement demand of the column under seismic loads, a two-dimensional finite element model of the pier was built using OpenSees (OpenSees 2011), as shown in Figure 5.5. The mass of superstructure is transferred to nine lumped masses, which correspond to nine girders, applied to the pier cap. As mentioned previously, four earthquake cases which are of magnitude 7.0 occurring at three different faults and of magnitude 5.9 occurring at the bridge location are considered for the vulnerability analysis. Based on the NEHRP (BSSC 1997) soil profile type classifications and the site geology conditions around the bridge area, the average shear wave velocity to a depth of 30m ($V_{S,30}$) is assumed to be 400 m/s. Given the magnitude of earthquake, epicentral distance, rupture distance, $V_{S,30}$ and number of samples which is set to 1000, the specified number of artificial ground motions can be generated using the approach provided by Yamamoto (2011).

By linking OpenSees (OpenSees 2011) with MATLAB (MathWorks 2009), the ductile tip displacements of each column associated with the 1000 ground motions

samples in one earthquake case are obtained. Then performing the distribution fitting to these displacements results in each earthquake case, the lognormal distribution is found to be the best fitting distribution and the associated distribution parameters are obtained. After obtaining the distribution types and the associated parameters of the ductile displacement capacity and demand of each column, the system failure probability is calculated using RELSYS.

5.4.2.3 *Both traffic and seismic loads*

Based on the prior assumptions that the traffic and earthquake loads are associated with the failure of the bridge's superstructure and substructure, respectively, the failure modes of the bridge given the occurrence of both the loads would be the failure of superstructure or substructure or both. Therefore, the vulnerability analysis under both traffic and seismic loads can be performed using the following equation:

$$P(F \mid H_L H_E) = P(F \mid H_L) + P(F \mid H_E) - P(F \mid H_L)P(F \mid H_E) \tag{5.19}$$

where the superstructure and substructure failure are assumed to be statistically independent.

5.4.3 Consequence Analysis

The consequences associated with the failure of bridge E-17-AH are evaluated from the following five aspects: rebuilding, running, time loss, safety loss, and removal costs. Based on the initial building cost of the bridge (Estes 1997), the rebuilding cost herein is estimated as $ 393,000. The removal cost per square meter C_1 is assumed to

be 376.74 $/m^2$ (Florida DOT 2011), and the width of the bridge is 15.2 m. The other parameters for the consequence evaluation are presented in Table 4.7.

5.4.4 Risk Assessment and Mitigation

After performing the hazards analysis, vulnerability analysis for the given hazards, and consequences analysis, the time-variant risk can be assessed. By comparing the risk caused by the earthquakes of magnitude 5.9 and 7.0 which occur at the bridge location and three faults, respectively, it is found that the earthquake of magnitude 5.9 leads to the highest risk to the bridge due to its shortest epicenter distance although its occurrence probability is not the largest among the four earthquakes investigated. Therefore, this risk is selected to represent the risk caused by earthquake loads.

The risks of bridge system failure due to traffic loads, seismic loads and the total risk which is evaluated using Equation (5.17) are plotted in Figure 5.6. It is evident that (a) compared with the risk caused by traffic load, the risk due to seismic load is much lower and can be neglected; therefore, the time-variant total risk is mainly controlled by the risk caused by traffic load; and (b) the total risk increases over time and the rate of change in the risk also increases over time. If a risk threshold 5.0×10^5 is assumed, the bridge service life will only be 47 years. In order to guarantee the bridge's safety within its target service life of 100 years, maintenance actions need to be applied.

5.4.4.1 *Essential maintenance*

Based on Estes (1997), four essential maintenance options are considered: replacing deck, replacing exterior girders, replacing deck and exterior girders, and replacing superstructure. Their associated costs are $225,600, $229,200, $341,800, and $487,100, respectively. As mentioned previously, the risk threshold 5.0×10^5 is reached at the year $t = 47$. To find the optimal EM option, each repair action is examined at this time and the one providing the lowest cost per year increase of service life is selected. The effects of each repair option on the service life extension are summarized in Table 5.2. It is found that (a) replacing exterior girders cannot extend the service life; and (b) although the extended years by replacing superstructure is longer than that by replacing deck, the cost associated with replacing superstructure is much more than that associated with replacing the deck. Therefore, replacing deck is the optimum option at $t = 47$ years.

The reasons for the resulting optimum EM option are explained by inspecting Figure 5.3: (a) since the failure probability of exterior girder, which is in the parallel position of the system model, is much lower than those of other girders, replacing exterior girders cannot mitigate the system risk; and (b) as previously mentioned, the system failure probability is mainly governed by the deck, therefore, the EM options including deck replacement (such as replacing deck, replacing superstructure) are very efficient in reducing system risk; in addition, due to the fact that the cost associated with replacing deck is the lowest, this option becomes the optimum EM option. The total risk is reduced significantly after the deck is replaced, as shown in Figure 5.7, and the service life is extended to $t = 88$ years. Once again, the procedure for seeking

the optimum EM option is repeated at this time and replacing deck was found to provide the minimum cost per year increase of service life by reaching the risk threshold at the time t =123 years, as listed in Table 5.3. Therefore, only two EM actions are required to maintain the total risk below the specified threshold 5.0×10^5 within the bridge's lifetime.

5.4.4.2 *Preventive maintenance*

Painting deck and coating girder aim to protect the bridge against corrosion. The corrosion initiates in the steel girder or the reinforcement in concrete deck when the service life of the painting or coating ends. Based on their roles in delaying the corrosion initiation time, recoating deck and repainting all the girders are considered as two preventive maintenance options for the bridge (Matsumoto *et al.* 1989, Almusallam *et al.* 2003). The effects of these two PM options on the corrosion depth of reinforcement and steel girder are shown qualitatively in Figure 5.8. The coating's service life is determined by Equation (5.6), while the painting's life is assumed to be a lognormal random variable with the mean and standard deviation of 6.15 years and 1.0 year, respectively (Matsumoto *et al.* 1989). The risk threshold used here is the same as that defined previously.

The optimum PM strategies with respect to different numbers of PM actions are obtained by the combined use of RELSYS and genetic algorithm toolbox in MATLAB (MathWorks 2009). It was found that repainting all the girders has no effect on the bridge service life extension. This can be attributed to: (a) the failure probability of exterior girder is much lower than other girders, although it varies significantly with

242

time; and (b) the failure probabilities of interior and exterior-interior girders change very slowly over time. Therefore, recoating deck becomes the only effective option in preventive maintenance and the optimum PM strategies associated with different numbers of PM actions are shown in Figure 5.9 to Figure 5.13.

Figure 5.9 presents the risk profiles in the case of applying deck recoating only once within the lifetime. It is observed that the risk threshold is reached at $t=47$ years if no PM action is applied. After recoating the deck at $t=37$ years which proves to be the optimal timing for PM application, the bridge's service life is extended to $t=57$ years. Figure 5.10 shows the results in the case of applying deck recoating twice during bridge's lifetime. The maximum years of service life that can be extended in this case is found to be 19 years when the deck is recoated at $t_1=23$ years and $t_2=48$ years. The results in the case of applying deck recoating three, four and five times are presented in Figure 5.11, Figure 5.12, and Figure 5.13, respectively. It is found that the bridge's service life can be extended by 31 years, 41 years, and 51 years, respectively when the deck recoating is applied at $t=[20, 42, 57]$ years, $t=[16, 37, 52, 69]$ years, and $t=[13, 34, 49, 68, 83]$ years, respectively.

It is observed from these figures that (a) since recoating deck aims to delay the propagation of corrosion of reinforcement in the concrete deck, the effect of PM on the lifetime risk profile is only to slow down the risk increase rate rather than reduce the risk immediately, which is the resulting effect of EM on lifetime risk; (b) as the number of PM actions increases, the lifetime risk profile with recoating becomes more flat, which implies a longer service life; (c) if only preventive maintenance is available, the maximum number of PM actions required for maintaining the system total risk

below the risk threshold during the bridge's entire lifetime (100 years) is five; and (d)

the minimum time interval between each PM application timings or between the first

PM application timing and the service life beginning timing in these five cases is 13

years, as shown in Figure 5.13; since the obtained coating's service life is lognormally

distributed with the mean and standard deviation of 10.77 years and 3.85 years,

respectively, the probability that the PM actions are applied after the service life of

previous coating ends is at least 98%; therefore, this indicates that the optimum PM

strategies for these five cases are reactive PM actions.

5.5 CASE STUDY 2: A HIGHWAY BRIDGE IN HIGH SEISMICITY REGION

The bridge investigated in Section 5.4 is assumed to be located in San Jose (California)

in this case study and its target lifetime is considered as 75 years.

5.5.1 Hazard Analysis

As mentioned in Section 5.4.1, the occurrence probability of traffic load is assumed to

be 1.0. From the Fault Activity Map of California (2010), it is seen that the bridge

location (latitude 37.33˚; longitude -121.89˚) is surrounded by some earthquake faults

(Figure 5.14) and all these faults are possible seismic sources which can generate

strong ground motions to the bridge. Since the radius of the investigated site region is

usually within 100km (Handfelt *et al.* 2011), a square region with the side length of

180km is used herein and the bridge is located in the square center, as shown in Figure

5.14. In order to perform detailed analysis of occurrence probabilities of earthquakes,

this region is discretized into 49 circular sub-regions with the radius of 15km by a grid consisting of 49 points. Each point represents an earthquake strike location.

According to the California Earthquake History (USGS 2009b), there were 15 large earthquakes whose magnitudes range from 6.6 to 7.9 occurred in California since 1850. Therefore, four discrete magnitudes 6.5, 7.0, 7.5, and 8.0 are analyzed for all the 49 earthquake locations. After inputting the desired time interval (75 years), radius of the investigated region (15 km), earthquake magnitude (6.5, 7.0, 7.5, and 8.0), and latitudes and longitudes of the 49 earthquake epicenter locations which can be derived from the latitude and longitude of bridge location, the occurrence probabilities of 196 earthquake scenarios are estimated using the 2009 Earthquake Probability Mapping (USGS 2009a).

5.5.2 Vulnerability Analysis

The vulnerability analysis under traffic load is presented in Section 5.4.2.1. The vulnerability analysis under seismic load in this case study is similar to that provided in Section 5.4.2.2. However, it should be noted that since the lifetime of the bridge in this case study is 75 years, the dimension of the displacement capacity matrix is 1000 (number of samples) ×75 (bridge lifetime). By performing the distribution fitting for each year, it is found that the displacement capacity is best modeled by lognormal distribution.

The finite element model discussed in Section 5.4.2.2 is also used herein to analyze the ductile displacement demand. As mentioned previously, 196 earthquake scenarios which are of four different magnitudes and occur at 49 different locations

are considered for the vulnerability analysis. By using the approach provided by Yamamoto (2011), the artificial ground motion associated with a specific earthquake scenario can be generated. Figure 5.15 shows a sample of the generated ground motions of magnitude 6.5 at the bridge location. After the samples of the ductile tip displacements of each column are obtained for each earthquake scenario, distribution fitting is performed and lognormal distribution is found to be the best fitting. Finally, the failure probability of the pier system is computed using RELSYS based on the statistical parameters of the displacement capacity and demand of each column. The vulnerability analysis under both traffic and seismic loads are presented in Section 5.4.2.3.

5.5.3 Risk Assessment

The consequences due to bridge failure are evaluated in Section 5.4.3. Based on the results from hazards, vulnerability, and consequence analyses, the point-in-time risk can be assessed. By comparing the risks caused by the 196 earthquake scenarios, it is found that the earthquake of magnitude 6.5 occurring at the bridge location causes the highest risk to the bridge due to its shortest epicenter distance (0 km) and highest occurrence probability ($P(H) = 0.199$). Therefore, this risk is selected to represent the risk resulting from earthquake loads. The risks of bridge system failure due to traffic load, seismic load and the total risk which is evaluated using Equation (5.17) are plotted in Figure 5.16.

It can be observed that (a) traffic and seismic and total risk increase over time; (b) the increase rate of seismic load risk is almost a constant during the service life,

246

whereas the traffic-load risk increases slowly in the first 40 years and then faster in the next 35 years; and (c) traffic load risk is lower than the seismic load risk in the first 59 years; afterward, it becomes higher than the seismic load risk and the difference between them increases over time. If a risk threshold 1.5×10^6 is assumed for total risk, the bridge service life will only be 47 years. In order to ensure the bridge's safety within its target service life of 75 years, maintenance actions need to be applied.

5.5.4 Risk Mitigation

5.5.4.1 *Essential maintenance*

Based on Estes (1997), five essential maintenance options are used in this case study and their associated costs are: replacing deck ($225,600), replacing piers ($298,000), replacing superstructure ($487,100), replacing deck and piers ($521,500), and replacing bridge ($659,900). Two different optimization criteria are considered herein to find the optimal EM solutions: (a) the optimum EM option at each time when the threshold is reached is the one providing the lowest cost per year increase of service life; and (b) the optimum EM strategy for the bridge's service life is the one which has the minimum life-cycle total EM cost.

As mentioned previously, the risk threshold 1.5×10^6 is reached at the year $t =47$. To find the optimal EM solution corresponding to the first criterion, each repair action is examined at this time and the effects of each repair option on the service life extension are summarized in Table 5.4. It is found that (a) replacing piers has the slightest effect on service life extension (only five years); (b) replacing deck is more effective than replacing piers; and (c) although the extended years by replacing bridge

is longer than that by replacing deck and piers, the cost associated with replacing bridge is also higher than that associated with replacing deck and piers; therefore, replacing deck and piers is the optimum option at $t = 47$ years.

The reasons for the above observations can be explained by examining Figure 5.3, Figure 5.16, and Figure 5.17: (a) although the traffic load risk is lower than the seismic load risk at $t = 47$ years, its increase rate is larger at this time; after replacing piers, the seismic load risk is reduced but the traffic load risk still increases rapidly; therefore, the risk threshold is reached again at $t = 52$ years after the piers are replaced; (b) as previously mentioned, the system failure probability under traffic load is mainly governed by the deck, therefore the EM options including deck replacement are efficient in reducing traffic load risk which increases rapidly during the last 35 years; although the seismic load risk cannot be mitigated by these EM options, it increases much slowly compared to the traffic load risk; thus, the service life extended by replacing deck (or superstructure) is more than that by replacing piers; and (c) since the total risk consists of seismic and traffic load risk, replacing deck and piers (or replacing bridge) which reduces the two risks simultaneously can significantly extend the bridge's service life.

The total risk is reduced by almost a half after the deck and piers are replaced at $t = 47$ years, as shown in Figure 5.17(a), and the service life is extended to $t = 71$ years. After repeating the procedure for seeking the optimum EM option at this time, replacing piers is found to be the optimal option by extending the service life to $t = 78$ years. Therefore, under the first optimization criterion, the optimum EM strategy

during the bridge's service life is to replace deck and piers at t =47 years and then replace only piers at t =71 years.

To determine the optimum EM strategy corresponding to the second optimization criterion, the costs of all possible EM solutions which can maintain the total risk below the predefined threshold 1.5×10^6 within the bridge's lifetime are compared and the optimum one which has the lowest total EM cost is found to be the combination of replacing deck at t =47 years and replacing piers at t =56 years, as shown in Figure 5.17(b). At t =47 years, bridge deck is replaced and the service life is extended by 9 years (see Table 5.4); at t =56 years, the traffic load risk is relatively low (since the deck was replaced in the previous EM action) and the seismic load risk is dominant; therefore, replacing piers at this moment can significantly reduce the total risk. By comparing the two EM strategies associated with two different optimization criteria, it is noticed that (a) different optimization criteria may lead to different optimum EM strategies; and (b) although the second EM strategy is more economical with a total cost of $523,600, the first EM strategy keeps the seismic load risk at a lower level during the lifetime (the traffic load risks in these two cases are the same).

5.5.4.2 *Preventive maintenance*

In addition to recoating deck that is discussed in Section 5.4.4.2, RC jacketing for piers is also used herein as a PM option to reduce the seismic load risk (Priestley *et al.* 1996). The side length of the column is assumed to increase by 30% after each RC jacketing. The sizes of the added ties and longitudinal rebars are the same as those in the original piers and the spacing of them is 150mm. The costs associated with

recoating the bridge deck and piers jacketing are assumed to be $40,000 and $15,000, respectively.

In this case study, the optimum PM strategy is determined by solving an optimization problem formulated as follows:

Find:

$$n_j, m_c, T_j = \left\{ t_{j,1}, t_{j,2}, ..., t_{j,i}, ..., t_{j,n} \right\}, T_c = \left\{ t_{c,1}, t_{c,2}, ..., t_{c,i}, ..., t_{c,m} \right\} \tag{5.20}$$

to minimize: the life-cycle total PM cost

subject to *the following constraints:*

the total risk during the service life is below the risk threshold 1.5×10^6

$$n_j \geq 0,\ m_c \geq 0 \tag{5.21}$$

$$t_{j,i} - t_{j,i-1} \geq 1,\ t_{c,i} - t_{c,i-1} \geq 1 \tag{5.22}$$

$$0 \leq t_{j,i} \leq 75,\ 0 \leq t_{c,i} \leq 75 \tag{5.23}$$

where n_j and m_c = numbers of column jacketing and deck recoating applied during the lifetime, T_j and T_c = vectors of application timings of column jacketing and deck recoating, and $t_{j,i}$ and $t_{c,i}$ = ith column jacketing and deck recoating time (years).

By combining RELSYS (Estes and Frangopol 1998) with genetic algorithm toolbox in MATLAB (MathWorks 2009), the optimum PM strategy is obtained with the objective value of 1.65×10^5. The risk profile under this optimum PM strategy is shown in Figure 5.18. It is observed that (a) the optimum PM strategy consists of 3 deck recoating (applied at T_c={19, 33, 49} years) and 3 column jacketing (applied at T_j={22, 39, 54} years); and (b) the effect of the ith column jacketing on decreasing seismic-load risk is more significant than that of the $(i-1)$th column jacketing because

the increased area of RC section associated with the i_{th} column jacketing is larger than the previous one.

5.6 CONCLUSIONS

In this chapter, a computational approach for assessing the time-variant risks due to traffic and earthquake loads and establishing the optimum essential and preventive maintenance strategies based on assessed risks is presented. The methodology used for the evaluation of commercial, safety and environmental consequences is improved by including three additional potential losses associated with bridge failure. A finite element model is used for a pier subjected to ground motions which are artificially generated to obtain the displacement ductility demand for the vulnerability analysis under earthquake load. Two different case studies in which the bridge is considered to be located in a low and high seismicity region, respectively, are investigated and the optimum EM and PM strategies are obtained. The following conclusions are drawn:

1. Consequence evaluation methods for the safety, environmental, and commercial losses associated with the unavailability of highway / railway or channel under the failed bridge are proposed in this chapter. In conjunction with the methods for running cost and time loss cost provided by other researchers and considering the money discount rate, Equation (5.16) presents an almost complete formulation for the time-variant consequences evaluation associated with bridge failure.

2. In case study 1, the increase rate of the risk due to traffic load is low in the first 60 years and then becomes very high in the next 40 years. This implies that for an essential maintenance option applied to reduce the risk due to traffic loads, its

effect on risk mitigation and service life extension will be weakened by postponing its application. This can be verified from Figure 5.7 and Table 5.2 and Table 5.3.

3. It is found from case study 2 that the optimum EM strategies associated with two different optimization criteria are different. One costs less money and the other keeps the bridge at a lower risk level during the lifetime. Choosing the solution that is more economical or safer as the final EM strategy depends not only on the financial budget but also on the decision-makers' attitude towards risk aversion.

4. In case study 2, the number of PM actions required for maintaining the system total risk below the risk threshold during the bridge's service life (75 years) is six, which is three times the number of EM actions; however, the total cost associated with the PM strategy is much less than those of EM strategies. Meanwhile, it keeps the seismic load risk at a lower level than the above two EM strategies within the lifetime. Therefore, it is considered as the optimum maintenance strategy.

5. During risk mitigation process, it was found that repainting girders have no improvement on bridge service life extension, which can be explained by the results from the vulnerability analysis under traffic load. This fact stresses the importance of analyzing and comparing the effects of the failure probability of each component on the system failure probability under a specific hazard during risk management.

Table 5.1 Parameters for the evaluation of ductile displacement capacity of longitudinal reinforcement in RC piers of Bridge E-17-AH.

Random variables	Mean	COV
Spacing of tie (mm)	305	0.1[a]
Initial longitudinal rebar diameter (mm)	25.4	0.015[b]
Distance from the center of longitudinal rebar to the edge of concrete cover (mm)	76	0.3[b]
Concrete compressive strength (MPa)	21	0.18[b]
Yield strength of longitudinal rebar (Mpa)	345	0.11[b]
Tensile strength of longitudinal rebar (Mpa)	450	0.11[b]
Elastic modulus of longitudinal rebars (Mpa)	2.06×10^5	0.06[b]

Note: [a] is assumed; and [b] is based on Estes (1997).

Table 5.2 Effects of each repair option on bridge service life extension at t =47 years in case study 1.

Options	Cost ($)	Lifetime extension (years)	Cost per year increase of service life ($)
Replacing deck	225,600	41	5,502
Replacing exterior girders	229,200	0	-
Replacing deck and exterior girders	341,800	41	8,336
Replacing superstructure	487,100	45	10,824

Table 5.3 Effects of each repair option on bridge service life extension at t =88 years
          in case study 1.

Options	Cost ($)	Lifetime extension (years)	Cost per year increase of service life ($)
Replacing deck	225,600	35	6,445
Replacing exterior girders	229,200	0	-
Replacing deck and exterior girders	341,800	35	9,765
Replacing superstructure	487,100	40	12,177

Table 5.4 Effects of each repair option on bridge service life extension at $t = 47$ years in case study 2.

Options	Cost ($)	Lifetime extension (years)	Cost per year increase in service life ($)
Replacing deck	225,600	9	25,066
Replacing piers	298,000	5	59,600
Replacing superstructure	487,100	13	37,469
Replacing deck and piers	521,500	24	21,729
Replacing bridge	659,900	27	24,440
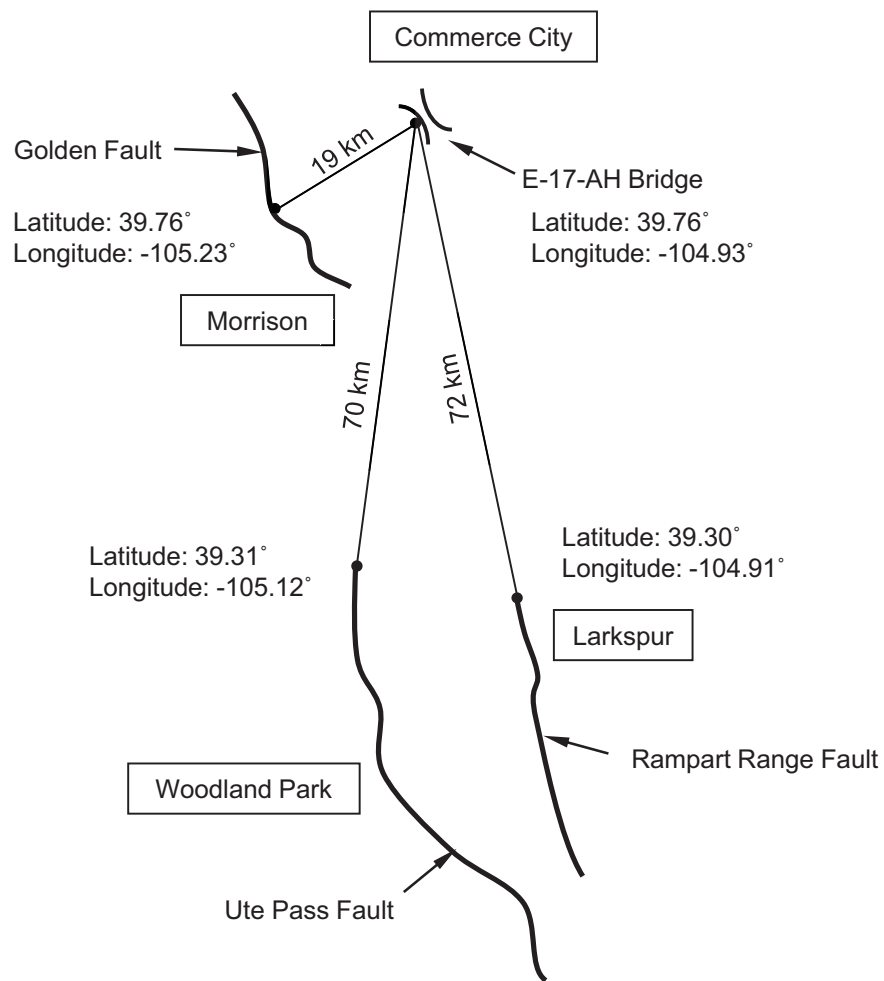
Figure 5.1 Locations of the three investigated faults and bridge E-17-AH.

Girder 1: Exterior girder
Girder 2: Exterior-interior girder
Girders 3 to 5: Interior girders
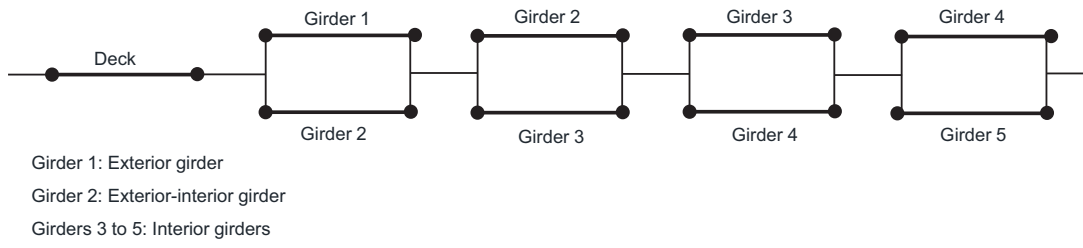
Figure 5.2 Series-parallel system model for vulnerability analysis under traffic load.
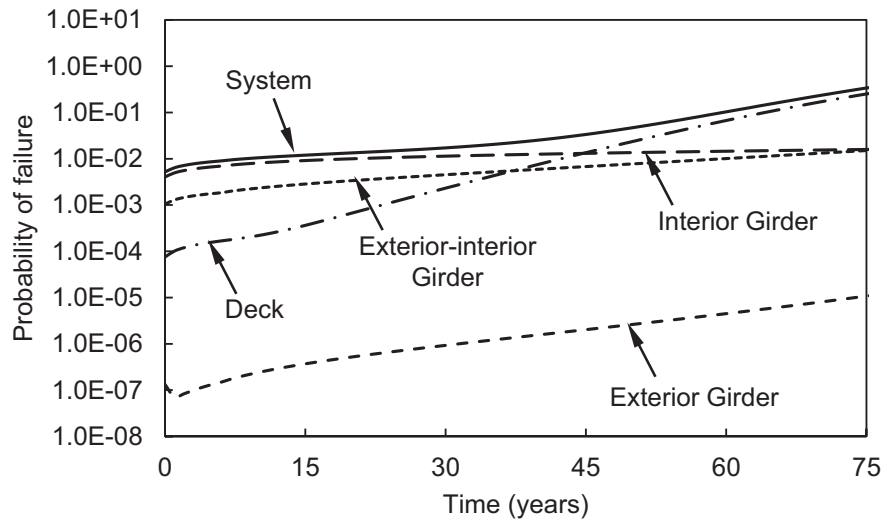
Figure 5.3 Failure probability profiles of each component and the system under traffic load.
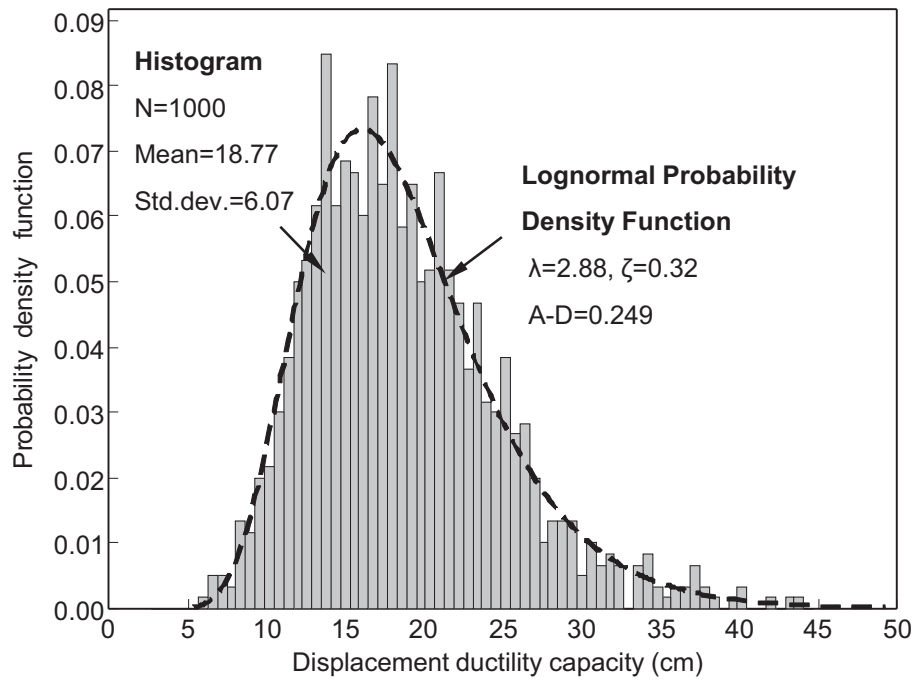
Figure 5.4 Lognormal distribution fitting of the displacement capacity at the year *t*=0.
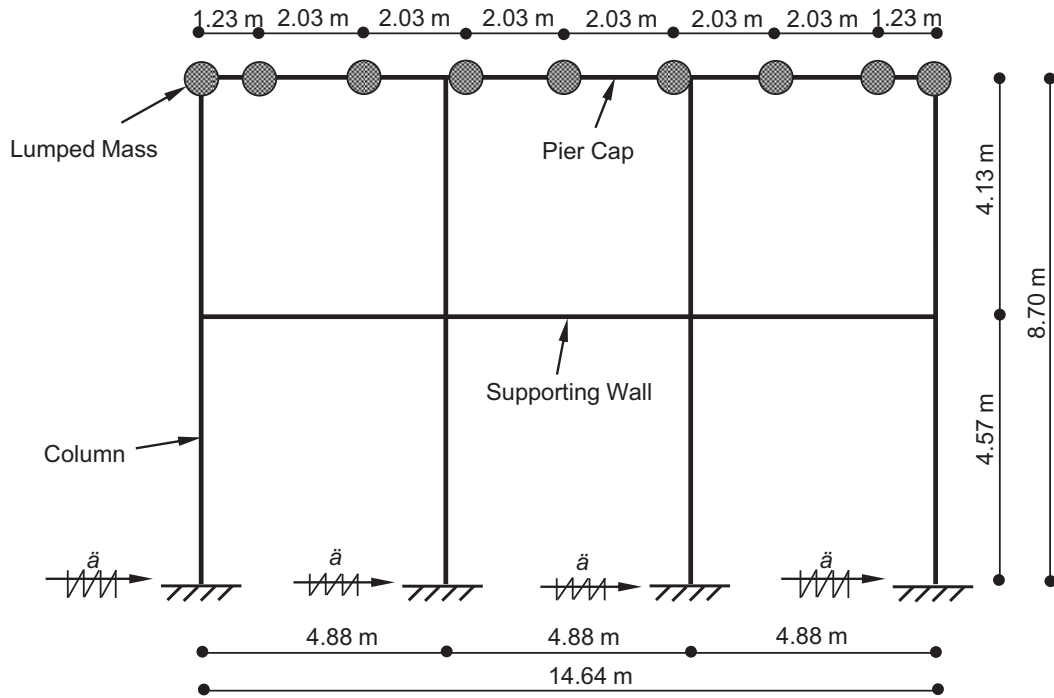
Figure 5.5 Two-dimensional finite element model of the pier.
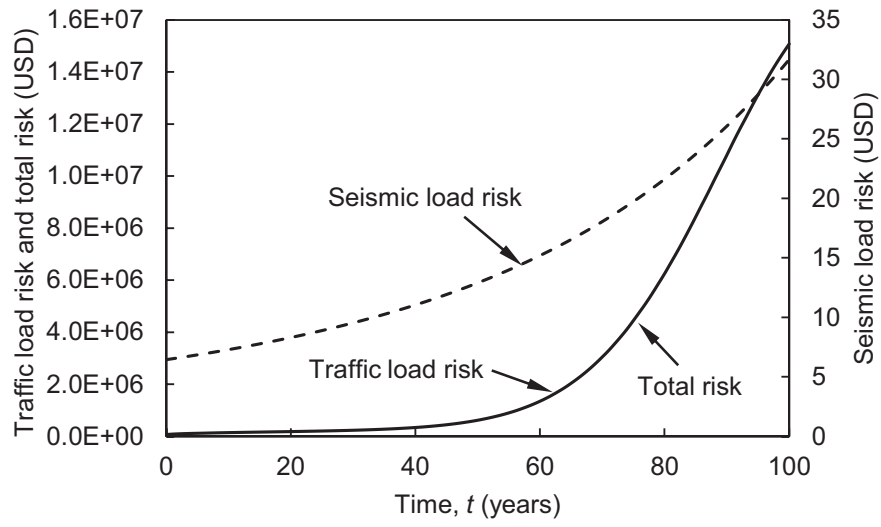
Figure 5.6 Profiles of traffic load risk, seismic load risk and total risk.
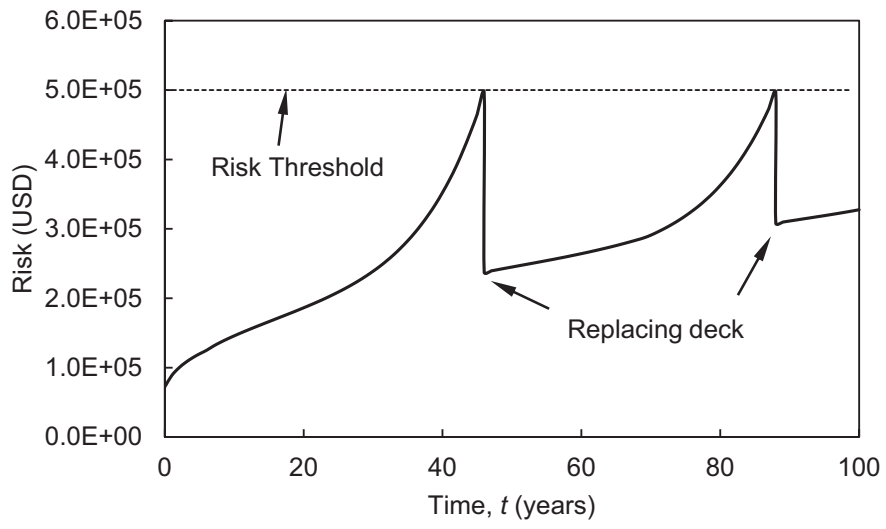
Figure 5.7 Total risk profile under optimum essential maintenance strategy.
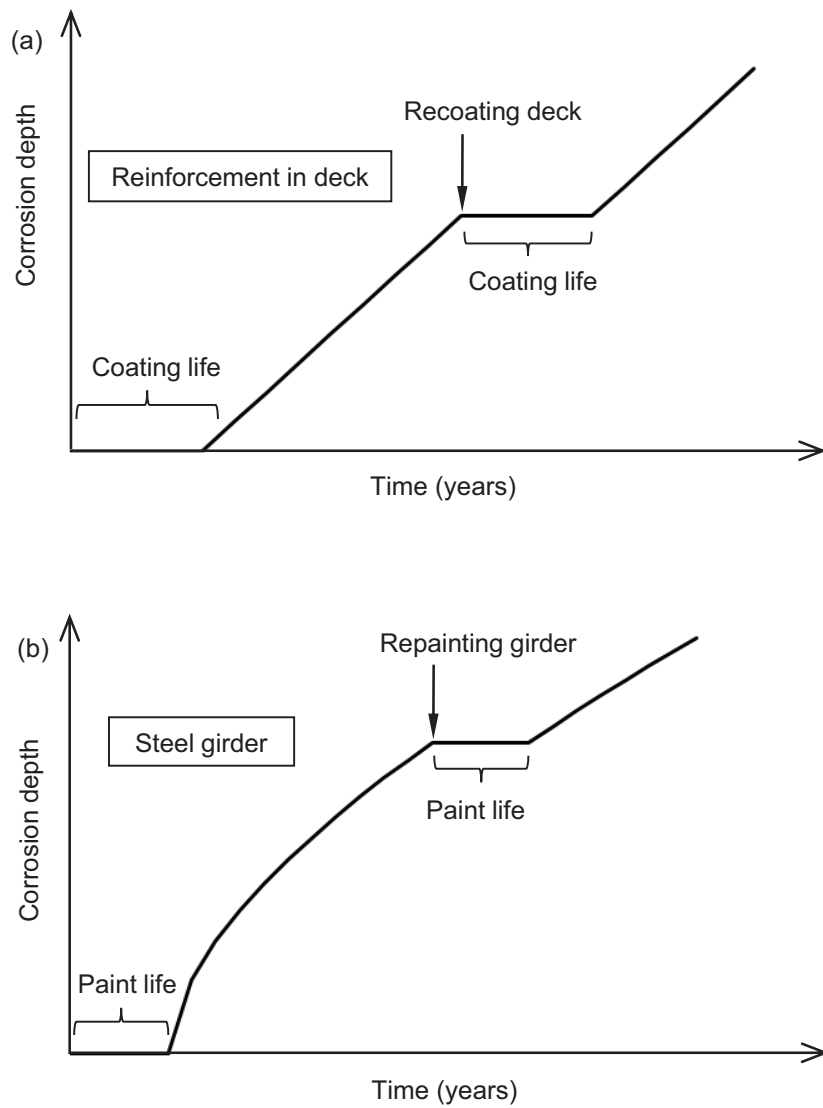
Figure 5.8 The effects of two preventive maintenance options on corrosion depth: (a) recoating deck; and (b) repainting girder.
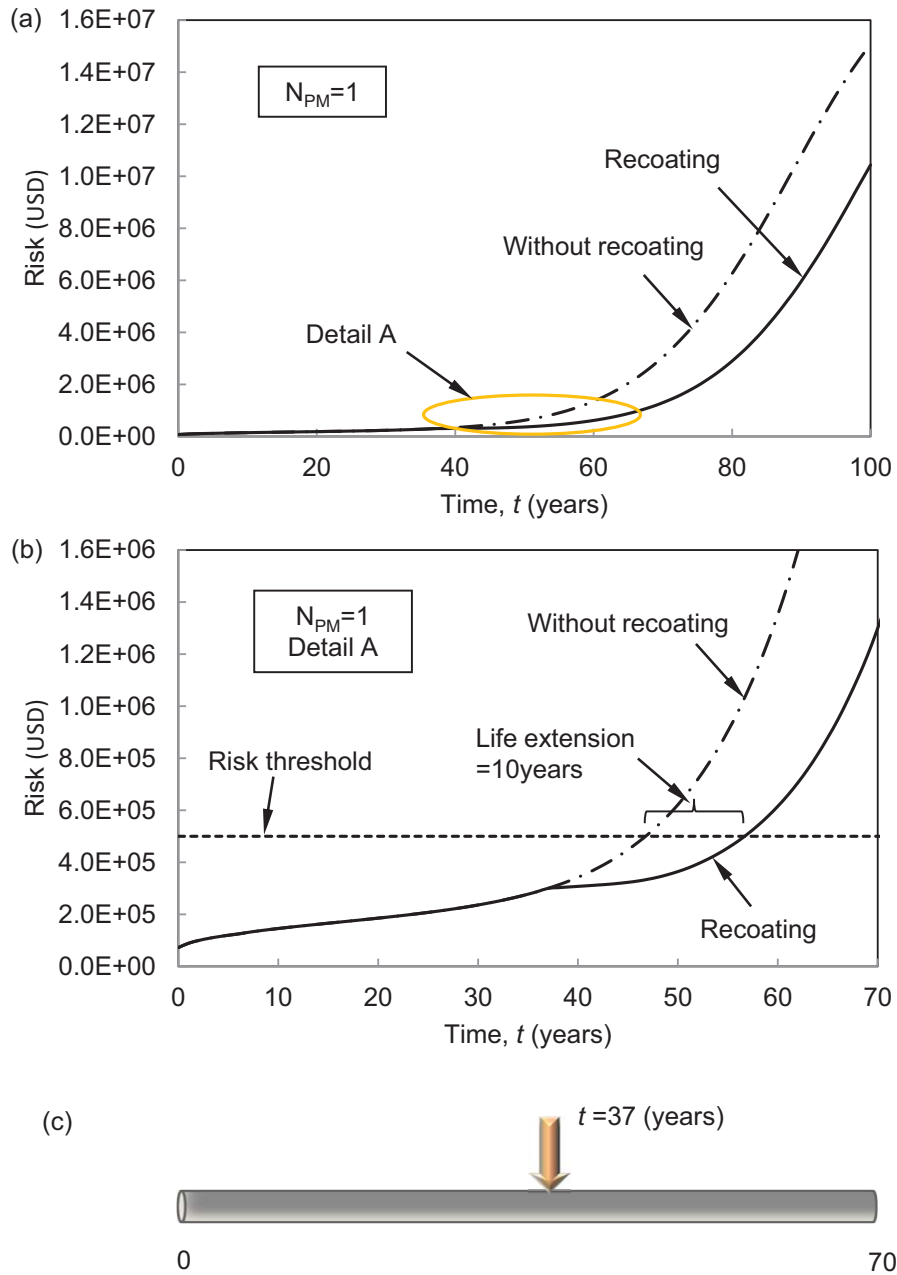
Figure 5.9 Risk profiles under one preventive maintenance: (a) total risk; (b) detail A;
and (c) optimum timing of PM application.
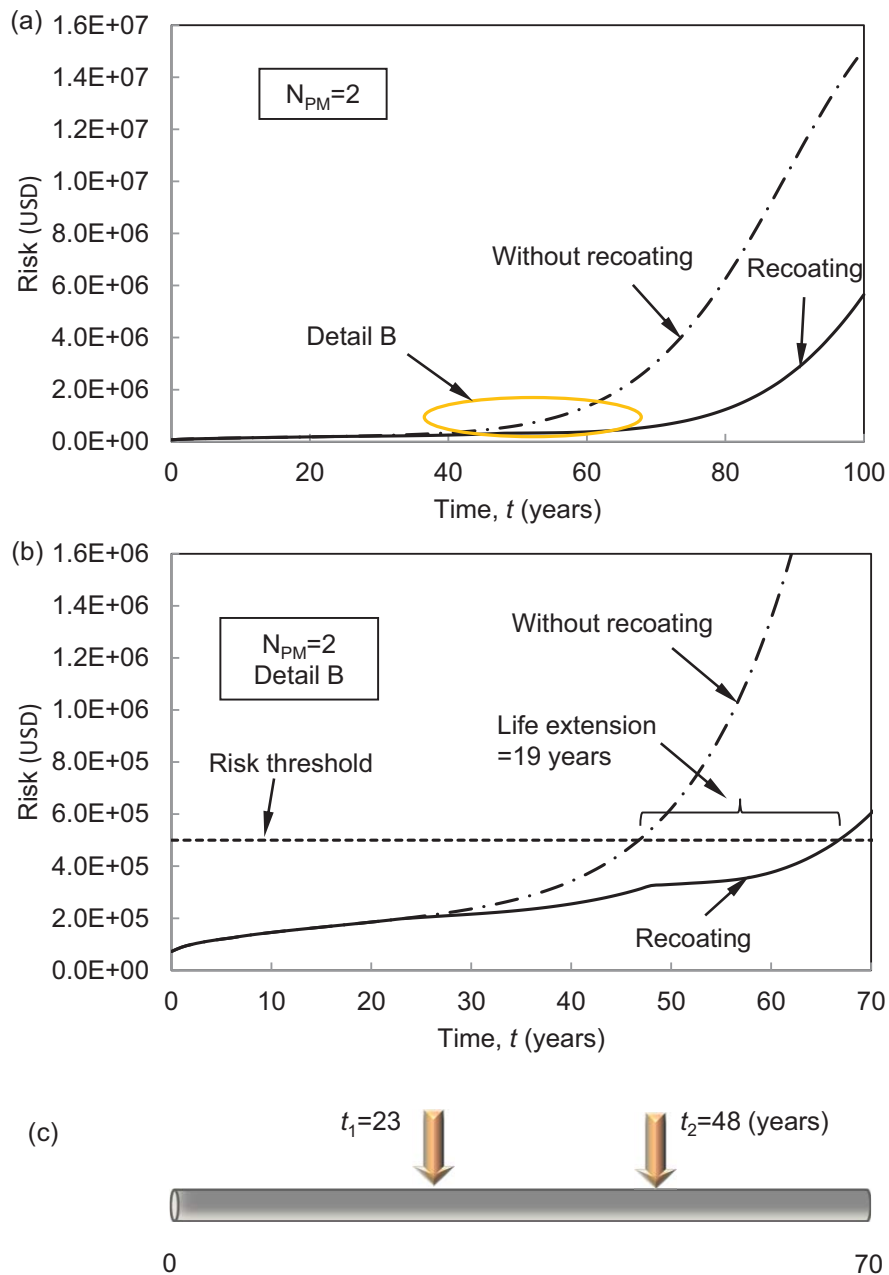
Figure 5.10 Risk profiles under two preventive maintenances: (a) total risk; (b) detail B; and (c) optimum timings of PM application.
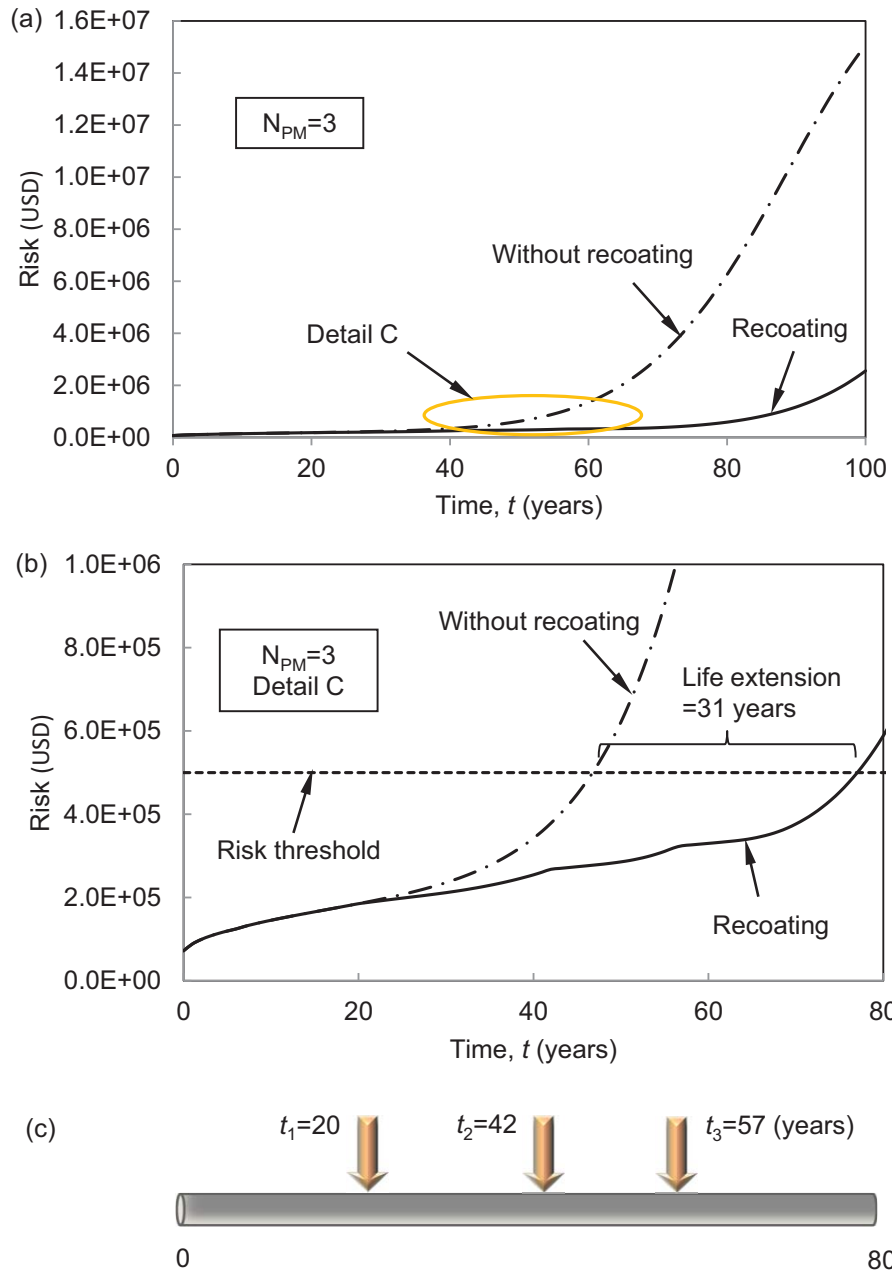
Figure 5.11 Risk profiles under three preventive maintenances: (a) total risk; (b) detail C; and (c) optimum timings of PM application.
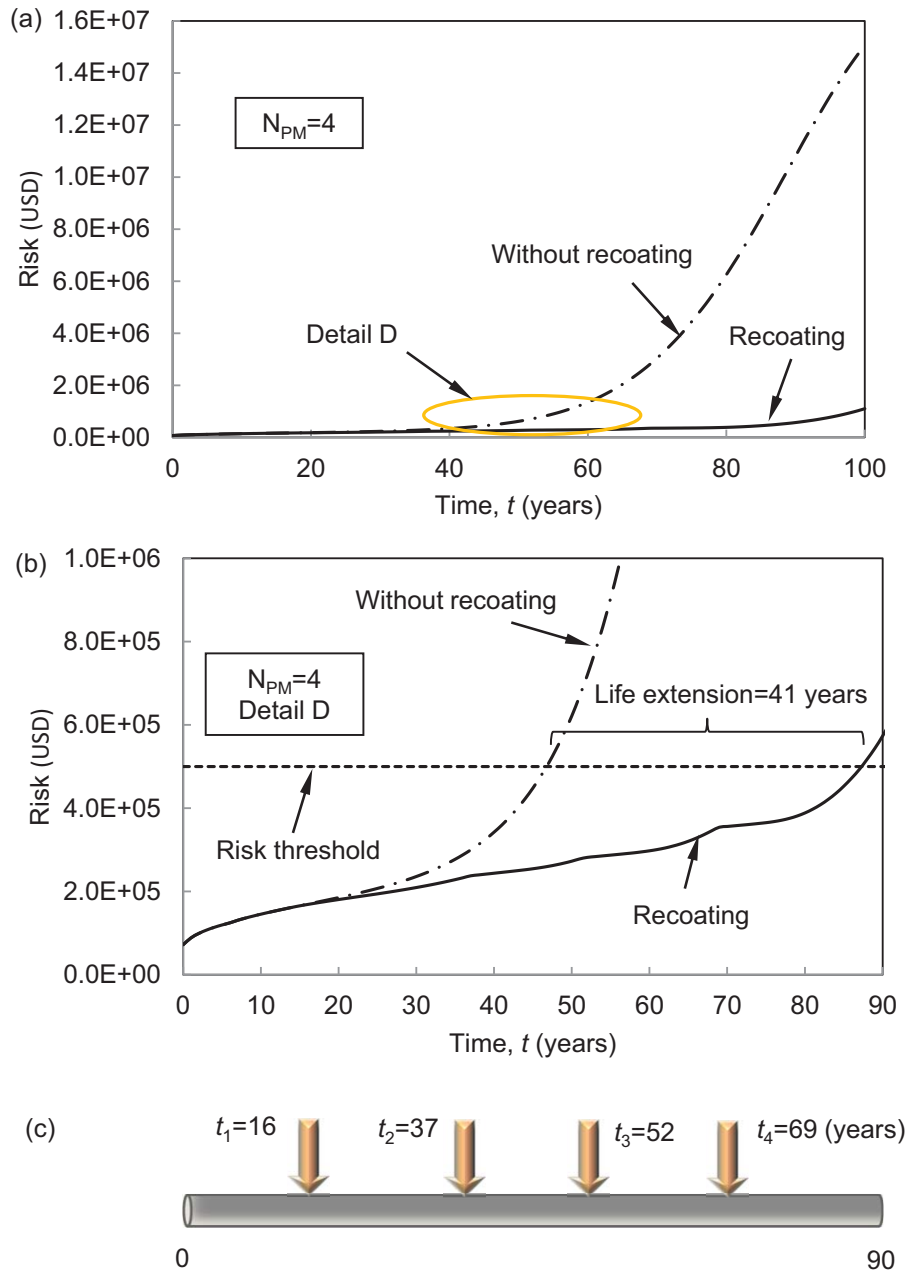
Figure 5.12 Risk profiles under four preventive maintenances: (a) total risk; (b) detail D; and (c) optimum timings of PM application.
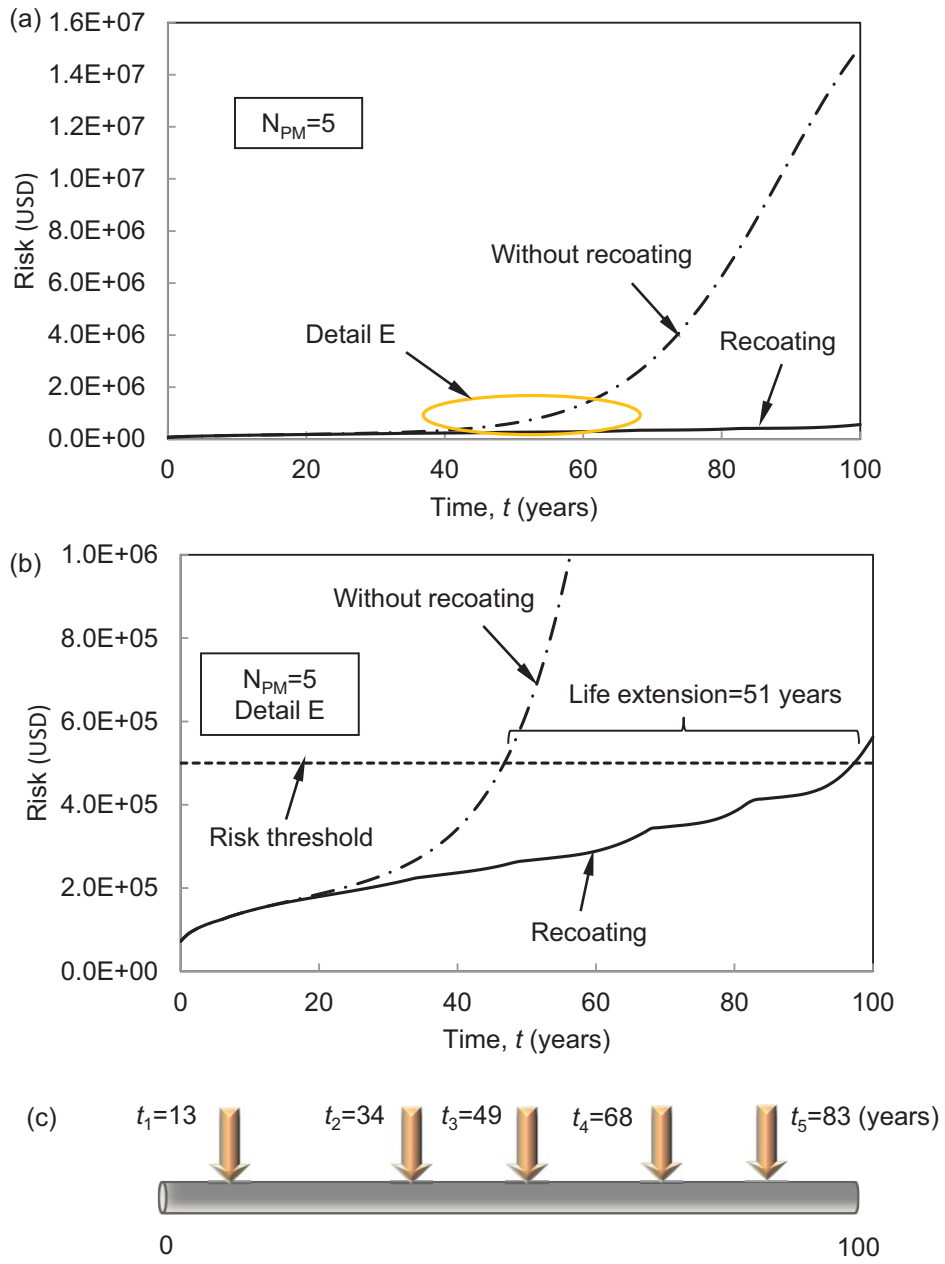
Figure 5.13 Risk profiles under five preventive maintenances: (a) total risk; (b) detail
E; and (c) optimum timings of PM application.
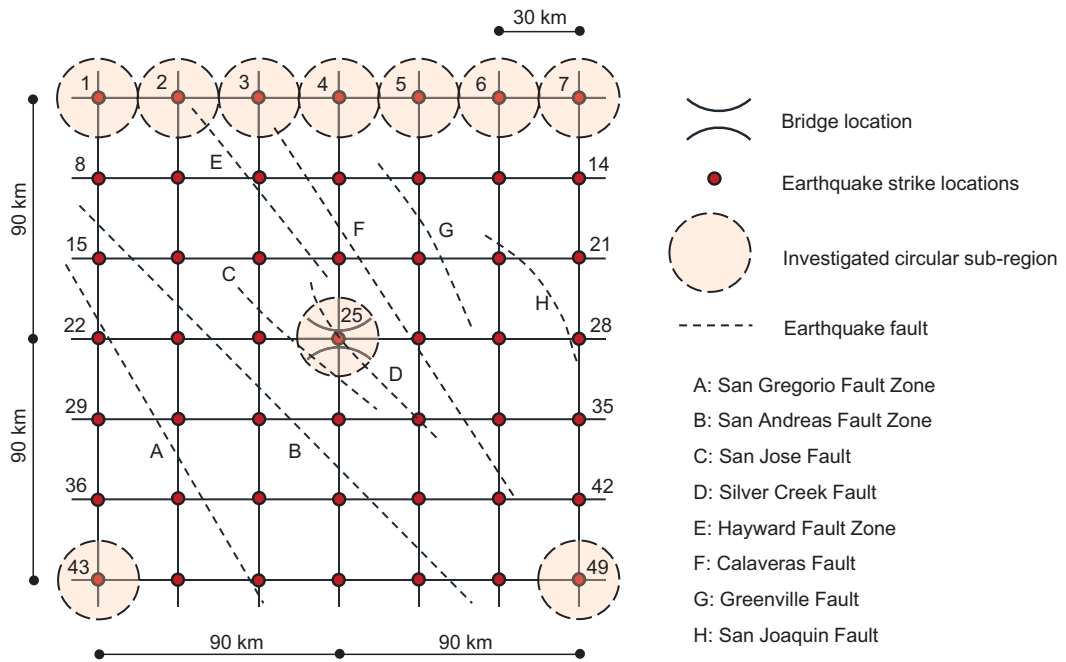
Figure 5.14   Locations of the investigated earthquakes, bridge and faults (Note: the
locations of the earthquake faults are approximate).
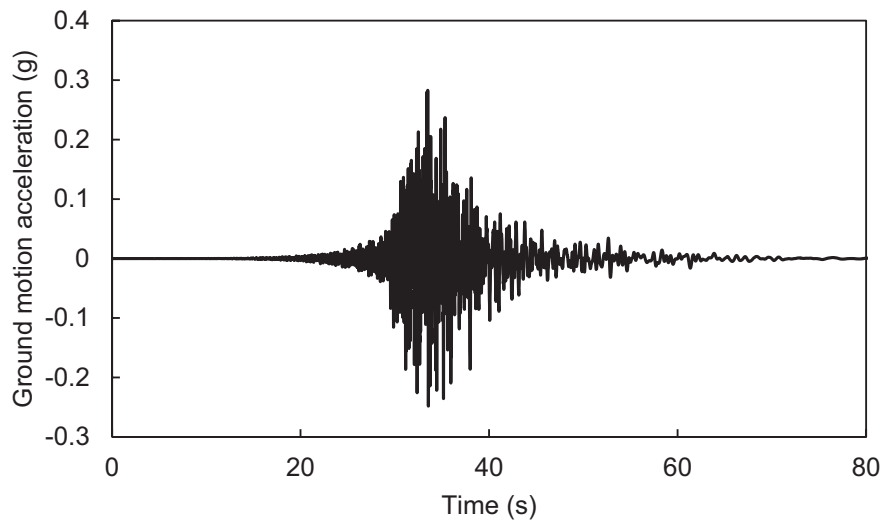
Figure 5.15 A sample of the generated artificial ground motions of magnitude 6.5 at
the bridge location.
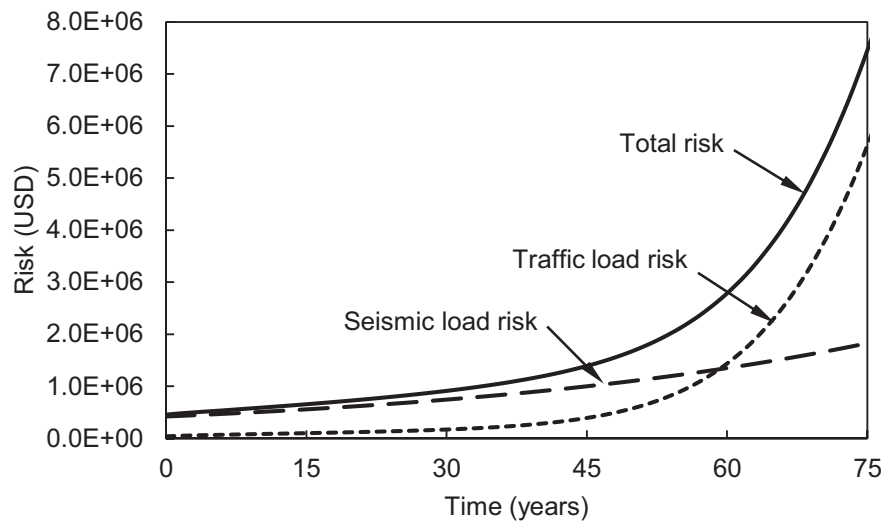
Figure 5.16 Profiles of traffic load risk, seismic load risk and total risk.
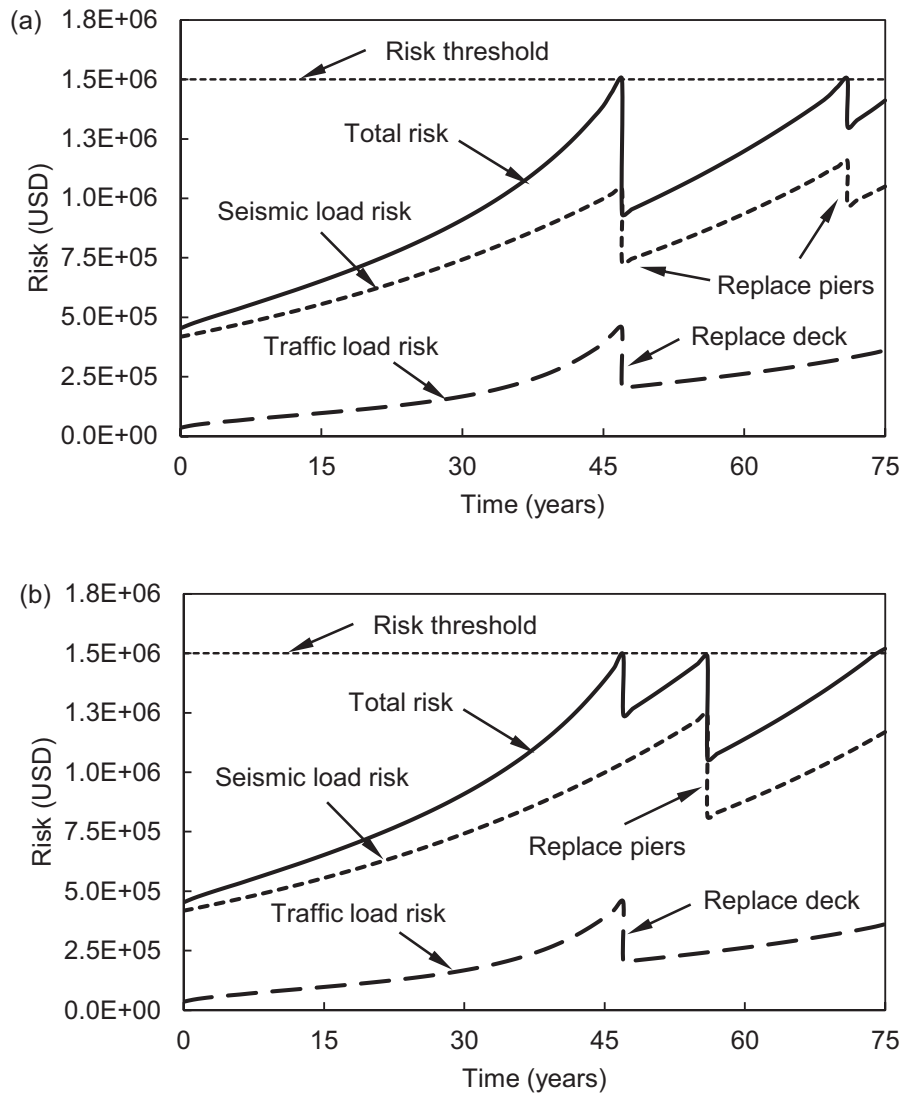
Figure 5.17 Risk profiles under two different optimum essential maintenance strategies: (a) lowest cost per year increase in service life; and (b) minimum life-cycle essential maintenance cost.
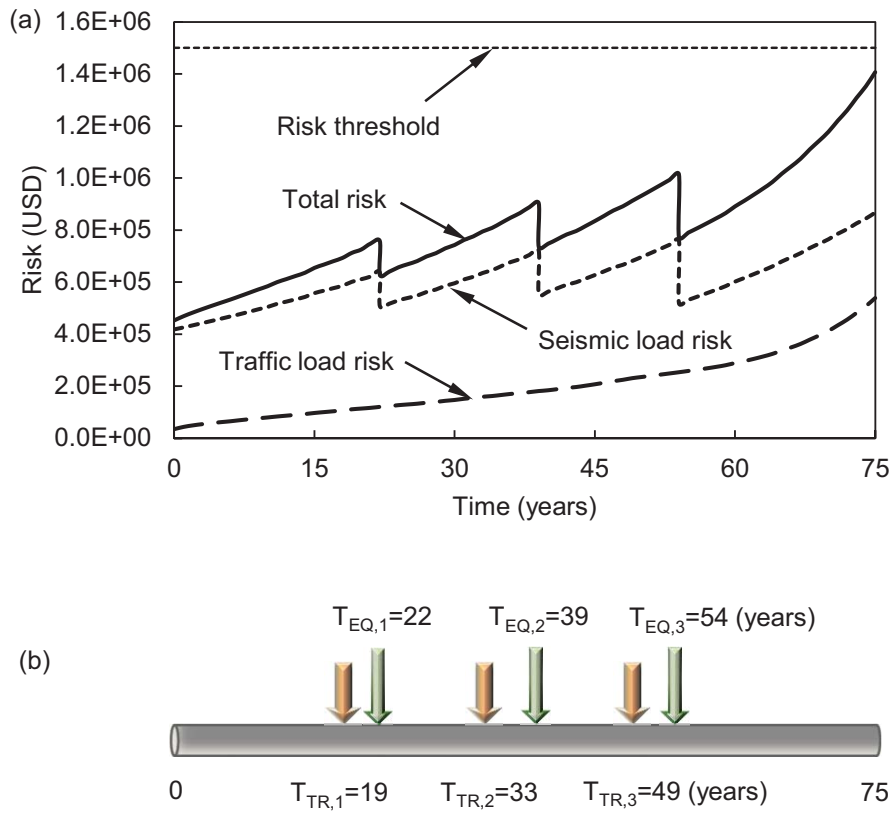
Figure 5.18 Risk profiles under preventive maintenance: (a) total, seismic and traffic risk profiles; and (b) optimum timings of PM application.

CHAPTER 6

TIME-VARIANT RISK ASSESSMENT OF BRIDGES WITH PARTIALLY AND FULLY CLOSED LANES DUE TO TRAFFIC LOAD AND SCOUR

6.1 INTRODUCTION

The deterioration of components strengths due to aging, observed growth of vehicular loads in both magnitude and volume, and the possible exposure to natural and / or man-made hazards have caused bridge safety concerns in many countries. In order to assess the level of structural safety to determine if maintenance actions are required, structural performance indicators, such as reliability, redundancy and robustness, were introduced and have been widely studied in recent decades (Frangopol and Curley 1987, Paliou *et al.* 1990, Ghosn and Moses 1998, Moan 2005, Okasha and Frangopol 2009a, Saydam and Frangopol 2011, Akiyama *et al.* 2013). These performance indicators reflect the uncertainties in resistance, load, and modeling. However, they do not take into account the consequences caused by malfunction or failure of structures. In this context, risk as a new performance indicator that provides means of combining the probability of failure or malfunction of a structure with the associated consequences was proposed. Much effort has been devoted by researchers to developing approaches and models for quantitatively assessing the risks of structures under different types of hazards (Stein *et al.* 1999, Lupoi *et al.* 2003, Adey *et al.* 2003, Decò and Frangopol 2011, Zhu and Frangopol 2013a).

Most previous studies on the risk assessment of bridge structures mainly focused on the risk due to the failure of the entire bridge system (Stein *et al.* 1999, Decò and Frangopol 2011, Yanmaz and Apaydin 2012, Zhu and Frangopol 2013a, Banerjee & Ganesh Prasad 2013). Although the consequences caused by the system failure are enormous, failure of the bridge system under a specific hazard is less likely to occur than the failures of its components. Since most bridges are designed with redundant load paths, failure of a component or a group of components may not lead to whole structure collapse but may cause partially or fully closure of bridge lanes. In this case, the functionality of bridge will be affected and the economic losses can be high. Therefore, it is necessary to assess the risk due to the unavailability of bridge lanes.

For a bridge with multiple lanes, there may be several different scenarios associated with the closure of bridge lanes (e.g., closing one, two, or all lanes). Generally, as the number of closed lanes increases, the resulted consequences become higher. However, it is difficult to predict which scenario will lead to the highest risk. Hence, it is essential to investigate all the possible lanes closure scenarios and assess their respective risks.

For bridges crossing rivers, traffic load and scour are two of the primary causes for bridge failure or closure of bridge lanes. Therefore, it is necessary to consider these two hazards in the risk assessment process. This chapter develops an efficient approach for assessing the time-variant risks associated with the closure of bridge lanes due to traffic load and scour. Section 6.2 introduces the traffic and scour hazard that are analyzed in this chapter. Section 6.3 identifies the possible scenarios of lanes closure due to the two hazards and evaluates the annual probabilities of occurrence of

these scenarios. Section 6.4 describes models for estimation of the consequences caused by closure of bridge lanes and assesses the time-variant risks. The proposed approach is applied to a highway bridge in Section 6.5. Finally, several conclusions are drawn in Section 6.6.

6.2 HAZARD EFFECTS CONSIDERED

As mentioned in Chapter 5, hazards are the situations or circumstances that pose a level of threat to the safety or functionality of structural systems. They can generally be classified into two types: (a) natural hazard, that are naturally occurring physical phenomena caused by rapid or slow natural events which can be hydrological (e.g., floods), geophysical (e.g., earthquakes and volcanic activity), among others; and (b) man-made hazards, that are caused by humans (e.g., traffic loading, collision, and fire).

Most bridges are built for passage of vehicles and pedestrians. Since the traffic on bridge usually increases over time, the original design features and geometries of the bridge may not be able to accommodate the current traffic volumes, vehicle sizes, and weights. In this context, overloading may occur on the bridge and the traffic loads may surpass the carrying capacity of the bridge. This will cause severe structural safety or functionality concerns of bridges especially when the increase of traffic loads is coupled with the deterioration of resistances of bridge members. Therefore, it is necessary to investigate the traffic hazard in the bridge risk assessment.

The other hazard studied in this chapter is scour, which is one of the most common causes of bridge failure in the United States (Wardhana and Hadipriono 2003). Scour is the engineering term for the water-induced erosion of the soil

surrounding bridge foundations during flooding events (Richardson and Davis 1995, Arneson *et al.* 2012). In connection with a bridge structure, three types of scour are recognized: long-term aggradation and degradation, contraction scour, and local scour (Lagasse *et al.* 2009, Arneson *et al.* 2012). Aggradation and degradation are long-term elevation changes in the streambed of the river or waterway cause by erosion and deposition of material. Contraction scour is due to the removal of material from river bed and the banks of a channel often resulted from constriction of the flow. Local scour involves the removal of material from around bridge piers and abutments. It is caused by an acceleration of flow and resulting vortices induced by obstructions to the flow.

While contraction scour and aggradation and degradation are less analyzed, local scour around bridge piers has been extensively studied over the past decades (Johnson 1991, Shen *et al.* 1969, Yanmaz and Altinbilek 1991, Melville and Chiew 1999, Breusers *et al.* 1997). Depending on the pattern of the approach flow sediment transportation, the local pier scour is classified into clear-water scour and live-bed scour (Chabert and Engeldinger 1956). Clear-water scour refers to the situation where there is no bed material transport; therefore, its scour hole is permanent. However, live-bed scour occurs when the bed material from the upstream is transported into the scour hole by the approach flow; therefore, it is cyclic in nature because it allows the scour hole that develops during the rising stage of the water flow to be refilled in the falling stage. The relation between the mean flow velocity V and the critical velocity V_c determines the scour condition is clear-water scour or live-bed scour. If $V > V_c$, live-bed scour occurs; otherwise, it is clear-water scour (Arneson *et al.* 2012).

For a bridge structure that spans a river or waterway, scour may occur during flooding events. In live-bed scour conditions, the scour hole generated during a flood is usually assumed to be refilled after the floodwater recedes (Ghosn *et al.* 2004). Although the precise information on the time needed for the foundation to regain its original strength is not provided in the available literature, it is suggested by bridge engineers that periods of three and six months are reasonable for clay and sand materials, respectively, to refill the scour hole (Ghosn *et al.* 2004). Assuming that the scour hole generated by the maximum yearly flood at year (t-1) is fully refilled when the maximum yearly flood at year t ($1 \leq t \leq 75$) occurs, the scour depths caused by annual maximum flood are considered as independent from year to year.

For the traffic hazard, the time-variant maximum loads acting on the bridge can be predicted using existing live load models. For the scour hazard, the scour depth at year t due to maximum yearly flood can also be estimated. Therefore, the annual probability of lanes closure caused by failure of bridge component(s) due to traffic load and scour can be evaluated, respectively, as will be presented in the following sections.

6.3 IDENTIFICATION AND ANALYSIS OF LANES CLOSURE SCENARIOS

6.3.1 Identification of Lanes Closure Scenarios

A bridge consisting of m lanes may have m or more different scenarios of lanes closure. For example, a steel girder bridge with four lanes may have the following possible lanes closure scenarios: (a) one lane is closed; (b) two lanes are closed; (c)

three lanes are closed; and (d) four lanes are closed. The two lanes closure case can be further divided into two scenarios: (a) two closed lanes are in the same direction; and (b) two closed lanes are in the different directions. The risks associated with these two scenarios might be different.

In the identification of the lanes closure scenarios, it should be noted that (a) failure of a single bridge component may lead to the closure of one lane or more lanes; for example, failure of an exterior girder may cause only one lane closure in a steel girder bridge; however, if an interior girder fails, two adjacent lanes may be closed; and (b) failures of different components (or different groups of components) may result in the same scenario of lanes closure. Therefore, the procedure for identifying the lanes closure scenarios is summarized as follows: (1) determine the lanes closure cases associated with failure of each critical bridge component (i.e., girders, piers); and (2) list the possible scenarios of lanes closure and express them in terms of the failure events of the investigated bridge components. For instance, consider a steel girder bridge having four lanes. From step (1) it is found that failure of the exterior girders A and B results in the closure of lane 1 and 4, respectively. Therefore, the scenario associated with the one lane closure can be described by the event

$$LC_1 = F_{A,only} \cup F_{B,only} \tag{6.1}$$

where LC_1 = one lane is closed, $F_{A,\,only}$ = only girder A fails, and $F_{B,\,only}$ = only girder B fails.

6.3.2 Analysis of the Scenarios

Since the lanes closure scenarios are represented by the failure events of bridge components, the failure probabilities of the components need to be calculated in order to evaluate the occurrence probabilities of these scenarios. For a given hazard, the maximum load it on a bridge component may exceed its resistance; therefore, the component failure occurs. Since the resistance of component may decrease due to deterioration and the load effect caused by the hazard may also vary over time, the limit state equation of the component including the time effect is

$$g(t) = R(t) - Q(t) = 0 \qquad\qquad\qquad (6.2)$$

where g = performance function, R = the resistance of the component, Q = load acting on the component under a given hazard, and t = time. With the limit state equation and other parameters that describe the uncertainties of R and Q, the time-variant failure probability of the component can be calculated.

6.3.2.1 *Traffic loading*

As mentioned in Chapter 5, traffic load is the most common type of loading that needs to be considered in the bridge design and performance assessment. Although bridge components may fail in different mechanisms under traffic load, only the flexural failure is investigated in this chapter with respect to the bridge superstructure components. The limit state equations of steel girders associated with flexural failure are provided in Equation (5.4). Corrosion is considered herein as the mainly factor that causes deterioration of girders and the corrosion model is provided in Equation (4.31)). In order to estimate the maximum bending moment of steel girder under traffic load,

the live load model presented in Chapter 4 is used herein. After obtaining the bending moment capacity and load effect that both vary with time, the annual failure probability of steel girder under traffic load can be determined based on the limit state equation given in Equation (5.4).

6.3.2.2 S*cour*

Bridges built in rivers are prone to scour around their piers during flooding events. The depth of scour is affected by the magnitude and duration of the flood. These two parameters associated with the maximum yearly flood usually vary from year to year. Therefore, in live-bed conditions, the scour depth in each year produced by maximum yearly flood is different. If the scour depth is significant, the stability of piers may be endangered and pier failure may occur. Assuming that the pier fails when the depth of scour hole reaches the bottom of pier footing (Johnson 1991), the limit state equation of the pier at year t is given as

$$g(t) = y_p - y_s(t) = 0 \qquad\qquad (6.3)$$

where y_p = pier depth, and y_s = scour depth.

During a flood event, the scour hole gradually develops and may reach the equilibrium scour depth if the flood is of long duration. For the live-bed scour, the time it takes to reach the equilibrium stage is less compared to clear-water scour. Therefore, it is assumed that the duration of the maximum yearly flood is long enough so that the equilibrium scour depth in live-bed condition can be reached. Extensive study has been conducted on the estimation of the equilibrium scour depth in the past decades and most of the proposed approaches are deterministic (Laursen 1958, Neill

1964, Shen *et al.* 1969, Yanmaz and Altinbilek 1991, Melville and Chiew 1999).

Among these approaches, the HEC-18 equation proposed by Richardson and Davis

(1995) for prediction of scour depth around bridge piers has been extensively used.

However, due to the presence of uncertainties in the parameters associated with stream

flow, pier shape, bed condition, and modeling, the scour depth needs to be evaluated

probabilistically. Therefore, a modified HEC-18 equation in which a modeling factor

is considered and most of the parameters are treated as random variables is used herein

to estimate the equilibrium scour depth (Ghosn *et al.* 2004):

$$y_s = 2\lambda_{mf} y_0 K_1 K_2 K_3 \left(\frac{D}{y_0}\right)^{0.65} Fr^{0.43} \tag{6.4}$$

where λ_{mf} = modeling factor, y_0 = the depth of flow upstream of the pier, K_1, K_2, and

K_3 = coefficients to take into account the nose shape of the pier, the angle between the

direction of the flow and the direction of the pier, and the stream bed condition,

respectively, D = the pier width, and the Froude number

$$Fr = V / \sqrt{(g_a y_0)} \tag{6.5}$$

in which V = mean flow velocity at the pier, and g_a = acceleration due to gravity.

The flow depth and flow velocity are related to the flow discharge rate, Q_f, and

the shape of the channel represented by the cross-sectional area of the stream, A, as

follows:

$$Q_f = AV \tag{6.6}$$

For a trapezoidal open channel with a constant bottom width, b, and side slope, z, the

cross-sectional area is calculated by

$$A = y_0(b + zy_0) \tag{6.7}$$

In addition, the flow velocity is related to the hydraulic radius, r, which is a function of the flow depth by Manning's equation:

$$V = \frac{1.49}{n} r^{2/3} S^{1/2} \tag{6.8}$$

where n = Manning roughness coefficient, and S = the slope of the bed stream.

Therefore, when the geometries parameters of the channel and the annual peak flow from maximum yearly flood event are provided, the flow depth and flow velocity can be calculated using Equations (6.6) to (6.8). Substituting the obtained depth and velocity of the flow into Equations (6.4) and (6.5) yields the equilibrium scour depth under the maximum yearly flood. Since most parameters in Equations (6.4) and (6.5) are modeled as random variables, Monte Carlo simulation is used to combine with these equations to obtain a probabilistic estimation of the equilibrium scour depth. Therefore, the annual failure probability of the pier column under scour can be computed using Equation (6.3).

As mentioned previously, the lanes closure scenarios are represented by the failure events of bridge components. After the time-variant failure probabilities of girders and piers are evaluated with respect to traffic load and scour, respectively, the occurrence probabilities of the identified scenarios of lanes closure can be calculated.

6.4 CONSEQUENCES EVALUATION

Failure of bridge components may lead to the partially or fully closure of bridge lanes. This will result in substantial interruption of traffic which will cause economic

disruption. Therefore, it is necessary to estimate the consequences due to the closure of bridge lanes in the risk assessment. In this chapter, consequences analysis is to quantitatively evaluate the economic loss stemming from the closure of bridge lanes caused by the failure of girder(s) or pier(s) under traffic load and scour. The economic loss is mainly estimated from the following three aspects: repair cost which is used to repair the failed bridge component(s) and the associated bridge parts, running cost and time loss cost due to closure of bridge lanes. The formula for estimation of the running and time loss costs are provided in Equations (4.32) and (4.33). However, it should be noted that when using these two equations in this Chapter, the average daily traffic A_{DT} should be replaced by the average daily traffic that are affected by the closure of bridge lane(s). Considering an annual money discount rate r_m, the total economic loss in future monetary value due to the closure of bridge lanes is

$$C_{FV} = \left(C_{RP} + C_{Running} + C_{TL}\right) \times \left(1 + r_m\right)^t \qquad (6.9)$$

where C_{RP} = repair cost, $C_{Running}$ and C_{TL} are defined in Chapter 4. After evaluating the time-variant occurrence probabilities of the identified scenarios of lane(s) closure and the associated economic loss, the time-variant risk related to these scenarios can be calculated using Equation (4.10).

6.5 CASE STUDY: A HIGHWAY BRIDGE

The bridge described in Section 4.4 is assumed to be located in Greene County, Ohio, crossing the Massies Creek. The lifetime of this bridge is considered as 75 years. The hazards analyzed herein are the traffic load and scour.

6.5.1 Identification of Lanes Closure Scenarios

Since this bridge has two lanes in each direction, the possible scenarios of lanes closure are: (a) closure of only one lane; (b) closure of two lanes in the same direction; (c) closure of two lanes in different directions; (d) closure of three lanes; and (e) closure of four lanes. As mentioned previously, the closure of bridge lanes under traffic load and scour is assumed to be caused by the failure of girders and pier columns, respectively; therefore, in order to identify the scenarios of lanes closure under the two respective hazards, the lanes closure cases due to the failure of each girder and pier column need to be determined.

The two exterior girders (Girders 1 and 9) mainly support the pedestrian traffic. Therefore, it is assumed that their failure has no effect on the vehicle traffic on the bridge. Consequently, only the seven interior girders (Girders 2 to 8) are considered in the scenarios identification process. Based on the assumption that the failure of an interior girder only affects its adjacent deck parts, the lanes closure cases associated with failure of each interior girder are shown in Table 6.1. It is seen from the table that only one lane will be closed if only Girder 2 or Girder 8 fails; therefore, the scenario associated with only one lane closure is expressed as the event

$$
\begin{aligned}
LC_{1,T} &= F_{G2,only} \cup F_{G8,only} \\
&= \left(F_{G2}S_{G3}S_{G4}S_{G5}S_{G6}S_{G7}S_{G8}\right) \cup \left(F_{G8}S_{G2}S_{G3}S_{G4}S_{G5}S_{G6}S_{G7}\right)
\end{aligned}
\tag{6.10}
$$

where $LC_{1,T}$ = only one lane is closed due to traffic load, $F_{G2,\ only}$ = only Girder 2 fails, $F_{G8,\ only}$ = only Girder 8 fails, F_{Gi} = Girder i fails (i = 2,3,…,8), and S_{Gi} = Girder i survives (i = 2,3,…,8).

For the scenario where two lanes in the same direction are out of service, two different cases are considered: (a) lanes 1 and 2 are closed; and (b) lanes 3 and 4 are closed. Therefore, based on Table 6.1, this scenario can be described in terms of the failure events of girders:

$$LC_{2S,T} = (L_1 \text{ and } L_2 \text{ are closed}) \cup (L_3 \text{ and } L_4 \text{ are closed})$$
$$= [(F_{G3} \cup F_{G4})S_{G5}S_{G6}S_{G7}S_{G8}] \cup [(F_{G6} \cup F_{G7})S_{G2}S_{G3}S_{G4}S_{G5}]$$

(6.11)

where $LC_{2S,T}$ = two lanes in the same direction are closed, and L_j = lane j (j = 1,2,3,4). Similarly, two cases are identified for the scenario in which two lanes in different directions are out of service: closure of lanes 2 and 3 that is caused by the failure of only Girder 5, and closure of lanes 1 and 4 which is resulted from the failure of Girders 2 and 8. The scenario is given as

$$LC_{2D,T} = (L_2 \text{ and } L_3 \text{ are closed}) \cup (L_1 \text{ and } L_4 \text{ are closed})$$
$$= (F_{G5}S_{G2}S_{G3}S_{G4}S_{G6}S_{G7}S_{G8}) \cup (F_{G2}F_{G8}S_{G3}S_{G4}S_{G5}S_{G6}S_{G7})$$

(6.12)

where $LC_{2D,T}$ = two lanes in the different directions are closed.

The scenario associated with the closure of three lanes consists of four cases: (a) lanes 1, 2, and 3 are closed; (b) lanes 1, 2, and 4 are closed; (c) lanes 2, 3, and 4 are closed; and (d) lanes 1, 3, and 4 are closed. Therefore, this scenario is written as

$$LC_{3,T} = (L_1, L_2 \text{ and } L_3 \text{ are closed}) \cup (L_1, L_2 \text{ and } L_4 \text{ are closed})$$
$$\cup (L_2, L_3 \text{ and } L_4 \text{ are closed}) \cup (L_1, L_3 \text{ and } L_4 \text{ are closed})$$
$$= [(F_{G3} \cup F_{G4})F_{G5}S_{G6}S_{G7}S_{G8}] \cup [(F_{G3} \cup F_{G4})F_{G8}S_{G5}S_{G6}S_{G7}]$$
$$\cup [(F_{G6} \cup F_{G7})F_{G5}S_{G2}S_{G3}S_{G4}] \cup [(F_{G6} \cup F_{G7})F_{G2}S_{G3}S_{G4}S_{G5}]$$

(6.13)

where $LC_{3,T}$ = three lanes are closed. Similarly, the scenario in which four lanes are out of service is identified as

$$LC_{4,T} = (L_1, L_2, L_3, \text{and } L_4 \text{ are closed})$$
$$= \left[(F_{G3} \cup F_{G4}) \cap (F_{G6} \cup F_{G7}) \right] \cup (F_{G2} \cap F_{G5} \cap F_{G8}) \qquad (6.14)$$

where $LC_{4,T}$ = four lanes are closed.

The lanes closure cases associated with failure of each pier column to determine the scenarios of lanes closure due to scour hazard is presented in Table 6.2. It is observed that the scenario associated with closure of two lanes in the same direction will not occur because the combination of failures of pier columns that leads to this scenario does not exist. Therefore, only the remaining four scenarios associated with lanes closure are investigated under the scour hazard. According to Table 6.2, the scenario associated with the closure of only one lane occurs when only Column 1 or Column 4 fails; therefore, this scenario is described by the following event:

$$LC_{1,S} = (L_1 \text{ is closed}) \cup (L_4 \text{ is closed}) = (F_{P1}S_{P2}S_{P3}S_{P4}) \cup (F_{P4}S_{P1}S_{P2}S_{P3})$$

$$(6.15)$$

where $LC_{1,S}$ = only one lane is closed due to scour, F_{Pi} = Column i fails (i = 1,2,3,4), and S_{Pi} = Column i survives (i = 1,2,3,4). Failure of both Columns 1 and 4 leads to the scenario where two lanes (different directions) are out of service:

$$LC_{2,S} = (L_1 \text{ and } L_4 \text{ are closed}) = (F_{P1}F_{P4}S_{P2}S_{P3}) \qquad (6.16)$$

where $LC_{2,S}$ = two lane are closed due to scour. The scenario associated with the closure of three lanes has two different cases: (a) lanes 1, 2, and 3 are closed; and (b) lanes 2, 3, and 4 are closed. Therefore, this scenario is expressed as the event

$$LC_{3,S} = (L_1, L_2 \text{ and } L_3 \text{ are closed}) \cup (L_2, L_3 \text{ and } L_4 \text{ are closed})$$
$$= (F_{P2}S_{P3}S_{P4}) \cup (F_{P3}S_{P1}S_{P2}) \qquad (6.17)$$

288

where $LC_{3,S}$ = three lane are closed due to scour. The last scenario in which four lanes are closed occurs when Columns 1 and 3 fail, or Columns 2 and 4 fail, or Columns 2 and 3 fail, shown as follows

$$LC_{4,S} = (L_1, L_2, L_3, \text{and } L_4 \text{ are closed}) = F_{P1}F_{P3} \cup F_{P2}F_{P4} \cup F_{P2}F_{P3} \qquad (6.18)$$

where $LC_{4,S}$ = four lanes are closed due to scour. With the relations between the identified lanes closure scenarios and the failure events of girders and pier columns, the probabilities of occurrence of these scenarios can be determined after the failure probabilities of girders and pier columns are obtained.

6.5.2 Analysis of the Scenarios

6.5.2.1 *Traffic loading*

As mentioned previously, the lanes closure scenarios due to traffic loading are caused by failures of interior girders. The limit state equations of the interior girders are provided in Equations (4.23) and (4.24) and the parameters of the random variables are presented in Table 4.5. Based on the limit state equations and the associated parameters, the annual failure probabilities of each girder are calculated using RELSYS (Estes and Frangopol 1998). The results are plotted in Figure 6.1. It is observed that (a) the probabilities of failure of all the girders increase over time; and (b) the failure probabilities associated with Girders 3 to 7 are higher than those associated with Girders 2 and 8; this is because the live loads distributed to Girders 3 to 7 are larger.

In the probability analysis of the lanes closure scenarios, two extreme correlation cases among the failure modes of girders are considered: (a) independent case; and (b)

perfectly correlated case. For the first scenario where only one lane is closed, its probability of occurrence can be calculated based on Equation (6.10) as follows:

$$P(LC_{1,T}) = P(F_{G2}S_{G3}S_{G4}S_{G5}S_{G6}S_{G7}S_{G8}) + P(F_{G8}S_{G2}S_{G3}S_{G4}S_{G5}S_{G6}S_{G7}) \qquad (6.19)$$

where $P(LC_{1,T})$ = probability associated with the closure of only one lane due to traffic loading. In the independent case, Equation (6.19) becomes

$$P(LC_{1,T}) = P(F_{G2})[1 - P(F_{G3})][1 - P(F_{G4})][1 - P(F_{G5})][1 - P(F_{G6})][1 - P(F_{G7})][1 - P(F_{G8})]$$
$$+ P(F_{G8})[1 - P(F_{G2})][1 - P(F_{G3})][1 - P(F_{G4})][1 - P(F_{G5})][1 - P(F_{G6})][1 - P(F_{G7})]$$

$$(6.20)$$

where $P(F_{Gi})$ = the probability of failure of Girder i. However, in the perfectly correlated case, Equation (6.19) is expanded as follows

$$P(LC_{1,T}) = \max\{0, P(F_{G2}) - \max[P(F_{G3}); P(F_{G4}); P(F_{G5}); P(F_{G6}); P(F_{G7}); P(F_{G8})]\}$$
$$+ \max\{0, P(F_{G8}) - \max[P(F_{G2}); P(F_{G3}); P(F_{G4}); P(F_{G5}); P(F_{G6}); P(F_{G7})]\}$$

$$(6.21)$$

By substituting the obtained probabilities of failure of each girder into Equations (6.20) and (6.21), the probabilities of occurrence associated with the closure of only one lane considering the two extreme correlation cases can be evaluated. Similarly, the probabilities of occurrence of the other four scenarios can be calculated based on Equations (6.11) to (6.14). The results are shown in Figure 6.2.

It is observed that in the independent case (a) the probabilities of occurrence associated with all scenarios increase over time; (b) among all the five scenarios, the probability of occurrence associated with the closure of four lanes is the lowest while its counterpart associated with the closure of two lanes in the same direction is the highest; (c) the occurrence probabilities of the closure of three and four lanes are very close; and (d) for the scenarios where two lanes are closed, the probability of

290

occurrence associated with the different directions is much lower than that associated with the same direction. However, in the perfect correlation case, the probability of occurrence associated with the closure of four lanes increases over time while the probabilities of the occurrence of the other four scenarios are nil. This is mainly due to the assumption of the relations between the lanes closure cases and the failure of girders (see Table 6.1). In addition, the fact that the failure probabilities of girders 3 to 7 are the same and they are lower than those of girders 2 and 8 also affects the results. The results will be different if any of these factors change. For example, if the failure probabilities of girders 2 and 8 are much higher than those of girders 3 to 7, the probability of occurrence associated with the closure of two lanes in different directions becomes the highest in the perfect correlation case.

6.5.2.2 *Scour*

Based on the bridge site information, a series of 60 consecutive historical data on the annual peak flow for the Massies Creek at the bridge location is obtained from the USGS National Water Information System (NWIS) (USGS 2014), as shown in Figure 6.3. Assuming that the annual peak flows are independent of each other and random (Ahearn 2003), a distribution fitting is performed to these recorded data and it is found that the annual peak flow is best modeled by a lognormal distribution. Figure 6.4 plots the histogram as well as the fitted distribution of the annual peak flow. Since the lifetime of the bridge is assumed to be 75 years, the recorded data is used as the annual peak flows for the next 60 years and another group of 15 samples are generated from

the obtained lognormal distribution to be used as the annual peak flows for the remaining 15 years.

According to the National Bridge Scour Database (USGS 2000), the geometry parameters of the channel (e.g., side slope, slope of the bed stream) at the bridge site are determined, as listed in Table 6.3. With the annual peak flow and the geometry parameters of the channel, the flow depth and flow velocity can be calculated using Equations (6.6) to (6.8). In the estimation of the annual maximum scour depth, the flow depth, flow velocity, modeling factor, and correction factor for bed condition are considered as random variables. Therefore, the flow depth and flow velocity obtained from Equations (6.6) to (6.8) are used as mean values and their probability distribution types and coefficients of variation (c.o.v.) are provided in Table 6.4.

Based on the information given in Table 6.4, a large number of samples (10^6) for the random variables are generated using Monte Carlo simulation. Substituting these samples into Equations (6.4) and (6.5) yields the samples of the annual equilibrium scour depth. Figure 6.5 shows the mean values of the annual equilibrium scour depth for the investigated time interval (i.e., 75 years). The depths of the pier columns are the same and they are assumed to follow normal distribution with the mean value and coefficient of variation of 3.0 and 0.1, respectively. Therefore, with the obtained samples of the annual equilibrium scour depth and the samples of the pier depth generated from the above distribution, the annual failure probabilities of the pier columns due to scour are computed based on Equation (6.3). The results are shown in Figure 6.6. It is found that (a) the highest annual failure probabilities of the pier columns occur at $t = 7$ and 11 years due to the largest annual peak flows associated

with the two years (see Figure 6.3); and (b) the failure probabilities associated with other years are much lower.

The scenarios associated with the closure of bridge lanes under scour can be represented by the failure events of pier columns, as presented in the previous section. Therefore, the relations between the probabilities of occurrence of these scenarios and the probabilities of failure of the pier columns can be derived. For example, based on Equation (6.16) that is associated with the closure of two lanes in different directions, the probability of occurrence of this scenario is:

$$P(LC_{2,S}) = P(F_{P1}F_{P4}S_{P2}S_{P3}) \tag{6.22}$$

where $P(LC_{2,S})$ = probability of occurrence associated with the closure of two lanes in different directions due to scour. If two extreme correlation cases (independent and perfectly correlated) among the failure modes of pier columns are considered, Equation (6.22) becomes

$$P(LC_{2,S}) = P(F_{P1}F_{P4}S_{P2}S_{P3}) = P(F_{P1})P(F_{P4})[1 - P(F_{P2})][1 - P(F_{P3})] \tag{6.23}$$

$$P(LC_{2,S}) = P(F_{P1}F_{P4}S_{P2}S_{P3}) = \max\{0, \min[P(F_{P1}); P(F_{P4})] - \max[P(F_{P2}); P(F_{P3})]\}$$

$$\tag{6.24}$$

for the independent case and perfectly correlated case, respectively. In the same manner, the probabilities of occurrence of the other three scenarios, $P(LC_{1,S})$, $P(LC_{3,S})$, and $P(LC_{4,S})$, can be determined based on Equations (6.15), (6.17), and (6.18), respectively.

The results associated with the independent case are shown in Figure 6.7 (a) and (b) while those associated with the perfect correlation case are presented in Figure 6.7

293

(c). It is found that in the independent case (a) the probability associated with three lanes closure is slightly higher than that associated with one lane closure; and (b) closure of three and two lanes closure has the highest and lowest probability, respectively. However, in the perfect correlation case, the probability associated with closure of four lanes is the highest while those associated with the scenarios where one, two, or three lanes are closed are nil.

6.5.2 Consequences Analysis

As mentioned previously, the consequences due to the closure of bridge lanes are evaluated considering three aspects: repair cost, running cost, and time loss cost. The repair costs associated the closure of different number of bridge lanes due to traffic load and scour are presented in Table 6.5. The parameters for evaluating the running and time loss cost are listed in Table 4.7. It should be noted that the average daily traffic (A_{DT}) and duration of detour (d) shown in this table are corresponding to the scenario where four lanes are closed. The values of these two parameters used in the other scenarios are assumed to be proportional to the values in Table 4.7: (a) the average daily traffic affected by the closure of one, two, and three lanes is 2125, 4200, and 6375 vehicles/day, respectively; and (b) the duration of detour associated the closure of one, two, and three lanes is 45, 90, and 135 days, respectively. Assuming the annual discount rate of money is 2%, the total consequences associated with different lanes closure scenarios can be evaluated using Equation (6.9).

6.5.3 Risk Assessment

After evaluating the occurrence probabilities of the identified lanes closure scenarios and the associated consequences, the risks associated with these scenarios are determined using Equation (4.10). The risks due to traffic loading considering two extreme correlation cases are plotted in Figure 6.8. It is observed that in the independent case (a) the highest and lowest lifetime risk is caused by the closure of two lanes in same direction and three lanes, respectively; (b) the risks due to the closure of three and four lanes are very close; and (c) closure of two lanes in the same direction leads to much higher risk than closure of two lanes in different directions. In the perfectly correlated case, the risk caused by the closure of four lanes is the highest while the risks associated with the other scenarios are nil.

Figure 6.9 shows the risks associated with different lanes closure scenarios due to scour. The results associated with the independent case are shown in Figure 6.9(a), (b) and (c) while those associated with the perfect correlation case are presented in Figure 6.9(d). It is noted that in the independent case (a) the highest and lowest risk are caused by the closure of three and two lanes, respectively; and (b) the time-variant risk caused by the closure of one lane is higher than that caused by four lanes closure except at $t = 7$ and 11 years; at these two years, the risks associated with the two scenarios are very close. In the perfectly correlated case, the risk caused by four lanes closure is the highest while the risks associated with the other scenarios are nil.

6.6 CONCLUSIONS

This chapter proposes an approach for assessing the time-variant risks associated with the closure of different number of bridge lanes due to traffic loading and scour. Possible lanes closure scenarios due to the two hazards are separately identified based on the lanes closure cases caused by the failure of each critical component related to bridge superstructure and substructure, respectively. The time-variant failure probabilities of girders under traffic loading are evaluated using a deterioration model to account for the decrease in resistance and a live load model to consider the increase in load effect. The annual failure probabilities of pier columns due to scour are estimated by comparing pier depth and scour depth caused by the annual peak flow. The probabilities of occurrence of the identified scenarios are computed based on the relations between these scenarios and the failure events of girders and pier columns. After evaluating the consequences associated with repair, running and time loss costs, the time-variant risks associated with different lanes closure scenarios are separately assessed for traffic loading and scour. The following conclusions are drawn:

1. As the number of closed lanes increases, the consequences increase; however, the probability of occurrence associated with more lanes closure might be lower than that associated with less lanes closure. Therefore, the risks associated with different lanes closure scenarios are different. This stresses the necessity of identifying all the possible scenarios and assessing the associated risks.

2. For a specific lanes closure scenario, the risks associated with two extremes

correlation cases among the failure modes of bridge components are significantly different. This indicates the significant effect of the correlation on the bridge risk and emphasizes the importance of correctly estimating the correlation coefficients in the risk assessment.

3. The risk due to the closure of bridge lanes is time-variant. For this reason, it is necessary to include the time effect in assessing this risk.

4. For the scenarios where the number of the closed lanes is the same, the risk due to the closure of lanes in the same direction is not the same with that associated with different directions. In this chapter, the difference in the obtained risks is mainly due to the difference in the probabilities of occurrence of the two scenarios. In fact, the consequences associated with two scenarios may also be different since the average daily traffic and the length of detour in each direction may not be the same. This difference needs to be taken into account in the risk assessment when detailed information on the average daily traffic and local transportation network is available.

Table 6.1 Lanes closure cases due to the failure of each interior girder.

Interior girder	Girder 2	Girder 3 or 4	Girder 5	Girder 6 or 7	Girder 8
Closed lane(s)	L_1	L_1, L_2	L_2, L_3	L_3, L_4	L_4

Note: L_1= lane 1, L_2= lane 2, L_3= lane 3, and L_4= lane 4.

Table 6.2 Lanes closure cases due to the failure of each pier column.

Pier column	Column 1	Column 2	Column 3	Column 4
Closed lane(s)	L_1	L_1, L_2, L_3	L_2, L_3, L_4	L_4

Note: L_1= lane 1, L_2= lane 2, L_3= lane 3, and L_4= lane 4.

Table 6.3 Deterministic parameters used for the evaluation of scour depth.

Parameters	Notation	Value	Reference
Side slope	z	2	USGS (2000)
Bottom width (m)	b	25	USGS (2000)
Slope of the bed stream	S	0.0035	USGS (2000)
Manning value	n	0.04	USGS (2000)
Correction factor for pier nose shape	K_1	1.1	Arneson *et al.* (2012)
Correction factor for angle of attack of flow	K_2	1.0	Arneson *et al.* (2012)
Pier width (m)	D	1.2	Estes (1997)

Table 6.4 Statistical parameters of the random variables used for the evaluation of scour depth.

Random variables	Notation	Distribution type	Parameters	Reference
Correction factor for bed condition	K_3	Uniform	[1.1, 0.05]	Ghosn *et al.* (2004)
Modeling factor	λ_{mf}	Asymmetric triangular	[0.8, 1.0, 1.0]	Johnson and Dock (1998)
Flow velocity (m/s)	V	Symmetric triangular	c.o.v. = 0.28	Ghosn *et al.* (2004)
Flow depth (m)	y_0	Symmetric triangular	c.o.v. = 0.1	Ghosn *et al.* (2004)

Note: The parameters for the normal and uniform distribution are the mean value and coefficient of variation; the parameters for the asymmetric triangular distribution are lower bound, upper bound, and mode.

Table 6.5 Repair costs associated with the closure of bridge lanes under traffic load and scour ($).

Scenarios	Under traffic load	Under scour
One lane closure	95,600	78,500
Two lanes closure	172,500	152,000
Three lanes closure	239,000	225,500
Four lanes closure	316,000	298,000
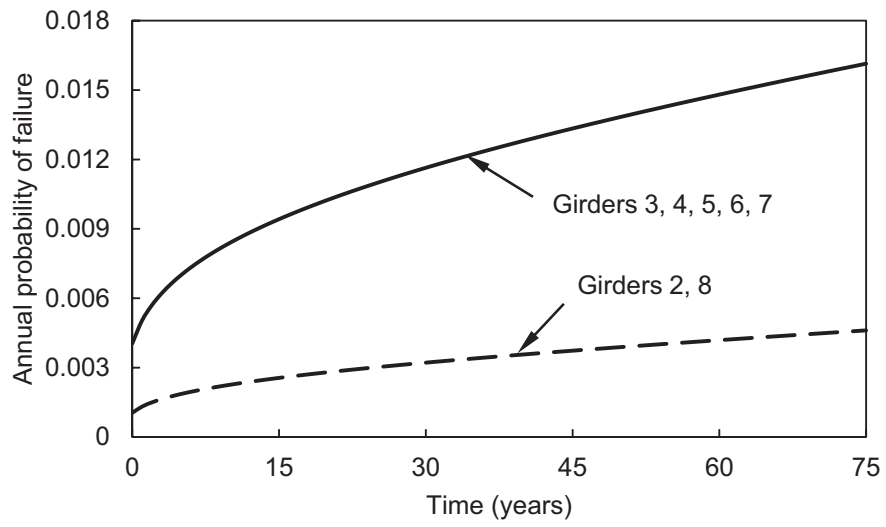
Figure 6.1 Profiles of annual failure probabilities of girders due to traffic loading.
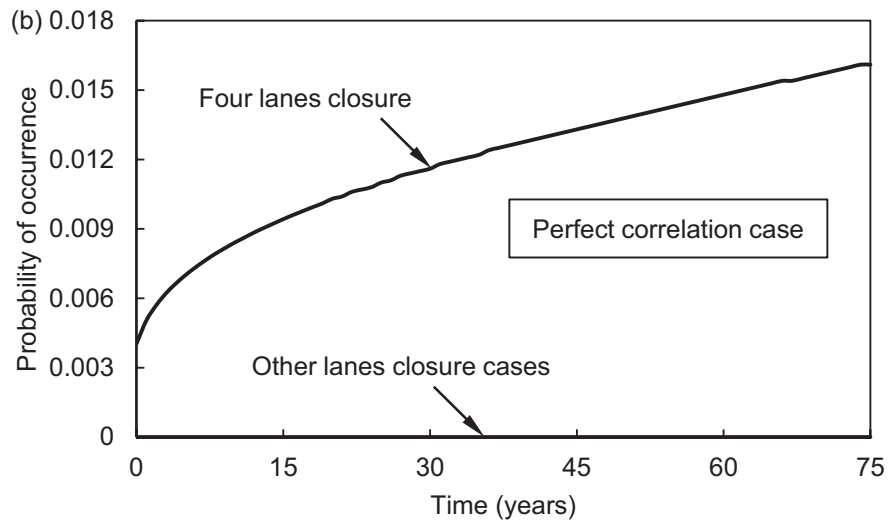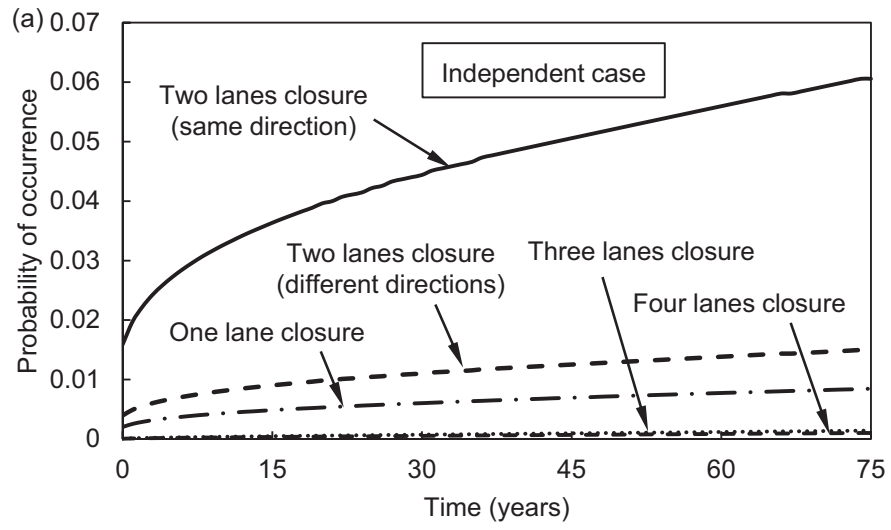
Figure 6.2 Profiles of time-variant occurrence probabilities of different lanes closure scenarios due to traffic loading.
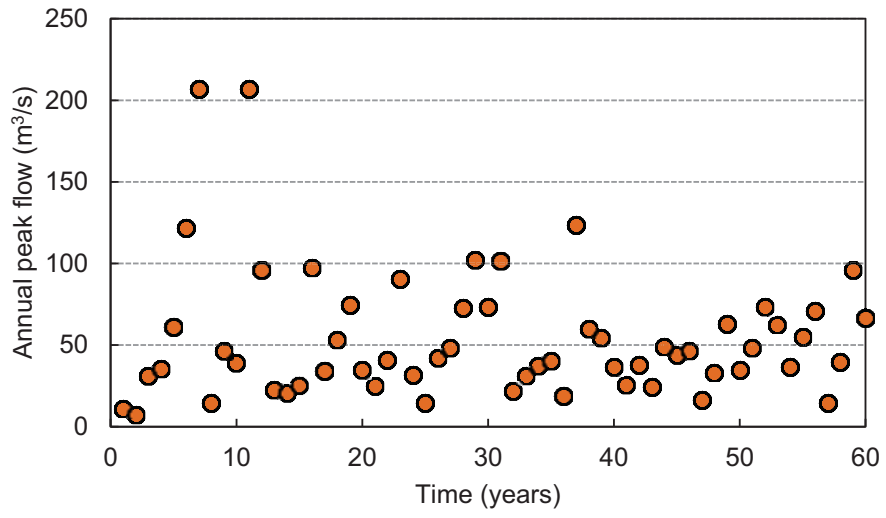
Figure 6.3 Annual peal flow for the Massies Creek (based on USGS (2014) data).
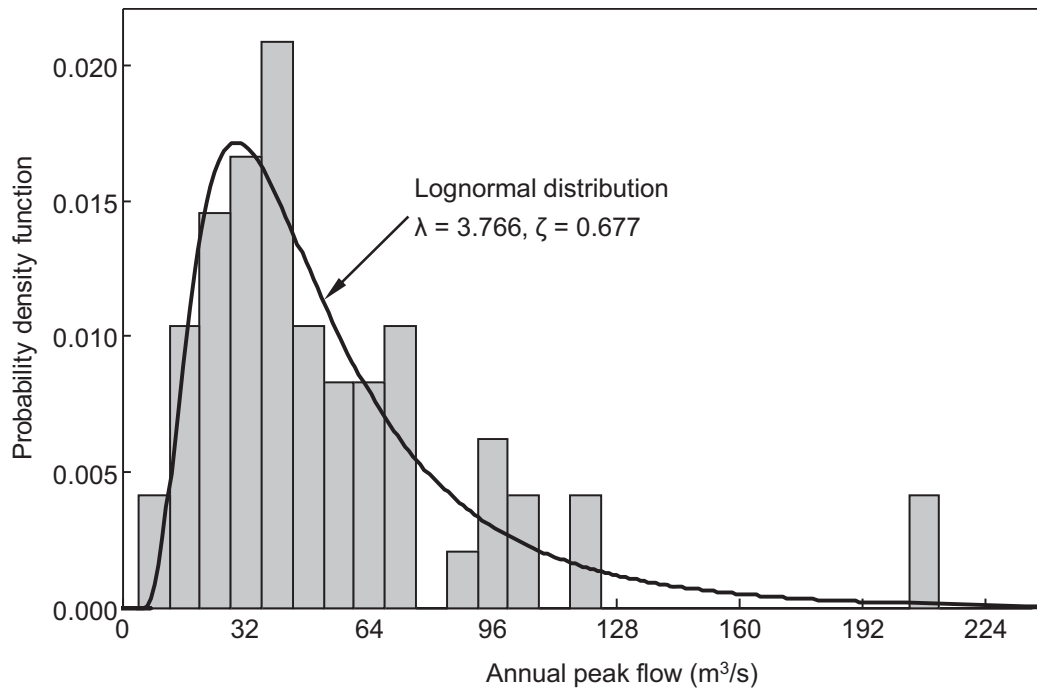
Figure 6.4 Histogram and lognormal distribution fitting of the annual peak flow.
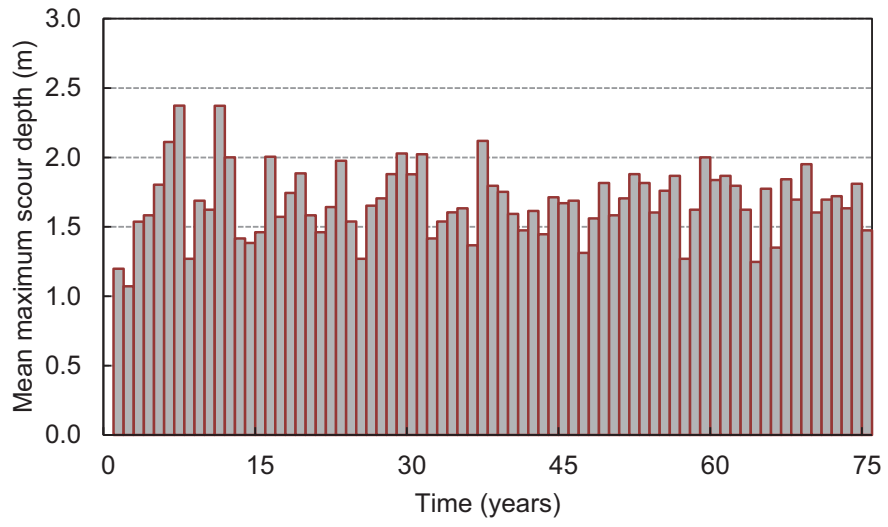
Figure 6.5 Histogram of mean value of the annual maximum scour depth.
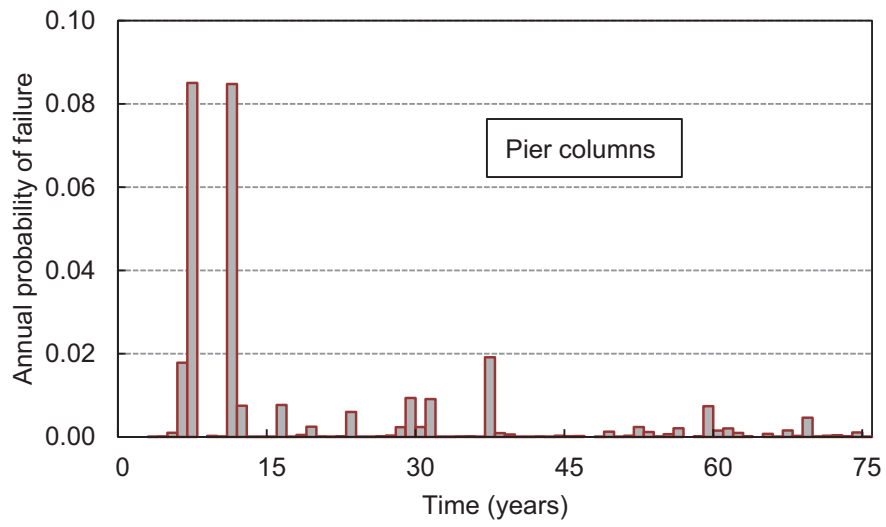
Figure 6.6 Annual failure probabilities of pier columns due to scour.
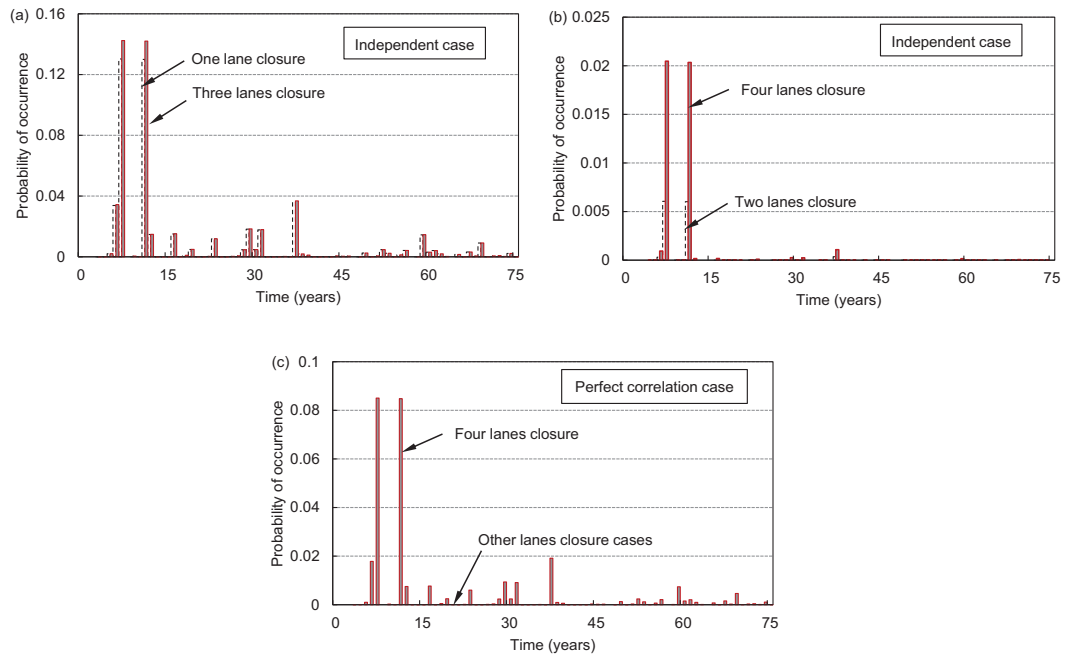
Figure 6.7 Annual occurrence probabilities of different lanes closure scenarios due to scour: (a) and (b) independent case; (c) perfect correlation case.
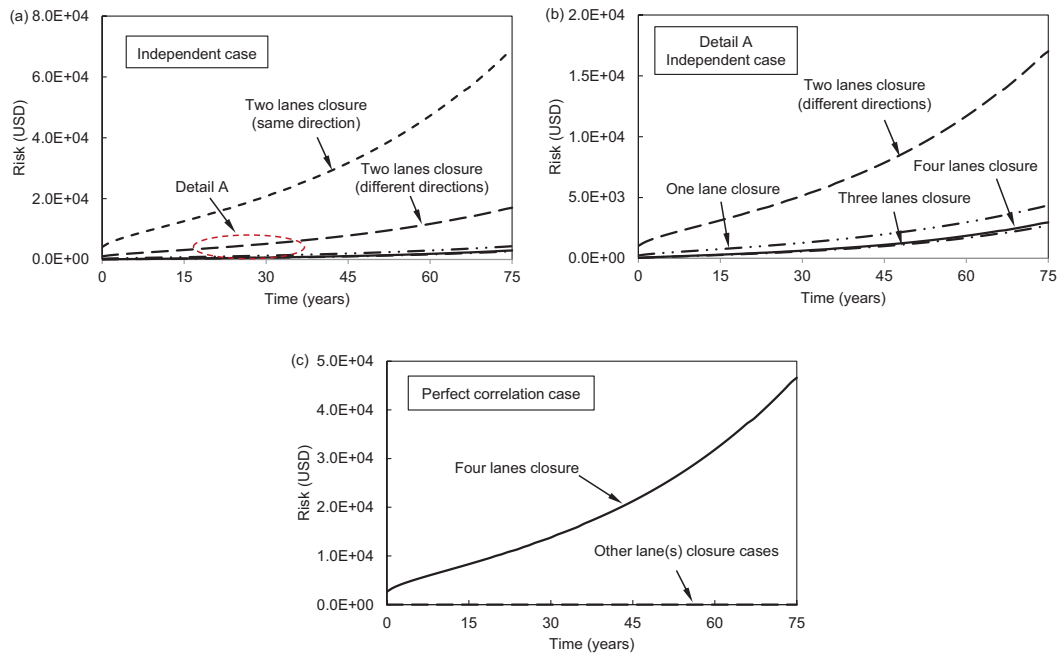
Figure 6.8 Annual risk associated with different lanes closure scenarios due to traffic loading: (a) and (b) independent case; (c) perfect correlation case.

310
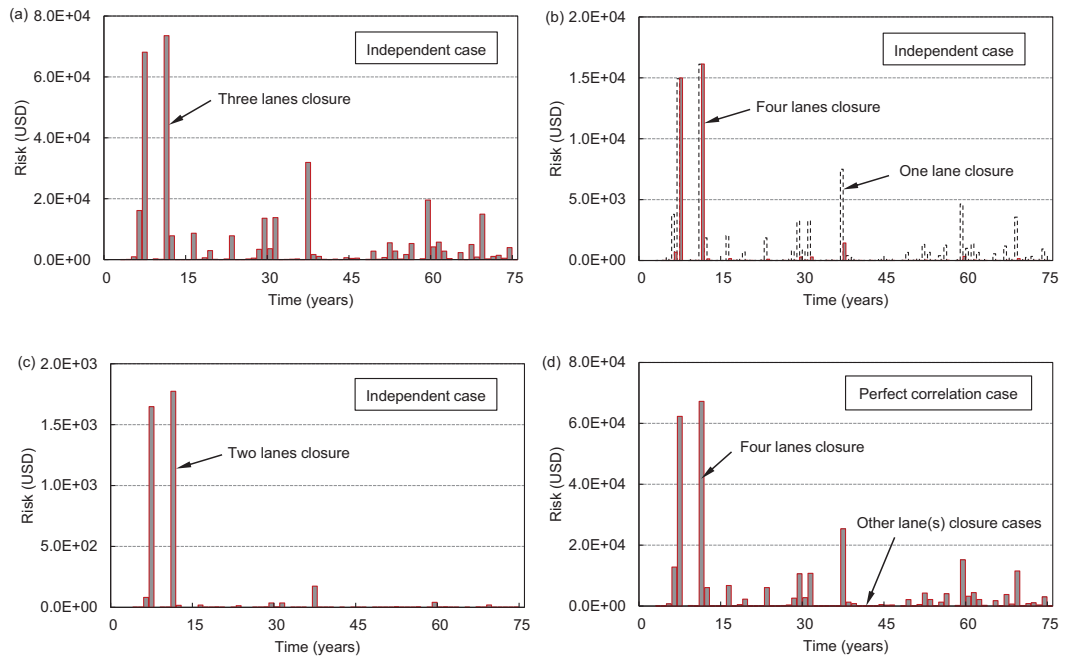
Figure 6.9 Annual risk associated with different lanes closure scenarios due to scour:
(a), (b) and (c) independent case; (d) perfect correlation case.

CHAPTER 7

INCORPORATION OF SHM DATA ON LOAD EFFECTS IN THE RELIABILITY AND REDUNDANCY ASSESSMENT OF SHIP CROSS-SECTIONS USING BAYESIAN UPDATING

7.1 INTRODUCTION

Due to the existence of uncertainties associated with materials properties, geometric configuration, failure modes, loadings and imperfect knowledge, probabilistic methods have been applied in the design and performance assessment of ship structures to quantify these unavoidable uncertainties. Studies on the evaluation of ship reliability index, which is an important probability-based performance indicator, have been extensively performed in the past decades (Ayyub *et al.* 2000, Hussein and Guedes Soares 2009, Luís *et al.* 2009, Mansour 1997, Nikolaidis *et al.* 1993). In addition to the reliability index, the redundancy index is also introduced in the performance assessment of marine structures in order to provide warning before the occurrence of structural collapse. Compared with the ship reliability, research on the ship redundancy is rarely conducted (Blagojevic and Ziha, Decò *et al.* 2011, 2012).

During the performance assessment and prediction of ship structures, the results are usually very sensitive to changes in the input parameters associated with the mechanical models and load conditions (Frangopol *et al.* 2012). Therefore, objective information on the real conditions of the ship strength and loadings is helpful in reducing the uncertainty in the results. Structural health monitoring (SHM) is a

powerful technology that can collect reliable data about the ship responses to various operational conditions, detect the emergence of damages, and perform real-time diagnosis of the ship structural behavior (Devine 2009, Okasha *et al.* 2011, Salvino and Collette 2009). The data acquired from SHM are usually limited in most circumstances and how to make efficient use of these data is particularly important. In such a case, Bayesian estimation approach is recommended since it can combine the judgmental information with objective SHM data to obtain a balanced estimation (Ang and Tang 2007).

Although Bayesian estimation is a very promising method, a review of the literature indicates that very few studies have been conducted on its application in naval engineering, especially in the safety assessment of ship structures. Only recently, Okasha *et al.* 2010 used this approach to integrate the SHM data in the performance prediction of ships by updating the wave-induced load effects. However, their study mainly focused on the long-term extreme values of the wave-induced load effects and the prior information is estimated simply based on the design codes. Since both the judgmental knowledge and the observation data are involved in the updating process, the accuracy of the prior information will influence the reliability of the parameters estimation. Inaccurate initial information (e.g., load effects from design codes) may lead to overly conservative or highly risky assessment results. Therefore, in this chapter, the prior information on the wave-induced load effects is calculated using the software PDSTRIP (PDSTRIP 2006) to obtain an accurate estimation.

Although the midship cross-section is usually of primary interest in the ship design and performance assessment, it cannot actually represent the performance of

the entire ship. Failures of some other cross-sections may also lead to the failure of the ship system; therefore, it is essential to investigate additional cross-sections in the ship performance assessment. This chapter proposes an approach for reducing the uncertainty in the reliability and redundancy assessment of ship cross-sections using Bayesian updating method. Section 7.2 describes the models for the probabilistic evaluation of the first and ultimate bending moments of a hull girder section. Section 7.3 presents the methods for the probabilistic estimation of the vertical bending moments induced by still water and waves. Section 7.4 provides the limit state equations for the first and ultimate failure of a ship cross-section and the definition of redundancy. Section 7.5 presents the Bayesian updating model and the method for determining the type and parameters of the updated distribution. In Section 7.6, the proposed approach is illustrated using the Joint High Speed Sealift (JHSS). Finally, several conclusions of this chapter are drawn in Section 7.7.

7.2 SHIP RESISTANCE

The determination of the ship hull strength is a critical step in the performance assessment of naval structures. In most practical cases, the vertical bending moment (VBM) of the hull girder is of the most interest since the bending moment is the primary load effect acting on the ship structure and the horizontal moment is usually very small compared with its vertical counterpart (Guedes Soares and Teixeira 2000, Hughes 1983). Methods developed in the past decades for the hull strength analysis are mostly deterministic (Hughes 1983, IACS 2008, Paik and Mansour 1995, Smith

1997). However, due to the uncertainties in the material properties, geometry and modeling, the strength of the ship hull needs to be evaluated probabilistically.

Based on the IACS (2008), it is known that the relation between curvature and bending moment can be described as a non-linear implicit function and the ultimate failure moment is defined as the peak value of the moment-curvature curve for a given cross-section. In order to improve the computing efficiency as well as ensure the accuracy, the optimization-based approach proposed by Okasha and Frangopol (2010b) is used in this chapter to determine the ultimate failure moment of the ship hull. In this approach, the ultimate failure moment is found by using an optimization search algorithm instead of a classic incremental curvature method. The main steps are summarized as follows (Okasha and Frangopol 2010b): (i) divide the hull girder transverse section into two types of elements: stiffened plates and hard corners; (ii) derive the stress-strain curves for all structural elements using the constitutive models in which various possible failure modes and initial imperfections are considered; in this step, four different modes of buckling failure are considered for the panels subject to compressive loads: beam-column buckling, torsional buckling, web local buckling of flanged profiles, and web local buckling of flat bars; (iii) provide the first trial of the curvature; and (iv) perform an optimization-based procedure to find the maximum bending moment. The obtained maximum moment is the ultimate failure moment of the investigated cross-section.

The evaluation of the first failure moment is based on the progressive collapse method presented in Hughes (1983). Two different failure modes are considered in this method: (i) compression failure of the stiffener; and (ii) compression failure of the

315

plating (IACS 2008). In the first mode the stiffener flange is compressed, therefore the stiffener is subject to local buckling effects by twisting about its line of attachment of the plating, which causes tripping stress. The failure stress of the stiffener is then the minimum between the yielding and the tripping stress. In the second mode, the nonlinear stress-strain relationship of the compressed plating is taken into account in the determination of its failure stress. Having obtained the failure stresses for each stiffener-plating system, the corresponding curvatures associated with the two failure modes can be calculated (Hughes 1983). Finally, the bending moment related to the minimum curvature is the first failure moment of the hull girder section.

In order to evaluate the ultimate and first failure bending moments probabilistically, the above two approaches are combined with a Latin-hypercube sampling simulation so that a number of moments samples (i.e. 5000 samples) can be generated. By performing distribution fitting to these output samples, it is found that the first and ultimate failure moments are best modeled by the lognormal distribution (Decò *et al.* 2011, Okasha and Frangopol 2010b).

7.3 LOAD EFFECTS ON SHIPS

One of the major aspects in the assessment of ship performance is the calculation of the load effects on ship structures due to still water and waves. According to Guedes Soares and Teixeira (2000), the primary load effects within the hull girder are the hogging and sagging vertical bending moments. Due to the unavoidable uncertainties in the prediction of the load effects, the still water and wave-induced VBMs have to be

evaluated probabilistically. In this section, the approaches for the probabilistic estimation of these VBMs are presented.

7.3.1 Still Water Bending Moment

Generally, the still water bending moment can be accurately calculated by integrating the difference between buoyancy and total weight along the length of the ship (Hughes 1983). However, in some circumstances, the information on the location and magnitude of the loads on a ship in still water is not sufficient or available. Therefore, approximation methods are needed to estimate the still water bending moment. IACS (2008) provides an approach to approximately estimate the hogging and sagging vertical bending moments for a given transverse cross-section:

$$M_{sw,hog} = 0.01 f_{sw} C_{wv} L^2 B (11.97 - 1.9 C_b) \qquad \text{for hogging} \qquad (7.1)$$

$$M_{sw,sag} = 0.05185 f_{sw} C_{wv} L^2 B (C_b + 0.7) \qquad \text{for sagging} \qquad (7.2)$$

where $M_{sw,hog}$ and $M_{sw,sag}$ = still water bending moments for hogging and sagging, respectively (Nm), f_{sw} = factor accounting for the variation of the vertical bending moment along the ship length, C_b = ship block coefficient (IACS 2008), L = ship length (m), B = ship breadth (m), and C_{wv} = wave coefficient calculated as follows (IACS 2008):

$$C_{wv} = \begin{cases} 10.75 - \left(\dfrac{300 - L}{100}\right)^{\frac{3}{2}} & \text{for } 150 < L \le 300 \\ 10.75 & \text{for } 300 < L \le 350 \\ 10.75 - \left(\dfrac{L - 350}{150}\right)^{\frac{3}{2}} & \text{for } 350 < L \le 500 \end{cases} \qquad (7.3)$$

317

In order to consider the uncertainties in the estimation of still water bending moment, Hussein and Guedes Soares (2009) proposed the use of a normal distribution with the mean and standard deviation to be taken as 70% and 20% of the maximum bending moment which is considered as 90% of the moment obtained by common rules (IACS 2008).

7.3.2 Statistical Description of Irregular Waves

The actual sea surface is highly irregular and random under all kinds of conditions. However, Pierson (1952) discovered that the irregularity of the sea surface can be approximately represented by the superposition of a large number of regular waves with different amplitudes and frequencies. This finding paved the way for further work on statistical description of sea surface. Based on a large amount of data collected in many years, various wave spectra have been proposed (Chakrabarti 1987). In this chapter, the wave spectrum for a fully developed sea, recommended by the International Ship and Offshore Structures Congress (ISSC) and International Towing Tank Conference (ITTC), is used (Faltinsen 1990):

$$S_w(\omega) = \frac{0.11 H_{1/3}^2 T_1}{2\pi} \left(\frac{\omega T_1}{2\pi}\right)^{-5} \exp\left[-0.44\left(\frac{\omega T_1}{2\pi}\right)^{-4}\right] \tag{7.4}$$

where $S_w(\omega)$ = wave spectrum for a given sea state, $H_{1/3}$ = significant wave height defined as the mean of the one third highest waves (m), T_1 = average wave period (s), and ω = absolute wave frequency (rad/s). For a particular operational condition, the wave spectrum is usually expressed in terms of encounter frequency ω_e, instead of ω,

to account for the ship speed and heading angle. The relationship between the encounter frequency and the absolutely wave frequency is:

$$\omega_e = \left| \omega - \frac{\omega^2 U}{g} \cos\theta_a \right| \qquad (7.5)$$

where U = speed of ship (m/s), θ_a = angle between the direction of wave and the direction in which the ship is heading (degree), and g = gravitational acceleration (m/s^2).

According to Hughes (1983), providing the instantaneous value of the ocean elevation has a Gaussian distribution with a zero mean, the peak elevation values follow a Rayleigh distribution:

$$f(A_w) = \frac{A_w}{m_{0,w}} \exp\left(-\frac{A_w^2}{2m_{0,w}} \right) \qquad (7.6)$$

where A_w = peak values of the wave elevation (m), and $m_{0,w}$ = zero-*th* moment of the wave spectrum, defined as:

$$m_{0,w} = \int_0^\infty \omega_e^{\ 0} S_w(\omega_e) d\omega_e \qquad (7.7)$$

7.3.3 Wave-induced Bending Moment

In many practical cases, the interaction between the ship and waves is considered to be linear when calculating the wave-induced vertical bending moment. Therefore, for the linear wave-ship system, the total response to the irregular waves can be obtained by computing the response to each regular wave separately and then superimposing these separate responses together. When the time-varying processes of the wave and

response are both represented in terms of spectral density functions, they can be directly related by a transfer function $\Phi(\omega_e)$ as follows:

$$S_M(\omega_e) = |\Phi(\omega_e)|^2 S_w(\omega_e) \tag{7.8}$$

where $S_M(\omega_e)$ = response spectrum for the wave-induced vertical bending moments, and $|\Phi(\omega_e)|^2$ = response amplitude operator (RAO). In this chapter, the RAO is calculated by combining MATLAB with PDSTRIP (2006), which is a software for linear response analysis under regular waves based on the strip theory.

Since the wave-ship system is linear herein, according to Hughes (1983), the peak values of the wave-induced VBMs can be considered to follow a Rayleigh distribution as:

$$f(M_w) = \frac{M_w}{m_{0,M}} \exp\left(-\frac{M_w^2}{2m_{0,M}}\right) \tag{7.9}$$

where M_w = peak values of the wave-induced VBM, and $m_{0,M}$ = zero-*th* moment of the VBM spectrum given by Equation (7.8). Therefore, the parameter α_M of the distribution, the mean μ_M and standard deviation σ_M of the random variable M_w can be obtained, respectively, as follows:

$$\alpha_M = \sqrt{m_{0,M}} \tag{7.10}$$

$$\mu_M = \sqrt{\frac{\pi \cdot m_{0,M}}{2}} \tag{7.11}$$

$$\sigma_M = \sqrt{\frac{(4-\pi) \cdot m_{0,M}}{2}} \tag{7.12}$$

7.4 RELIABILITY AND REDUNDANCY OF SHIP CROSS-SECTION

Reliability and redundancy are two important indicators for the assessment of structural performance. For ship structures, the reliability analysis is usually performed only respect to the midship cross-section. However, since a ship structure may fail due to the failure of other cross-sections, several additional cross-sections are also investigated in this chapter. Considering the modeling uncertainties of the resistance and load effects, the limit state equations for the ultimate and first failure of a cross-section are:

$$g_U = x_R M_{UR} - x_{sw} M_{sw} - x_w M_w = 0 \tag{7.13}$$

$$g_F = x_R M_{FR} - x_{sw} M_{sw} - x_w M_w = 0 \tag{7.14}$$

where g_U and g_F = performance functions for the ultimate and first failure, respectively, M_{UR} and M_{FR} = resisting bending moments for the ultimate and first failure, respectively, M_{sw} = still water bending moment, M_w = wave-induced bending moment, x_R = model uncertainty associated with the resistance determination, x_{sw} = model uncertainty related to the still water bending moment prediction, and x_w = model uncertainty associated with the wave-induced bending moment prediction.

Once the probability distributions and the associated statistical descriptors of the ultimate and first failure capacities, still water bending moment, wave-induced bending moment, and limit state equations presented above are determined, the reliability indices related to the ultimate and first failure of the investigated cross-sections are computed using the program RELSYS (Estes and Frangopol 1998). The assessment of cross-section redundancy is vital since it provides warnings before the

occurrence of cross-section collapse. Based on the cross-section reliability indices associated with the ultimate and first failure, the cross-section redundancy index RI can be calculated using the following definition (Frangopol 2011):

$$RI = \beta_U - \beta_F \tag{7.15}$$

where β_U and β_F = cross-section reliability indices related to the ultimate and first failure, respectively.

7.5 BAYESIAN UPDATING

Structural health monitoring has been proved to be a very powerful technique for collecting reliable information about the load effects acting on the ship structures and their responses to various operational conditions (Devine 2009, Okasha *et al.* 2011, Salvino and Collette 2009). If there is a large amount of observed data, classical approach is used to estimate the statistical descriptors of the distributions. However, when the available data are limited, as is often the case in structural engineering, the Bayesian approach which combines the judgmental information with the objective data will yield better estimation results. Different from the classical approach where the distribution parameters are considered as deterministic, Bayesian approach solves the estimation problem from another point of view: it deals with the uncertainty by treating the unknown parameters as random variables. In such a way, all sources of uncertainty related to the estimation of the parameters can be combined using the total probability theorem (Ang and Tang 2007).

Let $f_X(x)$ be the probability density function (PDF) of an underlying random variable X. The parameter of $f_X(x)$, denoted as θ, is considered as a random variable herein, and thus is described by a prior PDF $f'(\theta)$. Given a set of observation points $(x_1, x_2, \ldots, x_n)$ acquired from SHM, the likelihood function $L(\theta)$ is constructed by multiplying the PDFs of X evaluated at these SHM data values:

$$L(\theta) = \prod_{i=1}^{n} f_X(x_i \mid \theta) \qquad (7.16)$$

where n = size of the observed samples. Based on the Bayes theorem, the posterior density function of the parameter θ, $f''(\theta)$, is calculated as follows:

$$f''(\theta) = kL(\theta)f'(\theta) \qquad (7.17)$$

where k = normalizing constant, given as:

$$k = \left[\int_{-\infty}^{\infty} L(\theta)f'(\theta)d\theta \right]^{-1} \qquad (7.18)$$

Accounting for the uncertainty in the estimation of the parameter θ and the inherent variability of the underlying random variable X, the updated PDF of X, $f_X'(x)$, is obtained using the total probability theorem:

$$f_X'(x) = \int_{-\infty}^{\infty} f_X(x \mid \theta)f''(\theta)d\theta \qquad (7.19)$$

The distribution $f_X'(x)$ can be interpreted as a weighted average of all possible distributions $f_X(x \mid \theta)$ which are associated with different values of θ (Benjamin and Cornell 1970). It is noted from Equation (7.19) that (a) the parameter θ is not included in the final expression of $f_X'(x)$ since it has been "integrated out" of the equation; and (b) as more SHM data become available, the uncertainty associated with the

estimation of the distribution of the parameter θ will be reduced and therefore $f_X^{'}(x)$ will be closer to the true distribution of X (Benjamin and Cornell 1970).

Since the closed-form solutions for $f_X^{'}(x)$ are difficult to obtain in most practical cases, a more feasible approach to find an approximate solution for $f_X^{'}(x)$ provided in Okasha *et al.* (2010) is used herein. This approach consists of two steps: (1) calculate the cumulative distribution function (CDF) of the underlying random variable X by performing numerical integration of $f_X^{'}(x)$:

$$F_X^{'}(z_i) = \int_{-\infty}^{z_i} \int_{-\infty}^{\infty} f_X(u\,|\,\theta) f^{''}(\theta) d\theta du \qquad i = 1, 2, ..., k \qquad (7.20)$$

where $Z = [z_1, z_2, ..., z_i, ..., z_k]$ = array of values whose lower and upper bound is small and large enough, respectively, to cover the range of all probable values of X; moreover, the interval between z_i and z_{i-1} should be small enough to guarantee the precision of the approximate solution; and (2) perform distribution fitting to the values obtained from Equation (7.20) using the method of least square to determine the distribution parameters (Okasha *et al.* 2010, Bucher 2009).

7.6 CASE STUDY

The Joint High Speed Sealift (JHSS) is presented herein as a case study to demonstrate the process of assessing the reliability and redundancy of ship cross-sections and updating these performance indicators using the collected SHM data. The hull of JHSS is characterized by an unusually-fine hullform and a "gooseneck" bulbous bow for improved high-speed performance (Devine 2009). The general geometry properties of

the ship are provided as follows: overall length L = 294.06 m, breadth B = 32 m, height H = 22.3 m, and block efficient C_b = 0.4835 (Devine 2009). Three representative cross-sections: Station 5 (72.5 m aft of FP), Station 10 (145 m aft of FP) and Station 15 (217.5 m aft of FP) are investigated in this case study. Their design scantlings are shown in Figure 7.1 and the dimensions of the components are provided in Devine (2009).

7.6.1 Seakeeping Test and SHM Data

Seakeeping and structural loads tests were conducted for a scaled (λ =1:47.5255) segmented model of JHSS to obtain detailed ship motions and structural primary and secondary loadings in support of validation efforts for design simulation codes, specifically the Large Amplitude Motions Program (LAMP) (Devine 2009). The scaled JHSS structural segmented model is a four-screw self-propelled model encompassing segment cuts at Station 4 (58 m aft of FP), Station 7 (101 m aft of FP), Station 10 (145 m aft of FP), Station 13 (188 m aft of FP) and Station 16 (231.5 m aft of FP) (Devine 2009). The shell sections were connected with a continuous aluminum backspline beam that was instrumented with strain gages at each segment cut to provide measureable vertical, lateral and torsional bending moments and vertical and lateral shear forces resulting from combined quasi-static and dynamic seaways loads (Devine 2009). More details about the JHSS and the scaled segmented model can be found in Devine (2009).

Strain gages were installed at each segment cut to collect the SHM data of the wave-induced load effects. The obtained data contain 73,800 samples and the

sampling rate was 200 Hz, therefore, the total duration of the test was about 6.15 min (Okasha *et al.* 2010). Conversion of the test results of the scaled model to the full-scale ship follows the Froude-scaling guidelines, in which time is increased by $\sqrt{\lambda}$ and the bending moment is increased by $1.025\lambda^4$ (Okasha *et al.* 2010). Since the available data used in this case study were gathered under the operational condition of sea state 7, ship speed 35 knots and heading angle 0°, the wave-induced VBMs used as prior load effects for the later updating are calculated with respect to the operational case of sea state 7, ship speed of 35 knots for different heading angles ranging from 0° to 180°.

7.6.2 Resistances

In the probabilistic assessment of the first and ultimate failure moments of Stations 5, 10 and 15, the elastic modulus E, yielding stresses of plating and stiffener σ_{Yp} and σ_{Ys}, and plating thickness t_p are considered to be lognormal random variables with the coefficients of variation of 0.03, 0.1, 0.1 and 0.05, respectively (Paik and Frieze 2001). The mean values of the variates E, σ_{Yp} and σ_{Ys} are assumed to be 2.1×10^5 MPa, 351.6 MPa and 351.6 MPa, respectively (Devine 2009). 5000 samples are generated for these random variables using the Latin-Hypercube sampling to simulate the bending moments associated with the first and ultimate failure for both hogging and sagging. It is found that the generated output samples of these bending moments are best fitted by lognormal distributions. Their mean values and standard deviations related to the three cross-sections are presented in Table 7.1. The correlations among

the failure moments of different cross-sections are also obtained based on these output moments samples, as listed in Table 7.2 and Table 7.3.

7.6.3 Load Effects

Since the longitudinal loads distribution in still water of the JHSS is not available, the approximate approach provided in Equations (7.1) and (7.2) from IACS (2008) is used herein to estimate the hogging and sagging vertical bending moments at the three cross-sections. Based on Hussein and Guedes Soares (2009), the still water bending moments are assumed to be normally distributed and the obtained distribution parameters for the three cross-sections are presented in Table 7.4.

As mentioned previously, the wave-induced bending moments in this case study are calculated regarding sea state 7. For the selected wave spectrum (Equation (7.4)), the significant wave height and average wave period associated with sea state 7 are 7.62 m and 10 s, respectively (Resolute Weather 2012). 19 offset cross-sections spaced at 14.5 m and 95 wave lengths ranging from 24 m to 1300 m are used in PDSTRIP (2006) to compute the response amplitude operator for the ship speed of 35 knots and different heading angles ranging from 0° to 180° with an interval of 20°. Having obtained the response amplitude operator and selected the wave spectrum, the wave-induced VBM spectrum is calculated using Equation (7.8). Since the peak values of the bending moments are assumed to follow a Rayleigh distribution, the associated mean values and standard deviations can be evaluated in terms of the zero-*th* moment of the response spectrum.

Figure 7.2 shows the polar representation of the mean values of wave-induced bending moments for the three cross-sections. The bending moments between 0˚ and 180˚ are symmetric with those between 180˚ and 360˚. It is observed from that (a) for all cross-sections, the mean values of the VBMs obtained at the heading angle 0˚ are smaller than those obtained at the heading angle 180˚; and (b) the difference between the mean VBMs associated with 0˚ and 180˚ is more significant in the midship cross-section (i.e., Station 10) than in the other cross-sections.

7.6.4 Reliability and Redundancy of Cross-sections

After obtaining the distributions of the resistance, still water and wave-induced bending moments, the reliability indices of three cross-sections are assessed for both hogging and sagging under different heading angles, as shown in Figure 7.3. For the analyzed cross-sections, it is seen that (a) the reliability indices for sagging are all larger than those for hogging; and (b) the reliability indices at the heading angle 180˚ are all smaller than those obtained at the heading angle 0˚ for both sagging and hogging cases. It should be noted that the obtained reliability indices at the heading angle of 180º associated with the three cross-sections are relatively low. This is probably due to two reasons: (a) the operational condition investigated herein is sea state 7 and speed 35 knots, which is a very severe condition; therefore, the wave-induced bending moments acting on the cross-sections are very large; and (b) the dimensions used for the resistances evaluation are based on the preliminary design of JHSS; therefore, the estimated resistances might be relatively small compared with those based on the final design.

The cross-section redundancy is calculated using Equation (7.15), which is the difference between the reliability indices associated with the ultimate and first failure. The polar representations of redundancy indices associated with three cross-sections for hogging and sagging are plotted in Figure 7.4. It is found that (a) the lowest redundancy indices for both hogging and sagging occur at the heading angle of 180°; and (b) for Station 5, the redundancy indices for hogging are larger than those for sagging; this is contrary to the findings in the redundancy polar plots for Stations 10 and 15.

7.6.5 Performance Updating

Since Stations 5, 10 and 15 are investigated in the cross-section reliability and redundancy analysis, the SHM data associated with these stations are needed for the updating of the cross-section performance. However in the seakeeping loads test, Stations 5 and 15 were not monitored and the sections where the strains were measured are Stations 4, 7, 10, 13 and 16. Therefore, in order to demonstrate the updating process, the SHM data collected at Stations 4 and 16 are approximately used as the data at Stations 5 and 15 to update their prior load effects based on the fact that Stations 4 and 16 are close to Stations 5 and 15, respectively.

The load effects generated by sea waves consist of wave-induced bending moments associated with low frequency waves and slamming, springing and whipping effects related to high frequency excitations. In order to update the wave-induced bending moments, the low frequency signals are separated from the scaled SHM raw signals using the Butterworth filter in MATLAB signal processing toolbox

(MathWorks 2010) and then the positive and negative peaks which correspond to hogging and sagging bending moments are extracted from the filtered low frequency signals.

The available SHM data for the three cross-sections are associated with the operational case of sea state 7, ship speed 35 knots and heading angle 0˚. Therefore, only the points associated with this operational case in the polar plots (Figure 7.2 to Figure 7.4) can be updated. During the Bayesian updating of Rayleigh-distributed VBM, the distribution parameter α is treated as a random variable. Since α is always positive, it is considered to follow a lognormal distribution whose mean value μ_α is determined using PDSTRIP (2006) and coefficient of variation is assumed to be 10% (Okasha *et al.* 2010). For the given operational condition (sea state 7, ship speed 35 knots and heading angle 0˚), the mean values μ_α for Stations 5, 10 and 15 are found to be 2.21×10^8 Nm, 5.69×10^8 Nm and 4.47×10^8 Nm, respectively. By performing the signal filtering and peaks extraction, 406, 397 and 369 hogging and sagging peaks are obtained for Stations 4, 10 and 16, respectively. Based on Equations (7.16) to (7.18), the extracted VBM peaks are integrated with the prior PDFs and the samples of the posterior PDFs of α for the three sections are generated using the slice sampling algorithm. By using Minitab (2010), it is found that these posterior samples are best modeled by the lognormal distributions.

Figure 7.5 shows the generated samples and fitted PDF associated with Station 15 for both hogging and sagging. The prior and posterior PDFs of the parameter α related to Stations 5, 10 and 15 are plotted in Figure 7.6. Since the mean values of the prior PDFs are determined based on linear theory, the prior PDFs shown in Figure 7.6 are

the same for both hogging and sagging. However, the hogging and sagging peaks acquired from SHM data may be not the same and this might lead to the difference in the updated posterior PDFs between hogging and sagging.

It is noticed from Figure 7.6 that (a) the posterior PDFs associated with hogging and sagging are different at Stations 10 and 15 but almost the same at Station 5; (b) for Stations 10 and 15, the mean values of the posterior PDFs for hogging are larger than those for sagging; (c) after integrating with the SHM data, both the mean value and standard deviation of the parameter α at Station 5 are decreased; similar finding is also obtained at Station 15; and (d) for the midship section (Station 10), the mean value of α increases while the standard deviation decreases after updating. The decreases in the dispersion of the parameter in the three stations indicate that integration of the SHM data dramatically reduces the uncertainties in the parameter α for all these cross-sections.

The updated PDFs of the vertical bending moment can be determined by first obtaining the CDF of the VBM based on Equation (7.20) and then performing the distribution fitting to estimate the associated parameters. The original and updated PDFs and the SHM data for the three cross-sections are shown in Figure 7.7. Since the available SHM data are very limited, only the updated mean VBMs associated with heading angle 0° are presented in the polar plots of the original mean VBMs, as shown in Figure 7.8. It is found from Figure 7.7 and Figure 7.8 that (a) the mean and standard deviation associated with Stations 5 and 15 are reduced after the parameter α is updated; while for Station 10, the updated mean VBM is slightly increased; and (b) the

difference in the updated PDF between hogging and sagging is very slight for all the sections.

Figure 7.9 shows the updated reliability indices for heading angle 0° and the original reliability indices for different heading angles associated with three cross-sections. As shown in the figure, the updated reliability indices in Stations 5 and 15 are increased for both hogging and sagging cases at the heading angle 0°; while in Station 10, the updated reliability indices are slightly smaller than the originals. The updated cross-section redundancy indices for hogging and sagging associated with the heading angle of 0° are presented in the polar plot of original redundancy indices, as shown in Figure 7.10. It is found that for the three sections investigated, their redundancy indices before and after updated are almost the same.

7.7 CONCLUSIONS

This chapter presents an approach for improving the accuracy in the reliability and redundancy assessment of ship cross-sections by incorporating the objective SHM data related to the prior load effects. The vertical bending moments associated with the ultimate and first failure for a given cross-section are evaluated using an optimization-based method and the progressive collapse method, respectively. The prior information on the wave-induced load effects is calculated based on the linear theory. Bayesian updating is then performed to update the prior load effects using the hogging and sagging peaks extracted from the processed SHM data. The original and updated reliability and redundancy indices of the ship cross-sections are evaluated and the results are presented in polar plots. The following conclusions are drawn:

1. For a given sea state and ship speed, plotting the cross-section performance indicators in the polar coordinate system provides a straightforward representation of the effects of heading angle on the structural safety.

2. The cross-section reliability indices associated with sagging are larger than those associated with hogging for all heading angles. However, a similar conclusion cannot be obtained for the cross-section redundancy. For the investigated JHSS in the operational case of sea state 7 and ship speed of 35 knots, the lowest reliability and redundancy indices associated with the three stations occur at the heading angle of 180˚ for both hogging and sagging cases.

3. Integration of the SHM data can significantly reduce the uncertainty in a distribution parameter so that the updated performance indicators are closer to their true values. For the analyzed JHSS, the distribution types of the parameters α of three stations remain the same after updating while the mean values and standard deviations of α change. Therefore, the reliability and redundancy indices associated with the three stations at the heading angle 0˚ are changed although the differences before and after updating are slight.

4. In this chapter, only the performance indicators at the heading angle of 0º are updated due to lack of the SHM data. However, if the SHM information associated with different operational conditions is available, the proposed approach can be used to update the entire reliability / redundancy polar plots of different sea states and ship velocities. For a given sea state that a ship might encounter during a journey, the ship operator can use these updated polar plots as a guidance to adjust the speed and heading angle to maintain the

performance indicators above the defined thresholds.

Table 7.1 Statistical descriptors of the first and ultimate failure vertical bending moments for the three cross-sections ($\times 10^8$ Nm).

	Parameters		Station 5	Station 10	Station 15
Hogging	First failure	Mean	31.34	86.10	44.76
		Std.dev.	2.95	8.60	4.30
	Ultimate failure	Mean	35.94	99.83	46.42
		Std.dev.	3.05	8.88	3.98
Sagging	First failure	Mean	28.58	81.11	42.64
		Std.dev.	2.73	8.46	4.19
	Ultimate failure	Mean	32.11	95.05	51.62
		Std.dev.	3.12	7.85	4.16

Note: "Std.dev." denotes standard deviation.

Table 7.2   Correlation coefficients among the ultimate failure moments of three stations.

Station 5		Station 10		Station 15	
Sagging	Hogging	Sagging	Hogging	Sagging	Hogging
1.00	0.98	0.89	0.94	0.93	0.94
	1.00	0.92	0.96	0.95	0.94
		1.00	0.98	0.94	0.92
	Symmetric		1.00	0.95	0.94
				1.00	0.97
					1.00

Table 7.3 Correlation coefficients among the first failure moments of three stations.

Station 5		Station 10		Station 15	
Sagging	Hogging	Sagging	Hogging	Sagging	Hogging
1.00	0.95	0.87	0.88	0.90	0.92
	1.00	0.91	0.95	0.96	0.94
		1.00	0.99	0.95	0.94
	Symmetric		1.00	0.96	0.97
				1.00	0.99
					1.00

Table 7.4 Distribution parameters of the still water vertical bending moments for the three cross-sections ($\times 10^8$ Nm).

Distribution parameter	Hogging still water bending moment		Sagging still water bending moment	
	Stations 5 and 15	Station 10	Stations 5 and 15	Station 10
Mean	13.05	20.08	7.25	11.15
Standard deviation	3.73	5.74	2.07	3.19

Figure 7.1 Geometry of (a) Station 5, (b) Station 10, and (c) Station 15 (adapted from Decò *et al.* 2012).

339
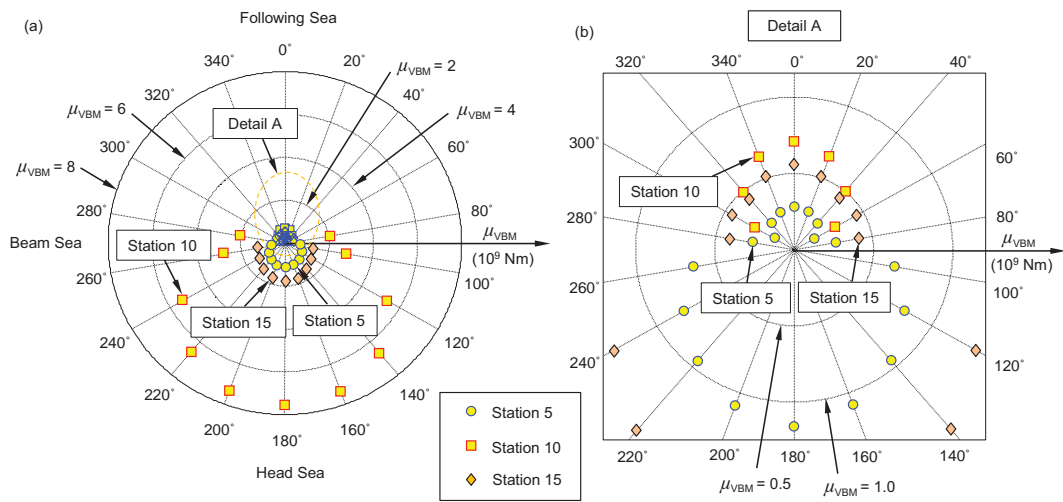
Figure 7.2 Polar representations of mean vertical bending moment (μ_{VBM}): (a) three sections (Stations 5, 10 and 15); and (b) Detail A.
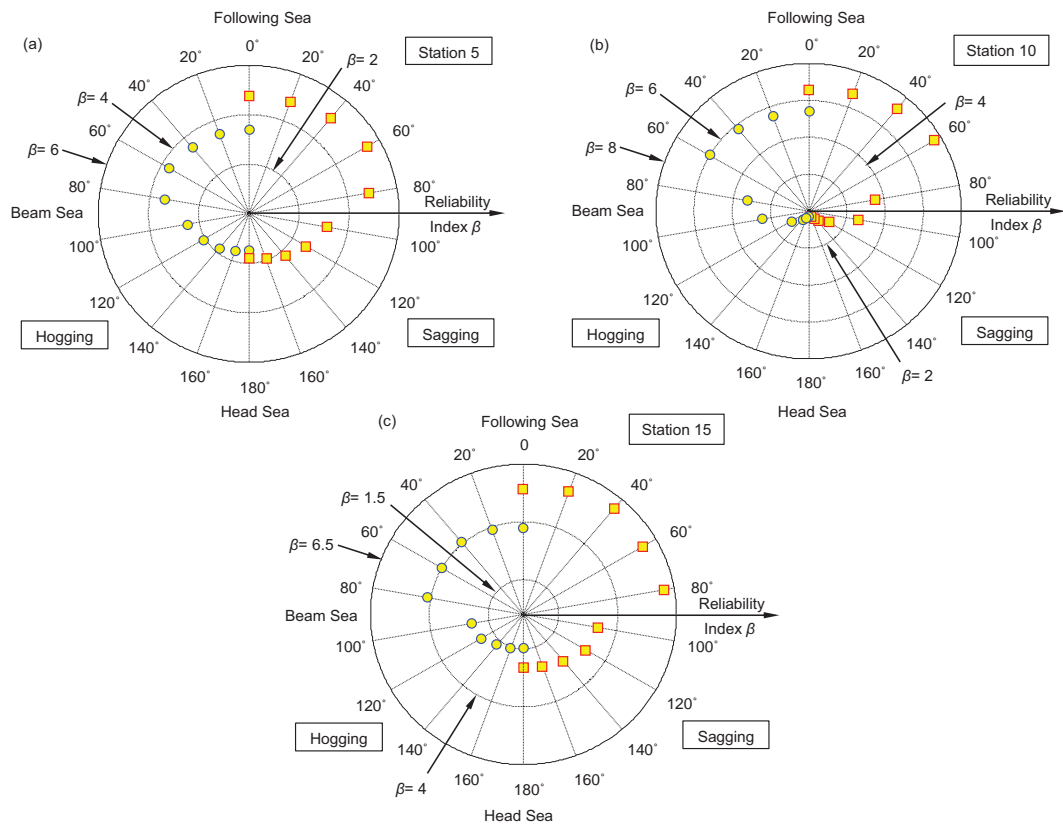
Figure 7.3 Polar representation of the reliability index (β) for both hogging and sagging associated with: (a) Station 5; (b) Station 10; and (c) Station 15.
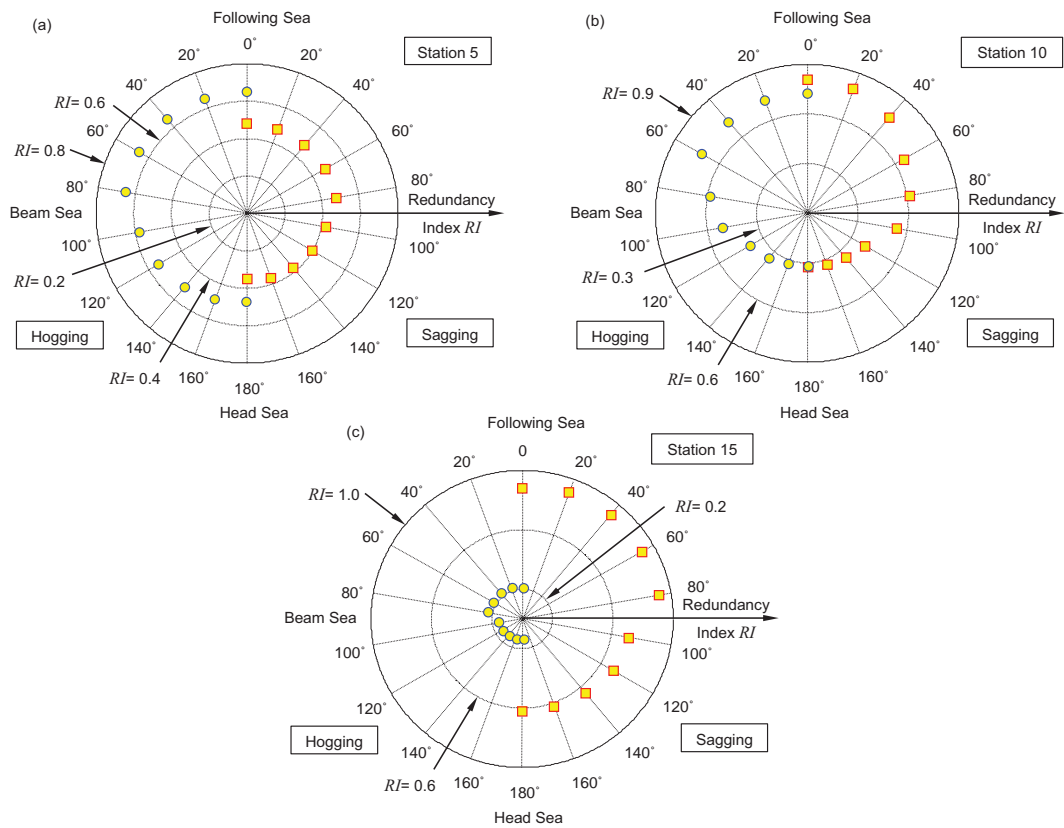
Figure 7.4 Polar representation of the redundancy index (*RI*) for both hogging and sagging associated with: (a) Station 5; (b) Station 10; and (c) Station 15.
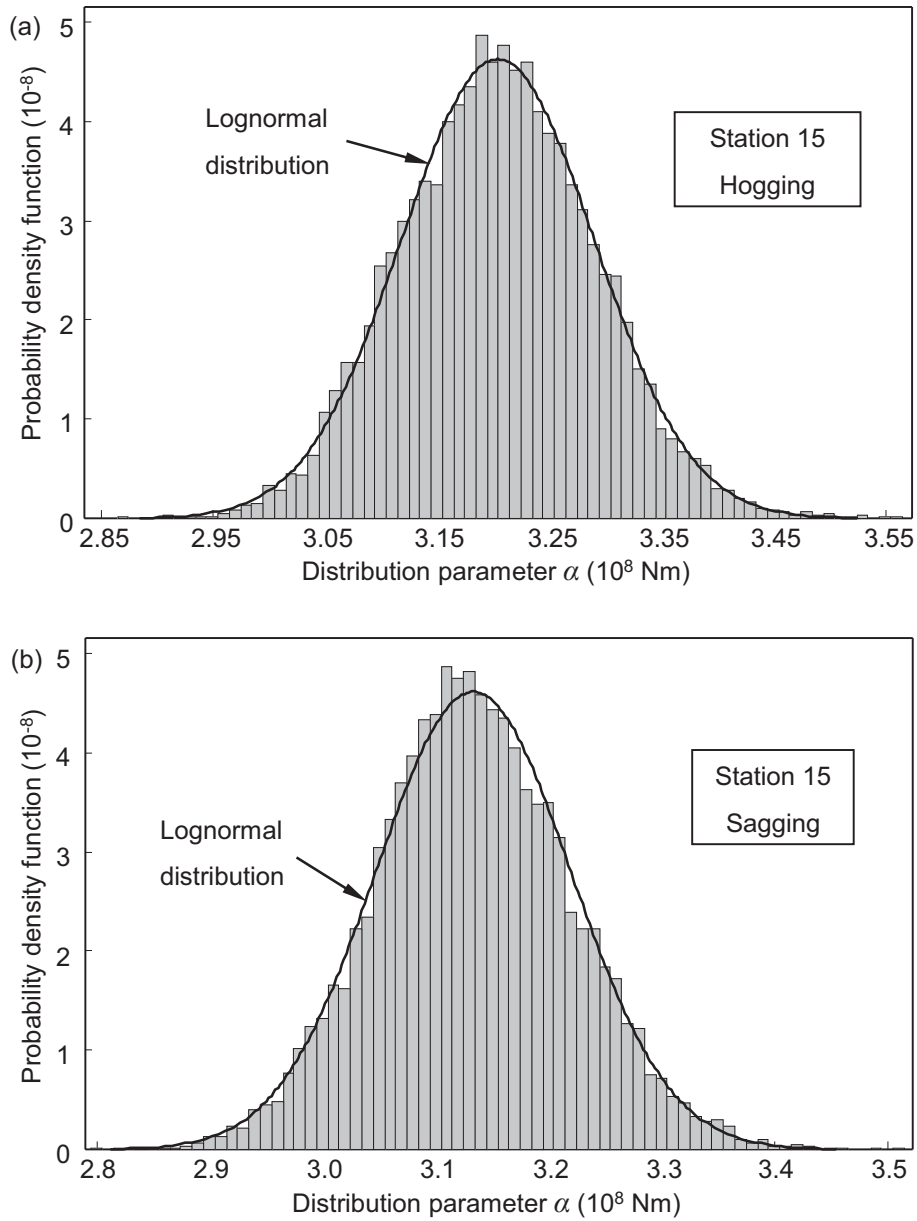
Figure 7.5 Histogram and fitted PDF of the generated posterior samples of parameter α in Rayleigh distribution associated with Station 15 for (a) hogging; and (b) sagging.
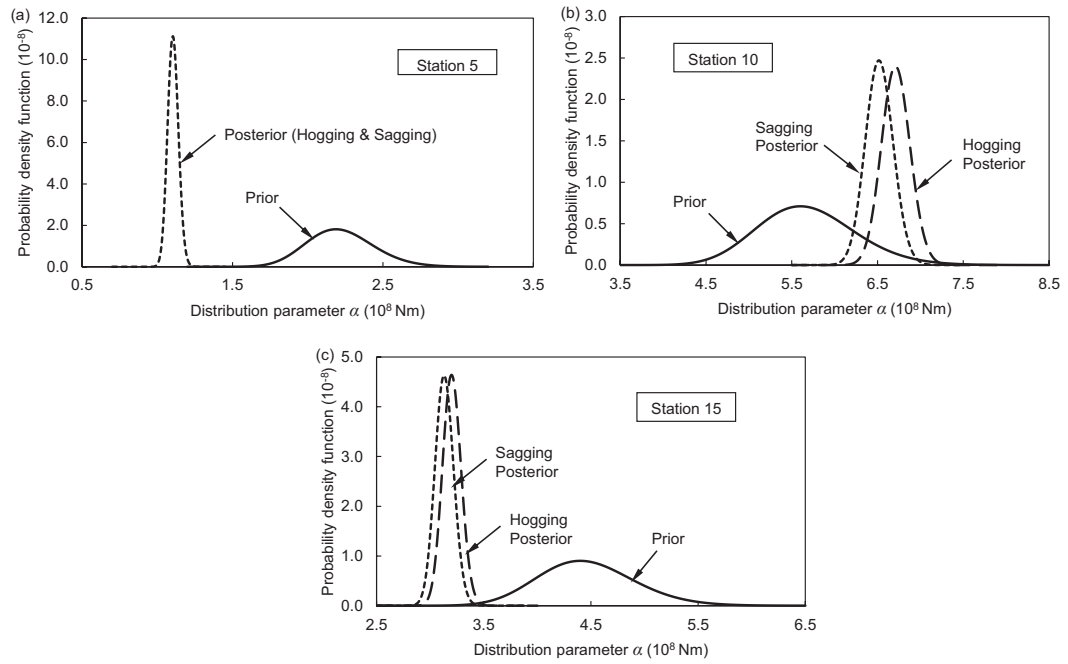
Figure 7.6   Prior and posterior PDFs of the parameter α in Rayleigh distribution associated with: (a) Station 5; (b) Station 10; and (c) Station 15.
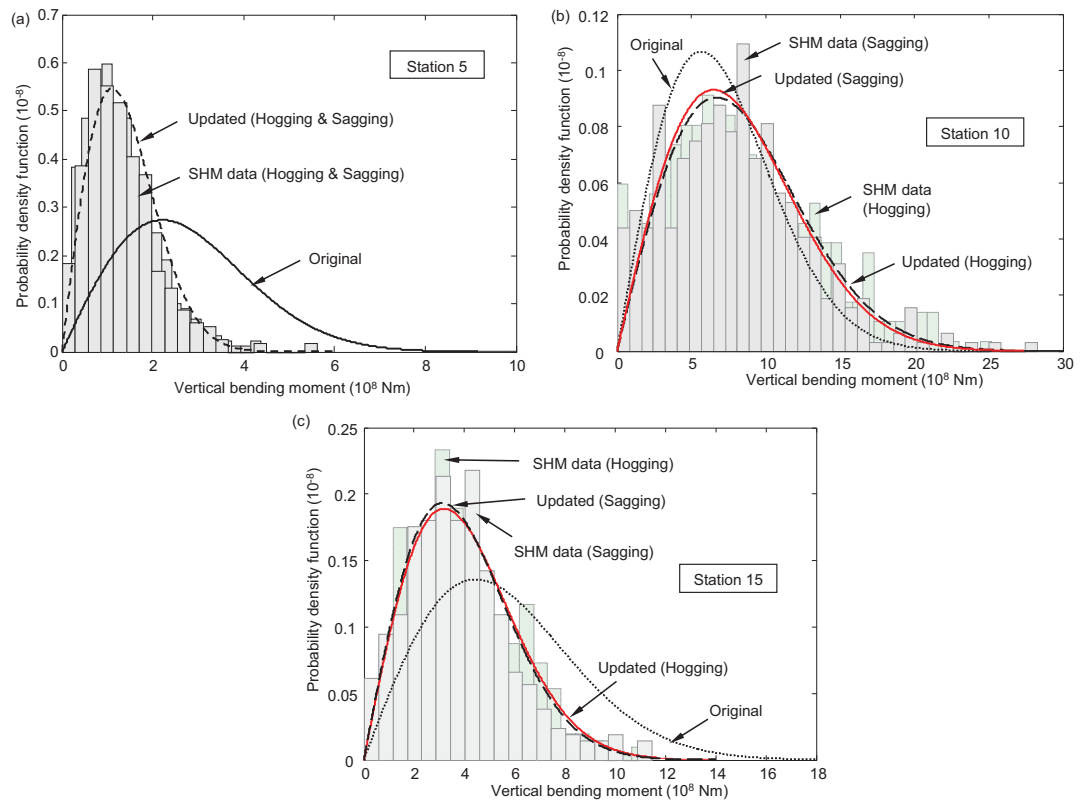
Figure 7.7 Original and updated PDFs of vertical bending moment associated with: (a) Station 5; (b) Station 10; and (c) Station 15.
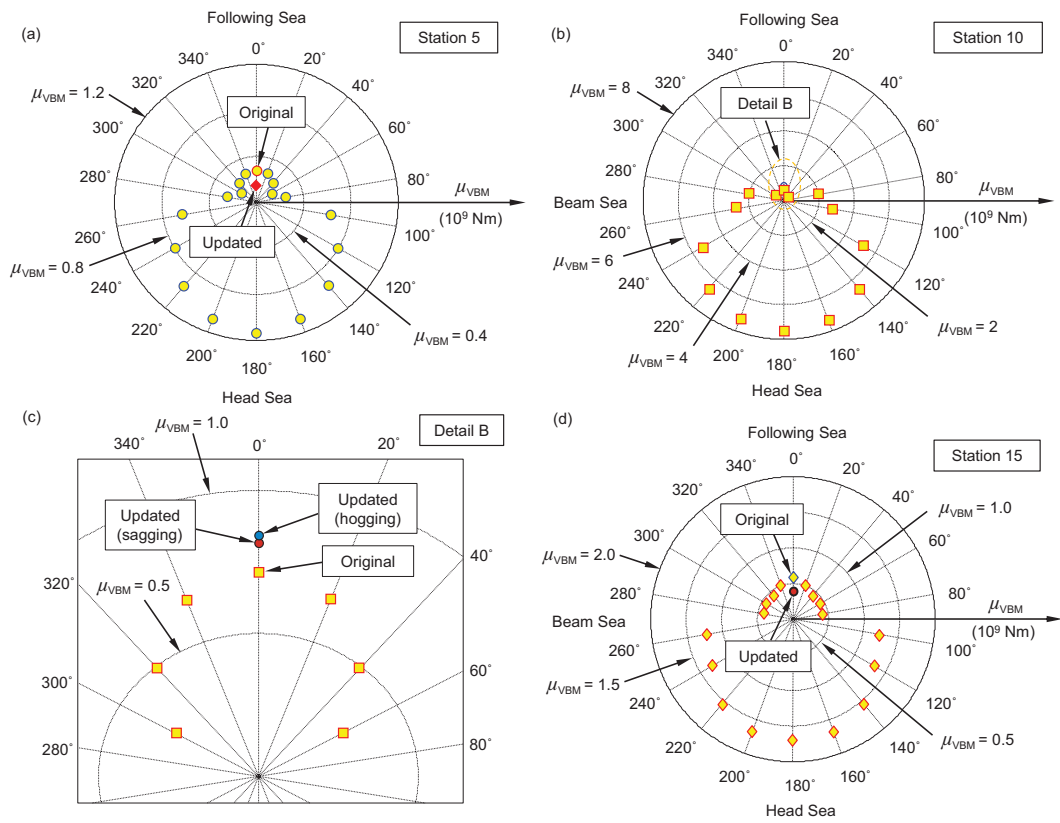
Figure 7.8 Polar representations of the original and updated mean vertical bending moment (μ_{VBM}) of: (a) Station 5; (b) Station 10; (c) detail B in Station 10; and (d) Station 15.

346
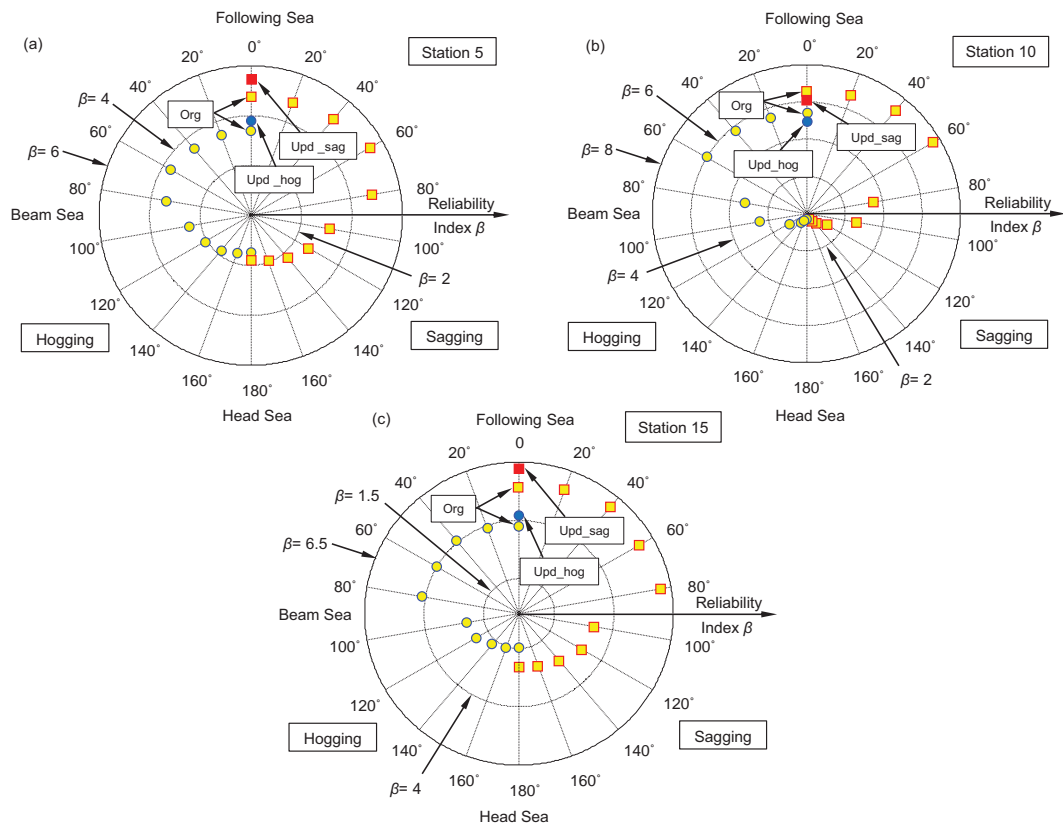
Figure 7.9 Polar representation of the original (denoted as "Org") and updated hogging (denoted as "Upd_hog") and sagging (denoted as "Upd_sag") reliability index (β) of: (a) Station 5; (b) Station 10; and (c) Station 15.
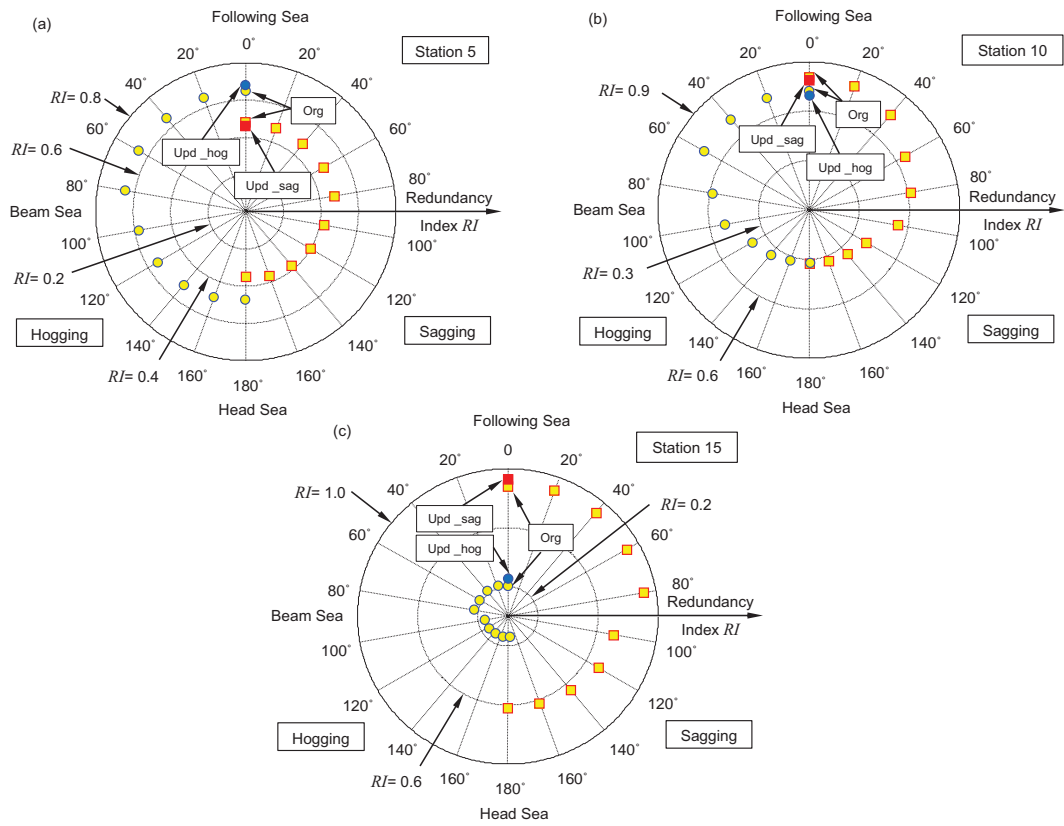
Figure 7.10   Polar representation of the original (denoted as "Org") and updated hogging (denoted as "Upd_hog") and sagging (denoted as "Upd_sag") redundancy index (*RI*) of: (a) Station 5; (b) Station 10; and (c) Station 15.

CHAPTER 8

RELIABILITY ASSESSMENT OF SHIP STRUCTURES USING BAYESIAN UPDATING

8.1 INTRODUCTION

Due to structural deterioration and the possible exposure to rough sea conditions during their lifetimes, the resistance of ships decreases and the wave loads acting on them may be very high. Therefore, it is necessary to assess structural performance to ensure an acceptable safety level of ships over their lifetimes. In the absence of the information on the real conditions of a ship structure, its responses to sea loads are estimated based on finite element models or design codes (Decò *et al.* 2012, Nikolaidis *et al.* 1993, Okasha *et al.* 2010). This may lead to conservative or risky assessment of ship performance. In this context, the availability of accurate information about the operational loads the ships are exposed to is helpful in improving the accuracy of performance assessment and validating the present information.

As mentioned in the previous chapter, structural health monitoring is a powerful technique for collecting reliable and objective data about the responses of ship structures to various operational conditions, detecting the appearance of damages, and performing real-time diagnosis of the ship structural behavior (Devine 2009, Okasha *et al.* 2010, Okasha *et al.* 2011, Salvino and Collette 2009). The amount of data collected depends on the time spans during which SHM is conducted. Classical

statistical approach is used to make accurate estimation of the parameters of a given probability distribution when a large amount of data is available. However, in most practical cases, the observed data is very limited. In such circumstances, Bayesian updating approach can be used to obtain a balanced estimation by combining the prior information with the observed data (Ang and Tang 2007).

Although Bayesian approach has been extensively used in some engineering fields (Enright and Frangopol 1999, Gaganis and Smith 2001, Geyskens *et al.* 1998, Rusk *et al.* 2011, Zhang and Mohammadian 2008, Zhang *et al.* 2009), few studies on its applications in marine engineering area, such as safety assessment of ship structures, have been performed. In Okasha *et al.* (2010), Bayesian approach was used to update the wave-induced load effects whose initial values were estimated based on the design codes by updating only one parameter in the Type I extreme value distribution. As implied earlier, both the initial information and acquired SHM data have impacts on the updated results. Inaccurate initial information (e.g., load effects from design codes) and partially incorporation with the SHM data (e.g., update only one parameter) may result in overly conservative or risky performance assessment results. In Zhu and Frangopol (2013b), the peak value of wave-induced bending moment is modeled by Rayleigh distribution and it is updated during the reliability and redundancy assessment of different ship cross-sections in hogging and sagging cases. Since Rayleigh distribution has only one parameter, the updating process focused on how to update the parameter in one-parameter distribution. However, in many practical cases, the distributions need to be updated may have two parameters, such as normal distribution and Type I extreme value distribution; therefore, it is vital to study the

process of updating two parameters in two-parameter distributions. This is the main objective of this chapter.

This chapter proposes an approach for updating the parameter(s) in a two-parameter distribution associated with the wave-induced load effects in the reliability assessment of ship structures using Bayesian method. Section 8.2 describes the models for the probabilistic evaluation of the ultimate strength of a hull girder considering time effect and the largest value of wave-induced bending moment. Section 8.3 presents a brief procedure for processing the raw SHM data to obtain the peak values of the wave-induced bending moment and develops the model for updating the parameter(s) of a two-parameter distribution. Section 8.4 studies four different updating cases associated with the Type I (largest) distribution which models the largest value of wave-induced bending moment. In Section 8.5, the proposed approach is applied to the Joint High Speed Sealift (JHSS). Finally, Section 8.6 summarizes the conclusions of this chapter.

8.2 RESISTANCE AND PRIOR LOAD EFFECTS MODELS

In most practical cases, the maximum vertical bending moment of the hull girder is of the most interest in the ship structure analysis (Guedes Soares and Teixeira 2000). As mentioned in the previous chapter, Okasha and Frangopol (2010b) proposed an efficient optimization-based approach for the determination of the probabilistic ultimate strength of the ship hull. It is proved to be as accurate as the rigorous incremental curvature method but needs significantly less computation time. In this

approach, the thickness loss of the ship hull elements due to corrosion can be considered by using the following corrosion model:

$$r(t) = C_1(t - t_0)^{C_2} \tag{8.1}$$

where $r(t)$ = thickness loss (mm), t_0 = corrosion initiation time depending on coating life (years), C_1 = annual corrosion rate (mm/years), C_2 = coefficient that determines the trend of corrosion progress, and t = time (years). The coefficient C_2 can take values ranging from 0.3 to 1.0. For practical design or assessment purposes, C_2 is usually assumed to be 1.0 (Paik and Thayamballi 2002). By combining this corrosion model with the optimization-based approach, the time-variant ultimate failure moment of a given cross-section can be obtained.

The primary load effects on the ship hull consist of the vertical bending moments induced by still water and waves. Estimation of the still water bending moment is provided in Chapter 7 (see Equations (7.1) and (7.2)). For the wave-induced bending moment, its peak value can be described by a Rayleigh distribution as:

$$f(M_w) = \frac{M_w}{\sigma^2} \exp\left(\frac{-M_w^2}{2\sigma^2}\right) \tag{8.2}$$

where M_w = wave-induced vertical bending moment, and σ = modal value. The detailed process for obtaining this Rayleigh distribution is presented in Chapter 7.

During the design or performance assessment of ships, the largest value (extreme value) of wave-induced bending moment, which may occur within the ship's lifetime, needs to be considered. Since the initial probability density function (PDF) of the peaks of vertical bending moment is Rayleigh distribution, the extreme value Y_n of these peaks converges to a Type I extreme value distribution (Ang and Tang 1984):

$$f_{Y_n}(y) = \frac{1}{\alpha_n} e^{-(y-u_n)/\alpha_n} \exp[-e^{-(y-u_n)/\alpha_n}] \tag{8.3}$$

where u_n = most probable value of Y_n, and α_n = measure of the dispersion of Y_n. For a given sample size n (number of peaks occurring within a design storm duration T), the above two parameters can be expressed in terms of n and σ (modal value of aforementioned Rayleigh distribution) as follows:

$$u_n = \sigma\sqrt{2\ln(n)} \tag{8.4}$$

$$\alpha_n = \frac{\sigma}{\sqrt{2\ln(n)}} \tag{8.5}$$

In order to find the number of peaks n, the peak rate must be determined. For a narrow-banded response, the peak rate can be approximated by the zero upcrossing rate (Pedersen 2000)

$$v_p = \frac{1}{2\pi}\sqrt{\frac{m_2}{m_0}} \tag{8.6}$$

where m_i = response spectral moments given by

$$m_i = \int_0^\infty \omega_e^i S_M(\omega_e) d\omega_e, \qquad i = 0, 1, 2,... \tag{8.7}$$

in which ω_e = encounter frequency, and S_R = response spectrum density, as defined in Chapter 7 (see Equation (7.8)). The design storm period T is assumed to be three hours in this chapter (Mansour and Mansour 1994). The number of peaks occurring within the duration T is

$$n = v_p \cdot T \tag{8.8}$$

8.3 SHM DATA PROCESSING AND BAYESIAN UPDATING

The load effects generated by sea waves consist of wave-induced bending moments associated with low frequency waves and slamming, springing and whipping effects related to high frequency excitations. In order to update the wave-induced bending moment, low frequency signals need to be separated from the collected SHM raw data using the signal filtering method. For the filtered low frequency signals, only the positive and negative peak values which correspond to hogging and sagging bending moments are of interest and thus extracted. The detailed process of peak extraction is described in (Okasha *et al.* 2010). With the obtained peak values, the prior wave-induced bending moments can be updated using Bayesian updating approach. In this chapter, the extracted hogging peaks are used to demonstrate the updating process.

Different from the classical estimation approach, Bayesian approach treats the unknown parameters of a distribution as random variables, instead of deterministic values; and more importantly, it provides room for incorporating the prior knowledge with the observed SHM data through the Bayes theorem to obtain a balanced estimation (Ang and Tang 2007). Bayesian approach for updating only one parameter in a distribution is discussed in Chapter 7. However, since most commonly used distributions have two parameters (such as normal, lognormal, Type I, Type II, and Gamma distribution), it is quite necessary to extend the approach to include the case of updating two parameters.

Consider a case of two parameters θ_1 and θ_2, which characterize the PDF $f_X(x)$ of an underlying random variable X, to be updated. In this case, the two parameters are

treated as random variables and have a prior joint PDF $f'(\theta_1, \theta_2)$. Given a group of observed information $(x_1, x_2, \ldots, x_n)$ of the underlying random variable X, the likelihood function $L(\theta_1, \theta_2)$ is constructed as:

$$L(\theta_1, \theta_2) = \prod_{i=1}^{n} f_X(x_i \mid \theta_1, \theta_2) \tag{8.9}$$

The general Bayesian updating equation becomes

$$f''(\theta_1, \theta_2) = kL(\theta_1, \theta_2)f'(\theta_1, \theta_2) \tag{8.10}$$

where $f''(\theta_1, \theta_2)$ = posterior joint PDF of θ_1 and θ_2, and k = normalizing constant to ensure $f''(\theta_1, \theta_2)$ is a proper PDF, given by:

$$k = \left[\int_{-\infty}^{\infty} \int_{-\infty}^{\infty} L(\theta_1, \theta_2)f'(\theta_1, \theta_2)d\theta_1 d\theta_2 \right]^{-1} \tag{8.11}$$

After incorporating the uncertainties in the estimation of both θ_1 and θ_2, the updated PDF of X becomes

$$f_X'(x) = \int_{-\infty}^{\infty} \int_{-\infty}^{\infty} f_X(x \mid \theta_1, \theta_2)f''(\theta_1, \theta_2)d\theta_1 d\theta_2 \tag{8.12}$$

Because the close-form expression for $f_X'(x)$ is difficult to obtain in most practical cases, the alternate approach provided in Section 7.5 which firstly calculates the cumulative distribution function of X and then performs distribution fitting to obtain the distribution type and parameters is used herein. Since an additional parameter is included in the updating process of a two-parameter distribution, the double integral in Equation (7.20) is expanded to triple integral as follows:

$$F_X'(z_i) = \int_{-\infty}^{z_i} \int_{-\infty}^{\infty} \int_{-\infty}^{\infty} f_X(u \mid \theta_1, \theta_2)f''(\theta_1, \theta_2)d\theta_1 d\theta_2 du \qquad i = 1, 2, \ldots, k \tag{8.13}$$

where $Z =[z_1, z_2, \ldots, z_i, \ldots, z_k]$ = array of values whose lower and upper bound is small and large enough, respectively, to cover the range of all probable values of X.

8.4 UPDATING CASES

Based on the aforementioned Type I (largest) distribution which models the extreme value of the peaks of the wave-induced bending moment, four updating cases are investigated herein: (a) update only u_n; (b) update only α_n; (c) update both u_n and α_n, assuming they are statistically independent; and (d) update both u_n and α_n, considering the correlation between them.

Case 1: update u_n only

Since u_n is the parameter to be updated, it is treated as a random variable in this updating process while the other parameter α_n is considered as deterministic. A lognormal distribution is assigned as a prior PDF to the variate u_n. Its mean μ_{u_n} is obtained from Equation (8.4) and the c.o.v. is assumed to be 10%.

Case 2: update α_n only

Contrary to Case 1, the parameter α_n in this case is regarded as a random variable while u_n is taken as a constant. Since α_n is positive in the Type I distribution, it is assumed to have a lognormal distribution with the mean value μ_{α_n} given by Equation (8.5) and the c.o.v. of 10%.

Case 3: update u_n and α_n both but separately

For a distribution containing two parameters, updating only one parameter at a time (as discussed in Cases 1 and 2) is much easier than updating both parameters simultanously, which involves finding the initial correlation coefficient of the prior joint PDF, generating bivariate random samples, and determining the best-fitted posterior joint PDF for the obtained samples, as will be seen subsequently in Case 4. Therefore, Case 3 where u_n and α_n are both but separately updated is investigated herein to see whether it can be used as an approximate alternative for Case 4.

In this tentative case, the two parameters u_n and α_n are separately updated using Equations (7.16) to (7.18). Therefore, they are considered as statistically independent and their posterior PDFs are the same as those obtained in Cases 1 and 2. Since both of them are updated, the new PDF of the underlying random variable Y_n becomes

$$f_{Y_n}^{'}(y) = \int_{-\infty}^{\infty}\int_{-\infty}^{\infty} f_{Y_n}(y\,|\,u_n,\alpha_n)f_{u_n}^{''}(u_n)f_{\alpha_n}^{''}(\alpha_n)du_n d\alpha_n \tag{8.14}$$

and the associated triple integral is rewritten as

$$F_{Y_n}^{'}(y_i) = \int_{-\infty}^{y_i}\int_{-\infty}^{\infty}\int_{-\infty}^{\infty} f_{Y_n}(y\,|\,u_n,\alpha_n)f_{u_n}^{''}(u_n)f_{\alpha_n}^{''}(\alpha_n)du_n d\alpha_n dy \qquad i = 1,2,...,k \tag{8.15}$$

Case 4: update u_n and α_n simultaneously, considering their correlation

Different from Case 4, u_n and α_n in this case are updated simultaneously and the correlation between them is taken into account during the updating process. In order to find the correlation coefficient, firstly, an $N{\times}N$ matrix of random numbers is generated from the original Type I distribution, where N is a large number (e.g. $N = 10^5$); therefore, the random numbers of each array (dimension $1{\times}N$) follow the Type I

distribution; then, for the i_{th} array ($i=1,2,3,…N$) consisting of N random numbers, the associated parameters $u_n(i)$ and $\alpha_n(i)$ can be found after the mean value and standard deviation with respect to the i_{th} array are determined; finally, the correlation coefficient between the parameters u_n and α_n, denoted as ρ_0, is calculated for the obtained $\boldsymbol{u_n}$ and $\boldsymbol{\alpha_n}$ vectors with the size of $N \times 1$; and the correlation coefficient between $\log(u_n)$ and $\log(\alpha_n)$, denoted as ρ, is also estimated from the $\log(\boldsymbol{u_n})$ and $\log(\boldsymbol{\alpha_n})$ vectors.

Since both parameters of the Type I distribution are positive, a bivariate lognormal distribution is assumed herein for the prior joint PDF of u_n and α_n (Abd Rabbo and Barakat 1979):

$$f(u_n,\alpha_n) = \frac{1}{2\pi\zeta_1\zeta_2\sqrt{(1-\rho^2)}} \cdot \frac{1}{u_n \cdot \alpha_n} \exp\left(-\frac{1}{2(1-\rho^2)}(A^2-2\rho AB+B^2)\right) \quad (8.16)$$

where

$$A = \frac{\log(u_n)-\lambda_1}{\zeta_1}, \qquad B = \frac{\log(\alpha_n)-\lambda_2}{\zeta_2} \quad (8.17)$$

in which (λ_1, ζ_1) and (λ_2, ζ_2) = parameters associated with u_n and α_n which are lognormally distributed, respectively, and ρ = correlation coefficient between $\log(u_n)$ and $\log(\alpha_n)$. The deterministic values of u_n and α_n obtained from Equations (8.4) and (8.5) are used as the expected values of u_n and α_n and their c.o.v.s are both assumed to be 10% in this prior joint PDF.

Based on Equations (8.9) to (8.11), the posterior samples of u_n and α_n are generated using the slice sampling algorithm. After finding the best-fitted posterior joint PDF for these samples, the updated PDF and CDF of Y_n are determined using

358

Equations (8.12) and (8.13). Since the safety of midship cross-section is a primary concern when assessing the performance of a ship hull structure (Guedes Soares and Teixeira 2000), the reliability analysis in this chapter is performed only with respect to the midship cross-section. The limit state equation for the ultimate failure of a cross-section is given in Equation (7.13). Based on the probability distributions and associated parameters for the resistance, still water bending moment, extreme value of the wave-induced bending moment and the limit state equation, the time-variant reliability index associated with the midship cross-section is computed using the program RELSYS (Estes and Frangopol 1998).

8.5 CASE STUDY

The Joint High Speed Sealift (JHSS) described in Section 7.6 is used herein as a case study to illustrate the concepts presented in this chapter. The design scantlings of the midship cross-section are shown in Figure 7.1(b) and the dimensions of the components are listed in Table 8.1 (Devine 2009). SHM data was collected during the seakeeping and structural loads tests which were conducted for a scaled (λ =1:47.5255) segmented model of JHSS. The data used in this case study provides the vertical bending moments at the midship cross-section associated with the operational case of 35 knot speed, heading angle 0°, and sea state 7. It contains 73,800 samples and the sampling rate was 200 Hz; therefore, the total duration of the test was about 6.15 min. Since no information on the measurement error is mentioned in (Devine 2009), it is assumed that there is no error in the measurement in the SHM data. Conversion of the test results of the scaled model to the full-scale ship is provided in Section 7.6.1. The

wave-induced bending moments associated with low frequency waves are filtered from the scaled bending moments using the Butterworth filter in MATLAB signal processing toolbox (MathWorks 2010). 397 positive peaks (hogging moments) are then extracted from the low frequency waves.

8.5.1 Time-variant Resistance and Prior Load Effects

The distribution type and parameters associated with the elastic modulus, yielding stresses of plating and stiffener and plating thickness of the midship cross-section are provided in Section 7.6.2. According to Akpan *et al.* (2002), the annual corrosion rate C_1 is assumed to follow lognormal distribution. The mean and standard deviation of C_1 with respect to the location of the stiffened plates are presented in Table 8.2, and the parameters associated with deck stiffener web and side stiffener web are the same as those associated with deck plating and side shell plating, respectively (Okasha *et al.* 2010).

　　The corrosion initiation time t_0 is also treated as a lognormally distributed random variable with the mean of 5 years and coefficient of variation of 0.4 (Decò *et al.* 2011). However, since the coefficient C_2 was treated as a deterministic value in most previous studies (Akpan *et al.* 2002, Paik and Thayamballi 2002, Decò *et al.* 2011, Qin and Cui 2003) and no information on the suggested distribution type, mean value and coefficient of variation of C_2 is found from the reference papers, C_2 is considered as deterministic herein. 5000 samples are generated for these random variables using the Latin-Hypercube sampling to simulate the ultimate bending moment which is found to be best fitted by a lognormal distribution. Since the corrosion effect is considered

during the ship's service life taken as 30 years, the above procedure (sampling-simulating-fitting) needs to be performed 16 times at a two-year increment to obtain the time-variant resistance of the midship cross-section. The lifetime profiles of the mean and mean plus and minus one standard deviation of the ultimate bending moment (hogging) are shown in Figure 8.1. It is obvious that the bending moment decreases over time due to the corrosion effect.

The vertical bending moment (hogging) due to still water is computed using Equations (7.1) and (7.3). Based on Hørte *et al.* (2007) and Hussein and Guedes Soares (2008), the obtained bending moment for the midship cross-section is assumed to be normally distributed with mean and standard deviation of 2.008×10^9 Nm and 5.736×10^8 Nm, respectively.

For the operational condition of speed 35 knots, heading angle 0° and sea state 7, three steps are required to obtain the Rayleigh distribution for the peaks of the wave-induced vertical bending moments: (1) determine the Response Amplitude Operator (RAO) curve for this operational case using the program PDSTRIP (2006); (2) combine the sea spectrum of sea state 7 and the RAO curve to assess the response spectrum; and (3) find the square root of the area under the spectral density function of the response spectrum, and this is the parameter σ of the Rayleigh distribution in Equation (8.2). Having performed the steps above, the parameter σ for this operational case is found to be 5.69×10^8 Nm. Based on Equations (8.4) and (8.5), the parameters u_n and α_n of the Type I extreme value (largest) distribution are found to be 2.13×10^9 Nm and 1.52×10^8 Nm, respectively.

8.5.2 Bayesian Updating Cases

Generally, long-term SHM data of real ship structures is rarely available. For the investigated concept ship JHSS, although its seakeeping load test was conducted on a segmental model in the laboratory, the SHM data available is still very limited (the duration of the SHM test converted to the full-scale ship was about 43 minutes) and only 397 low-frequency peaks were extracted (Devine 2009). However, since the main objectives of this chapter are to (a) demonstrate the process of updating the parameters in a two-parameter distribution and (b) study the effects of different updating cases on the results rather than perform strict reliability analysis for structural design or performance assessment of real ships, all the obtained peaks are used to update the two-parameter Type I (largest) distribution.

As mentioned previously, four updating cases associated with estimating the parameter(s) in the Type I extreme value (largest) distribution are investigated herein: (a) update only u_n; (b) update only α_n; (c) update both u_n and α_n but separately; and (d) update u_n and α_n simultaneously, considering the correlation between them.

Case 1: update u_n only

The parameter u_n in this case is considered as a lognormally distributed random variable with the mean and c.o.v. of 2.13×10^9 Nm and 0.1, respectively. Based on Equations (7.16) to (7.18), the obtained 397 peaks of the vertical bending moments are integrated with this prior PDF and the samples of the posterior PDF of u_n are generated using the slice sampling algorithm. By using Minitab (2010), it is found that these posterior samples are best modeled by the lognormal distribution. The histogram

and fitted PDF of these samples are plotted in Figure 8.2(a). It is noted that after including the SHM data, the distribution type of u_n changes from the assumed lognormal distribution to normal distribution.

Figure 8.2(b) shows the prior and posterior PDFs of u_n. It is observed that both the mean and standard deviation of u_n decrease significantly after updating; this indicates that integration of the SHM data dramatically reduces the uncertainty in the parameter u_n. The updated PDF of the largest value of VBM is plotted in Figure 8.3. It is found that (a) compared with the original PDF, the updated PDF is shifted to the left; this implies that the mean value of the largest VBM is significantly reduced after the location parameter u_n is updated; and (b) the shape of the updated PDF is not changed; this is because the scale parameter α_n is deterministic in this case, which means the dispersion of the largest VBM keeps the same.

Case 2: update α_n only

The following hyper-parameters are considered for the lognormal random variable α_n: λ_{α_n} =18.84 and ζ_{α_n} =0.1, based on the assumed mean and c.o.v. of 1.52×10^8 Nm and 0.1, respectively. By applying the Equations (7.16) to (7.18), the samples of the posterior PDF of α_n are generated and plotted in Figure 8.4(a). It is noticed that these posterior samples are best fitted by lognormal distribution, which is of the same type as the prior PDF of α_n. Figure 8.4(b) shows both the prior and posterior PDFs of α_n. It is observed that both the mean and standard deviation of α_n increase after updating. Therefore, integrating SHM data does not necessarily reduce the dispersion of a parameter, which characterizes its aleatory uncertainty. Whether this uncertainty

increases or not depends on the initial assumption of the dispersion of the parameter. If the initial dispersion is assumed to be a small value while the true dispersion is a larger one, the aleatory uncertainty of this parameter will increase after updating because integration of SHM data makes the updated dispersion of this parameter closer to its true value. However, the epistemic uncertainty associated with this parameter will be reduced because our knowledge about the hyper-parameters of the parameter is improved after the observed information is included.

The original and updated PDFs of the largest value of the vertical bending moments are plotted in Figure 8.5. It is found that (a) the mean values of both PDFs are almost the same because the location parameter u_n is considered as deterministic in this case; and (b) the dispersion of the updated PDF is much larger than that associated with the original one due to the significant increase of the mean of α_n, as shown in Figure 8.4.

Case 3: update both u_n and α_n but separately

The PDFs of the underlying variate before and after updating are plotted in Figure 8.6. It shows that (a) the location and shape of the updated PDF are changed compared to the original one since both u_n and α_n are updated in this case; and (b) although the posterior PDFs of u_n and α_n are the same as those in Cases 1 and 2, the obtained location and scale parameters of the updated Type I distribution in this case are different from the obtained location parameter in Case 2 and the scale parameter in Case 3.

Case 4: update u_n and α_n simultaneously, considering the correlation between them

The deterministic values of u_n and α_n in the original Type I largest distribution (2.13 $\times 10^9$ Nm and 1.52 $\times 10^8$ Nm, respectively) are used as the mean values of u_n and α_n in the prior joint distribution and their c.o.v.s are both assumed to be 0.1. By using the method for determining the correlation coefficient that was discussed previously and setting the sample size N to be 10^5, the correlation coefficient between u_n and α_n is found to be 0.19. With the prior joint PDF provided by Equations (8.16) and (8.17) and the 397 hogging peaks of VBM, the posterior samples of u_n and α_n are obtained based on Equations (8.9) to (8.11), as plotted in Figure 8.7. It is observed that (a) although the prior marginal distributions of u_n and α_n are lognormal, the posterior marginal distributions are best fitted by normal distribution; and (b) the correlation between the two parameters increases after incorporation of the SHM data.

The prior and posterior marginal distributions of u_n and α_n are shown in Figure 8.8. It is noticed that after incorporation of the SHM data, (a) the mean and standard deviation of u_n decrease while the mean of α_n increases; these observations are similar to those in Cases 1 and 2; (b) the standard deviation of α_n decreases rather than increases as found in Case 2; and (c) compared with the previous cases, the differences in the mean values (standard deviations) between the prior and posterior PDFs of the both u_n and α_n in this case are less significant.

The multivariate normal distribution has some properties and two of them are recalled here: (1) if a random vector follows a multivariate normal distribution, its marginal distributions are normal; however, the reverse conclusion may not be true; and (2) a random vector is said to have the multivariate normal distribution if every

linear combination of its components is normally distributed. Therefore, although the marginal distributions of u_n and α_n are normal, it cannot be concluded that their joint distribution is a bivariate normal distribution. Based on the second property above, an approximate method used herein for assessing the bivariate normality is described as follows: (1) generate two random numbers a and b; (2) examine whether the random variable $Y = a \cdot u_n + b \cdot \alpha_n$ is normally distributed using the Anderson-Darling test (Anderson and Darling 1952); (3) repeat steps (1) and (2) q times, where q is a large number; and (4) if all the results from step (2) are "Yes" for the q times, the random variables u_n and α_n can be approximately regarded to have a joint normal distribution. By performing the above procedures and setting q to be 10^7, the posterior joint distribution of u_n and α_n is found to be a bivariate normal distribution, as shown in Figure 8.9.

The updated PDF of the largest vertical bending moment is obtained by first substituting the above posterior joint PDF into Equations (8.12) and (8.13) and then performing distribution fitting. Figure 8.10 shows the original and updated PDFs with the SHM data. It is found that (a) similar to the observation in Case 3, the updated PDF in this case has a smaller mean value and a larger standard deviation compared to the original PDF; the reason for this is twofold: (1) incorporation of the SHM data makes the mean and standard deviation of the updated PDF move towards to those associated with the SHM data; and (2) the mean and dispersion of the SHM data are smaller and larger than the mean and dispersion of the original PDF, respectively; and (b) compared with the result in Case 3, updating the two parameters simultaneously

and taking the correlation between them into account lead to smaller mean and standard deviation of the updated PDF.

By comparing the results in Cases 1-4, it is concluded that (a) for the case of only one parameter is updated (Cases 1 and 2), if this parameter is related to the location (or scale) of the PDF, the location (or scale) changes in the new obtained PDF while the scale (or location) keeps almost the same (see Figure 8.3 and Figure 8.5); (b) for the cases where both parameters are updated (Cases 3 and 4), the location and scale of the updated PDF are altered compared to the original PDF (see Figure 8.6 and Figure 8.10); (c) since the SHM data contains the information related to both parameters, updating only one parameter excludes the influence of the SHM data on the other parameter; therefore, the results in Cases 1 and 2 which partially integrate the SHM data are not reliable; and (d) the independence assumption in Case 3 is not reasonable because the two parameters u_n and α_n are actually correlated and the correlation coefficient increases as more SHM data are included, and the results in this tentative case deviate significantly from those in Case 4. Thus, the obtained PDF of the largest VBM in Case 4 is closer to the true result than those in the other three cases.

8.5.3 Time-variant Reliability Index

The time-variant reliability indices associated with Cases 1-4 are plotted in Figure 8.11. It is observed that for the investigated operational condition (speed 35 knots, heading angle 0°, and sea state 7), (a) updating only u_n (Case 1) and only α_n (Case 2) result in the highest and lowest lifetime reliability, respectively; (b) updating both parameters separately (Case 3) also leads to very low lifetime reliability; and (c) the

367

reliability associated with updating the correlated parameters simultaneously (Case 4) is slightly higher than the reliability without integrating SHM data.

In order to obtain a better updating result based on the limited data, an additional case (denoted as "Case 5") where a set of largest samples from the peaks of vertical bending moment are used for updating is studied herein. In this case, the extracted 397 regular peaks are divided into 10 groups and the maximum values from each group are approximately used as the extreme samples to update the Type I distribution. The time-variant reliability indices associated with Cases 4 and 5 are shown in Figure 8.12. It is noticed that the updated lifetime reliability indices based on the regular peaks and largest samples are very close.

8.5 CONCLUSIONS

This chapter presents an approach for reducing the uncertainty in the performance assessment of ship structures by updating the wave-induced load effects with the information acquired from SHM. Bayesian updating is performed to estimate the parameters in the Type I extreme value (largest) distribution which models the largest values of the peaks of wave-induced bending moment. Three general cases associated with updating (a) only one parameter, (b) two parameters separately, and (c) two correlated parameters simultaneously in a two-parameter distribution are investigated. The following conclusions are drawn:

1. Incorporation of SHM data does not necessarily reduce the uncertainty of a parameter; instead, the dispersion of the parameter may increase after updating. The role of SHM data is to reduce the epistemic uncertainty and make the updated

information of a parameter be closer to its true values. The probability distribution types of the parameters and the correlations between them may change after updating.

2. Although the posterior PDFs of u_n and α_n in Case 3 (u_n and α_n are separately updated) are the same as those in Cases 1 and 2, the obtained location and scale parameters of the updated Type I distribution in this case are different from the obtained location parameter in Case 1 (only u_n is updated) and the scale parameter in Case 2 (only α_n is updated). Since the two parameters are separately integrated with the SHM data and independence is assumed between them, the obtained results associated with Case 3 differ significantly from the true values, and it cannot be used as an approximate alternative for Case 4.

3. The reliability indices associated with updating only one parameter in a two-parameter distribution deviate heavily from the true values since the influence of the SHM data on the other parameters is excluded during the updating process. To ensure the reliability of the obtained results, both the parameters in the distribution should be simultaneously updated and the correlations among them need to be taken into account. Updating only one parameter yields conservative or risky results in the design or performance assessment of structures.

4. Since the available SHM data is very limited, the peak values of vertical bending moments are used to update the Type I distribution in order to demonstrate the process of updating the parameters in a two-parameter distribution. If sufficient SHM data becomes available in the future, the largest samples extracted from a set of design storms have to be used to update the Type I distribution.

Table 8.1 Geometric properties of the components in midship cross-section (adapted from Okasha *et al.* (2010)).

Component No.	Designation	d (mm)	t_w (mm)	b (mm)	t_f (mm)
1	5×4×6 T	125.5	4.8	100.6	5.3
2	8×4×10 I-T	200.4	4.3	100.1	5.2
3	10×4×12 I-T	250.7	4.8	100.6	5.3
4	8×4×15 I-T	206.0	6.2	102.1	8.0
5	12×4×16 I-T	304.5	5.6	101.3	6.7
6	12×4×19 I-T	308.9	6.0	101.9	8.9
7	10×5 ¾ ×22 I-T	258.3	6.1	146.1	9.1
8	14×5×22 I-T	349	5.8	127	8.5
9	8×6 ½ ×28 I-T	204.7	7.2	166.1	11.8
10	7×8×21.5 T	173.5	7.7	203.2	22.1
11	24×9×94 I-T	616.7	13.2	230.1	22.1
12	24×12×119 I-T	616.2	14.0	325.1	21.6
13	24×14×146 I-T	628.4	16.5	327.7	27.7
14	36×16 ½ ×230 I-T	911.4	19.6	418.3	32.0

Note: d = stiffener depth, t_w = web thickness, b = web width, and t_f = flange thickness.

Table 8.2 Distribution parameters of the annual corrosion rate C_1 based on Okasha *et al.* (2010).

Location	Mean (mm/year)	Standard deviation (mm/year)
Deck plating	0.008125	0.000406
Side shell plating	0.003750	0.000188
Bottom shell plating	0.021250	0.001063
Bottom stiffener web	0.008125	0.000406
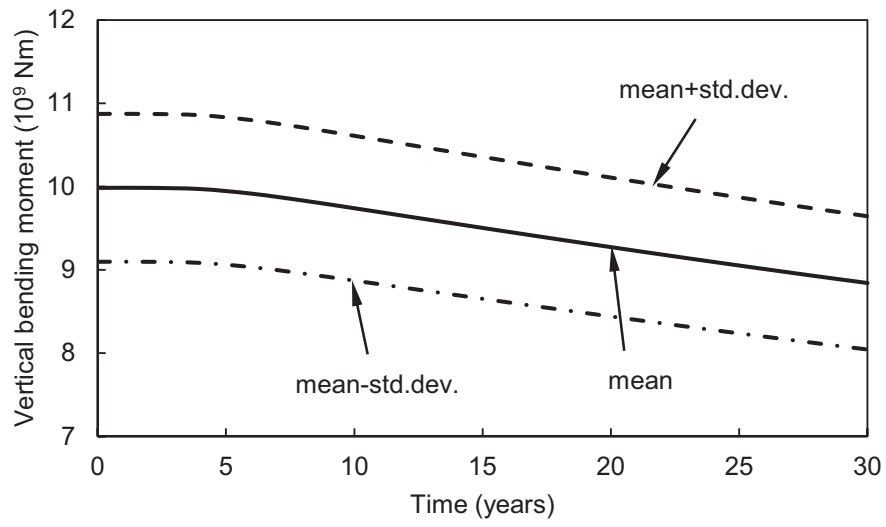
Figure 8.1 Profile of mean and mean plus and minus one standard deviation of the ultimate failure moment at the midship cross-section.
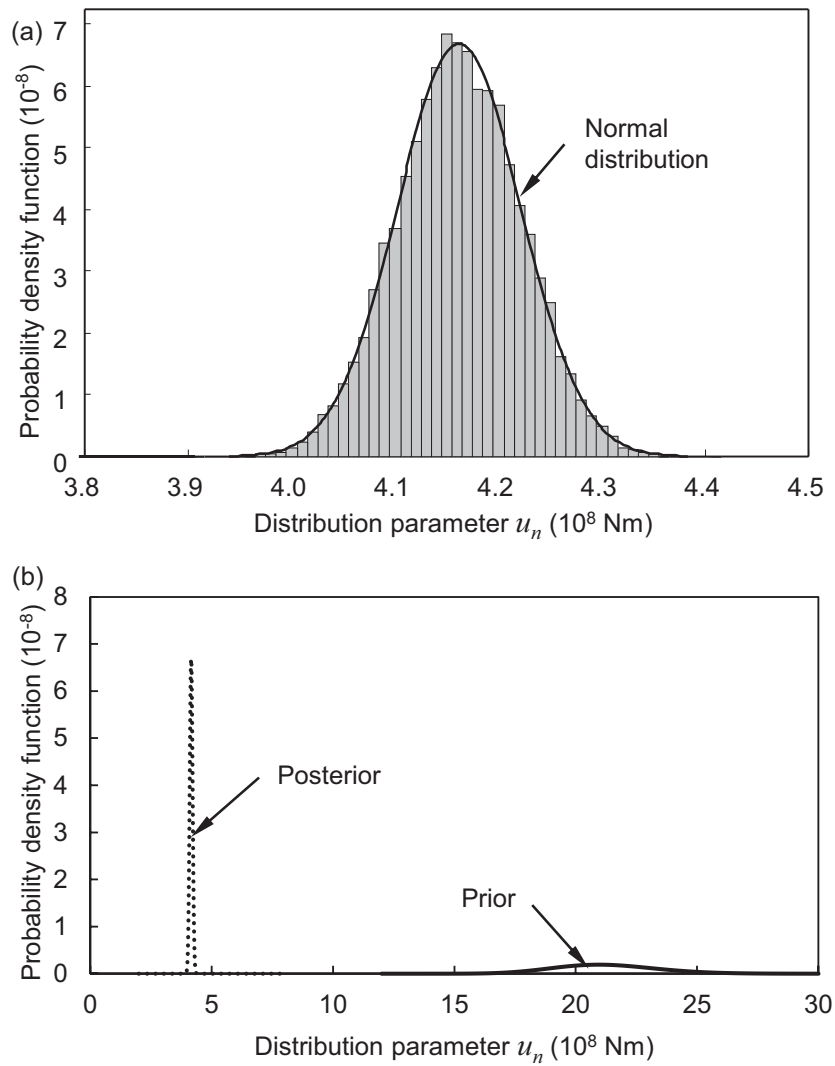
Figure 8.2 (a) Histogram and fitted PDF of the generated posterior samples of parameter u_n; and (b) prior and posterior PDFs of the parameter u_n in the Type I extreme value distribution.
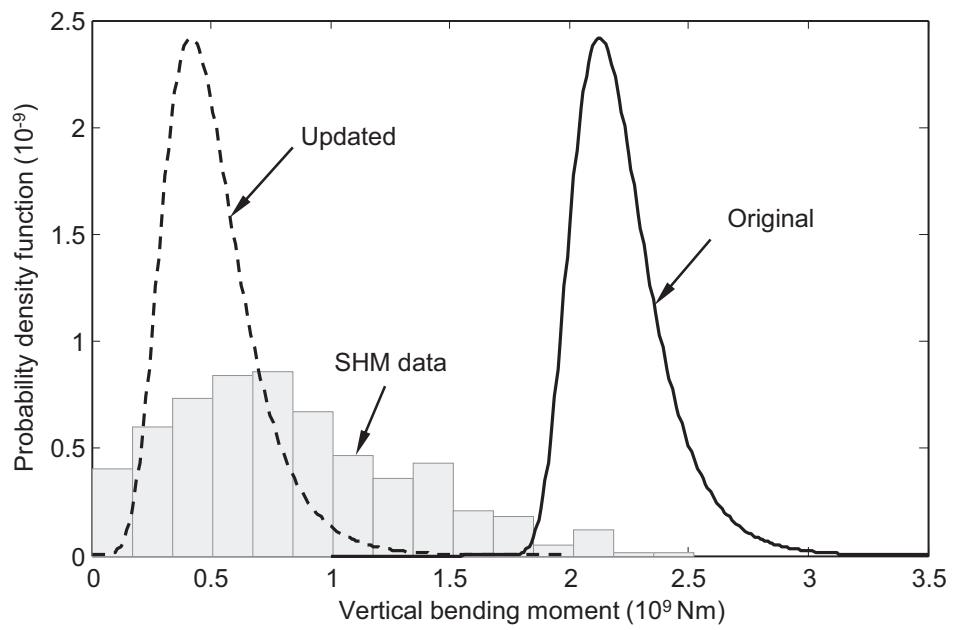
Figure 8.3 Original and updated PDFs of the largest values of vertical bending moment in the case when only u_n is updated.
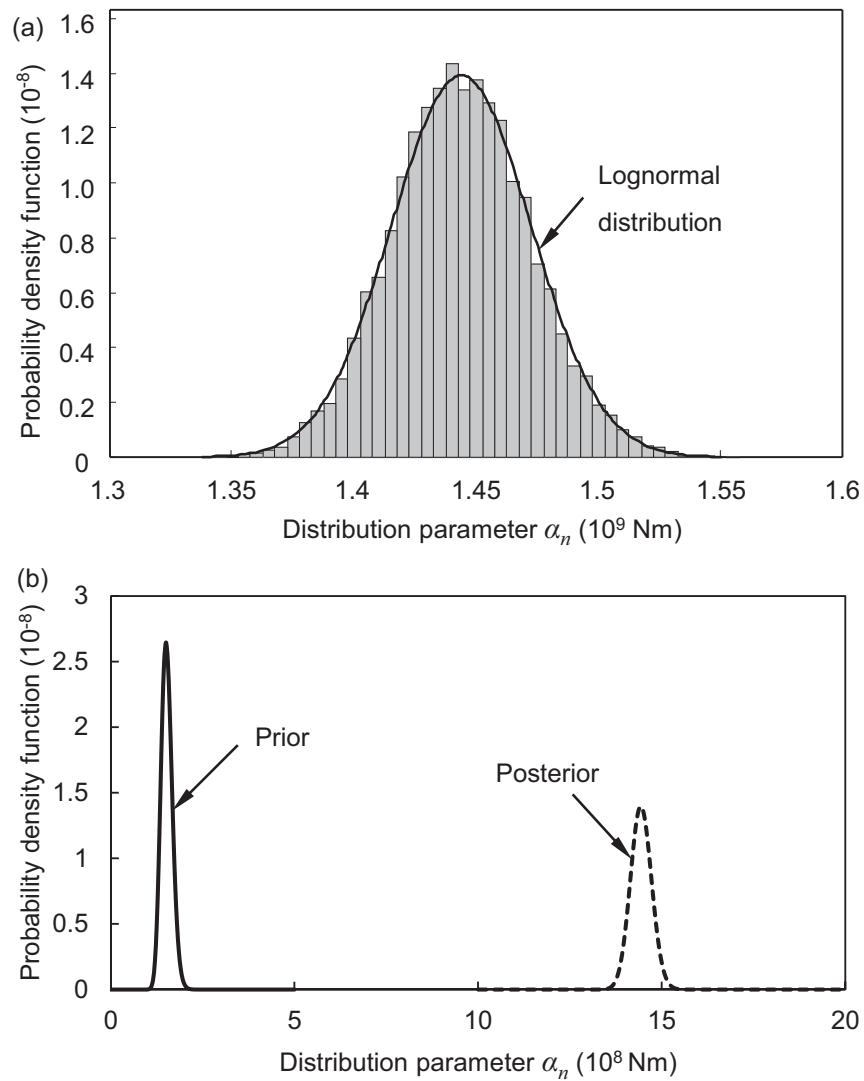
Figure 8.4   (a) Histogram and fitted PDF of the generated posterior samples of parameter α_n; and (b) prior and posterior PDFs of the parameter α_n in the Type I extreme value distribution.
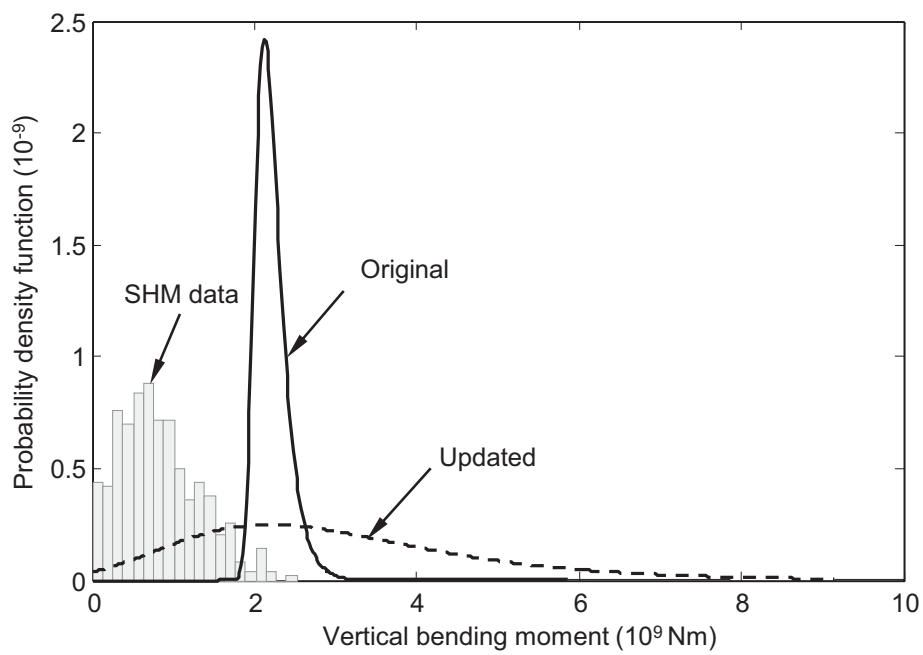
Figure 8.5 Original and updated PDFs of the largest values of vertical bending moment in the case when only α_n is updated.
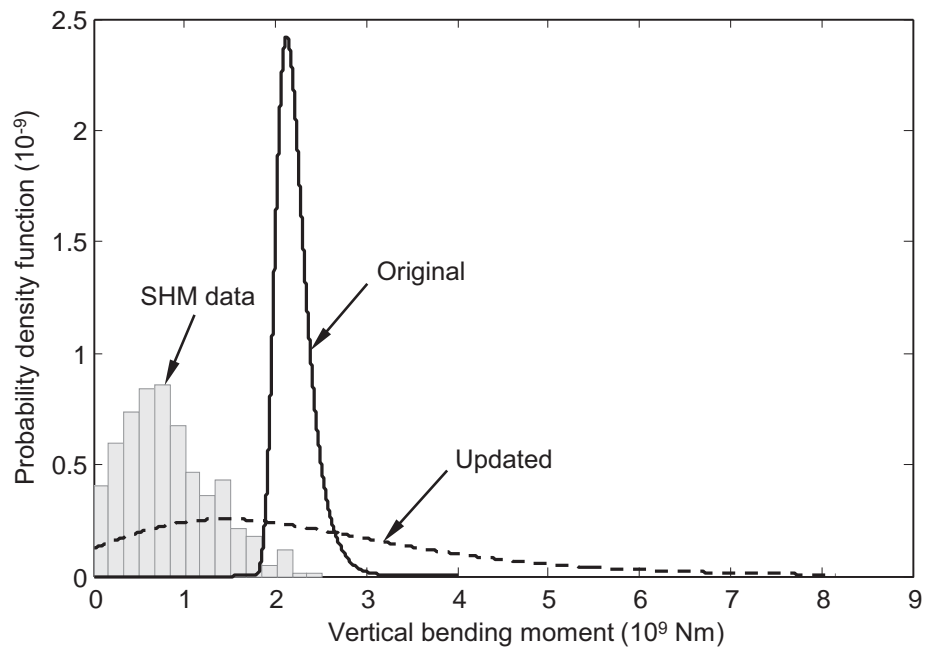
Figure 8.6 Original and updated PDFs of the largest values of vertical bending moment in the case when u_n and α_n are updated separately.
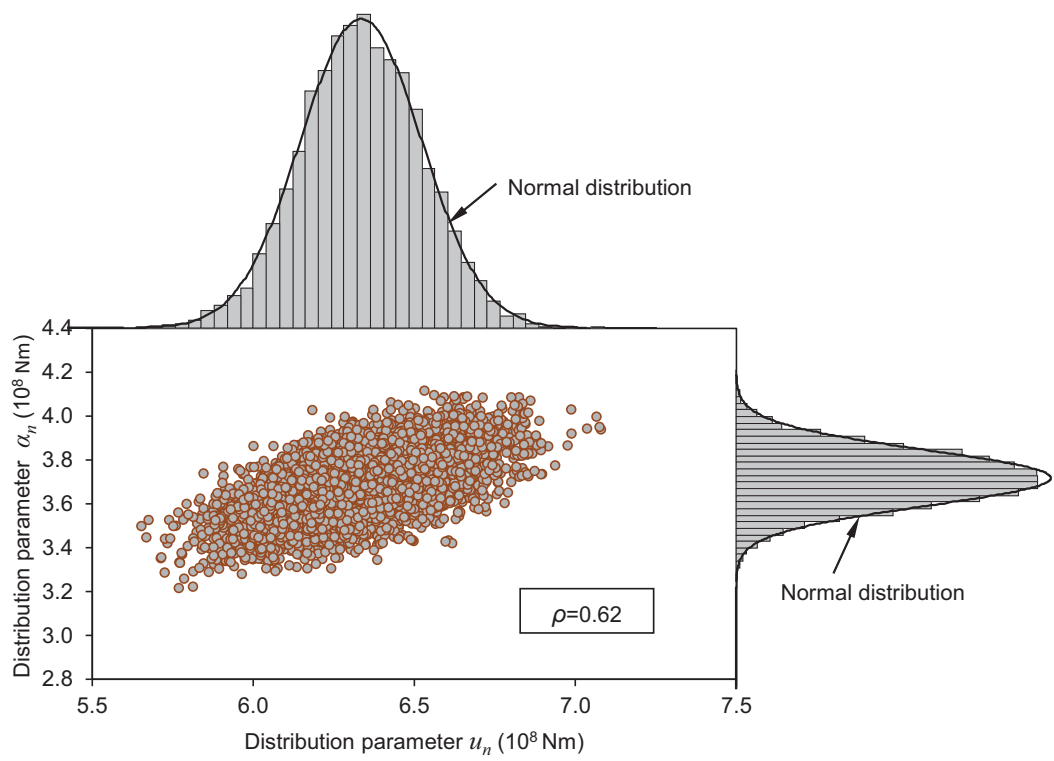
Figure 8.7 Histograms and fitted marginal PDFs of the generated posterior samples of parameters u_n and α_n in the Type I extreme value distribution.
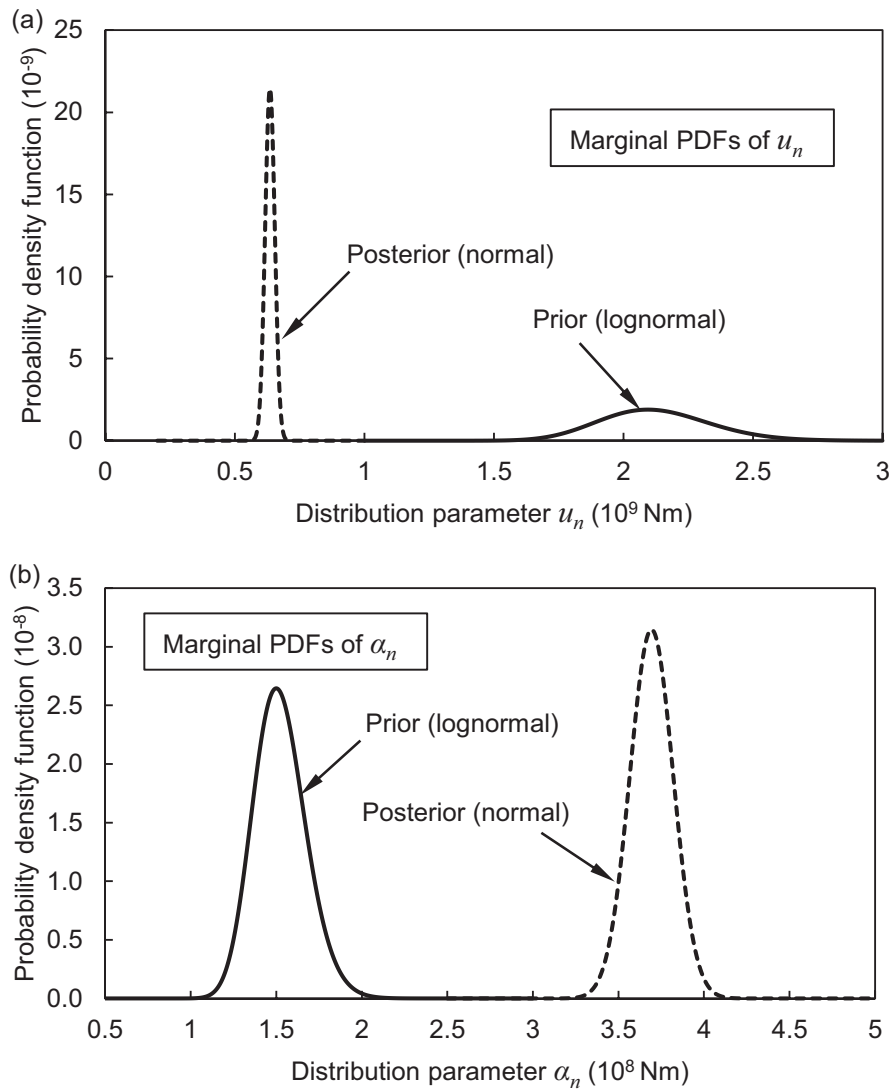
Figure 8.8 Prior and posterior marginal PDFs of (a) parameter u_n and (b) parameter α_n in the Type I extreme value distribution.
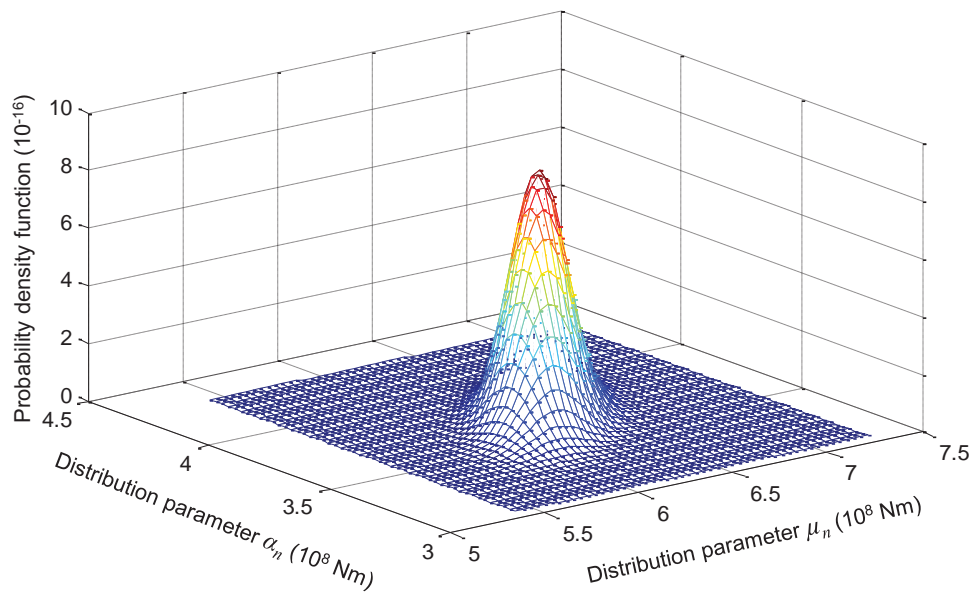
Figure 8.9 Posterior joint PDF of the parameters u_n and α_n in the Type I extreme value distribution.
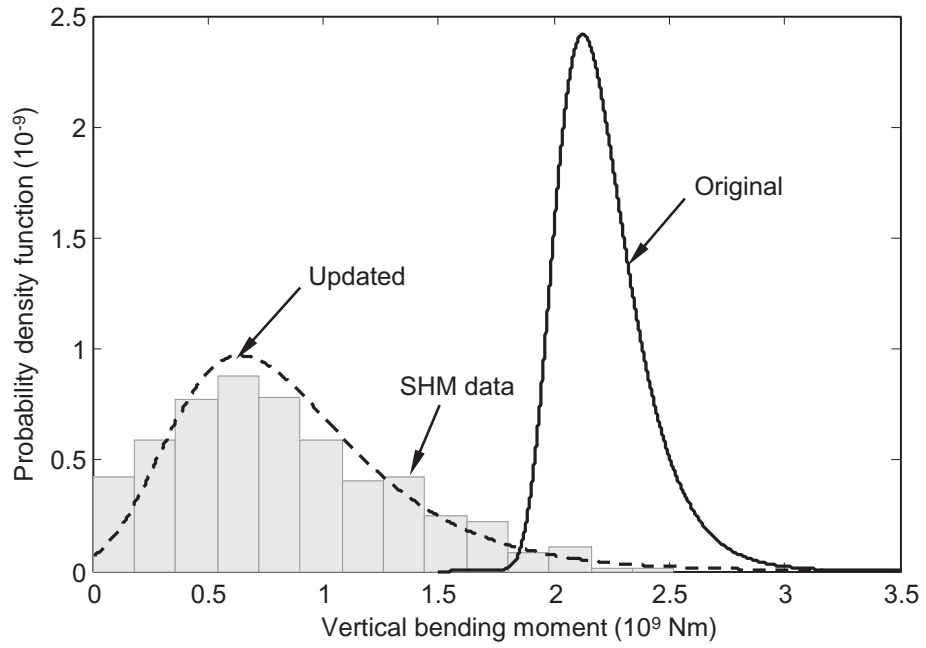
Figure 8.10   Original and updated PDFs of the largest values of vertical bending moment in the case of u_n and α_n are updated simultaneously with the correlation between them taken into account.
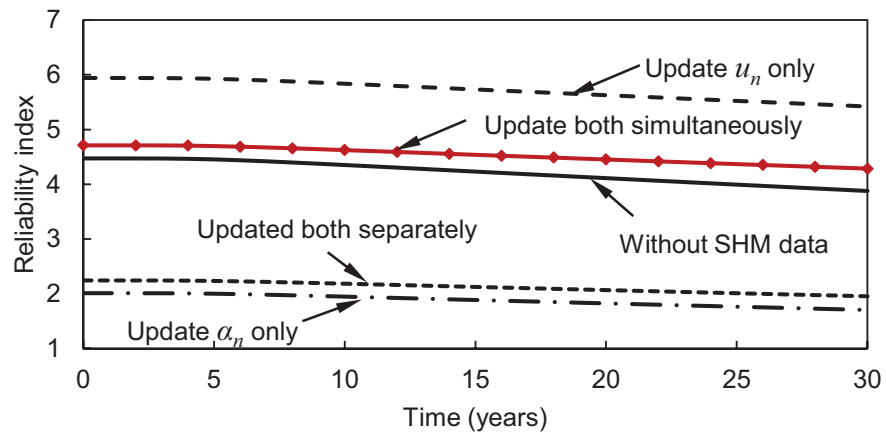
Figure 8.11 Profiles of time-variant reliability index before and after updating associated with Type I extreme value distribution.
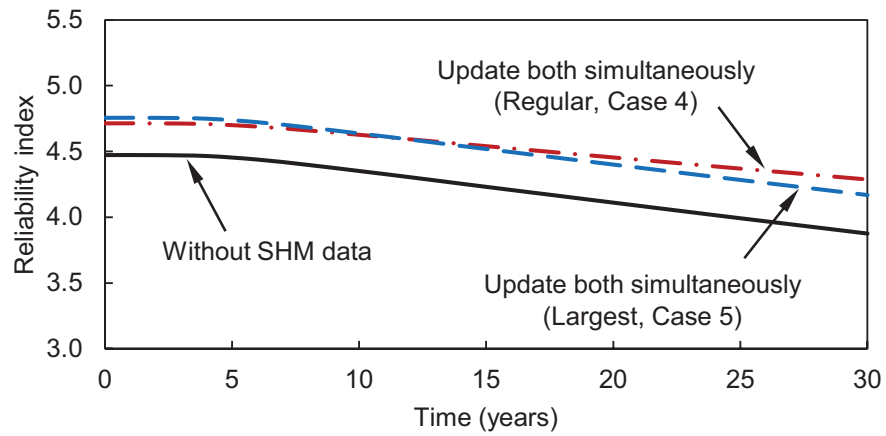
Figure 8.12   Profiles of the time-variant reliability index associated with updating Cases 4 and 5.

CHAPTER 9

SUMMARY, CONCLUSIONS, AND SUGGESTIONS FOR

FUTURE WORK

9.1 SUMMARY

This study has proposed a redundancy factor considering the effects of several parameters and developed approaches for integrating the reliability- and risk-based performance indicators in the life-cycle management framework for structures. The tasks of the life-cycle management framework investigated in this study include (a) performance assessment and prediction, (b) optimization of maintenance strategies, and (c) performance updating using structural health monitoring data. The proposed redundancy factor aims at providing a more rational reliability-based design of structural components. The developed approaches are intended to serve as useful tools for obtaining accurate assessment results of structural performance for decision making.

Due to the subjective evaluation of the factor relating to redundancy in the current AASHTO bridge design specifications, a redundancy factor considering the effects of several parameters, such as number of components, correlation among the resistances of components, system type, and post-failure material behavior, was proposed. The impacts of the parameters describing the uncertainties of resistances and load effects of components on the redundancy factor were studied using idealized systems.

384

Redundancy factors of ductile and brittle systems consisting of many components were evaluated considering three correlation cases.

Since the load and resistance factors in the LRFD codes were calibrated to achieve a uniform level of reliability for all components, the reliability of systems consisting of uniform reliability components was investigated. Effects of the post-failure behavior and the statistical parameters associated with resistances and load effects on the system reliability were studied. Reliability indices of ductile and brittle systems with many uniform reliability components were analyzed.

Reliability, redundancy and risk are important performance indicators in the life-cycle management process. An approach for evaluating these structural performance indicators considering the effects of time, deterioration of structural resistance, system modeling type and correlations among failure modes of components was presented. Event-tree models were utilized to evaluate the direct and indirect risks caused by failure of components or system. Idealized systems consisting of three components were used to study the effects of the aforementioned factors on these performance indicators.

A risk-based maintenance optimization methodology for bridges subjected to traffic and earthquake loads was proposed to seek the optimum essential and preventive maintenance strategies. The risks due to traffic and earthquake load, respectively, and the total risk under both hazards were assessed by performing hazard analysis, vulnerability analysis and consequences analysis. A more complete formulation for consequences evaluation was presented. Two case studies in which the bridge was located in a low and high seismic region were investigated.

An approach for assessing the risks due to the closure of bridge lanes under traffic load and scour was developed. Scenarios of lanes closure due to the two hazards were identified. After obtaining the annual failure probabilities of girders and pier columns, the occurrence probabilities of the scenarios were evaluated based on the relations between the scenarios and the failure events of girders and pier columns. Consequences caused by lanes closure were evaluated from three aspects. The risks associated with the identified scenarios were assessed considering two correlation cases among the failure modes of bridge components.

In order to reduce the uncertainty in structural performance assessment, an approach for incorporating structural heath monitoring data in the reliability and redundancy assessment of ship cross-sections using Bayesian updating was presented. The prior information on the wave-induced load effects was analyzed based on linear theory. The peak values of low frequency waves used for updating were extracted from the filtered SHM raw signals. Bayesian updating method was used to integrate the objective SHM data with the Rayleigh-distributed prior load effects to obtain a balanced estimation. The original and updated reliability and redundancy indices of the ship cross-sections were evaluated and compared.

Since the two-parameter distributions are more commonly used in the engineering field, a methodology for updating two parameters was developed based on the approach mentioned previously for updating one parameter. This methodology was applied to ship structures to improve the accuracy in the reliability assessment of ships. The load effects to be updated was the largest values of the wave-induced vertical bending moments modeled by Type I extreme value distribution. Three general cases

associated with updating (a) only one parameter, (b) two parameters separately, and (c) two correlated parameters simultaneously were investigated. The reliability indices associated with these updating cases were evaluated considering the time effects.

9.2 CONCLUSIONS

From the analyses of the proposed redundancy factor and the life-cycle performance of bridge and ship structures, the following conclusions are drawn:

- The redundancy factor proposed in this study and the factor relating to redundancy in the AASHTO bridge design specifications are of the same nature. The major difference is that the factor relating to redundancy in the AASHTO specifications is determined based on a general classification of redundancy levels while the proposed redundancy factor is more rational because it is based on a comprehensive system reliability-based approach considering the effects of several parameters including the system type, correlation among the resistances of components, post-failure material behavior, and number of components in the system.

- The approach proposed for simplifying the system model of a brittle system enables the redundancy factor analysis of a brittle system with a large number of components. This approach in conjunction with the developed MCS-based program and the methodology presented for redundancy factor analysis of ductile system paves the way for generating standard tables of redundancy factors to facilitate the component design process.

- Deterioration of structural components causes the degradation of reliability and the increase of risk over time. However, the tendency of redundancy changing with time is uncertain. The direct and indirect risks caused by the failure of component or system can be evaluated using the proposed event-tree model. It has been found that the direct risk due to a single component failure is independent of the system type while the associated indirect risk is affected not only by the system type but also by the position of component in the system. In addition, the correlation among the failure modes of components has significant effect on the direct and indirect risks.

- This study developed methods for evaluation of the safety and environmental losses due to bridge failure and the commercial losses associated with the unavailability of highway / railway or channel under failed bridge. These methods as well as the existing approaches for analysis of the running cost and time loss cost present a more complete formulation for the total consequences evaluation caused by bridge failure.

- As expected, it has been observed that the risks due to traffic and seismic loads increase over time due to the deterioration in the structural strength and increase in the traffic volume. The effect of an essential maintenance action on risk mitigation under a specific hazard is affected by the increase rate of the time-variant risk profile associated with this hazard. Analyzing the impact of the failure probability of a component on the system failure probability can help predicting the effect of a maintenance action associated with the component (i.e., replacing, repainting, or recoating, etc.) on risk mitigation.

- Different optimization criteria yield different optimum maintenance strategies. Selecting the solution that is more economical or the one providing lower lifetime risk as the final optimum strategy depends not only on the financial budget but also on the decision-makers' attitude towards risk aversion.

- Although the consequences increase as the number of closed lanes increases, the risk associated with the closure of more lanes is not necessarily higher than that associated with the closure of fewer lanes. Correlation among the failure modes of bridge components has significant effect on the risk due to lanes closure.

- The scenarios of bridge lanes closure need to be classified not only based on the number of closed lanes but also on the directions of the closed lanes. For the scenarios where the number of the closed lanes is the same, the risk due to the closure of lanes in the same direction may be different from that associated with closure of lanes in different directions.

The following conclusions are drawn from the performance assessment of ship structures:

- Polar plot of the reliability / redundancy index provides a straightforward representation of the structural safety associated with different heading angles for a given sea state and ship speed.

- It has been found that the reliability indices of a ship cross-section associated with sagging are usually larger than those associated with hogging for all heading angles. However, this conclusion cannot be extended for the redundancy indices of the cross-section.

- Integration of the SHM data can significantly reduce the epistemic uncertainty in estimation of the distribution parameters so that the updated performance indicators are closer to their true values. The probability distribution types of the parameters and the correlations between them may change after updating.

- The reliability indices associated with updating only one parameter in a two-parameter distribution or updating both parameters separately deviate heavily from the true results. Therefore, these updating cases cannot be used as approximate alternatives for the case where the correlated parameters are simultaneously updated.

- When the SHM information associated with different operational conditions is available, the proposed approach can be used to update the entire reliability / redundancy polar plots with respect to different sea states and ship velocities. For a given sea state that a ship might encounter during a journey, the ship operator can use these updated polar plots as guidance to adjust the speed and heading angle to maintain a satisfactory safety level of the ship system.

9.3 SUGGESTIONS FOR FUTURE WORK

The suggestions for future work are presented as follows:

- This study generated standard tables of the proposed redundancy factor for a representative case where the coefficients of variation of resistances and load effects are assumed to be commonly-used values. Further effort is needed to

develop standard tables for other frequently-used coefficients of variation cases to form a complete set of tables for structural component design.

- The proposed approach for assessing the direct and indirect risks caused by failure of single component needs to be extended to multiple components. The total risks associated with failure of different groups of components can provide guidance on determining the maintenance priorities of components.

- The hazards investigated in the risk assessment of this study are considered as independent. Further research is needed to develop approaches for risk analysis under correlated hazards by evaluating their conditional probabilities and the sequential effects on the vulnerability analysis and consequences analysis.

- The essential and preventive maintenance actions are significantly different in the costs and effects on the risk mitigation; therefore, combination of the two types of actions may be more efficient and economical than using only one of them. Hence, maintenance options that combine both essential and preventive maintenance should be considered in the optimization process.

- In the reliability and redundancy assessment of ship structures, the dynamic effects induced by waves are not included. Therefore, research effort is needed to develop approaches for analyzing these effects and updating them with the processed SHM data.

- As is the case with bridge structures, the consequences caused by failure of ship structures can be enormous. Therefore, it is necessary to assess the risk of ships under specific operational conditions and integrate SHM information in the risk analysis using Bayesian updating.

- For a multi-objective optimization of maintenance strategies, a group of optimum solutions can be obtained. Selection of the final optimum strategy is determined by the decision-makers' attitude. Therefore, further studies are required to develop approaches for rational decision making.

REFERENCES

AASHTO. (1992). Standard specifications for highway bridges. 15th Edition. American Association of State Highway and Transportation Officials, Washington, DC.

AASHTO. (1994). LRFD bridge design specifications. 1st Edition. American Association of State Highway and Transportation Officials, Washington, DC.

AASHTO. (2007). LRFD bridge design specifications, 4th Edition. American Association of State Highway and Transportation Officials, Washington, DC.

AASHTO. (2010). LRFD bridge design specifications. 5th Edition. American Association of State Highway and Transportation Officials, Washington, DC.

AASHTO. (2012). LRFD Bridge Design Specifications. 6th Edition. American Association of State Highway and Transportation Officials, Washington, D.C.

Abd Rabbo, N.A. and Barakat, H.M. (1979). Estimation problem in bivariate lognormal distribution. *Indian Journal of Pure Applied Mathematics*, 10(7), 815-825.

Adey, B., Hajdin, R. and Bruhwiler, E. (2003). Risk-based approach to the determination of optimal interventions for bridges affected by multiple hazards. *Engineering Structures*, 25(7), 903-912.

Ahearn, E.A. (2003). Peak-flow frequency estimates for U.S. Geological Survey stream flow-gaging stations in Connecticut. *Water-Resources Investigations Report 03-4196*, Department of the Interior, U.S. Geological Survey, Reston, VA.

Akiyama, M., Frangopol D.M., Arai, M. and Koshimura, S. (2013). Reliability of bridges under tsunami hazard: emphasis on the 2011 Tohoku-Oki earthquake. *Earthquake Spectra*, 29(S1), S295-S317.

Akiyama, M., Frangopol, D.M. and Matsuzaki, H. (2011). Life-cycle reliability of RC bridge piers under seismic and airborne chloride hazards. *Earthquake Engineering and Structural Dynamics*, 40(15), 1671-1687.

Akpan, U.O., Koko, T.S., Ayyub, B. and Dunbar, T.E. (2002). Risk assessment of aging ship hull structures in the presence of corrosion and fatigue. *Marine Structures*, 15(3), 211-231.

Albrecht, P. and Naeemi, A.H. (1984). Performance of weathering steel in bridges. *NCHRP Report 272,* National cooperative highway research program,

transportation research board, Washington, D.C., July.

Almusallam, A.A., Khan F.M., Dulaijan S.U. and Al-Amoudi O.S.B. (2003). Effectiveness of surface coatings in improving concrete durability. *Cement and Concrete Composites*, 25(4-5), 473-481.

Anderson, T.W. and Darling, D.A. (1952). Asymptotic theory of certain 'goodness-of-fit' criteria based on stochastic processes. *Annals of Mathematical Statistics*, 23:193-212.

Andrews, J.D. and Dunnett, S.J. (2000). Event tree analysis using binary decision diagrams. *IEEE Transactions on Reliability*, 49(2), 230-239.

Ang, A.H.-S. and Tang, W.H. (1975). Probability concepts in engineering planning and design, vol. I. *John Wiley & Sons*, New York.

Ang, A.H-S. and Tang, W.H. (1984). Probability concepts in engineering planning and design: decision, risk and reliability, vol. II. *John Wiley & Sons*, New York.

Ang, A.H.-S. and Tang, W.H. (2007). Probability concepts in engineering. Emphasis on applications to civil and environmental engineering. 2nd Edition. *New York: Wiley & Sons*.

Arneson, L.A., Zevenbergen, L.W., Lagasse, P.F. and Clopper, P.E. (2012). Evaluating scour at bridges, 5th Edition. *Hydraulic Engineering Circular No. 18*, FHWA-NIF-12-003. Federal Highway Administration, U.S. Department of Transportation, Washington, D.C.

Augusti, G., Ciampoli, M. and Frangopol, D.M. (1998). Optimal planning of retrofitting interventions on bridges in a highway network. *Engineering Structures*, 20(11), 933-939.

Ayyub, B.M., Assakkaf, I.A. and Atua, K.I. (2000). Reliability-based load and resistance factor design (LRFD) of hull girders for surface ships. *Naval Engineers Journal*, 112(4), 279–96.1.

Babu, S.G.L. and Singh, V.P. (2011). Reliability-based load and resistance factors for soil-nail walls. *Canadian Geotechnical Journal*, 48 (6), 915-930.

Balendra, T., Tan, K. and Kong, S. (1999). Vulnerability of reinforced concrete frames in low seismic region when designed according to BS 8110. *Earthquake Engineering and Structural Dynamics*, 28(11), 1361–1381.

Baker, J.W., Schubert, M. and Faber, M.H. (2006). On the assessment of robustness. *Structural Safety*, 30(3), 253–267.

Banerjee, S. and Ganesh Prasad, G. (2013). Seismic risk assessment of reinforced concrete bridges in flood-prone regions. *Structure and Infrastructure Engineering*, 9(9), 952-968.

Benjamin, J.R. and Cornell, C.A. (1970). Probability, statistics, and decision for civil engineers. New York: McGraw-Hill Book Company.

Blagojevic, B. and Ziha, K. (2008). On the assessment of redundancy of ship structural components. *In: Proceedings of the international conference on offshore mechanics and arctic engineering (OMAE)*, Estoril, Portugal, June 15–20, 2008, vol. 2, pp. 673–68.

Bocchini, P. and Frangopol, D.M. (2012). Bridge network performance, maintenance, and optimization under uncertainty: accomplishments and challenges. *Structure and Infrastructure Engineering*, 8(4), 341-356.

Breusers, H.N.C., Nicollet, G. and Shen, H.W. (1997). Local scour around cylindrical piers. *Journal of Hydraulic Research*, 15(3), 211-252.

Bruneau, M. (1992). Evaluation of system-reliability methods for cable-stayed bridge design, *Journal of Structural Engineering*, 118(4), 1106-1120.

Bucher, C. (2009). Computational analysis of randomness in structural mechanics: Vol. 3. *Structures and infrastructures book series*. Taylor & Francis, London.

Building Seismic Safety Council (BSSC). (1997). NEHRP recommended provisions for seismic regulations for new buildings, Part 1-Provisions. Federal Emergency Management Agency (FEMA) 302, 290.

Burdekin, F.M. (2007). General principles of the use of safety factors in design and assessment. *Engineering Failure Analysis*, 14(3), 420-433.

Burton, B. and Verijenko, V. (2002). Structural health monitoring in marine structures. *ASME 21st International Conference on Offshore Mechanics and Arctic Engineering*, June 2002, Oslo, Norway, Volume 2, pp 243-249.

Cavaco, E.S., Casas, J.R. and Neves, L.A.C. (2013). Quantifying redundancy and robustness of structures. *Proceedings of IABSE Workshop on Safety, Failures and Robustness of Large Structures*, International Association for Bridge and Structural Engineering (IABSE), Zurich, Switzerland.

Chabert, J. and Engeldinger, P. (1956). Etude des affouillements autour des piles de points (Study of scour at bridge piers). Bureau Central d'Etudes les Equipment d'Outre-Mer, Laboratoire National d'Hydraulique. Chatou, France, (in French).

Chakrabarti, S.K. (1987). Hydrodynamics of offshore structures. *Computational Mechanics Publications*, Berlin, Germany.

Chen, W. F. and Duan, L. (1999). Bridge engineering handbook. CRC, Boca Raton, FL.

Cheng, J. and Li, Q.S. (2009). Reliability analysis of long span steel arch bridges against wind-induced stability failure. *Journal of Wind Engineering and Industrial Aerodynamics*, 97(3-4), 132-139.

Colorado State Patrol. (2011). Colorado driver handbook. Denver, Colorado. Webpage: www.colorado.gov.

Decò. A. and Frangopol, D.M. (2011). Risk assessment of highway bridges under multiple hazards. *Journal of Risk Research*, 14(9), 1057-1089.

Decò, A. and Frangopol, D.M. (2013). Life-cycle risk assessment of spatially distributed aging bridges under seismic and traffic hazards. *Earthquake Spectra*, 29(1), 1-27.

Decò, A., Frangopol, D.M. and Okasha, N.M. (2011). Time-variant redundancy of ship structures. *Journal of Ship Research*, 55(3), 208-219.

Decò, A., Frangopol, D.M. and Zhu, B. (2012). Reliability and redundancy assessment of ships under different operational conditions. *Engineering Structures*, 42, 457-471.

DesRoches, R. and Fenves, G.L. (2000). Design of seismic cable hinge restrainers for bridges. *Journal of Structural Engineering*, 126(4), 500–509.

DesRoches, R., Choi, E., Leon R.T. and Pfeifer, T.A. (2004). Seismic response of multiple span steel bridges in central and southeastern United States. II: Retrofitted. *Journal of Bridge Engineering*, 9(5), 473-479.

Devine, E.A. (2009). An overview of the recently-completed JHSS monohull and trimaran structural seaways loads test program. *Naval Surface Warfare Center*, Carderock Division (NSWCCD), PowerPoint Briefing.

Ditlevsen, O. and Bjerager, P. (1986), Methods of structural systems reliability. *Structural Safety*, 3(3-4), 195-229.

Ellingwood, B.R. (2001). Acceptable risk bases for design of structures. *Progress in Structural Engineering and Materials*, Wiley & Sons, 3(2), 170-179.

Ellingwood, B.R. (2005). Risk-informed condition assessment of civil infrastructure: state of practice and research issues. *Structure and Infrastructure Engineering*, 1 (1), 7 – 18.

Ellingwood, B., Galambos, T.V., MacGregor, J.G. and Cornell, C.A. (1980). Development of a probability based load criterion for American National Standard A58. *NBS Special Publication 577*, National Bureau of Standards, Washington, D.C.

Enright, M.P. and Frangopol, D.M. (1999). Condition prediction of deteriorating concrete bridges using Bayesian updating. *Journal of Structural Engineering*, 125(10), 1118-1125.

Estes, A.C. (1997). A system reliability approach to the lifetime optimization of inspection and repair of highway bridges. *PhD Thesis*, Department of Civil, Environmental, and Architectural Engineering, University of Colorado, Boulder, CO.

Estes, A.C. and Frangopol, D.M. (1998). RELSYS: A computer program for structural system reliability. *Structural Engineering & Mechanics*, 6(8), 901–999.

Estes, A.C. and Frangopol, D.M. (1999). Repair optimization of highway bridges using system reliability approach. *Journal of Structural Engineering*, 125(7), 766-775.

Estes, A.C. and Frangopol, D.M. (2001). Bridge lifetime system reliability under multiple limit states. *Journal of Bridge Engineering*, 6(6), 523-528.

Faltinsen, O.M. (1990). Sea loads on ships and offshore structures. *Cambridge (UK): Cambridge University Press*. 328p.

Farrar, C.R. and Worden, k. (2007). An introduction to structural health monitoring. *Philosophical Transactions of the Royal Society A*, 365, February 2007, pp303-315.

Fault Activity Map of California. (2010). Geologic data map No. 6. *California Geological Survey*. Department of Conservation, Sacramento, CA.

Florida Department of Transportation. (2011). Bridge costs. *Transportation costs report*.

Frangopol, D.M. (2011). Life-cycle performance, management, and optimization of structural systems under uncertainty: accomplishments and challenges. *Structure and Infrastructure Engineering*, 7(6), 389-413.

Frangopol, D.M., Bocchini, P., Decò, A., Kim, S., Kwon, K., Okasha, N.M. and Saydam, D. (2012). Integrated life-cycle framework for maintenance, monitoring, and reliability of naval ship structures. *Naval Engineers Journal*, 124(1), 89-99.

Frangopol, D.M. and Curley, J.P. (1987). Effects of damage and redundancy on structural reliability. *Journal of Structural Engineering*, 113 (7), 1533–1549.

Frangopol, D.M., Iizuka, M. and Yoshida, K. (1992). Redundancy measures for design and evaluation of structural systems. *Journal of Offshore Mechanics and Arctic Engineering*, 114(4), 285-29.

Frangopol, D.M. and Klisinski, M. (1989a). Material behavior and optimum design of structural systems. *Journal of Structural Engineering*, 115(5), 1054-1075.

Frangopol, D.M. and Klisinski, M. (1989b). Weight-strength-redundancy interaction in optimum design of three-dimensional brittle-ductile trusses. *Computers and Structures*, 31(5), 775-787.

Frangopol, D.M., Lin, K.-Y. and Estes, A.C. (1997). Life-cycle cost design of deteriorating structures. *Journal of Structural Engineering*, 123(10), 286–297.

Frangopol, D.M. and Nakib, R. (1991). Redundancy in highway bridges. *Engineering Journal, American Institute of Steel Construction*, 28(1), 45-50.

Fu, G. (1987). Modeling of Lifetime structural system reliability. *Ph.D. Dissertation, Report no. 87-9*. Cleveland, OH: Department of Civil Engineering, University of Case Western Reserve University.

Gaganis, P. and Smith, L. (2001). A Bayesian approach to the quantification of the effect of model error on the predictions of groundwater models. *Water Resources Research*, 37(9), 2309-2322.

Geyskens, P., Der Kiureghian, A. and Monteiro, P. (1998). Bayesian prediction of elastic modulus of concrete. *Journal of Structural Engineering*, 124(1), 89–95.

Ghosh, J. and Padgett, J.E. (2010). Aging considerations in the development of time-dependent seismic fragility curves. *Journal of Structural Engineering*, 136(12), 1497–1511.

Ghosh, J., Rokneddin, K., Padgett, J.E. and Dueñas–Osorio, L. (2014). Seismic reliability assessment of aging highway bridge networks with field instrumentation data and correlated failures. I: methodology. *Earthquake Spectra*, 30(2), 795-817.

Ghosn, M. and Moses, F. (1998). Redundancy in highway bridge superstructures. *NCHRP Report 406*, Transportation Research Board, Washington, DC.

Ghosn, M., Moses, F. and Frangopol, D.M. (2010). Redundancy and robustness of highway bridge superstructures and substructures. *Structure and Infrastructure Engineering*, 6(1-2), 257-278.

Ghosn, M., Moses, F. and Wang, J. (2004). Design of highway bridges for extreme events. *NCHRP Report 489*, Transportation Research Board, Washington, D.C.

Guedes Soares, C. and Teixeira, A.P. (2000). Structural reliability of two bulk carrier designs. *Marine Structures*, Elsevier, 13(2), 107-128.

Handfelt, L.D., Wong, I., and Kavanagh, N. (2011). Seismic hazard evaluation for design of San Vicente dam raise. *21st Century Dam Design - Advances and Adaptations, 31st Annual USSD Conference*, U.S. Society on Dams, Denver.

Hansell, W.C. and Viest, I.M. (1971). Load factor design for steel highway bridges. *AISC Engineering Journal*, American Institute of Steel Construction, 8(4), 113-123.

Hendawi, S. and Frangopol, D.M. (1994). System reliability and redundancy in structural design and evaluation. *Structural Safety*, 16(1-2), 47-71.

Hess, P.E., III. (2007). Structural health monitoring for high speed naval ships. *In: Proceedings of the 6th international workshop on structural health monitoring: quantification, validation, and implementation*, September 2007, Stanford, California, 3–15.

Hessami, A.G. (1999). Risk management: A systems paradigm. *Systems Engineering*, 2(3), 156–167.

Hsiao, L., Yu, W. and Galambos, T. (1990). AISI LRFD method for cold-formed steel structural members. *Journal of Structural Engineering*, 116(2), 500–517.

Hughes, O.F. (1983). Ship structural design: a rationally-based, computer-aided, optimization approach. *Wiley and Sons, New York*, 582p.

Hussein, A.W. and Guedes Soares, C. (2008). Partial safety factors assessment for double hull tankers following the new common structural rules. *In: Proceedings of the 27th International Conference on Offshore Mechanics and Arctic Engineering*.

Hussein, A.W. and Guedes Soares, C. (2009). Reliability and residual strength of double hull tankers designed according to the new IACS common structural rules. *Ocean Engineering*, 36(17-18), 1446-1459.

Hørte, T., Wang, G. and White N. (2007). Calibration of the hull girder ultimate capacity criterion for double hull tankers. *Proceedings of the 10th International*

Symposium on Practical Design of Ships and Other Floating Structures. Houston, USA, vol (1), 553-564.

IACS. (2008). Common structural rules for double hull oil tankers. *International Association of Classification Societies (IACS), London, UK*.

Imai, K. and Frangopol, D.M. (2001). Reliability-based assessment of suspension bridges: application to the Innoshima Bridge. *Journal of Bridge Engineering*, 6 (6), 398–411.

Imai, K. and Frangopol, D.M. (2002). System reliability of suspension bridges. *Structural Safety*, 24(2-4), 219-259.

Imam, B. and Chryssanthopoulos, M.K. (2010). A review of metallic bridge failure statistics. *In: International Association for Bridge Maintenance and Safety Conference*, July 2010, Philadelphia, USA.

Janssens, V., O'Dwyer, D.W. and Chryssanthopoulos, M.K. (2012). Assessing the consequences of building failures. *Structural Engineering International*, 22(1), 99-104.

Johnson, P.A. (1991). Reliability-based pier scour engineering. *Journal of Hydraulic Engineering*, 118(10), 1344-1358.

Johnson, P.A. and Dock, D.A. (1998). Probabilistic bridge scour estimates. *Journal of Hydraulic Engineering*, 124(7), 750-754.

Jung, W.S., Han S.H. and Ha J. (2004). A fast BDD algorithm for large coherent fault trees analysis. *Reliability Engineering and System Safety*, 83(3), 369-374.

Kececioglu, D. (1995). Maintainability, availability, and operational readiness engineering handbook. Prentice-Hall, Upper Saddle River, NJ.

Kim, J. (2010). Finite element modeling of twin steel box-girder bridges for redundancy evaluation. *Dissertation*, The University of Texas at Austin, Austin, Texas.

Kim, S, Frangopol, D.M. and Zhu, B. (2011). Probabilistic optimum inspection/repair planning of deteriorating structures. *Journal of Performance of Constructed Facilities*, 25(6), 534-544.

Kirkwood, C.W. (1993). An algebraic approach to formulating and solving large models for sequential decisions under uncertainty. *Management Science*, 39 (7), 900-913.

Ko, J.M. and Ni, Y.Q. (2005). Technology developments in structural health monitoring of large-scale bridges. *Engineering Structures*, 27(12), 1715-1725.

Kong, J.S. and Frangopol, D.M. (2003). Life-cycle reliability-based maintenance cost optimization of deteriorating structures with emphasis on bridges. *Journal of Structural Engineering*, 129(6), 818-828.

Kong, J.S., Frangopol, D.M. and Gharaibeh, E.S. (2000). Life prediction of highway bridges with or without preventive maintenance. *Proceedings of 8th ASCE Specialty Conference on Probabilistic Mechanics and Structural Reliability*, July 2000, University of Notre Dame, Norte Dame, Indiana.

Kulicki, J.M., Mertz, D.R. and Wassef, W.G. (1994). LRFD design of highway bridges. *NHI Course 13061*, Federal Highway Administration, Washington, D. C.

Kulicki, J.M., Prucz, A., Clancy, C.M., Mertz, D.R. and Nowak, A.S. (2007). Updating the calibration report for AASHTO LRFD code. *NCHRP 20-7/186*, Transportation Research Board, Washington, D.C.

Lagasse, P.F., Clopper, P.E., Pagán-Ortiz, J.E., *et al.* (2009). Bridge Scour and Stream Instability Countermeasures—Experience, Selection, and Design Guidance, 3rd Edition. *Hydraulic Design Series No. 23*, FHWA Publication No. FHWANHI-09-111 & 112.

Laursen, E.M. (1958). Scour at bridge crossings. *Bulletin No. 8*, Iowa Highways Research Board, Ames, Iowa.

Leemis, L.M. (1995). Reliability, probabilistic models and statistical methods. Prentice Hall, NJ, USA.

Lin, K-Y. and Frangopol, D.M. (1996). Reliability-based optimum design of reinforced concrete girders. *Structural Safety*, 18(2-3), 239-258.

Lin, S., Yu, W. and Galambos, T. (1992). ASCE LRFD method for stainless steel structures. *Journal of Structural Engineering*, 118(4), 1056–1070.

Liu, M. and Frangopol, D.M. (2005a). Multi-objective maintenance planning optimization for deteriorating bridges considering condition, safety, and life-cycle cost. *Journal of Structural Engineering*, 131 (5), 833–842.

Liu, M. and Frangopol, D.M. (2005b). Time-dependent bridge network reliability: novel approach. *Journal of Structural Engineering*, 131(2), 329-337.

Liu, M., Frangopol, D.M. and Kim, S. (2009). Bridge system performance assessment from structural health monitoring: a case study. *Journal of Structural Engineering*, 135(6), 733-742.

Liu, W.D., Neuenhoffer, A., Ghosn, M. and Moses, F. (2001). Redundancy in highway bridge substructures, *NCHRP Report 458*. Transportation Research Board, Washington, DC.

Luís, R.M., Teixeira, A.P. and Guedes Soares, C. (2009). Longitudinal strength reliability of a tanker hull accidentally grounded. *Structural Safety*, 31(3), 224–33.

Lupoi, A., Franchin, P. and Schotanus, M. (2003). Seismic risk evaluation of RC bridge structures. *Earthquake Engineering and Structural Dynamics*, 32:1275-1290.

Manning, R. (1891). On the flow of water in open channels and pipes. Transactions of the Institution of Civil Engineers of Ireland, 20, 161-207.

Mansour, A.E. (1997). Assessment of reliability of ship structures. *SSC-398*, April 30, 1997. Ship Structure Committee, Washington D.C.

Mansour, A.E. and Hovem, L. (1994). Probability Based Ship Structural Safety Analysis. *Journal of Ship Research*, SNAME, 38(4), 329-339.

MathWorks. (2009). Statistics toolbox, MATLAB 7.9. Natick, MA, The Mathworks, Inc.

MathWorks. (2010). Signal processing toolbox, MATLAB 7.10. Natick, MA, The MathWorks, Inc.

Matsumoto, M., Shiraishi, N., Rungthongbaisuree, S. and Kikuta, T. (1989). Corrosion of steel bridges-its long-term prediction and effect on the safety. *Structural Engineering / Earthquake Engineering*, 6(2), 229-237.

Melville, B.W. and Chiew, Y.M. (1999). Time scale for local scour at bridge piers. *Journal of Hydraulic Engineering*, 125(1), 59-65.

Minitab. (2010). Graphing data, Minitab 16.0. State College, PA, Minitab, Inc.

Moan, T. (2005). Reliability-based management of inspection, maintenance and repair of offshore structures. *Structure and Infrastructure Engineering*, 1 (1), 33–62.

Moses, F. (1974). Reliability of structural systems. *Journal of the Structural Division*, *Proceedings of the American Society of Civil Engineers*, 100(ST9), September 1974.

Moses, F. (1982). System reliability development in structural engineering, *Structural Safety*, 1(1), 3–13.

Naito, H., Akiyama, M. and Suzuki, M. (2011). Ductility evaluation of concrete-

encased steel bridge piers subjected to lateral cyclic loading. *Journal of Bridge Engineering,* 16(1), 72-81.

Neill, C.R. (1964). River-bed scour: a review for engineers. Canadian Good Roads Association, Technical Publication No. 23.

Nikolaidis, E., Hughes, O., Ayyub, B.M. and White, G.J. (1993). A method for reliability assessment of ship structures. *Ship Symposium*, November 16-17, 1993, SSC/SNAME, Arlington, Virginia, US, pp H1-H10.

Nishitani, M., Umebara, T. and Fukui, J. (2002). Development of seismic retrofitting technologies for existing foundations. *Proceedings of the 18th US-Japan Bridge Engineering Workshop,* Panel on Wind and Seismic Effects, UJNR, 18: 284-297.

Okasha, N. M. and Frangopol, D. M. (2009a). Time-dependent redundancy of structural systems. *Structure and Infrastructure Engineering*, 6(1-2), 279 – 301.

Okasha, N.M. and Frangopol, D.M. (2009b). Lifetime-oriented multi-objective optimization of structural maintenance, considering system reliability, redundancy, and life-cycle cost using GA. *Structural Safety*, 31 (6), 460-474.

Okasha, N.M. and Frangopol, D.M. (2010a). Novel approach for multi-criteria optimization of life-cycle preventive and essential maintenance of deteriorating structures. *Journal of Structural Engineering*, 136(8), 1009-1022.

Okasha, N.M. and Frangopol, D.M. (2010b). Efficient method based on optimization and simulation for the probabilistic strength computation of the ship hull. *Journal of Ship Research*, SNAME, 54(4), 1-13.

Okasha, N.M, Frangopol, D.M. and Decò, A. (2010). Integration of structural health monitoring in life-cycle performance assessment of ship structures under uncertainty. *Marine Structures*, 23(3), 303-321.

Okasha, N.M., Frangopol, D.M., Saydam, D. and Salvino, L.M. (2011). Reliability analysis and damage detection in high-speed naval craft based on structural health monitoring data. *Structural Health Monitoring*, 10(4), 361-379.

OpenSees. (2011). Open system for earthquake engineering simulation, OpenSees 2.2.2. Berkeley, CA, Pacific Earthquake Engineering Research Center, University of California.

Paik, J.K. and Frieze, P.A. (2001). Ship structural safety and reliability. *Progress in Structural Engineering and Materials*, Wiley and Sons, 3(2), 198-210.

Paik, J.K., Kim, S.K. and Lee, S.K. (1998). Probabilistic corrosion rate estimation model for longitudinal strength members of bulk carriers. *Ocean Engineering*, 25(10), 837-860.

Paik, J.K. and Mansour, A.E. (1995). A simple formulation for predicting the ultimate strength of ships. *Journal of Marine Science and Technology*, 1(1), 52-62.

Paik J.K. and Thayamballi A.K. (2002). Ultimate strength of ageing ships. *Journal Engineering for the Maritime Environment*, 216, 57-77.

Paikowsky, S.G. (2004). Load and resistance factor design (LRFD) for deep foundations, *NCHRP Report 507*. Transportation Research Board, Washington, DC.

Paliou, C., Shinozuka, M. and Chen, Y.-N. (1990). Reliability and redundancy of offshore structures. *Journal of Engineering Mechanics*, 116 (2), 359–378.

PDSTRIP. (2006). Program PDSTRIP: Public Domain Strip Method. Website: http://sourceforge.net/projects/pdstrip.

Pedersen, T. (2000). Wave load prediction – a design tool. *PhD Thesis*, Department of Naval Architecture and Offshore Engineering, Technical University of Denmark, Lyngby.

Pedersen, P.T. (2002). Collision risk for fixed offshore structures close to high-density shipping lanes. *Proceedings of the Institution of Mechanical Engineers, Part M: Journal of Engineering for the Maritime Environment*, 216 (1), 29-44.

Pierson, W.J. (1952). A unified mathematical theory for the analysis of propagation and refraction of storm-generated ocean surface waves, part I and 11, *New York University*.

Priestley, M.J.N., Seible, F. and Calvi, M. (1996). Seismic design and retrofit of bridges. *John Wiley & Sons*, New York.

Qin, S. and Cui, W. (2003). Effect of corrosion models on the time-dependent reliability of steel plated elements. *Marine Structures*, 16(1), 15-34.

Rabi, S., Karamchandani, A. and Cornell, C.A. (1989). Study of redundancy of near-ideal parallel structural systems. *Proceeding of the 5th International Conference on Structural Safety and Reliability*, New York, 975–982.

Rackwitz, R. (2002). Optimization and risk acceptability based on the Life Quality Index. *Structural Safety*, 24(2-4), 297-331.

Rakoczy, A.M. (2012). Development of system reliability models for railway bridges. *Ph.D. Dissertation*, University of Nebraska.

Resolute Weather. (2012). Pierson–Moskowitz sea spectrum. www.eustis.army.mil/weather.

Richardson, E.V. and Davis, S.R. (1995). Evaluating scour at bridges, 3rd edition. Report No. FHWA-IP-90-017, *Hydraulic Engineering Circular No. 18*, Federal Highway Administration, Washington, DC.

Rusk, D.T., Lin, K.Y., Swartz, D.D. and Ridgeway, G.K. (2011). Bayesian updating of damage size probabilities for aircraft structural life-cycle management. *Journal of Aircraft*, 39(4), 689-696.

Salvino, L.M. and Collette, M.D. (2009). Monitoring marine structures. *New York: John Wiley & Sons*.

Saydam, D. and Frangopol, D.M. (2011). Time-dependent performance indicators of damaged bridge superstructures. *Engineering Structures*, 33(9), 2458-2471.

Seo, J-W. and Linzell, D.G. (2010). Probabilistic vulnerability scenarios for horizontally curved, steel, I-Girder bridges under earthquake loads. *Transportation Research Record: Journal of the Transportation Research Board*, 3(2202), 206-211.

Shen, H.W., Schneider, V.R. and Karaki, S. (1969). Local scour around bridge piers. *Journal of the Hydraulics Division*, 95(HY6), 1919-1940.

Smith, C. (1997). Influence of local compressive failure on ultimate longitudinal strength of a ship's hull. *In: Proceedings of the PRADS: international symposium on practical design in shipbuilding*, Tokyo, Japan, 18–20 October 1977, Society of Naval Architects of Japan: 73-79.

Stein, S.M., Young, G.K., Trent, R.E. and Pearson, D.R. (1999). Prioritizing scour vulnerable bridges using risk. *Journal of Infrastructure Systems*, 5(3), 95-101.

Tangchawal, S. (2011). Proposed reliability techniques on soil and rock excavations. *Energy Research Journal*, 2(1), 17–21.

Thoft-Christensen, P. and Baker, M.J. (1982). Structural reliability theory and its applications. Springer-Verlag, Berlin, Heidelberg, New York.

Thoft-Christensen, P. and Murotsu, Y. (1986). Application of structural systems reliability theory. Springer-Verlag, Berlin, Heidelberg, Tokyo.

Tobias, D.H. (2011). Perspectives on AASHTO load and resistance factor design. *Journal of Bridge Engineering*, 16(6), 684–692.

Tsopelas, P. and Husain, M. (2004). Measures of structural redundancy in reinforced concrete buildings. II: Redundancy response modification factor RR. *Journal of Structural Engineering*, vol 130, 1659-1666.

Uddin, N. and Ang, A.H-S. (2011). Quantitative risk assessment for natural hazards. American Society of Civil Engineers. VA.

USGS. (2000). USGS National Bridge Scour Database. Department of the Interior, U.S. Geological Survey, Reston, VA.

USGS. (2009a). Earthquake probability mapping. Department of the Interior. U.S. Geological Survey, Reston, VA.

USGS. (2009b). Earthquake hazards program. Department of the Interior. U.S. Geological Survey, Reston, VA.

USGS. (2014). USGS National Water Information System. Department of the Interior, U.S. Geological Survey, Reston, VA.

Vu, K. and Stewart, M.G. (2000). Structural reliability of concrete bridges including improved chloride-induced corrosion models. *Structural Safety,* 22(4)**,** 313-333.

Wang, C-H. and Wen, Y-K. (2000). Evaluation of pre-northridge low-rise steel buildings. II: Reliability. *Journal of Structural Engineering*, 126(10), 1169–1176.

Wardhana, K. and Hadipriono, F.C. (2003). Analysis of recent bridge failures in the United States. *Journal of Performance of Constructed Facilities*, 17(3), 144-150.

Wen, Y.K. and Song, S.H. (2003). Structural reliability / redundancy under earthquakes. *Journal of Structural Engineering*, 129(1), 56-67.

Wilson, J. and Holmes, K. (2007). Seismic vulnerability and mitigation during construction of cable-stayed bridges. *Journal of Bridge Engineering*, 12(3), 364–372.

Wright, T, DesRoches R. and Padgett, J.E. (2011). Bridge seismic retrofitting practices in the central and southeastern United States. *Journal of Bridge Engineering*, 16(1), 82-92.

Yang, S.I., Frangopol, D.M. and Neves. L.C. (2006). Optimum maintenance strategy for deteriorating structures based on lifetime functions. *Engineering Structures*, 28(2), 196–206.

Yamamoto, Y. (2011). Stochastic model for earthquake ground motion using wavelet packets. *Ph.D. Thesis*. Department of Civil and Environmental Engineering, Stanford University, Stanford, CA.

Yanmaz, A.M. and Altmbilek, H.D. (1991). Study of time-variant local scour around bridge piers. *Journal of Hydraulic Engineering*, 117(10), 1247-1268.

Yanmaz, A.M. and Apaydin, M. (2012). Bridge scour risk assessment and countermeasure design. *Journal of Performance of Constructed Facilities*, 26(4), 499-506.

Zhang, Y. and Mohammadian, A. (2008). Bayesian updating of transferred household travel data. *Transportation Research Record*, Issue 2049, 111-118.

Zhang, J., Zhang, L.M. and Tang, W.H. (2009). Bayesian framework for characterizing geotechnical model uncertainty. *Journal of Geotechnical and Geoenvironmental Engineering*, 135(7), 932-940.

Zhao, Y.G. and Ono, T. (2001). Moment methods for structural reliability. *Structural Safety*, 23(1), 47-75.

Zhu, B. and Frangopol, D.M. (2012). Reliability, redundancy and risk as performance indicators of structural systems during their life-cycle. *Engineering Structures*, vol 41, 34-49.

Zhu, B. and Frangopol, D. M. (2013a). Risk-based approach for optimum maintenance of bridges under traffic and earthquake loads. *Journal of Structural Engineering*, 139(3), 422-434.

Zhu, B. and Frangopol, D. M. (2013b). Incorporation of SHM data on load effects in the reliability and redundancy assessment of ship cross-sections using Bayesian updating. *Structural Health Monitoring*, 12(4), 377-392.

APPENDIX

LIST OF NOTATIONS

A.1 NOTATIONS OF CHAPTER 2

$E_c(R)$	=	mean resistance of a single component
$E_c(M_{U,ext})$	=	mean resistance of exterior girder when its reliability index is 3.5
$E_c(M_{U,int})$	=	mean resistance of interior girder when its reliability index is 3.5
$E_{cs}(R)$	=	mean resistance of a component in a system
$E_{cs}(M_U)$	=	final mean resistance of girder
$E(P)$	=	mean value of load effect
F	=	failure event
g_i	=	performance function of component i
G	=	limit state equation matrix
LN	=	lognormal distribution
$M_{DL,ext}$	=	bending moment acting on exterior girder due to dead load
$M_{DL,int}$	=	bending moment acting on interior girder due to dead load
$M_{L,ext}$	=	total bending moment acting on exterior girder
$M_{L,i}$	=	total bending moment acting on girder i
$M_{L,int}$	=	total bending moment acting on interior girder
M_{LL}	=	maximum bending moment at the mid-span cross-section of bridge
$M_{LL,ext}$	=	maximum bending moment acting on exterior girder due to live load
$M_{DL,int}$	=	maximum bending moment acting on interior girder due to live load
$M_{U,i}$	=	ultimate moment capacity of girder i
N	=	number of components in a system
N	=	normal distribution
q_{ext}	=	lateral load distribution factor of exterior girder
q_{int}	=	lateral load distribution factor of interior girder

R	=	resistance
R_i	=	resistance of component i
R_n	=	nominal resistance
R_r	=	factored resistance
P	=	load effect
P_f	=	probability of failure
Q_i	=	force effect
$V(R)$	=	coefficients of variation of resistance
$V(P)$	=	coefficients of variation of load effect
w	=	number of simulation samples
$w_{a,ext}$	=	the uniform load on exterior girder due to the self-weight of asphalt pavement
$w_{a,int}$	=	the uniform load on interior girder due to the self-weight of asphalt pavement
w_{ext}	=	the total uniform load on exterior girder due to the self-weight of superstructure
$w_{g,i}$	=	the uniform load on girder i due to its self-weight
w_{int}	=	the total uniform load on interior girder due to the self-weight of superstructure
$w_{r,ext}$	=	the uniform load on exterior girder due to the self-weight of railing
$w_{s,ext}$	=	the uniform load on exterior girder due to the self-weight of slab
$w_{s,int}$	=	the uniform load on interior girder due to the self-weight of slab
β_c	=	reliability index of a single component
β_{ext}	=	component reliability index of exterior girder
β_{int}	=	component reliability index of interior girder
β_{sys}	=	system reliability index
$\beta_{sys,target}$	=	target system reliability index
η_D	=	factor relating to ductility
η_i	=	load modifier
η_l	=	factor relating to operational classification
η_R	=	redundancy factor (factor relating to redundancy)

$\rho(R_i, R_j)$	=	correlation coefficient between the resistances of components i and j
δ	=	post-failure behavior factor
γ_i	=	load factor
ϕ	=	resistance factor
ϕ_R	=	redundancy modifier

A.2 NOTATIONS OF CHAPTER 3

$E_{cs}(M_{U,ext})$	=	mean resistance of exterior girder when its reliability index is 3.5
$E_{cs}(M_{U,int})$	=	mean resistance of interior girder when its reliability index is 3.5
$E_{cs}(R)$	=	mean resistance of a component in a system
$E(P)$	=	mean value of load effect
g_i	=	performance function of component i
LN	=	lognormal distribution
$M_{L,ext}$	=	total bending moment acting on exterior girder
$M_{L,i}$	=	total bending moment acting on girder i
$M_{L,int}$	=	total bending moment acting on interior girder
$M_{U,i}$	=	ultimate moment capacity of girder i
N	=	number of components in a system
N	=	normal distribution
R	=	resistance
R_i	=	resistance of component i
P	=	load effect
$V(R)$	=	coefficients of variation of resistance
$V(P)$	=	coefficients of variation of load effect
β_{cs}	=	reliability index of a component in a system
β_{sys}	=	system reliability index
$\rho(R_i, R_j)$	=	correlation coefficient between the resistances of components i and j
δ	=	post-failure behavior factor

A.3 NOTATIONS OF CHAPTER 4

A	=	cross-sectional area
A_{DT}	=	average daily traffic
A_{DTT}	=	average daily truck traffic
b	=	branch in event-tree model
c	=	average corrosion penetration
C	=	consequences
C_{DIR}	=	direct consequences
C_{FV}	=	future monetary value of the consequences
C_{IND}	=	indirect consequences
C_{PV}	=	present monetary value of the consequences
C_{Reb}	=	rebuilding cost
$C_{Running}$	=	running cost
C_{SL}	=	safety loss cost
C_{TL}	=	time loss cost
C_{Tva}	=	value of time per adult
C_{Tvtk}	=	value of time for truck
C_{Veh}	=	average running cost for vehicles
d	=	duration of detour
D	=	length of detour
D_S	=	safe following distance during driving
DF	=	traffic load distribution factor
DR	=	deterioration rate
E_i	=	failure of component i
$\overline{E}_i$	=	survival of component i
F_i	=	failure of the damaged system without component i
$\overline{F}_i$	=	survival of damaged system without component i
$F_{comp,i}$	=	component i fails

411

F_{subsys}	=	subsequent system fails
$\overline{F}_{subsys}$	=	subsequent system survives
F_y	=	yield stress
g	=	performance function
G	=	girder
I_{beam}	=	impact factor
l	=	ratio between the traffic load moment and the HS-20 moment
L	=	bridge length
M_{trk}	=	traffic load moment
M_{max}	=	critical traffic load moment under the HS-20 truck load
O_{Car}	=	average vehicle occupancy for cars
O_{Trk}	=	average vehicle occupancy for trucks
p	=	regression random variable for estimation of corrosion penetration
P	=	probability
P_f	=	probability of failure
q	=	regression random variable for estimation of corrosion penetration
r	=	resistance
r_m	=	money discount rate
R	=	risk
R_{DIR}	=	direct risk
R_{IND}	=	indirect risk
R_{TOT}	=	total risk
RI	=	redundancy index
s	=	load effect
S	=	average detour speed
t	=	time
T_{Trk}	=	average daily truck traffic in percent
Z	=	plastic section modulus
β	=	reliability index

β_{fc}	=	reliability index associated with the probability of the first component failure
β_s	=	system reliability index
μ_R	=	mean value of the resistance of a component
μ_{Fy}	=	mean value of the material yield stress
σ_R	=	standard deviation of the resistance of a component
σ_{Fy}	=	standard deviation of the material yield stress
ρ	=	correlation coefficient
γ	=	Euler number
γ_{mfg}	=	modeling uncertainty factor of girder
λ_{asph}	=	weight uncertainty factor of asphalt
λ_{conc}	=	weight uncertainty factor of concrete
λ_{steel}	=	weight uncertainty factor of steel
δ	=	coefficient of variation
Φ	=	standard normal cumulative distribution function

A.4 NOTATIONS OF CHAPTER 5

A	=	cross-sectional area of reinforcement
A_r	=	remaining cross-sectional area of reinforcement
A_{rl}	=	cross-sectional area of longitudinal rebar
A_{rt}	=	cross-sectional area of tie
C_0	=	surface chloride concentration
C_1	=	removal cost per square meter
C_a	=	displacement ductility capacity
C_{corr}	=	corrosion coefficient
C_{cr}	=	critical chloride concentration
C_{Rem}	=	removal cost
C_{under}	=	loss associated with the channel, highway or railway under the bridge

d	=	effective cross-sectional depth
d_0	=	initial diameter
d_r	=	remaining diameter
d_{se}	=	distance from the center of cross-section of the longitudinal rebar to the edge of the cover
d'	=	distance from extreme compression longitudinal rebar to extreme tensile longitudinal rebar
D	=	chloride diffusion coefficient
$erfc$	=	complementary error function
E_s	=	elastic modulus
f_c	=	concrete compressive strength
f_m	=	tensile strength of longitudinal rebar
f_{wy}	=	yield strength of tie
f_y	=	yield strength of longitudinal rebar
g	=	performance function
h	=	shear span of RC pier
H	=	hazard
H_E	=	earthquake hazard
H_L	=	traffic hazard
i_{corr}	=	parameter related to the rate of corrosion
I	=	impact factor
M_{deck}	=	traffic load moment acting on the deck
M_{dl_asph}	=	dead load moment caused by asphalt
M_{dl_conc}	=	dead load moment caused by concrete
M_{dl_steel}	=	dead load moment caused by steel
M_{ll}	=	traffic load moment
M_u	=	ultimate moment capacity
N_B	=	number of spaces between ties associated with buckling length
N_L	=	number of longitudinal rebars perpendicular to the loading direction
N_w	=	number of ties in the region involved in the instability of the rebar

P	=	probability
Q	=	load effect
R	=	resistance
R_{Total}	=	total risk
S	=	tie spacing
T	=	corrosion initiation time
T_c	=	application timing of deck recoating
T_j	=	application timing of column jacketing
w	=	weight of intact cross-section of rebar
w_2	=	remaining weight after removing the rust
W	=	bridge width
x	=	concrete cover depth
α_1	=	reduction parameter
γ_{mfc}	=	modeling uncertainty factor of concrete deck
δ_u	=	Displacement capacity of a RC pier
η	=	traffic load distribution factor
Δ_e	=	displacement ductility demand
ϕ_y	=	yield curvature
ϕ_u	=	ultimate curvature

A.5 NOTATIONS OF CHAPTER 6

A	=	cross-sectional area of an open channel
b	=	bottom width of an open channel
C_{RP}	=	repair cost
CP_f	=	cumulative failure probability
D	=	pier width
F_G	=	girder failure event
F_P	=	pier column failure event

Fr	=	Froude number
g	=	performance function
g_a	=	acceleration due to gravity.
K_1	=	coefficient to consider the nose shape of the pier
K_2	=	coefficient to consider the angle between the direction of the flow and the direction of the pier
K_3	=	coefficient to consider the stream bed condition
LC	=	lane(s) closure event
n	=	Manning roughness coefficient
P	=	probability of failure
Q	=	load effect
Q_f	=	flow discharge rate
r	=	hydraulic radius
R	=	resistance
S	=	slope of the bed stream
S_G	=	girder survival event
S_P	=	pier column survival event
V	=	mean flow velocity
V_c	=	critical velocity
y_0	=	depth of flow upstream of the pier
y_P	=	pier depth
y_s	=	scour depth
z	=	side slope
λ_{mf}	=	modeling factor

A.6 NOTATIONS OF CHAPTER 7

A_w	=	peak value of the wave elevation

B	=	ship breadth
C_b	=	ship block coefficient
C_{wv}	=	wave coefficient
E	=	elastic modulus
f_{sw}	=	factor accounting for the variation of the vertical bending moment along the ship length
f_X	=	original probability density function of random variable X
f'	=	prior probability density function
f''	=	posterior probability density function
f'_X	=	updated probability density function of random variable X
F'_X	=	updated cumulative distribution function of random variable X
g_U	=	performance function for the ultimate failure
g_F	=	performance function for the first failure
H	=	ship height
$H_{1/3}$	=	significant wave height
k	=	normalizing constant
L	=	ship length
$L(\theta)$	=	likelihood function
$m_{0,w}$	=	zero-*th* moment of the wave spectrum
$m_{0,M}$	=	zero-*th* moment of the vertical bending moment spectrum
M_{FR}	=	resisting bending moment for the first failure
M_{sw}	=	still water bending moment
M_{UR}	=	resisting bending moment for the ultimate failure
M_w	=	peak value of the wave-induced vertical bending moment
n	=	size of the observed samples
RI	=	redundancy index
S_M	=	response spectrum for the wave-induced vertical bending moment
S_w	=	wave spectrum for a given sea state

417

t_p	=	plating thickness
T_1	=	average wave period
U	=	ship speed
x_R	=	model uncertainty associated with the resistance determination
x_{sw}	=	model uncertainty related to the still water bending moment prediction
x_w	=	model uncertainty associated with the wave-induced bending moment prediction
α_M	=	parameter of Rayleigh distribution
β_F	=	cross-section reliability index related to the first failure
β_U	=	cross-section reliability index related to the ultimate failure
σ_{Yp}	=	yielding stresses of plating
σ_{Ys}	=	yielding stresses of stiffener
ω	=	absolute wave frequency
ω_e	=	encounter frequency
Φ	=	transfer function
θ	=	parameter of the probability density function of random variable X
θ_a	=	angle between the direction of wave and the direction in which the ship is heading
μ_M	=	mean value of the peaks of wave-induced vertical bending moment
σ_M	=	standard deviation of the peaks of wave-induced vertical bending moment
λ	=	scale of the segmented model

A.7 NOTATIONS OF CHAPTER 8

C_1	=	annual corrosion rate
C_2	=	coefficient that determines the trend of corrosion progress
f'	=	prior probability density function

f''	=	posterior probability density function
f'_X	=	updated probability density function of random variable X
F'_X	=	updated cumulative distribution function of random variable X
k	=	normalizing constant
m	=	response spectral moment
M_w	=	wave-induced vertical bending moment
n	=	number of peaks occurring within a design storm duration T
N	=	number of simulation samples
r	=	thickness loss
t_0	=	corrosion initiation time
T	=	design storm period
u_n	=	most probable value of the Type I extreme value distribution
v_p	=	peak rate
Y_n	=	largest value of the peaks of vertical bending moment
α_n	=	measure of the dispersion of the Type I extreme value distribution
σ	=	modal value of the Rayleigh distribution
ρ	=	correlation coefficient between $\log(u_n)$ and $\log(\alpha_n)$
ρ_0	=	correlation coefficient between u_n and α_n
θ_i	=	parameter of the probability density function of random variable X
λ_1	=	parameter of lognormal distribution of u_n
ζ_1	=	parameter of lognormal distribution of u_n
λ_2	=	parameter of lognormal distribution of α_n
ζ_2	=	parameter of lognormal distribution of α_n

VITA

Benjin Zhu was born in Hefei, China, to Lixuan Zhu and his wife, Conglan Kong. She obtained her Bachelor of Science Degree in Civil Engineering from Hefei University of Technology, Hefei, China in 2004. Benjin received her Master of Science Degree in Bridge Engineering from Tongji University, Shanghai, China in 2007. From 2007 to 2009, she worked as a bridge engineer in the Architectural Design and Research Institute of Tongji University, Shanghai, China. In the August of 2009, she joined the Ph.D. program at Lehigh University, Bethlehem, PA, working under the supervision of Prof. Dan M. Frangopol.